A STUDY OF THERMO-STRUCTURAL DESIGN CONCEPTS FOR LIFTING ENTRY VEHICLES

by J. Newell

19960502 125

DEPARTMENT OF DEFENSE
PLASTICS TECHNICAL EVALUATION CENTER
PICATINNY ARSENAL, DOVER, N. J.

NATIONAL AERONAUTICS AND SPACE ADMINISTRATION • WASHINGTON, D. C. • JUNE 1965

DISCLAIMER NOTICE

UNCLASSIFIED

Technical Report
distributed by

**DEFENSE
TECHNICAL
INFORMATION
CENTER**

DTIC Acquiring Information-
Imparting Knowledge

Cameron Station
Alexandria, Virginia 22304-6145

UNCLASSIFIED
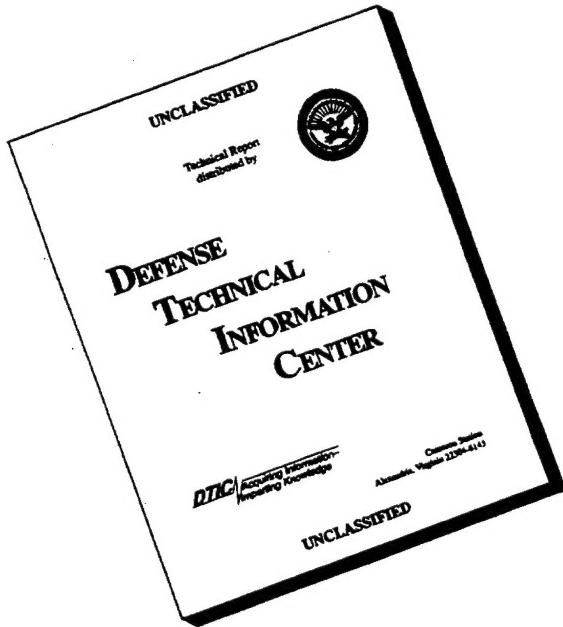
THIS DOCUMENT IS BEST QUALITY AVAILABLE. THE COPY FURNISHED TO DTIC CONTAINED A SIGNIFICANT NUMBER OF PAGES WHICH DO NOT REPRODUCE LEGIBLY.

A STUDY OF THERMO-STRUCTURAL DESIGN CONCEPTS

FOR LIFTING ENTRY VEHICLES

By J. Newell

ABSTRACT

This report contains the results of an investigation which was performed concerning the feasibility of various structural concepts for future space vehicles such as the HL-10 configuration. Various combinations of ablator and substructure were analyzed to survive the environments of ascent, space flight, and reentry at velocities between 26,000 and 36,500 feet per second. The concepts were applied to representative locations on the vehicle and evaluated in terms of thermal and structural performance; weight, which is a measure of efficiency of performance; ease of fabrication; reusability and/or refurbishability; and fabrication and assembly costs. To aid in the evaluation, comparisons were made between double and single wall concepts. The merits of integrated wall construction were examined in conjunction with the double wall concept. The term "integrated wall" as applied herein refers to reliance on the load-carrying ability of the ablator material in the structural design of an ablator-substructure composite shell.

FOREWORD

The purpose of this document is to present the final results of a feasibility study which was performed by the Research and Advanced Development Division, Avco Corporation, Wilmington, Massachusetts under NASA Contract NAS-1-3531. The study consisted of an investigation into "Thermo-Structural Design Concepts for Lifting Entry Vehicles." The work was administered under the direction of the Structures Research Division of the National Aeronautics and Space Administration, Langley Research Center, Hampton, Virginia. Mr. H. Bush of the Thermal Analysis Section, Entry Structures Branch, was project engineer for the division.

The study, which began 18 November 1963 and was concluded on 20 November 1964, was divided into two phases. Phase I consisted of a preliminary evaluation of the candidate concepts for construction of a lifting entry vehicle as reported in Avco RAD document RAD-SR-64-24, dated 29 January 1964. The results of Phase II of the study are documented herein.

Mr. J. Newell was the project engineer responsible for all technical aspects of the study assisted by other members of Avco's technical staff including: P. Andrews, N. Seelye, and A. Woodhull. Sincere acknowledgement is also made to H. Blumstein, R. Harmon, A. Machera, P. Miles, J. Morrison, D. Parker, and F. Simpson for their contributions.

CONTENTS

ILLUSTRATIONS

ILLUSTRATIONS (Cont'd)

ILLUSTRATIONS (Cont'd)

ILLUSTRATIONS (Cont'd)

ILLUSTRATIONS (Cont'd)

ILLUSTRATIONS (Cont'd)

TABLES

NOMENCLATURE

B   - extensional stiffness

C   - vehicle length

C_L - lift coefficient

C_p - specific heat

D   - bending rigidity

D_N - vehicle nose diameter

E   - modulus of elasticity

F_{cu} - ultimate compressive stress, psi

F_{tu} - ultimate tensile stress, psi

FG   - fiberglass

FHC   - filled honeycomb ablator

FPS   - feet per second

Ft   - feet

h_c - honeycomb core height

H/C, H.C.   - honeycomb

I   - moment of inertia

°K   - degrees, Kelvin

K_s - solar flux constant, 442 BTU/hr-ft^2

k   - thermal conductivity

L/D   - lift/drag ratio

M   - moment; Mach number

N   - normal force/inch

OML   - outer mold line

p   - pressure

Q   - integrated heating, BTU/ft^2

q   - dynamic pressure

$\dot{q}$ - convective heat flux, BTU/ft^2-sec.

R_{e_∞} - free stream Reynolds Number

S   - distance from windward ℄ around perimeter of vehicle cross-section

T   - temperature

t   - thickness

V_e - reentry velocity

$W/C_D A$ - ballistic coefficient

Z_e - reentry altitude

α - angle of attack, degrees; thermal diffusivity; coefficient of thermal expansion, in/in/°F

ρ - density

δ_e, δ_f - elevon deflection angle, degrees

ϵ - strain

σ - stress

ν - Poisson's ratio

subscripts:

a   - ablator

BL   - bond line (ablator-structure interface)

NOMENCLATURE (Concl'd)

subscripts: (Concl'd)

e   -   reentry

eff   -   effective

F.S.   -   honeycomb sandwich face sheet

fg   -   fiberglass

max   -   maximum

s, stag -   stagnation

1.0 INTRODUCTION

The purpose of this document is to present the results of a 12 month study per-formed by Avco RAD for the National Aeronautics and Space Administration, Langley Research Center, Hampton, Virginia, under contract NAS 1-3531, con-cerning the feasibility of various thermo-structural concepts for lifting reentry vehicles. The basic design is a double-wall type of construction consisting of either a metallic or nonmetallic outer shell housing an inner shell(s) which are essentially removable pods to accomodate both cargo and crew. Integration of the wall elements was considered in conjunction with the double wall concepts in an effort to further reduce vehicle weight. The term "integrated" as applied to the analyses herein refers to those cases where the ablator was considered to be part of the load carrying structure. This approach was used only with the nonmetallic outer shell. The feasibility of various double wall concepts was studied and evaluated in terms of thermodynamic and structural performance, weight, ease of fabrication, cost, reusability, and turnaround time for a multi-mission vehicle. Similar studies of a single wall concept were made for com-parison with the double wall analyses.

The program was divided into two phases. Phase I was concerned with the preliminary evaluation of combinations of three ablators (filled honeycomb, molded and laminated) and two types of fiberglass construction (honeycomb and stiffened sheet). Each combination was to be evaluated at representative locations on the vehicle and compared in terms of weight and ease of fabrica-tion. On the basis of this comparison, promising combinations were to be selected for further study during Phase II of the program. The results of the preliminary evaluation study are reported in reference 1. For low curvature regions on the vehicle the two most promising combinations were the filled honeycomb and laminated ablators on fiberglass honeycomb sandwich substructure, while on the highly curved areas of the vehicle the laminated and molded ablators on fiberglass sheet were recommended instead.

Phase II of the program was broken down into three general categories: 1) performance analyses, 2) comparison analyses, and 3) parametric studies. The intent of the performance analyses (Item I) was to obtain a more detailed definition of the structural and thermodynamic aspects of the selected design concepts and their associated problem areas. The objective of the analyses in Item 2 was to compare the double wall concepts for vehicle construction to a more conventional single wall configuration. It was during this phase of the program that weights, initial fabrication costs and feasi-bility of refurbishing or replacing the exterior shell were studied in detail in order to determine the relative advantages and disadvantages of the various concepts. Finally, parametric studies (Item 3) were made to determine the effects of changes in thermal and structural material properties on weight and performance of the selected concepts. These studies yielded information concerning the material property changes needed to improve the overall feasibility of the design concept.

2.0 STUDY SUMMARY AND CONCLUSIONS

2.1 Summary

The major effort in this study was devoted to evaluating the feasibility of selected double wall concepts in terms of design weight, which is a measure of thermodynamic and structural performance; fabrication cost; and re-using or refurbishing the structure. To provide a basis for comparison, an aluminum single shell vehicle with the filled H/C ablator was also analyzed. Each vehicle was designed to survive environments of ascent, space flight, reentry, and approach to touchdown. The load-carrying ability of the ablator was relied upon in the structural design of some of the double wall concepts. However, in all cases, cracking of the ablator was not allowed during ascent or reentry. The thermal design of the heat shield was based on a maximum ablator-structure interface temperature of 700°F in all cases except for the single aluminum shell concept, where 300°F was used because of the strength reduction of aluminum at higher temperatures. All double wall concepts were assumed to contain identical aluminum pressure shells.

    a.   Weight

A percentage comparison of the weights of each of the concepts analyzed in the study, in relation to the lightest weight system (integrated fiber-glass shell with filled H/C ablator), are presented in table I.

    1)   Double Wall versus Single Wall Construction

The single aluminum shell design with the filled H/C ablator proved to be about 27 percent heavier than the double shell designs. This large weight difference was due primarily to the additional ablator weight ($\sim$ 70 percent) required for a 300°F bond line temperature instead of a 700°F limitation.

    2)   Fiberglass versus Steel Outer Shell

The nonintegrated concepts with steel outer shells were approximately 2 and 4 percent heavier for the filled H/C ablator and laminated ablator designs, respectively, than their nonintegrated fiberglass outer shell counterparts. These slight differences are attributed to increases in structure and insulation weights and not those of the ablators, whose weights were the same for steel as for fiberglass structure. If the loads had been greater, steel might have shown a weight advantage over fiberglass, but here the design was minimum gauge-limited over much of the vehicle.

3) <u>Integrated versus Nonintegrated Outer Shell</u>

Table I indicates that only minor weight savings (between 0.4 and 2.5 percent) would be obtained by relying on the load-carrying ability of the ablator in a double shell design.

The lightest weight vehicle was the filled H/C ablator with an integrated fiberglass outer shell. The filled H/C ablator is lighter and more thermally efficient than the laminated ablator but has less structural strength. Its weight proved to be 17 percent lighter than the laminated ablator but required a 45 percent heavier outer shell substructure.

The structural design environment for the entire bottom surface of the integrated fiberglass shell with filled H/C ablator was max "q" reentry, which required the substructure to be stiff enough to prevent cracking of the ablator. This was in contrast to the laminated ablator design, in which cracking was not a problem and whose structure was amost completely designed by the approach to touchdown condition.

b. Fabrication and Assembly

Fabrication and assembly techniques were investigated to determine a feasible method whereby the outer shell could be assembled and dis-assembled around a single pressure vessel that was assumed to conform to the outer shape of the vehicle. The method chosen consisted of attaching the inner shell at various frame locations by fittings that would permit the thermal expansion and contraction of the shells relative to one another and at the same time provide sufficient paths between them for transfer of loads. The outer shell would be manufactured in several sections consisting of a nose cap, right and left hand body shells, and upper and lower closure strip, fins and elevons. The various sections would be bolted or unbolted, as the case may be, around the inner pressure shell in a manner that would require a minimum amount of perturbation in the heat shield.

c. Cost

Total material and fabrication costs for the various concepts indicate that the steel outer shell — aluminum pressure shell vehicle would be 53 percent more expensive than the fiberglass outer shell — aluminum pressure shell vehicle while the single aluminum shell vehicle would be 22 percent cheaper. Comparing the costs of just the two ablators, the laminated one would be 13 percent cheaper to fabricate than the filled H/C ablator. Costs for the structural shells themselves indicate that the single aluminum shell would be 6 percent more expensive and the steel outer shell would be 270 percent more expensive to fabricate than the outer fiberglass shell.

-3-

d. Reusability and Turnaround Time

1) Double Wall Concepts

Reusability of the double wall concepts would consist of reusing
the inner pressure vessel and either replacing or refurbishing
the used outer shell with new ablator. Short turnaround times
are possible with double wall construction because the outer shell
is removable. After a mission, the outer shell would be dis-
assembled and replaced by a new unit, fabricated beforehand.
The vehicle could then be readied for another flight. In the mean-
time, refurbishing of the used shell could be initiated to make it
ready for a future mission, if so desired. Thus, the time in-
volved in refurbishing would not affect the turnaround time of the
vehicle.

Whether to refurbish or discard a used outer shell is dependent
on several factors. First, because fiberglass degrades at 700°F,
a lower bond line temperature of about 500°F would be the maxi-
mum allowable temperature for a structure that is to be reused.
This would imply an increase in ablator weight of about 25 percent,
or 800 lbs. for a superorbital mission. The reliability problems
associated with reuse or refurbishment should also be considered.

Another consideration is cost. The cost of refurbishing a used
outer shell by machining was found to be between 70 and 82 percent
of the original shell cost, a difference of $118,000 for the filled
H/C ablator. Total savings could range from $500,000 to
$3,600,000 depending on the ablator type used for missions in-
volving from six to twenty-four flights yearly.

2) Single Wall Concepts

The basic cost of refurbishing a single shell vehicle would be the
same as that for refurbishing the outer shell of a double wall
vehicle. However, it would have to be done on the vehicle itself
so that the turnaround time must include the time required to
remove the used ablator and to fabricate and inspect a new one.
Also, refurbishing a single shell vehicle could well require re-
moving electronic and other sensitive equipment because of the
relatively high curing temperatures ($\sim$ 300°F) of the ablator and
bond, and thus may increase cost significantly to insure reliability.

-4-

e. Parametric Studies: Areas of Improvement

The parametric studies performed concerning the thermodynamic properties of the ablator indicated that the greatest weight savings would be accomplished by reducing the density and thermal conductivity of the material. Since the ablator accounts for about half of the total weight of a double shell vehicle, significant percentage reductions in its weight would have an important effect on overall vehicle weight.

The structural parametrics and results of weight comparisons of various concepts indicate that, with the design criterion of no ablator cracking, the ultimate strain capability of the ablator can significantly affect the structural and overall weight of the vehicle. For instance, an increase in ultimate strain of the lightweight filled H/C ablator from 0.4 to 1.2 percent would lead to overall vehicle weight savings of 6.7 percent with the fiberglass outer shell, 3.1 percent with the steel outer shell, and 12 percent with the single aluminum shell.

TABLE I

VEHICLE WEIGHT COMPARISONS

Design Concept		Percentage Weight Increase	
Ablator	Structure	26,000 fps	36,500 fps
1. Filled H/C	Integrated, fiberglass outer shell	ref.	ref.
2. Filled H/C	Fiberglass outer shell	0.5	0.4
3. Laminated	Integrated, fiberglass outer shell	0.5	2.4
4. Laminated	Fiberglass outer shell	2.9	4.6
5. Filled H/C	Steel outer shell	2.3	2.4
6. Laminated	Steel outer shell	7.6	8.7
7. Filled H/C	Aluminum single shell	27.9	26.2

2.2 Conclusions

Based upon the results of the study, the following conclusions may be drawn:

a. Double wall construction, with a fiberglass outer shell and an internal pressure pod, would show the following advantages over single aluminum shell construction:

1) With its potential of high ablator-structure bond line temperature, double wall construction would remain lighter than single wall construction as long as the latter was limited to materials with a considerably lower bond line temperature allowable.

2) Although the initial cost of a double shell vehicle would be more than that of a single shell one, the reusability of its inner shell would make the costs more competitive if several missions are contemplated.

3) Double wall construction would be more amenable for reuse and short turnaround times than single wall construction because the outer shell could be removed, replaced by another, and then refurbished. If several missions with short time intervals between them are contemplated, fewer double shell vehicles would be needed than single shell vehicles because of their shorter turnaround times.

b. A fiberglass honeycomb outer shell for the concepts considered would be somewhat lighter and considerably less expensive to fabricate than a stainless steel honeycomb outer shell.

c. Rather insignificant weight savings would be achieved for the missions analyzed by relying on the load-carrying capability of the ablator for double shell concepts. However, weight savings could probably be more significant for other missions if the structural loads of ascent or early reentry, when the ablator's strength can be utilized, were larger relative to the loads of touchdown than those considered in this study.

d. Significant weight savings would result from an increase in the strain to failure capability of the filled H/C ablator or by a reduction in its density or conductivity.

3.0 PERFORMANCE ANALYSIS

Performance analyses were conducted to determine the design trade-offs between various double and single wall composites as the primary load-carrying and thermal protection system for the class of lifting entry vehicles having a hypersonic L /D of about of 1.2. The HL -10 configuration is typical of this class of vehicles and, hence, was used as the reference geometry for the study. This investigation consisted of performing analytical studies in the areas of aerodynamics, thermodynamics, structures, and design in an effort to determine the characteristic behavior and associated weight trade-offs involved for the various design concepts. In each instance typical stagnation and afterbody geometries (i.e., segments of spheres, cones, cylinders and panels with appropriate attachments and supports) were used as analytical models to idealize various locations and portions of the vehicle. The type of studies performed and the results obtained are presented in this section of the report.

3.1 Design Concepts

The various combinations of ablator and substructure materials and construction techniques considered for both double and single wall concepts are described in the following paragraphs. Cross sectional views of each type of construction are shown in figure 1 while characteristic thermal and mechanical properties of the materials at representative temperatures are given in table II.

3.1.1 Double Wall Concept

3.1.1.1 Nonintegrated Designs

The double wall designs consisted of an outer shell composite of an ablative material bonded to either a fiberglass or steel substructure with insulation, surrounding a removable inner aluminum pressure shell that conformed to the external shape of the vehicle. The same inner pressure shell was used for all double shell designs. Circumferential frames within the outer and inner shells were located at discrete stations along the vehicle. The various designs investigated are described below.

   a. Fiberglass Shell-Filled H/C Ablator

   One outer shell design considered a charring ablator loaded into the cells of a reinforcing fiberglass honeycomb that had been bonded to a substructure of fiberglass honeycomb sandwich construction. This concept is adaptable to flat or low curvature areas of the vehicle. In regions of high curvature, such as the nose or leading edge of fins, the use of

DOUBLE WALL CONCEPT

SINGLE WALL CONCEPT

+250°F AT START OF REENTRY

700°F (MAX)

ABLATOR*

BOND

FIBERGLASS OR STAINLESS STEEL HONEYCOMB OUTER SHELL

Q-FELT INSULATION

200°F MAX (70°F AT START OF REENTRY)

ALUMINUM HONEYCOMB PRESSURE SHELL (70°F)

+250°F AT START OF REENTRY

300°F (MAX)

ABLATOR*

BOND

ALUMINUM HONEYCOMB PRESSURE SHELL

Q-FELT INSULATION

200°F MAX AT END OF REENTRY (70°F AT START OF REENTRY)
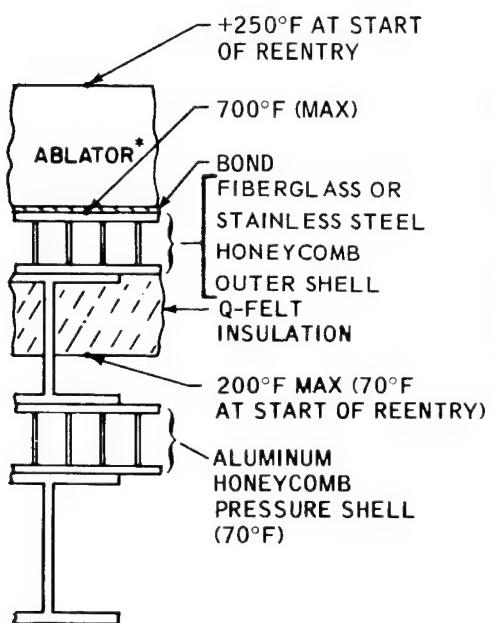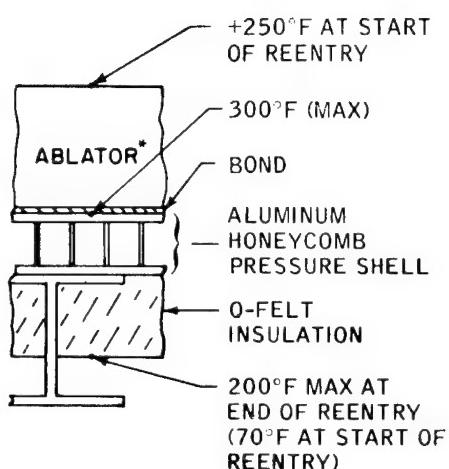
*FILLED HONEYCOMB AND/OR LAMINATED ABLATOR
64-8006

Figure 1 DESIGN CONCEPTS

TABLE II

REPRESENTATIVE MATERIAL PROPERTIES

Materials	Density lb/ft³	Specific Heat(BTU/hr-ft-°F)	Thermal Conductivity at 250°F (BTU/hr-Ft-F)	Emissivity	Temp. °F	Modulus of Elasticity psi	Coefficient of Thermal Expansion Relative to 200°F	Ult. Tensile Strain Percent	Ftu psi	Fcu psi
Fiberglass 91-LD-181	110	0.21	0.24		-250. 125. 500. 700.	3.3×10^6 3.2 2.7 2.2	5.1×10^6 5.1 4.0 3.5	1.2 1.2 1.2 1.2	40,000. 35,000. 26,500. 20,000.	40,000. 35,000. 26,500. 12,500.
Steel PH-15-Mo TH 1050	479	0.11	11.30		125 700	29.0×10^6 26.0×10^6	6.1×10^{-6} 6.1×10^{-6}	3.0	188,000. 157,000.	176,000. * 147,000. *
Aluminum 2014-T6	175	0.23	113.0		125 300	10.4×10^{-6} 10.0×10^{-6}	12.5×10^{-6} 12.5×10^{-6}	6.0	66,000 56,100	60,000. * 49,200. *
H/C Filled Ablator	31	0.37	0.054	0.75	-250. 125. +250. 500.	0.25×10^6 0.03 0.02 0.02	10.5×10^{-6} 6.0 5.5 2.5	0.4 1.2 0.4 0.4	750. 300. --- 100.	--- --- --- 150.
Molded Ablator	38	0.38	0.078	0.75	-250 125 +250 500.	0.5×10^6 0.07 .025 0.02	12.8×10^{-6}	0.5 1.4 1.2 0.5	2,000. 700 --- 200	--- --- --- 700.
Laminated Ablator	45.4	0.44	0.060	0.76	-250. 125. +250 500	0.56×10^6 0.22 0.21 0.20	13.6×10^{-6} 4.8 3.0 3.0	1.2 1.2 1.2 1.2		

*Fcy

honeycomb as the matrix for the ablator is not recommended because of the difficulty and expense involved in fabrication. Accordingly, in such areas a molded charring ablator bonded to fiberglass sheet was used as the construction technique. The fiberglass laminate considered was a phenolic resin in combination with 181 glass cloth, which has high temperature strength capability. This laminate was also considered for the circumferential frames. The insulation, which was bonded to the inner surface of the shell, consisted of a layer of Q-Felt material.

The inner pressure shell was of aluminum honeycomb sandwich construction supported circumferentially by aluminum frames. In the analyses, material properties typical of 2014-T6 and 7075-T6 alloy were used, respectively, for the skins and frames. (See table II and reference 2.)

b.   Fiberglass Shell-Laminated Ablator

Another outer shell design considered a laminated felt ablator (in which the felt layers had been reinforced with open weave fiberglass scrim cloth) bonded to a fiberglass honeycomb sandwich substructure for regions of high curvature. Due to the addition of the scrim cloth, this ablator has considerably more strength than the filled H /C and molded ablators, but its density is higher.

c.   Steel Shell-Filled H /C Ablator

A third outer shell design considered the filled H / C ablator bonded to a substructure of stainless steel brazed honeycomb, except that sheet construction was used in the regions of high curvature. The steel alloy considered for the analyses was PH 15-7 Mo TH 1050, properties of which can be found in table II and in reference 2.

d.   Steel Shell-Laminated Ablator

A fourth outer shell design considered the laminated ablator bonded to the stainless steel substructure described above.

3.1.1.2 Integrated Designs

Two integrated fiberglass outer shell designs were analyzed in an effort to reduce vehicle weight:

-10-

     a. Integrated Fiberglass Shell, Filled H /C Ablator

     b. Integrated Fiberglass Shell, Laminated Ablator

These were conceptually the same as the fiberglass shell designs described previously, the only difference being that the ablators in this instance were considered to be an integral part of the load carrying structures.

3.1.2 Single Wall Concept

The single wall design considered in the study consisted of the filled H / C ablator bonded to an aluminum honeycomb substructure, supported circumferentially by aluminum frames. This aluminum shell was also the pressure shell. A layer of Q-Felt insulation was bonded to its inner surface.

3.2 Mission Requirements and Environmental Criteria

The environmental conditions associated with the various phases of a typical mission profile such as launch, abort, space flight, reentry and touchdown considered in this study are presented below. The thermal and structural design criteria developed on the basis of these conditions are described in sections 3.4 and 3.5, respectively.

   I. Launch Conditions

     A. Trajectory -- Saturn C-1

     B. Angle of attack = ± 15 degrees (loads)

     No trajectory perturbations considered

     C. Initial surface temperature = + 125°F

   II. Abort Conditions

     A. Pad: 10g

     B. Maximum dynamic pressure (M = 1.5)

        1) 6 g axial loading plus 750 lb/ft^2 dynamic pressure

        2) 2 g axial loading plus 1000 lb/ft^2 dynamic pressure

        No tumbling is allowed. Angle of attack for pressure effects = ± 15°.

III. Space Conditions

    A. Maximum surface temperature = + 250°F

    B. Minimum surface temperature = -250°F

IV. Reentry Conditions

    A. Initial surface temperature, ± 250°F

    B. Reentry Trajectories (Z_e = 400,000 ft)

        1) $C_{L\,max}$ conditions (W/CDA = 42 psf, a = 60°)

            a. V_e = 26,000 ft/sec, 12 g undershoot, L/D = 0.6 to touchdown

            b. V_e = 26,000 ft/sec, 12 g undershoot, L/D = 0.6 to altitude hold to touchdown

            c. V_e = 36,500 ft/sec, overshoot, L/D = 0.6 to altitude hold to touchdown

            d. V_e = 36,500 ft/sec, 12 g undershoot, L/D = 0.6 to altitude hold to touchdown

        2) L/D_{max} conditions (W/CDA = 147 psf, a = 30°)

            a. V_e = 26,000 ft/sec, L/D = 1.2 to altitude hold (257,000 ft) to equilibrium glide to touchdown

            b. V_e = 36,500 ft/sec, 12 g undershoot, L/D = 1.2 to altitude hold to equilibrium glide to touchdown

            c. V_e = 36,500 ft/sec, overshoot, L/D = 1.2 to altitude hold to equilibrium glide to touchdown.

V. Touchdown Conditions

One psi differential between internal pressure and ambient pressure, due to lag in venting. The vent location is assumed to be in the middle of the upper surface of the vehicle.

3.3 Aerodynamic Analysis

3.3.1 Trajectories

For this study complete atmospheric flight profiles have been considered. Although no specific ascent abort trajectories were analyzed, maximum

pressures and accelerations typical of a C-1 launched manned vehicle were estimated in order to obtain structural design loads. Pertinent trajectory parameters for the significant design trajectories specified in section 3.2 are shown in figures 2 through 6.

3.3.2 Pressure Distributions

All pressure distributions have been generated theoretically using the Newtonian-Prandtl Meyer Method. [3] Comparisons made with available data have indicated this to be a reasonable approach along the vehicle's windward plane of symmetry. The method should give adequate results elsewhere on the windward surface. On the leeward side of the vehicle, the mixing line was assumed to trail from the leading edge parallel to the free-stream velocity vector, and no pressure gradient through the shear layer was assumed.

The effects of elevon deflection were examined both analytically (Newtonian plus centrifugal effects)[3] and experimentally.[4] It was found that, although the analytical method underestimated the experimental pressure peak in the vicinity of flow reattachment, it predicted adequately the mean pressure over the windward surface of the elevon. Accordingly, the flap pressure was assumed to be constant over the lower surface of the elevon at the theoretical value ($p_{} /p_s = .475$ for $\delta_e = 20°$). Pressures on the upper surface of the elevons (when deflected downwards) were assumed to be the same as the pressure over the vehicle upper surface. Upward elevon deflection (the $C_{L\,max}$ condition) did not produce design loads.

Typical axial and circumferential pressure distributions are shown in figures 7 and 8 (zero elevon deflection).

3.3.3 Heat Transfer

3.3.3.1 Convective

At the stagnation point the theoretical predictions of Van Tassell and Pallone[5] were employed. These results include the most up-to-date transport property estimates and agree well with test data at velocities up to 40,000 ft/sec. Vorticity interaction effects were included using the results of Hoshizaki[6], which also show good agreement with test data. The velocity gradient was determined

using the method of Waldman and Thyson[7] in excellent agreement with the NASA/Langley test data.[8] Heat transfer calculations for various trajectories are shown in figures 9 through 12, and are summarized in table III. Typical stagnation enthalpy time histories are shown in figure 13.

Laminar convective distributions were obtained from NASA-Langley test data modified to remove what appeared to be effects of low density and boundary layer transitional conditions (at different running conditions). Pressure interaction or transport property effects which would be a function of axial station were considered to be small. The ascent distribution was computed using two-dimensional local similarity theory.

Boundary-layer transition was considered, and as a criterion a wetted length Reynolds number of 900,000 was chosen for ascent flight (no ablation) and 150,000 for reentry flight (ablation occuring). Turbulent heating was then calculated using a flat plate, zero pressure gradient approach. Typical turbulent heating results are shown in figure 14 for ascent flight and in figure 15 for the L/D_{max} 12 g undershoot reentry. Such heating did not produce design conditions.

The heating perturbations due to elevon deflections were estimated based on NASA-Langley data[8] in which significant effects were observed only for downward elevon deflections. Heating increases were largely confined to the windward surface of the elevon itself. Accordingly, heating perturbations in the vicinity of the elevons were neglected.

Since the test data was for a 30° elevon deflection, it had to be adjusted for the L/D_{max} trim condition which required about a 20° deflection. This was accomplished by scaling with the square root of the elevon pressure as theoretically determined.[3] The moderate Reynolds number test data was used as being more consistent with flight conditions (see figure 6). Based on this data, therefore, a design heating value of 0.3 $\dot{q}_{stag}$ was chosen, constant over the surface.

-14-

TABLE III

STAGNATION POINT HEATING CONDITIONS

Reentry Velocity		26,000 (fps)	26,000 (fps)	36,500 (fps)	36,500 (fps)	36,500 (fps)	36,500 (fps)
Trajectory	Ascent	U/NM-C_{Lmax}	L/D_{max}AH*	O/AH-C_{Lmax}	U/AH-C_{Lmax}	O/HA-L/D_{max}	U/AH-L/D_{max}
$\dot{q}_{cmax}$, Btu/ft^{2}sec	4.2	242	78.5	290	600	346	1,080
Q_c, Btu/ft^2	370.	14,800	115,000	78,000	37,200	220,000	81,700
$\dot{q}_{ermax}$	--	--	--	<5	65	<5	650
Q_{er}	--	--	--	<500	1,370	<500	13,700
$\dot{q}_{nermax}$	--	7.0	7.5	67	70	67	67
Q_{ner}	--	500	7,000	11,800	290	18,000	<500

*Altitude hold at 257,000 feet

O – Overshoot boundary
U – Undershoot boundary
AH – Altitude hold
NM – No modulation
c – convective
er – equilibrium radiation
ner – nonequilibrium radiation

3.3.3.2 Equilibrium Radiative

Equilibrium radiative heating calculations were based on the results of Kivel and Bailey, [9] modified due to recent theoretical and experimental information on the continuum radiation from nitrogen. [10] These new data, though by no means complete, do indicate that for temperatures above 9000°K, Kivel's and Bailey's results considerably overestimate the radiation intensity. The calculations, therefore, reflect this new information (see figure 10).

Stagnation point shock detachment distances have been estimated assuming a two-dimensional flow, which is reasonable for this type of body at these angles of attack.

Heating distributions have been made for the windward side as-suming a plane, optically thin slab model with linear temperature and density gradients normal to surface (see figure 16). The flux to the leeward surface was neglected. The shock geometry was derived from NASA-Langley schlieren photographs.

3.3.3.3 Nonequilibrium Radiative

Nonequilibrium radiative heating calculations have been based entirely on the experimental data of Allen et al. [11] No density dependence was considered (i.e., truncation effects, etc., neglected) and an arbitrary altitude cut-off of 280,000 feet was assumed (see figures 11 and 12).

Heating distributions were estimated using a two-dimensional flow model with shock geometry given as noted above (see figure 17).

3.3.4 Wall Shear

Cold wall shear calculations were performed for both laminar and turbulent flow conditions by assuming Reynolds analogy valid. Typical results are shown in figure 18. The maximum shear value was approximately 8 psf.

-16-
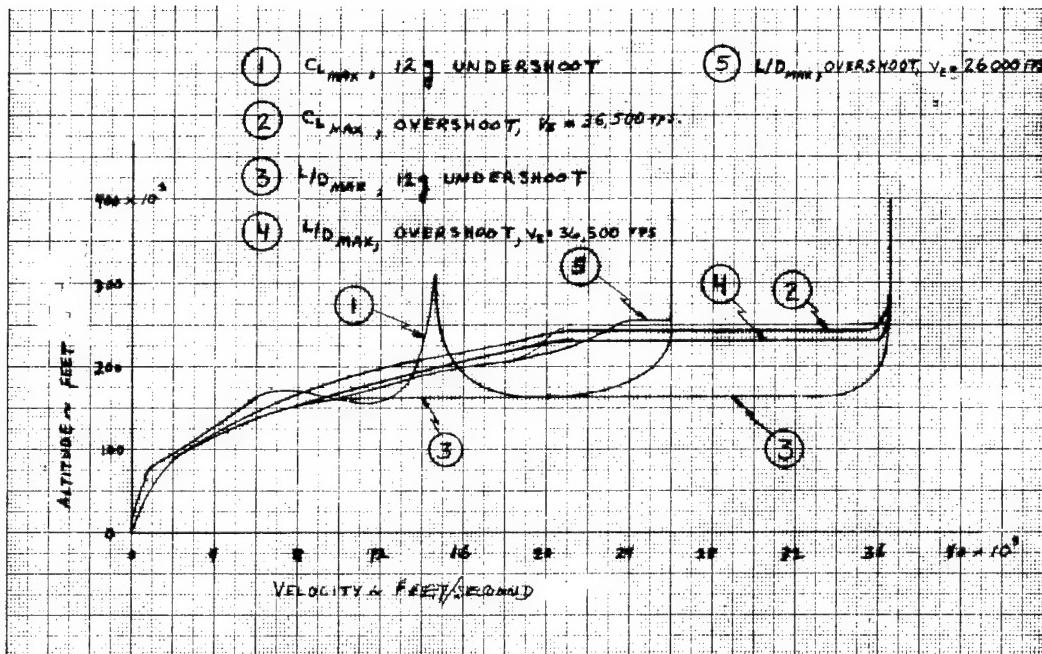
Figure 2 VELOCITY-ALTITUDE PROFILE
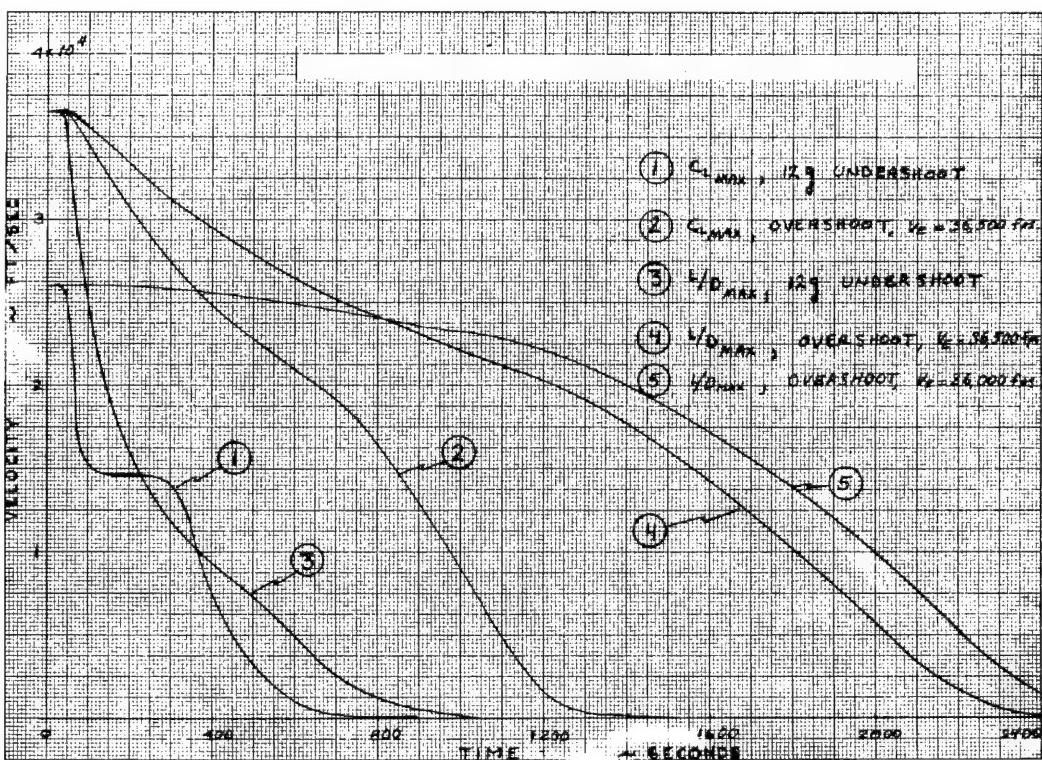
Figure 3 VELOCITY-TIME HISTORIES--REENTRY

-17-
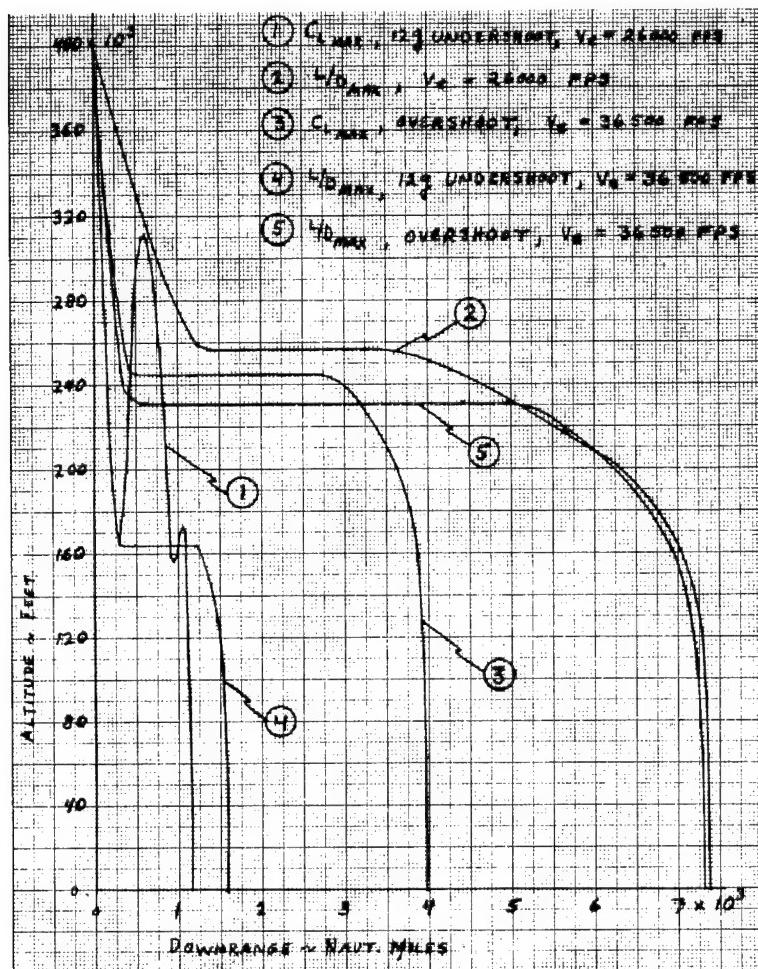
Figure 4 DOWNRANGE CAPABILITY
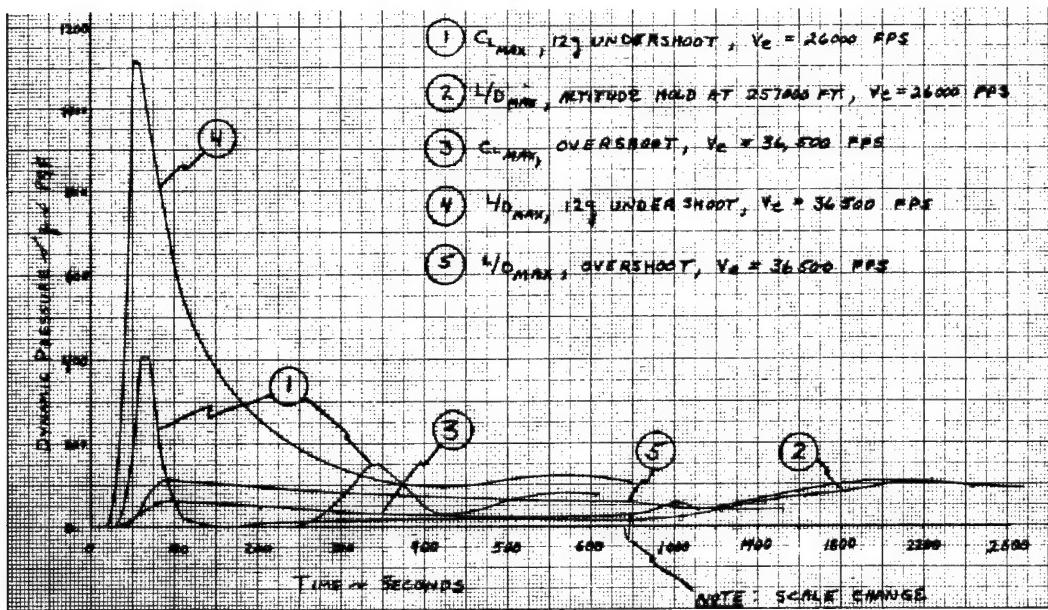
Figure 5 DYNAMIC PRESSURE-TIME HISTORIES--REENTRY

-18-

Figure 7 REENTRY PRESSURES–AXIAL DISTRIBUTION, $\alpha = 30°$

Figure 6 FREE-STREAM REYNOLDS NUMBER TIME HISTORIES

-19-
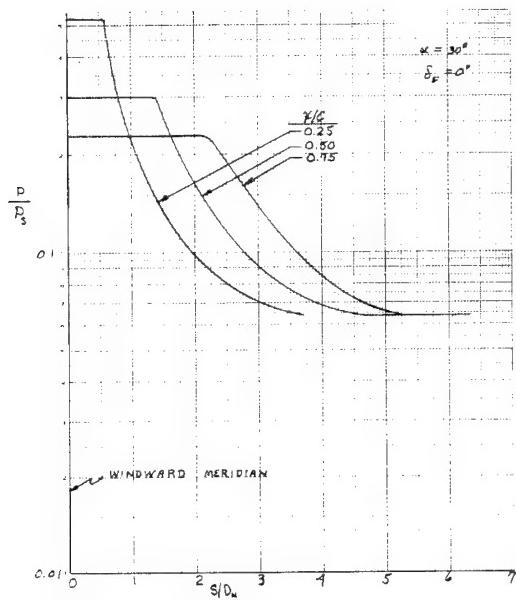
Figure 8 REENTRY PRESSURES-CIRCUMFERENTIAL DISTRIBUTION, $\alpha = 30°$
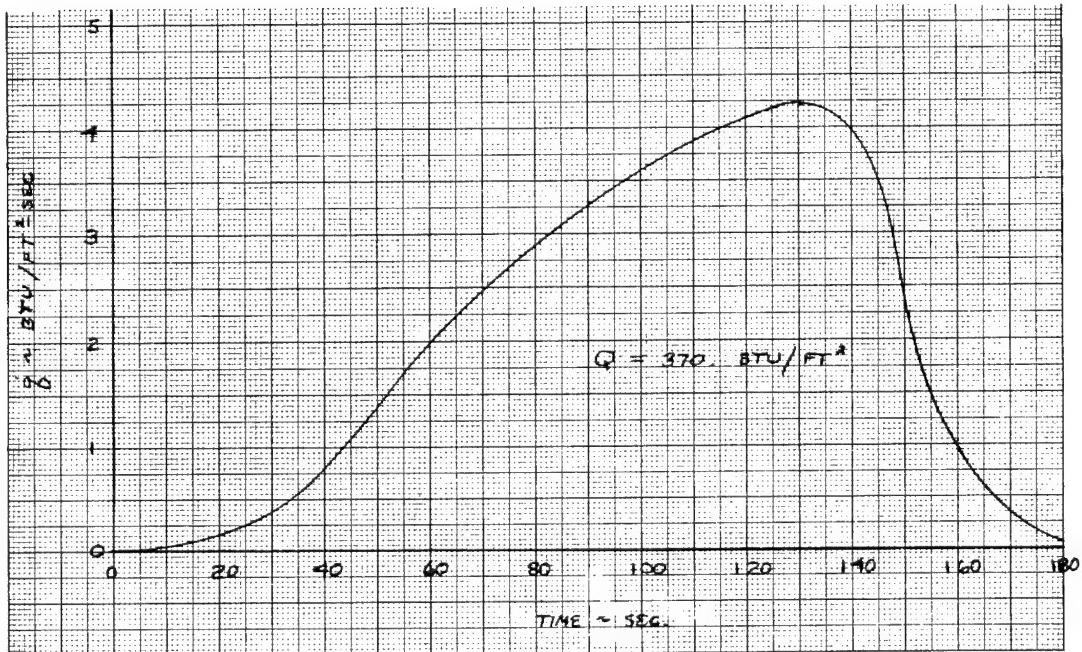
Figure 9 ASCENT STAGNATION POINT HEATING, $\alpha = 0°$
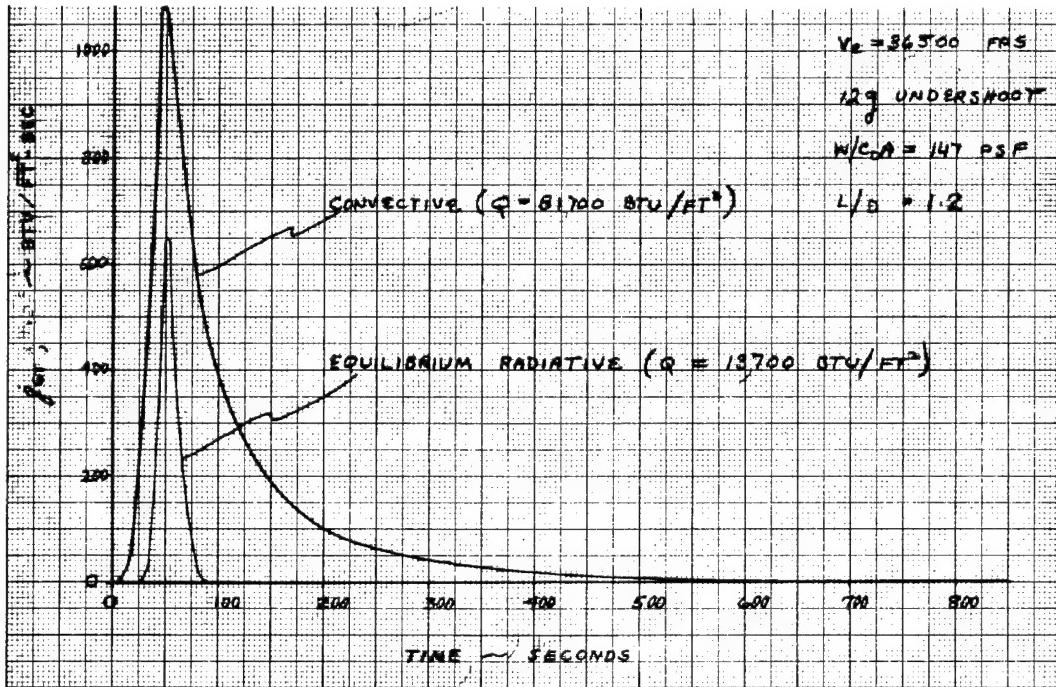
Figure 10 STAGNATION POINT HEAT TRANSFER TIME HISTORIES--REENTRY,
(L/D)$_{max}$, 12 g UNDERSHOOT, V$_E$ = 36,500 FPS
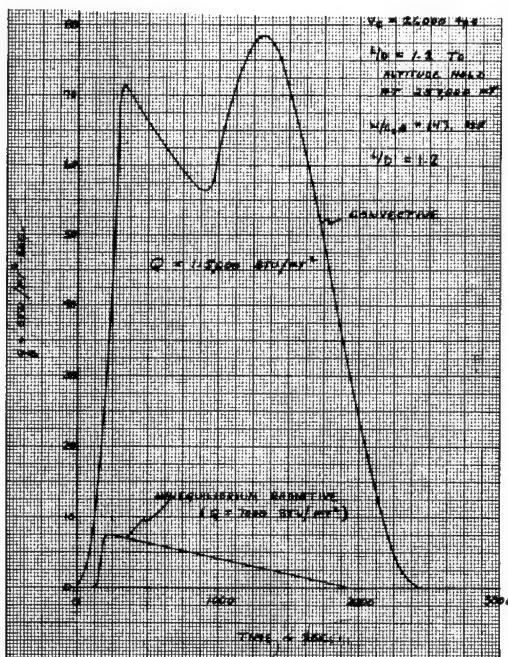
Figure 11 STAGNATION POINT HEAT TRANSFER TIME HISTORIES--REENTRY,
V$_E$ = 26,000 FPS, (L/D)$_{max}$, OVERSHOOT

-21-
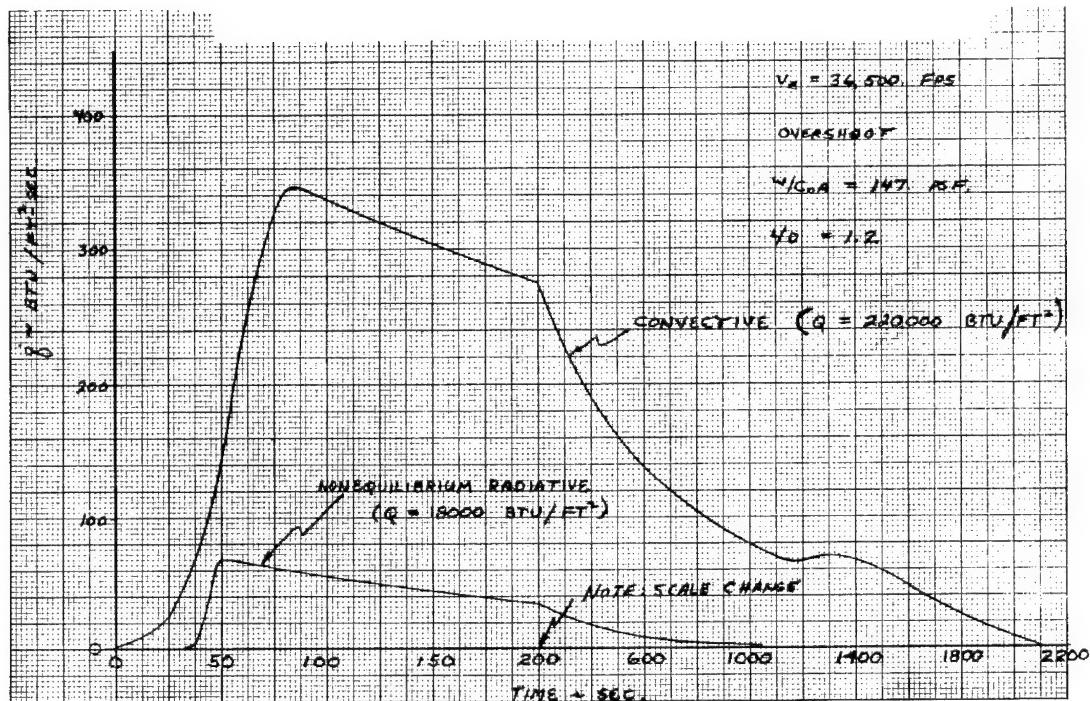
Figure 12 STAGNATION POINT HEAT TRANSFER TIME HISTORIES--REENTRY,
$V_E = 36,500$ FPS, $(L/D)_{max}$, OVERSHOOT
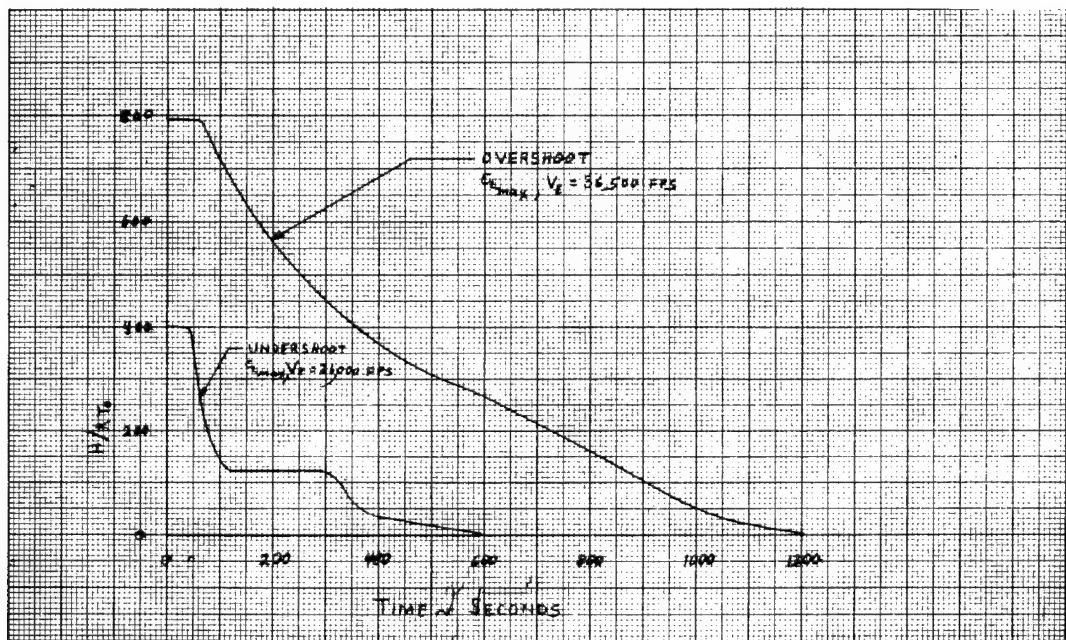
Figure 13 TYPICAL NON-DIMENSIONAL STAGNATION ENTHALPY
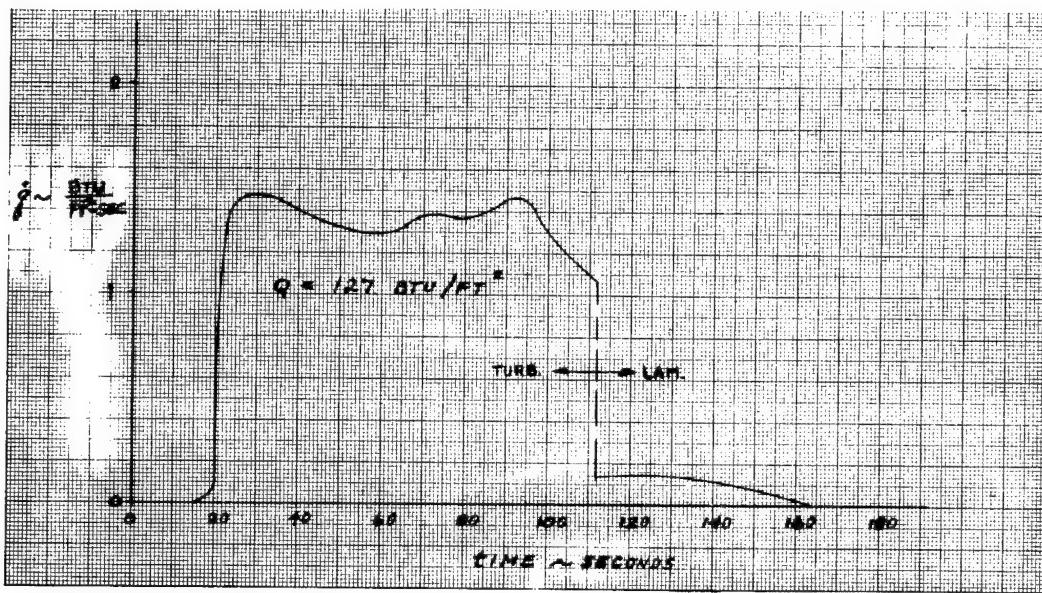
Figure 14 ASCENT HEATING AT STATION X/C = 0.5, $\alpha = 0°$, UPPER SURFACE
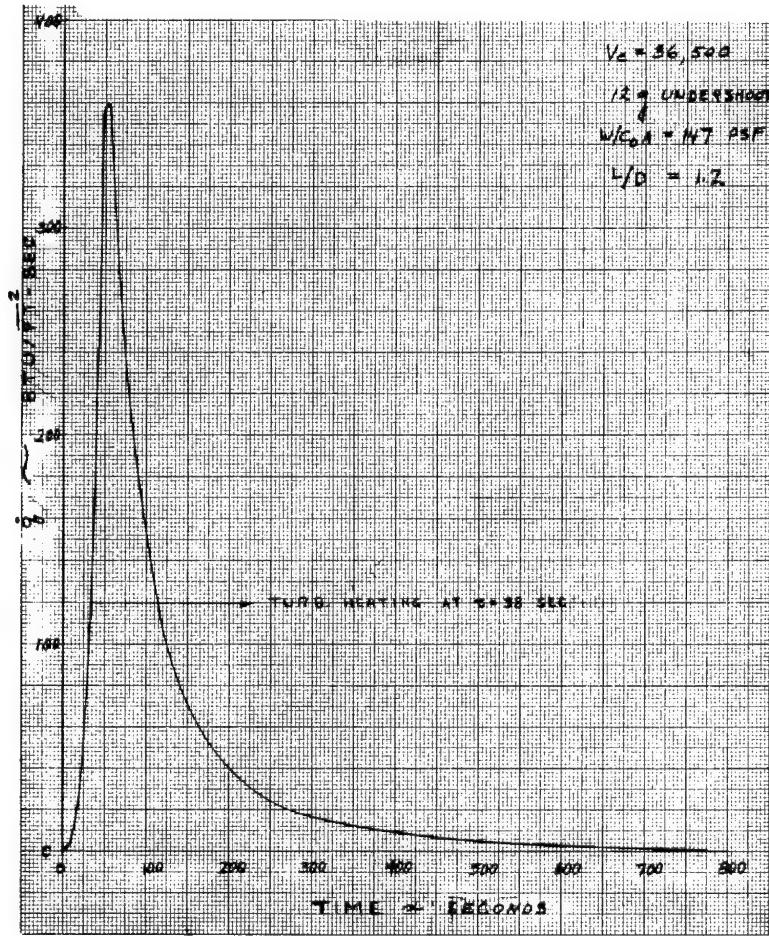
Figure 15 CONVECTIVE HEAT TRANSFER AT X/C = 0.5
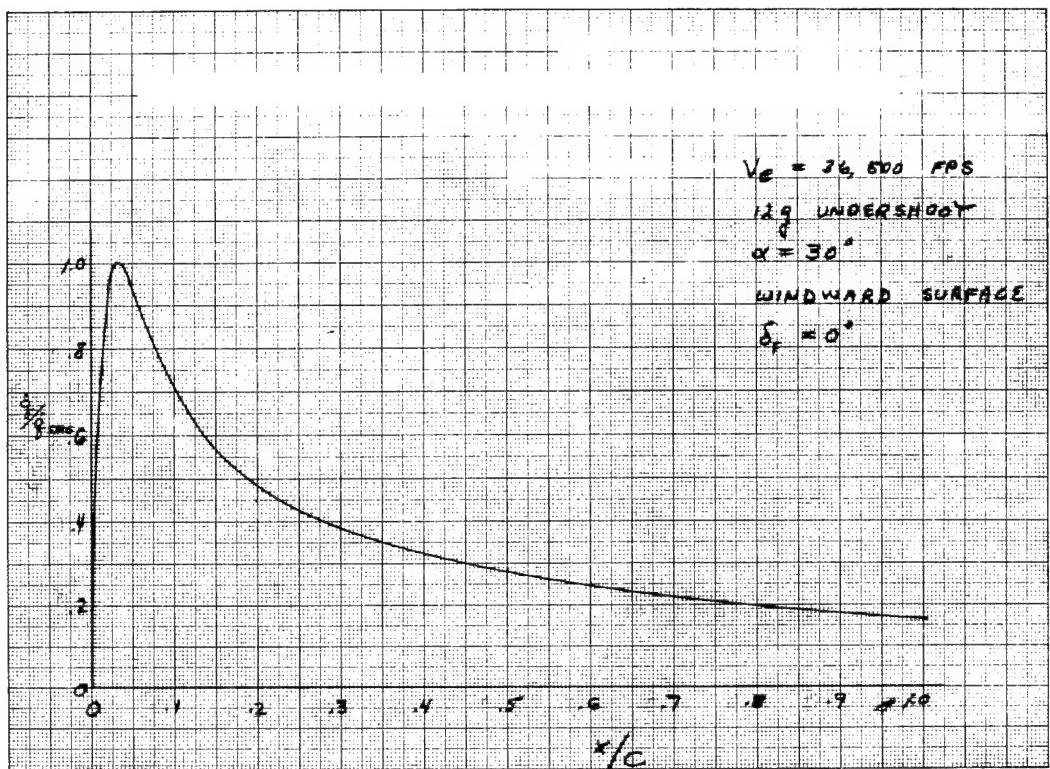
Figure 16 EQUILIBRIUM RADIATIVE HEATING DISTRIBUTION,V_E = 36,500 FPS,
12 g UNDERSHOOT, α = 30°
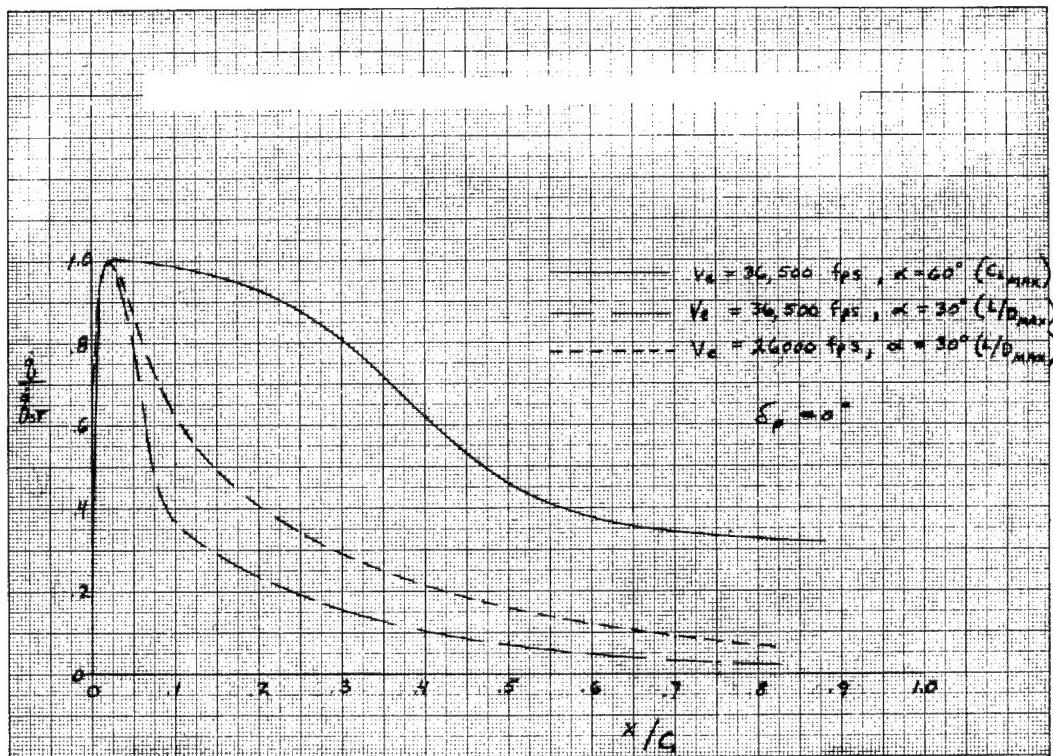
Figure 17 NON-EQUILIBRIUM RADIATIVE HEATING DISTRIBUTIONS

-24-
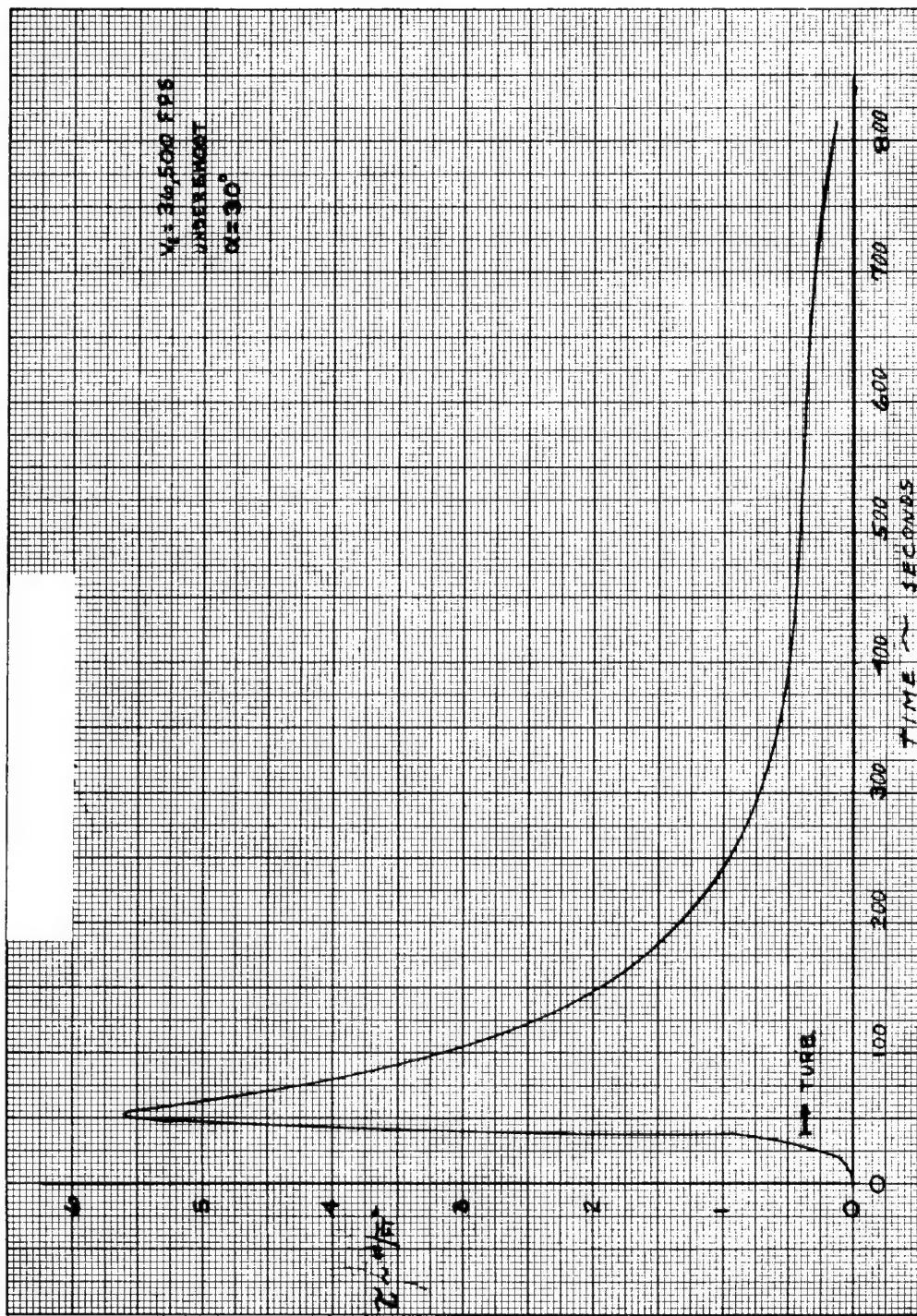
Figure 18 WALL SHEAR HISTORY, X/C = 0.5, V_E = 36,500 FPS, UNDERSHOOT, α = 30°

3.4 Thermodynamic Analysis

This section details the thermodynamic analysis performed to determine ablator and insulation requirements for the double and single wall concepts described in section 3.1, subject to the environmental and design criteria of sections 3.2 and 3.4.1, respectively. A separate design for each concept was obtained for reentries at 26,000 fps and at 36,500 fps.

In the paragraphs below, the calculation model upon which the analyses were based is described, followed by the results of the various analyses.

Paragraph 3.4.3 contains the ablator and insulation thicknesses and unit weights for the double wall concept, fiberglass shell designs. The additional ablator requirements for ascent heating protection are also presented. Paragraph 3.4.4 presents the results for the steel outer shell designs, and those for the single aluminum shell appear in paragraph 3.4.5. In the final section, 3.4.6, the overall ablator and insulation weights for all the design concepts are listed.

3.4.1 Thermal Design Criteria and Assumptions

The following criteria were adopted for this study:

a. The thermal characteristics of a complete heat shield composite (ablator, bonding material, substructure, and backup insulation) were considered in calculating ablating material thicknesses.

b. A bond line temperature of 700°F, reflecting the present state of materials technology, was used for the fiberglass and stainless steel honeycomb structures of the double wall concept while a 300°F criterion was selected for the single aluminum structure vehicle. Insulation requirements were based on a 70°F initial rear face of insulation temperature which was then allowed to attain a maximum of 200°F during reentry. For the fiberglass and stainless steel vehicles an initial temperature differential of 175°F was assumed through the insulation; for the aluminum substructure vehicle an 80°F differential was assumed.

c. The thermal conductivity values of the ablative materials were assumed to increase irreversibly with increasing temperatures. Thermal properties of other materials were assumed independent of temperature.

d. Ablative materials subjected to temperatures in excess of 500°F during ascent (Saturn C-1) were considered to be unacceptable for reentry protection.

-26-

e.   Ablation temperatures required as computer program inputs
were determined from experimental data as a function of hot wall
heating rates, but were assumed to be constant for an average
hot wall heating value during the ablation process.

f.   Calculations were performed using nominal thermal proper-
ties and ablation characteristics, as well as nominal values for
aerodynamic heating.   The safety margin thus afforded is restricted
to structural considerations only.

3.4.2 Calculation Model and Methods of Analysis

3.4.2.1 Geometry

The composite sections upon which the calculations were based
consisted of an ablator, bond, substructure, and Q-Felt insulation,
as shown in figure 19. At the start of reentry the outside face of
the ablator was at +250°F, the back face of the insulation was at
70°F. For the double wall concept designs, the space in between
the shells was vented and thus was at essentially zero pressure.
Since the conductivity of the Q-Felt in a near vacuum (.0005
BTU/hr-ft-°F) is much smaller than that of the ablator or sub-
structure (.03 to .05), nearly the entire temperature drop from
+250°F to 70°F would occur through the insulation, as is shown in
figure 19. For the single aluminum shell concept with an internal
pressure of 7 psi, the conductivity of the Q-Felt is not as low, and
the initial temperature distribution through the composite would
be as pictured in figure 19.

Reentry ablator and insulation thicknesses for the double wall
concepts were determined concurrently based on the two require-
ments that the maximum temperature of the ablator-structure
bond interface not exceed 700°F and the insulation rear face not
exceed 200°F at any time before touchdown. For the aluminum
single shell concept, bond line temperature was limited to 300°F
instead of 700°F. For reentry calculations the conductivity of
the Q-Felt was taken at its one atmosphere pressure value of
0.015 BTU/hr-ft-F°.

3.4.2.2 Mathematical Formulation

The computation technique for the thermodynamic analyses was
based on a transient one-dimensional heat conduction model
composed of slabs of the various materials in the composite.
Adiabatic conditions were assumed to exist at the rear and sides
of the model. A standard computer program, capable of treating

convective heating, surface recession, and transpiration effects, was used. The mathematics of this program, detailed in references 12 and 13, are briefly described below.

The differential equation used to describe the thermal response of a point in the ablative material, transformed to accommodate a receding surface is:

$$\rho C_P \frac{\partial T}{\partial t} - \dot{s} \rho C_P \left(\frac{1-y}{L-s}\right) \frac{\partial T}{\partial y} = \frac{1}{(L-s)^2} \frac{\partial}{\partial y} \left(k \frac{\partial T}{\partial y}\right)$$

where

ρ = density

C_P = specific heat

T = temperature

t = time

$\dot{s}$ = rate of surface recession

L = original ablator thickness

s = total thickness ablated at time t

y = $\dfrac{x - s(t)}{L - s(t)}$

k = thermal conductivity

The thermal properties may be functions of position and temperature.

Provisions are made so that the thermal properties may be specified as irreversible functions of temperature. The effects of the charring of an ablative material on the thermal conductivity are therefore considered. The ablator conductivity-temperature relations used in the analyses are shown in figure 20.

For the bond material, substructure, and insulation, the problem is one of transient heat conduction described as

$$\rho C_P \frac{\partial T}{\partial t} = \frac{\partial}{\partial x} \left(k \frac{\partial T}{\partial x}\right)$$

Boundary conditions are as follows:

At the front surface

$$\dot{q}_c \left[1 - \frac{H_w}{H_g} \right] - \sigma \epsilon T_w^4 = \dot{q}_{eff} = \frac{k \, \partial T}{(L-s) \partial y} \bigg|_{y=0} + \rho \dot{s} F$$

where:

$\dot{q}_c$ = convection heat flux for a 500°R wall temperature

H_g = stagnation enthalpy

H_w = wall enthalpy = $0.0068 \, T_w + 0.37 \times 10^{-6} \, T_w^2$

ϵ = surface emissivity

T_w = wall temperature

$\dot{q}_{eff}$ = net heat flux

$\dot{s}$ = surface recession rate

F = $H_v + \eta \, (H_s - H_w)$

H_v = heat of vaporization

η = blowing coefficient

Interface conditions are described by

$$\frac{k}{L-s} \, \frac{\partial T}{\partial y} \bigg|_{ablator} = k \, \frac{\partial T}{\partial x} \bigg|_{substructure}$$

in conjunction with

$$T_{ablator} \, (1,t) = T_{substructure} \, (L,t)$$

at the first interface and similar terms at other interfaces.

The adiabatic back face is described by $k \, \dfrac{\partial T}{\partial x} = 0$.

In the calculation process, the surface recession rate is zero until the surface temperature reaches the ablation temperature.

Once the ablation temperature is reached the recession rate is controlled by the aerothermodynamic environment (heat flux and enthalpy). Program 1327.1 is equipped to account for surface recession rates being a function of temperature. The values of ablation temperatures as functions of heat flux used for the analyses are presented in figure 21.

Radiative heating was treated separately from convective heating by computing the appropriate ablator thicknesses required and then adding these to the convective heating thicknesses to obtain the total ablator thicknesses. Radiation thicknesses were determined by the expression:

$$\Delta L_{rad} = \frac{\int_{t_o}^{t} \dot{q}_R \, dt}{\rho_{abl.} \, q^*_{rad.}}$$

where $\int_{t_o}^{t} \dot{q}_R \, dt$ is the total radiation heating of a given trajectory, $\rho_{abl.}$ is ablator density and q^*_{rad} is specific radiant heat capacity of the ablative material. This is an approximate treatment of the radiation effects but was deemed sufficient to ascertain comparative trends within the scope of this study.

3.4.2.3 Calculation Procedure

The method used to obtain required ablator and insulation thicknesses for given maximum bond line and rear face temperatures involved a double iteration process because a change in ablator thickness would affect the required insulation thickness, and vice versa, although to a much lesser extent. The procedure involved selecting an ablator thickness, associating with this thickness three arbitrary insulation thicknesses, and solving for bond line and rear face temperatures. The process was then repeated for two other ablator thicknesses. These bond line and rear face temperatures were then plotted as functions of ablator thickness, and the ablator thickness required to yield a 700°F maximum bond line temperature was used to select a rear face temperature for each of the insulation thicknesses chosen. These rear face temperatures were then replotted as functions of insulation thickness, and the insulation thickness required to yield a maximum 200°F rear face temperature determined.

3.4.3 Double Wall Concept, Fiberglass Shell

3.4.3.1 Calculation Results

a. Reentry Ablator Thicknesses and Unit Weights

Thicknesses for the filled H/C and laminated ablator designs required for protection against the convective heating of the

-30-

26,000 and 36,500 fps reentry trajectories are shown in figure 22. For the filled H/C ablator design, a molded ablator is used on the nose cap, and its thickness at the stagnation point is marked on the graph by an "X".

These thicknesses along the vehicle were obtained with the aid of NASA heating distribution curves[8] and figure 23, which is a plot of required ablator thicknesses as a function of percent of stagnation point heating for particular trajectories. Stagnation point heating data was summarized in table III.

The L/D_{max} trajectory proved to be more severe than the $C_{L_{max}}$ trajectories for reentries at 26,000 fps because of its much longer flight time (see figure 3) and correspondingly larger integrated heating. Similarly, for reentry at 36,500 fps, the L/D_{max} overshoot trajectory required greater convective heating ablator thicknesses than the $C_{L_{max}}$ overshoot or any of the undershoot trajectories.

The laminated ablator, because of its greater density and heat capacity per unit volume would require between 15 and 30 percent smaller thicknesses than those of the filled H/C ablator, the larger percentage differences occurring in regions of high heating such as the nose cap and leading edges.

Ablator thickness distributions required for radiative heating protection along the vehicle's bottom surface are shown in figures 24 and 25. None is required for the upper surface since no radiative heating is experienced. Note that the thicknesses required for the 26,000 fps reentry are quite small, and that for reentry at 36,500 fps the thicknesses needed for the $C_{L_{max}}$ trajectory are significantly larger than those for the L/D_{max} trajectory. The reason for this is that for the $C_{L_{max}}$ conditions, the vehicle would be flying at a 60° angle of attack, thus exposing the lower surface considerably more to the flow than for the 30° angle of attack of an L/D_{max} condition.

Total ablator thicknesses, representing both convective and radiative requirements, are shown in figures 26 and 27 and the corresponding unit weights at selected vehicle locations are listed in table IV. For all main body locations the required laminated ablator weights average about 20 percent heavier than those for the filled H/C ablator design due primarily to the differences in material density and resultant insulating efficiency between the two ablators, the only exception being in the stagnation region. For the filled H/C ablator design the molded ablator was used for this area

of the vehicle because of its ease of fabrication. Since the thermal conductivity of the molded ablator is higher than that of the laminated ablator, its resultant weight is slightly higher. Either the molded or laminated ablators could be used in this region of the vehicle with relatively little weight penalty.

With the addition of the radiative thicknesses, the L/D_{max} trajectories remained the designing ones for the entire vehicle for reentries at 26,000 fps and for all but a small area at the aft end of the bottom surface of the vehicle for reentries at 36,500 fps. This area, as shown in figure 28 was designed by the $C_{L_{max}}$ overshoot trajectory chiefly because of the larger radiation effects.

Typical bond line temperature responses at two locations on the vehicle for reentry at 36,500 fps under various flight conditions are shown in figure 29 and 30. These curves clearly show that the ablator thicknesses required for the L/D_{max} overshoot trajectory because of the larger total integrated heating are more than ample to meet all other flight conditions.

For the L/D_{max} and $C_{L_{max}}$ flight conditions the control surfaces (elevons) are deflected downwards 20° and upwards 60°, respectively, in order to obtain the proper angle of attack. In designing for the L/D_{max} condition ablator thickness were calculated to satisfy both the convective and nonequilibrium radiative heating inputs at this location which were approximately 25 to 30 per cent of the stagnation point heat input. Total ablator thicknesses required to meet these conditions are given below:

Ablator	26,000 fps	36,500 fps
Filled H/C	1.79 inches	2.14 inches
Laminated	1.26 inches	1.55 inches

b.   Insulation Thicknesses and Unit Weights

The Q-Felt insulation used in the design has a density of 6 lbs/ft^3 and a conductivity of 0.015 BTU/hr-ft-°F. The thicknesses required to limit its back face temperature to 200°F are shown in figures 31 and 32 for both ablator designs and reentry velocities. Unit weights at certain locations on the vehicle are included in table IV.

At the stagnation point the insulation requirement for both ablator designs is almost identical. Except for minor variations the same is true for the leeward side of the vehicle. However, along the windward side approximately 0.5 inch more insulation is required for the laminated ablator than for the filled H/C ablator design since the required substructure for the filled H/C ablator has a considerably deeper cross section, resulting in a larger thermal gradient requiring less insulation.

For reentry at 36,500 fps, the $C_{L_{max}}$ trajectory was found to yield greater heating than the $(L/D)_{max}$ trajectory in the area adjacent to the bottom centerline at $X/C = .75$ (see figure 28). The shorter trajectory time (1522 seconds versus 2484 seconds) is the primary reason for the sharp decrease in insulation requirements at this location.

c.   Ascent Heating Protection

The total reentry ablator thickness distributions listed in table IV were exposed to the heating environment of a Saturn C-1 launch. Temperature gradients at various body locations were determined using the same calculation method and computer program described in section 3.4.2. The criterion for ascent protection was that any ablator material exposed to temperatures in excess of 500 °F would be deemed unacceptable for reentry protection and, consequently, additional ablator thicknesses would have to be added to those required for reentry. Since ascent heating is not too severe, these additional thicknesses are required for only the nose region of the vehicle. These thicknesses add less than 7 pounds to the ablator weight. Representative thicknesses for the 26,000 fps vehicles are listed below.

Body Location	Filled H/C Ablator	Laminated Ablator
Stagnation Point	0.084* inch	0.052 inch
X/C = .125 Windward	0.04	0.01
Leeward	0	0

*Molded Ablator

3.4.3.2 Ablation History

Figure 33 shows the ablation and surface temperature histories of the double wall concept employing filled honeycomb ablator at three

-33-

vehicle locations when exposed to the 36,000 (L/D) trajectory environment. These locations include the stagnation region (A), and main body stations, X/C = 0.5 windward (B) and X/C = 0.3, leeward (C). Typical cross-sectional views of the composite at these locations are shown on figure 33. When the heating rates at "A" are normalized the rates at "B" and "C" are 0.095 and 0.02, respectively. The ablation temperatures at these stations were chosen as functions of total heat flux to be 3440, 2140, and 1500° F respectively.

It will be noted that ablation persists for approximately 860 seconds at section "A" resulting in a total surface recession of 1.187 inches. Approximately 33 percent of the total heating load is absorbed through the ablation process. At section "B" ablation persists for about 400 seconds, and causes a surface recession of 0.038 inches as it dissipates about 9.7 percent of the total heat load. At section "C" the ablation temperature is never attained and the total heat load, 4386 BTU/sq. ft., is accounted for by the conduction and reradiation mechanism.

3.4.3.3 Substructure Trade-Off Study

In addition to obtaining ablator and insulation thicknesses based upon the minimum fiberglass substructure honeycomb core depths required for structural adequacy of the design, the core depths were varied, and ablator and insulation thicknesses required to maintain a 700°F bond line and 200°F rear face temperature were recalculated at X/C = 0.5 on the windward and leeward sides in order to find the effect on the total weight of the composite. Figures 34 and 35 indicate the variation in total heat shield unit weight as a function of honeycomb core height alone.

Figure 36 illustrates the dependency of thermal diffusivity and unit weight on core height. As the core height is varied from zero to some intermediate height, the thermal diffusivity will decrease for a given face sheet thickness and then increase as the core height is increased.

The characteristic shape of the thermal diffusivity versus honeycomb core height curve is caused by the following considerations:

Thermal diffusivity a is defined as:

-34-

$$a = \frac{k}{\rho C_p}$$

where

k = thermal conductivity

ρ = density

C_p = specific heat

The honeycomb is composed of a core and two face sheets, which will have different values of k, ρ, and C_p. The complex geometry is idealized to a homogeneous structure in order to simplify the computer calculations. This is accomplished by using the concept of "effective properties," defined as

$$k_{eff} = \frac{2L_1 + L_2}{\dfrac{2L_1}{k_1} + \dfrac{L_2}{k_2}}$$

$$C_{p_{eff}} = \frac{2\,\rho_1\,L_1\,C_{p_1} + \rho_2\,L_2\,C_{p_2}}{2\,\rho_1\,L_1 + \rho_2\,L_2}$$

$$\rho_{eff} = \frac{2\,\rho_1\,L_1 + \rho_2\,L_2}{2L_1 + L_2}$$

where L_1 and L_2 refer to the face sheet and core section thicknesses, respectively. If L_2 goes to zero (i.e., no core section) the diffusivity is high, reflecting face sheet properties only. For finite values of L_2 the value of a changes to reflect the relative influence of k_{eff}, ρ_{eff}, and $C_{p_{eff}}$. Reversal occurs because small values of L_2 change k significantly, but not ρ. Then as L_2 approaches infinity, k and ρ approach their initial values.

This effect is illustrated for two face sheet thicknesses of 0.020 and 0.030 inch. Along the leeward side of the vehicle, where the ablator thickness is comparatively small, this substructure effect is noticed (see figure 34). It is concluded that the required substructure core height of about 0.22 inch is fairly close to the optimum height. Along the windward side at $X/C = 0.5$, however, structural requirements dictate a core height of 1.91 inch. In this case, additional height

will increase core weight, so that the minimum weight design would be the one with the smallest adequate core height.

3.4.4 Double Wall Concept, Steel Shell

The ablator thicknesses required to limit bond line temperatures to 700°F for the steel outer shells were, in general, within 2 percent of those required for the fiberglass shells. Q-Felt insulation thicknesses at the stagnation point and along the leeward side were also nearly the same as those required for the fiberglass shell designs. Along the windward side, however, the steel shell with the filled H/C ablator required about a half inch more insulation than the fiberglass shell, due primarily to the greater conductivity of the steel substructure than that of the deep cross section of the fiberglass honeycomb substructure. For the laminated ablator this difference was not as pronounced, because the fiberglass core depth was nowhere nearly as great.

The difference in conductivities between the fiberglass and steel substructures had very little effect on the required ablator weights. For example, at $X/C = 0.5$ on the bottom surface, the steel honeycomb substructure depth was 1.11 inch with a conductivity of 0.24 BTU/hr-ft-°F, compared to the fiberglass honeycomb's 1.91 inch depth and 0.038 BTU/hr-ft°F conductivity. The factor of 6 difference in conductivities created only a 2 percent difference in ablator weights.

Ablator and insulation unit weights for the steel outer shell designs are listed in table V.

3.4.5 Single Wall Concept, Aluminum Shell

Required thicknesses of the filled honeycomb ablator were determined to provide protection against convective heating by limiting bond line temperatures to 300°F. Insulation requirements were determined which limited rear face temperatures to 200°F; however, a different initial temperature gradient was assumed, as noted in figure 19. The same calculation procedures and methods were used to determine convective and radiative heating thicknesses that were described in section 3.4.2.

The resulting total ablator thicknesses are plotted as functions of body location and heating ratios in figures 37 and 38. Insulation thicknesses are shown in figure 39, and unit weights of ablator and insulation are included in table VI.

3.4.6 Total Ablator Weights

The total ablator and insulation weights for reentries at 26,000 fps and 36,500 fps are presented in tables VII and VIII, respectively.

The filled H/C ablator total weights are about 17 percent lighter than those for the laminated ablator, and the weight penalty for a 300°F maximum bond line temperature compared to a 700°F temperature averages at 70 percent.

-36-

TABLE IV

TOTAL ABLATOR AND INSULATION UNIT WEIGHTS
DOUBLE WALL CONCEPT-INTEGRATED
FIBERGLASS SHELL

(700°F, maximum bondline, 200°F maximum rear face temperature)

Body Location	26,000 fps		26,000 fps		36,500 fps		36,500 fps	
	Filled H/C	Insulation	Laminated	Insulation	Filled H/C	Insulation	Laminated	Insulation
Stagnation Point	8.072 lb/ft² (molded)	0.980 lb/ft²	7.150 lb/ft²	0.980 lb/ft²	10.784 lb/ft² (molded)	0.980 lb/ft²	9.383 lb/ft²	0.960 lb/ft²
Windward:-								
X/C = 0.06	5.801	0.985	6.053	1.025	6.904	0.945	7.264	0.980
X/C = 0.375	3.465	0.890	4.162	1.065	4.132	0.775	4.918	1.050
X/C = 0.5	3.003	0.850	3.632	1.075	3.696	0.775	4.426	1.065
X/C = 0.75	2.336	0.935	2.875	1.125	3.208	0.675	4.162	0.805
Leeward:-								
X/C = 0.1	1.386	1.28	1.589	1.280	1.899	1.290	2.346	1.275
X/C = 0.3	1.309	1.255	1.589	1.245	1.899	1.260	2.346	1.240
X/C = 0.75	1.283	1.105	1.627	1.125	1.874	1.150	2.308	1.185

TABLE V

TOTAL ABLATOR AND INSULATION UNIT WEIGHTS
DOUBLE WALL CONCEPT-
STEEL SHELL

(700°F maximum bondline, 200°F maximum rear face temperature)

Body Location	26,000 fps				36,500 fps			
	Filled H/C	Insulation	Laminated	Insulation	Filled H/C	Insulation	Laminated	Insulation
Stagnation Point	7.168 lb/ft² (molded)	0.950 lb/ft²	6.772 lb/ft²	1.040 lb/ft²	10.659 lb/ft² (molded)	0.965 lb/ft²	9.307 lb/ft²	0.940 lb/ft²
Windward:-								
X/C = 0.06	5.801	0.970	6.051	1.020	6.865	0.985	7.301	0.865
X/C = 0.5	2.944	1.080	3.591	1.090	3.655	1.075	4.389	1.075
X/C = 0.75	2.277	1.140	2.849	1.140	2.928	0.845	3.492	0.860
Leeward:-								
X/C = 0.3	1.335	1.290	1.665	1.280	1.874	1.310	2.308	1.290
X/C = 0.75	1.283	1.290	1.627	1.280	1.822	1.285	2.308	1.285

TABLE VI

TOTAL ABLATOR AND INSULATION UNIT WEIGHTS
SINGLE WALL CONCEPT-
ALUMINUM SHELL

(300°F maximum bondline, 200°F maximum rear face temperature)

Body Location	26,000 fps		36,500 fps	
	Filled H/C	Insulation	Filled H/C	Insulation
Stagnation Point	9.568 lb/ft^2 (molded)	0.575 lb/ft^2	12.496 lb/ft^2 (molded)	0.535 lb/ft^2
Windward:-				
X/C = 0.06	7.264	0.575	8.405	0.575
X/C = 0.5	5.049	0.590	5.503	0.650
X/C = 0.75	4.612	0.645	4.673	0.655
Leeward:-				
X/C = 0.375	4.055	0.660	4.620	0.665
X/C = 0.5	4.055	0.670	4.620	0.665
X/C = 0.75	3.978	0.670	4.543	0.655

TABLE VII

ABLATOR WEIGHT BREAKDOWN

26,000 FT/SEC VEHICLE

	Filled H/C Ablator Weight, Pounds			Laminated Ablator Weight, Pounds		
	Single Wall-Aluminum Shell	Double Wall-Steel Shell	Double Wall-Integrated Fiberglass Shell	Single Wall-Aluminum Shell	Double Wall-Steel Shell	Double Wall-Integrated Fiberglass Shell
Nose Cap Plus Bond	121	101	101	--	89	89
Body Plus Bond	3408	1918	1918	--	2291	2291
Elevons (2) Plus Bond	566	319	319	--	361	361
Total Ablator and Bond Weight	4095	2338	2338	--	2741	2741
Insulation	295	538	482	--	542	519

TABLE VIII

ABLATOR WEIGHT BREAKDOWN

36,500 FT/SEC VEHICLE

	Filled H/C Ablator Weight, Pounds			Laminated Ablator Weight, Pounds		
	Single Wall-Aluminum Shell	Double Wall-Steel Shell	Double Wall-Integrated Fiberglass Shell	Single Wall Aluminum Shell	Double Wall-Steel Shell	Double Wall-Integrated Fiberglass Shell
Nose Cap Plus Bond	152	131	131	--	111	111
Body Plus Bond	3839	2326	2326	--	2789	2789
Elevons (2) Plus Bond	638	393	393	--	446	446
Total Ablator and Bond Weight	4629	2850	2850	--	3346	3346
Insulation	299	529	459	--	526	504
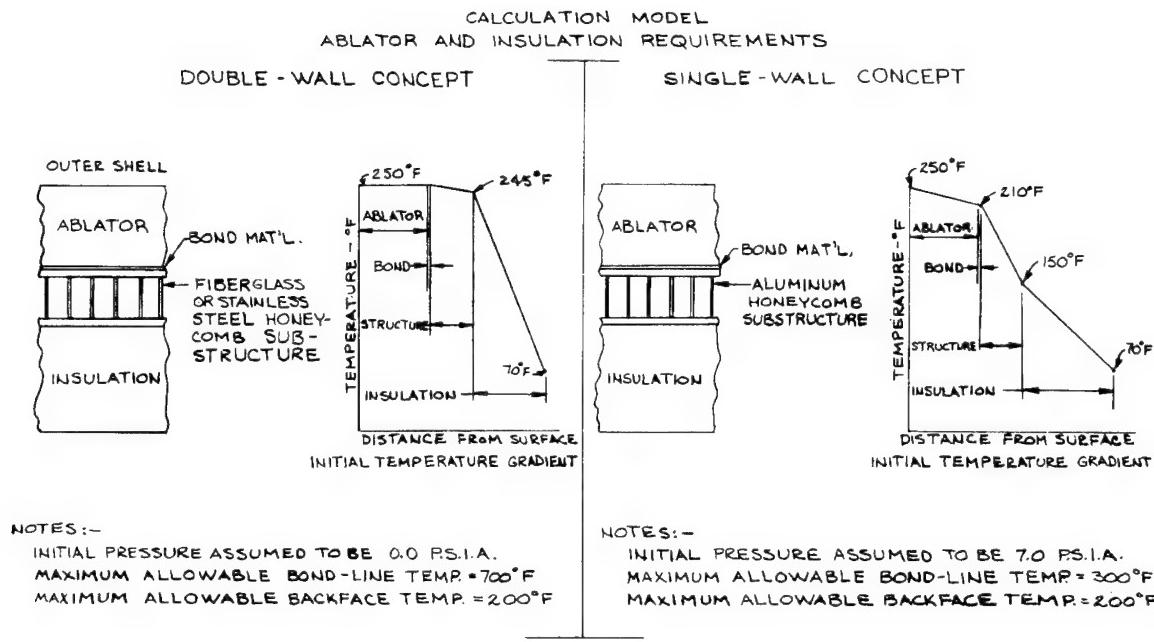
Figure 19 CALCULATION MODEL, ABLATOR AND INSULATION TEMPERATURE
REQUIREMENTS
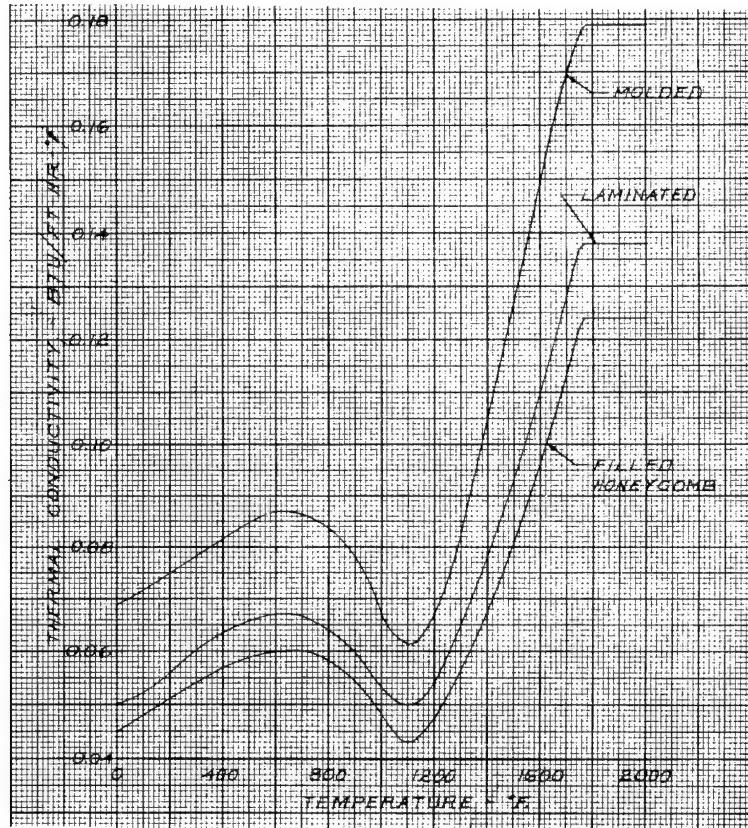
Figure 20 ABLATOR THERMAL CONDUCTIVITY VERSUS TEMPERATURE
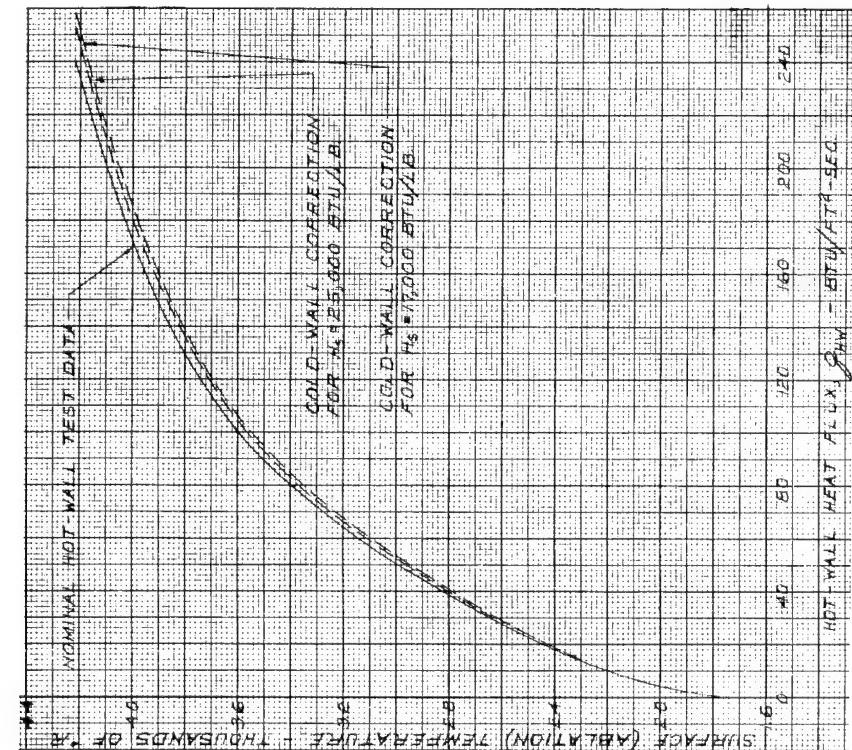
Figure 21 ABLATION TEMPERATURE VERSUS CONVECTIVE HEATING RATE
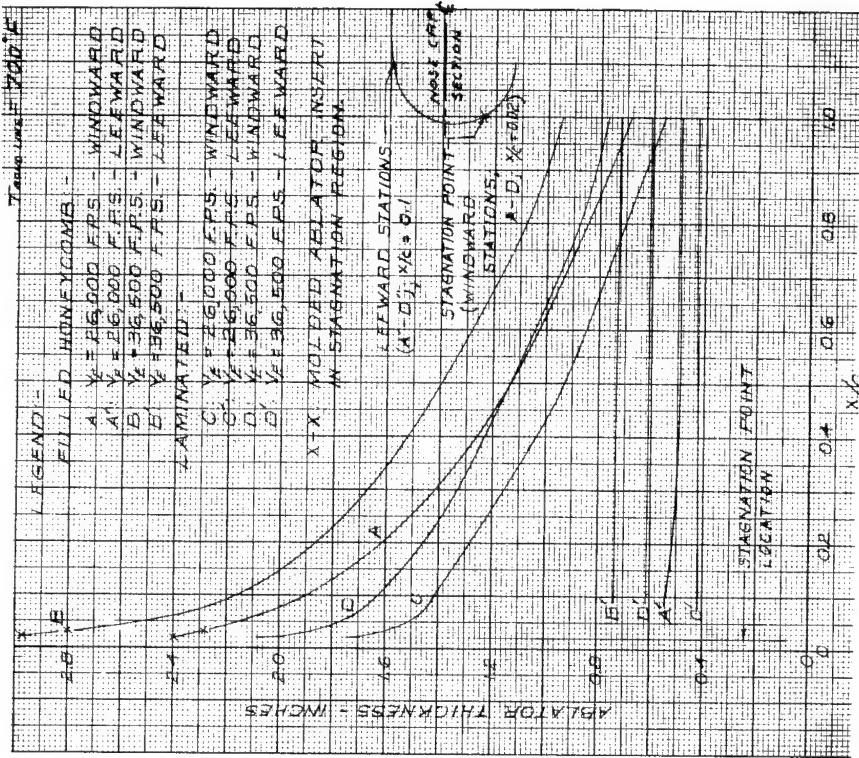
Figure 22 CONVECTIVE HEATING ABLATOR THICKNESS VERSUS BODY LOCATION
DOUBLE WALL CONCEPT, FIBERGLASS OUTER SHELL

-43-
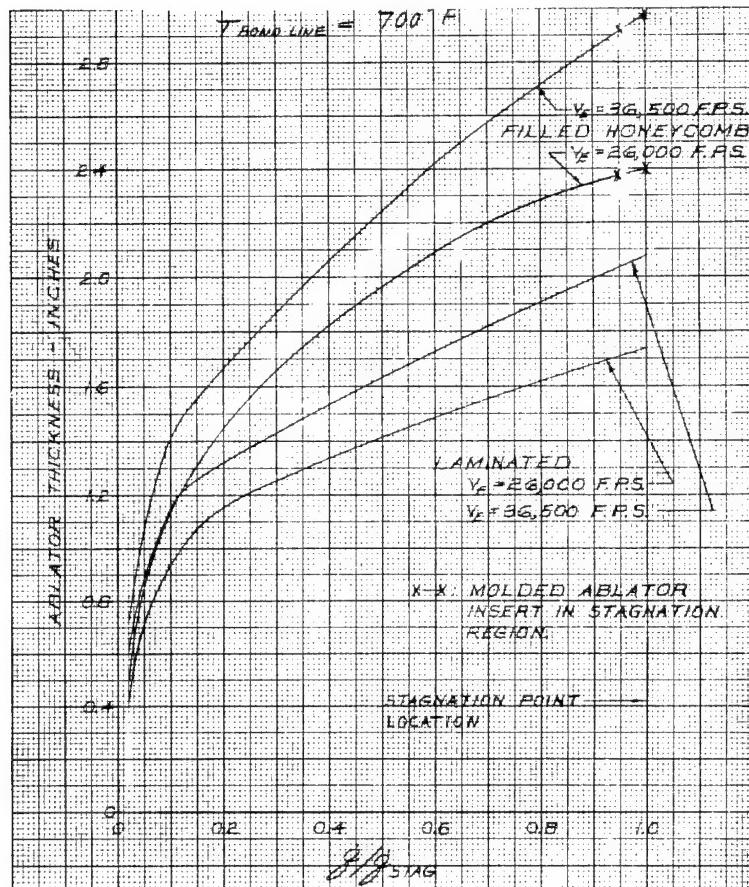
Figure 23 ABLATOR THICKNESS VERSUS LOCAL CONVECTIVE HEATING, DOUBLE
WALL CONCEPT, FIBERGLASS OUTER SHELL
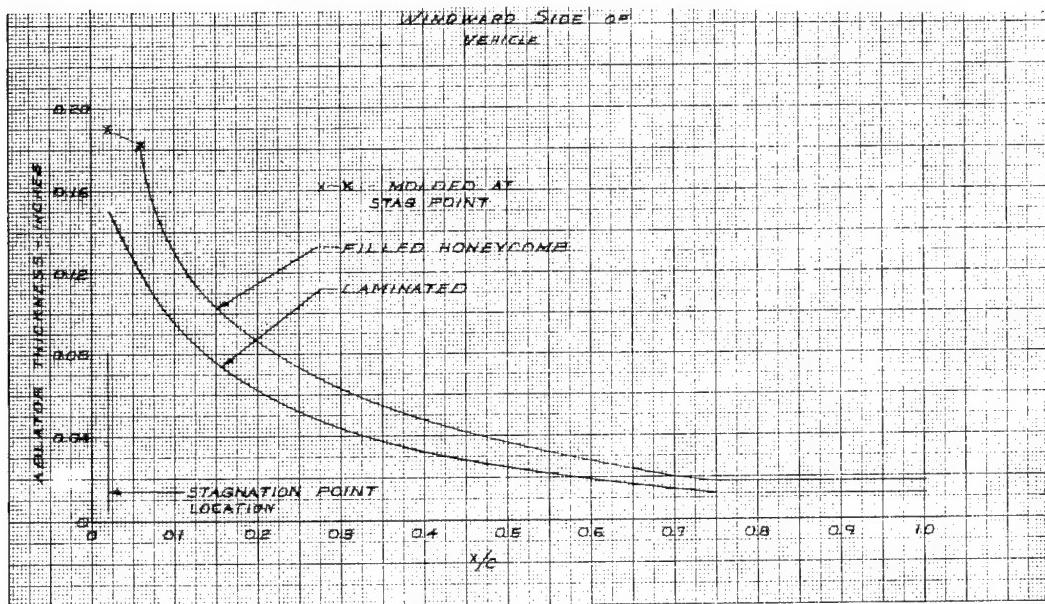
Figure 24 ABLATOR THICKNESS REQUIREMENTS, RADIATIVE HEATING,
$(26,000 \ (L/D)_{max}$ TRAJECTORY)

-44-
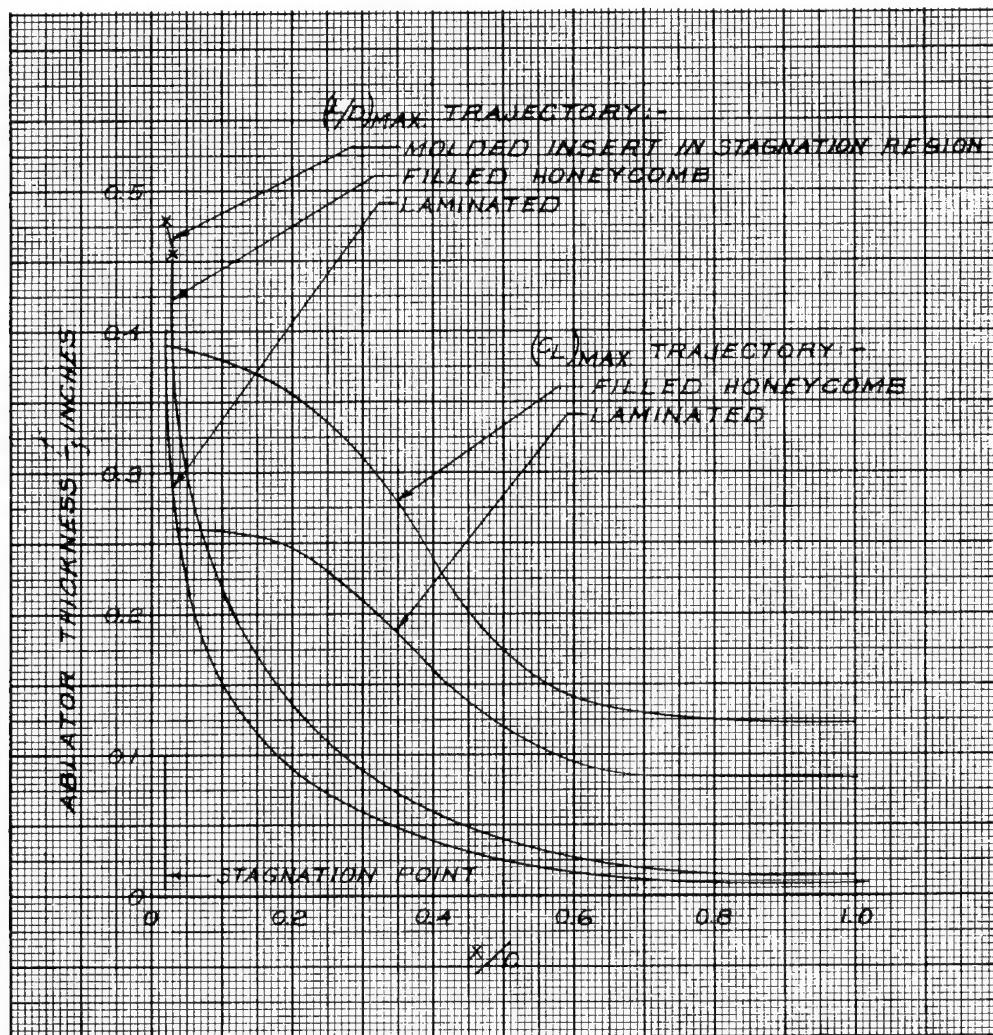
Figure 25 ABLATOR THICKNESS REQUIREMENTS, RADIATIVE HEATING,
(36,500 FPS TRAJECTORIES)
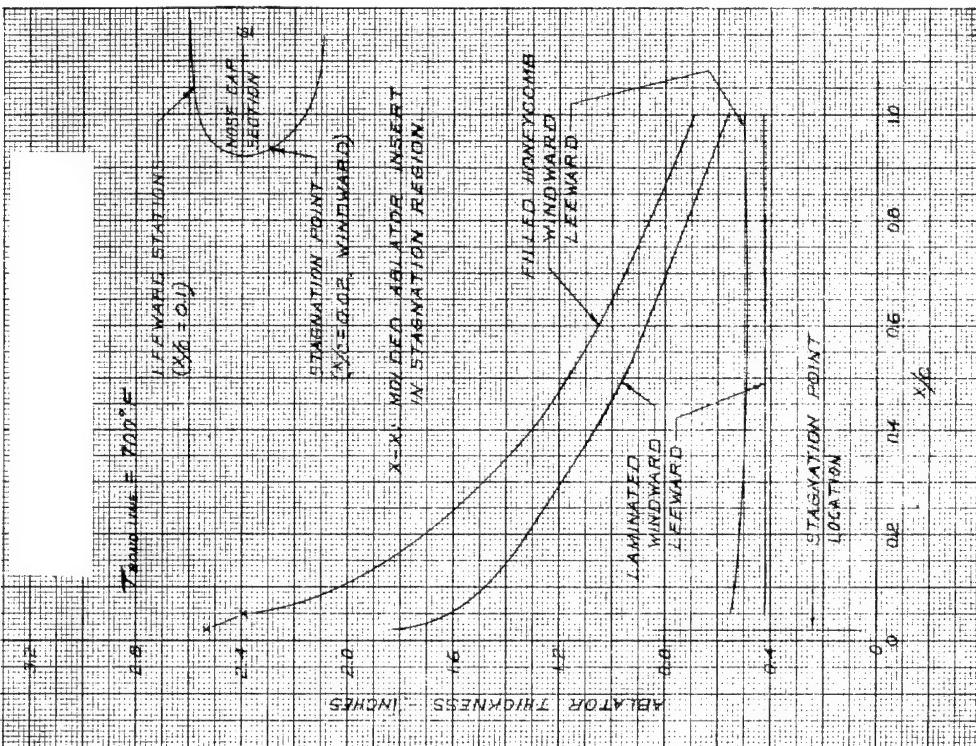
Figure 26 TOTAL ABLATOR THICKNESSES VERSUS BODY LOCATION, DOUBLE WALL   Figure 27 TOTAL ABLATOR THICKNESSES VERSUS BODY LOCATION, DOUBLE WALL
CONCEPT, 26,000 FPS REENTRY   CONCEPT, 36,500 FPS REENTRY
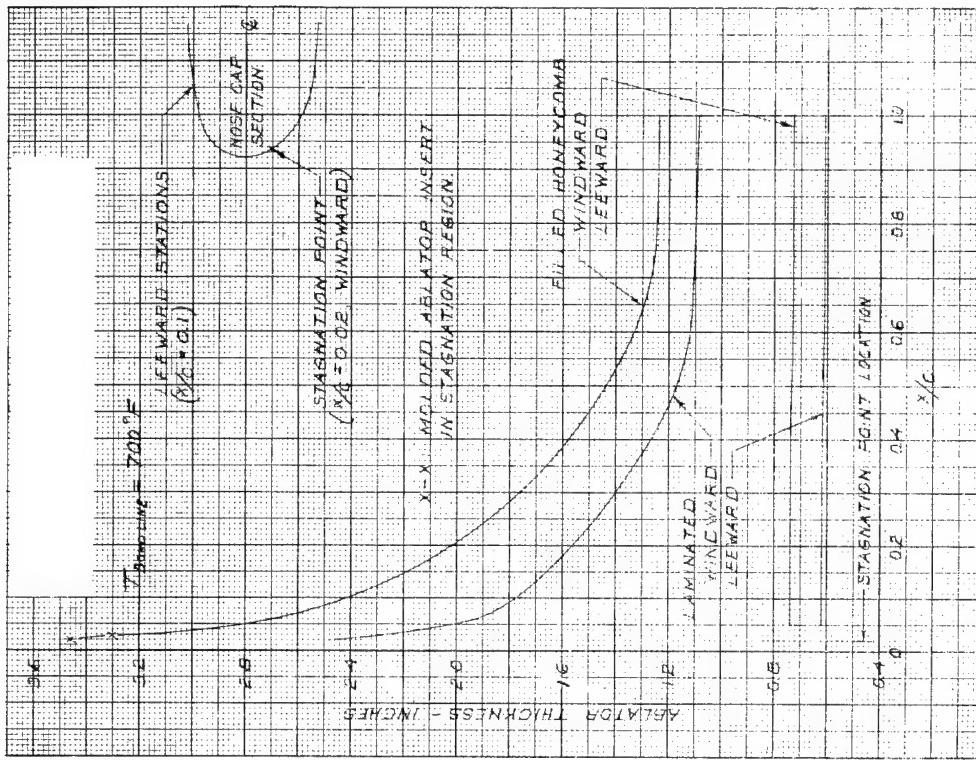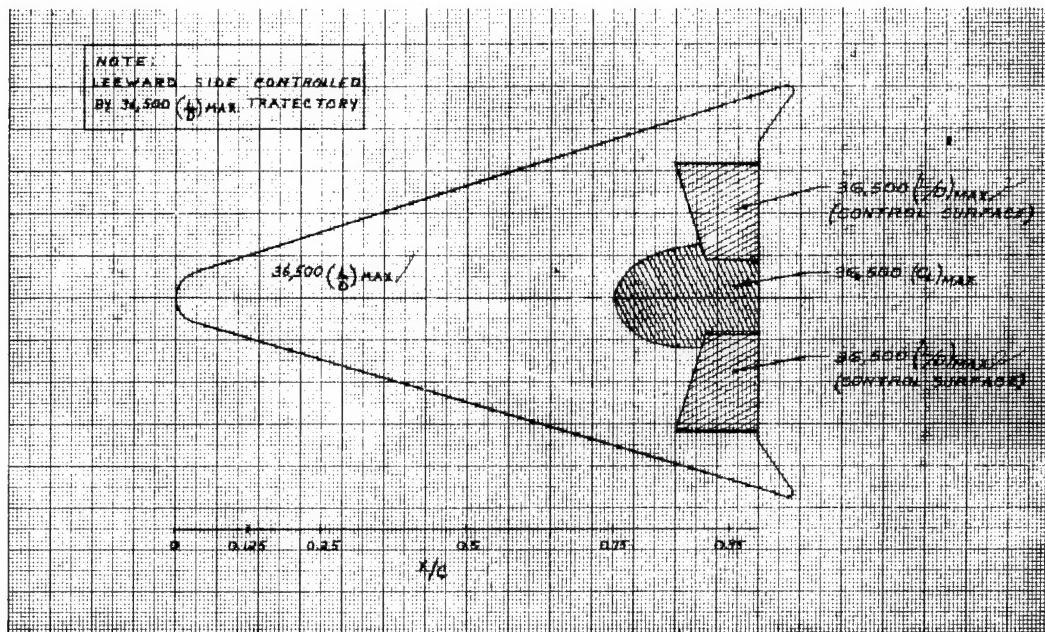
Figure 28 TRAJECTORY DESIGN AREAS, 36,500 FPS
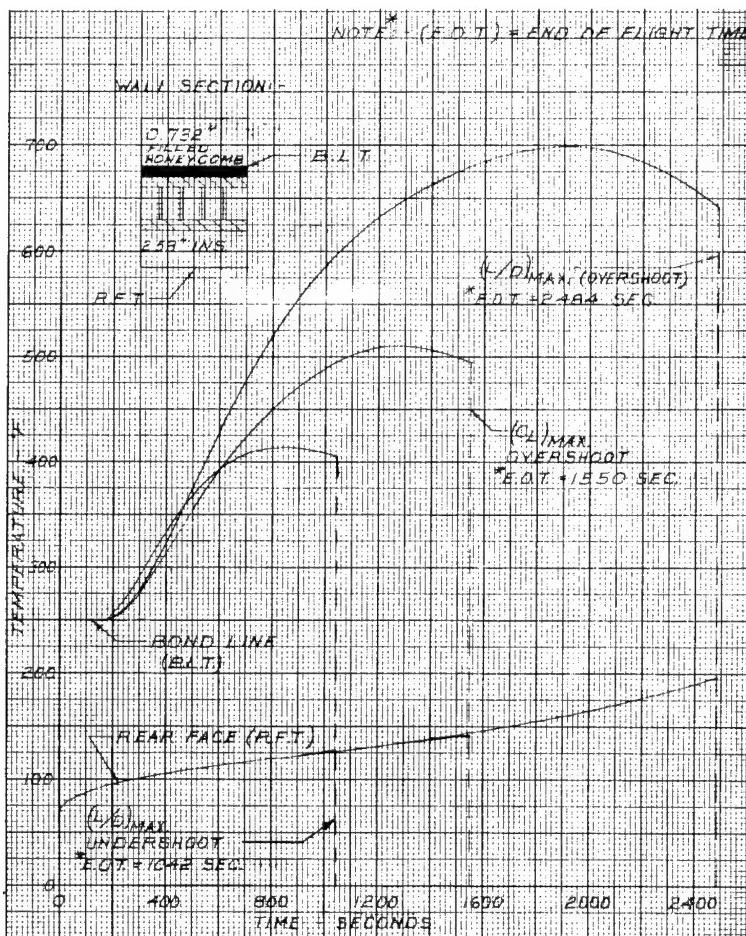
Figure 29 BOND LINE AND REAR FACE TEMPERATURE HISTORIES--36,500 FPS--
X/C = 0.3 LEEWARD
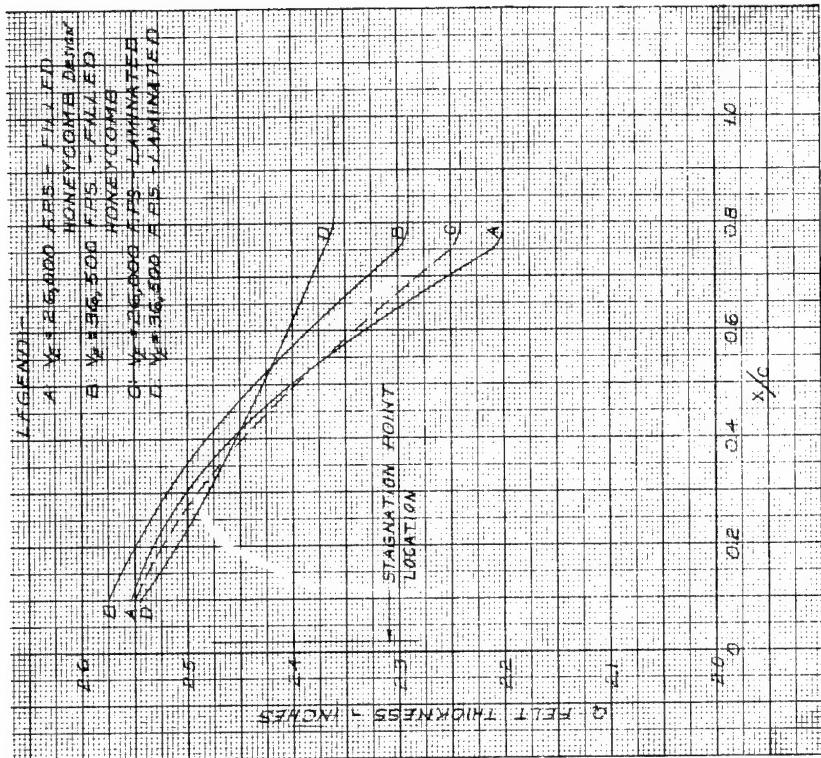
Figure 31 Q-FELT INSULATION THICKNESS, LEEWARD SIDE, DOUBLE WALL
CONCEPTS, FIBERGLASS OUTER SHELL

Figure 30 BOND LINE AND REAR FACE TEMPERATURE HISTORIES--36,500 FPS--
X/C = 0.50 WINDWARD
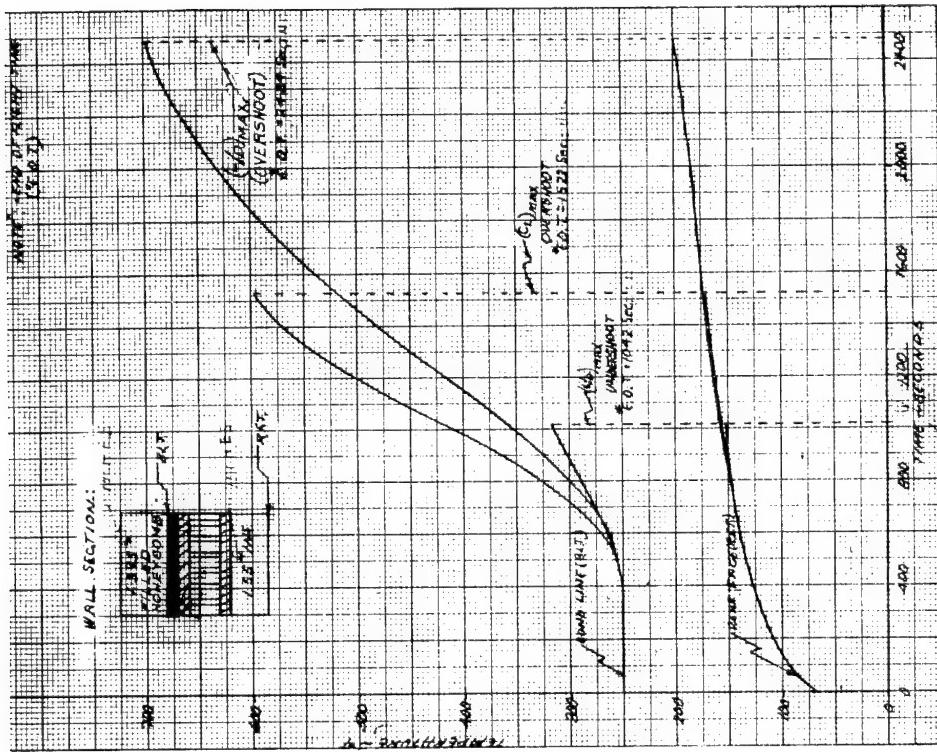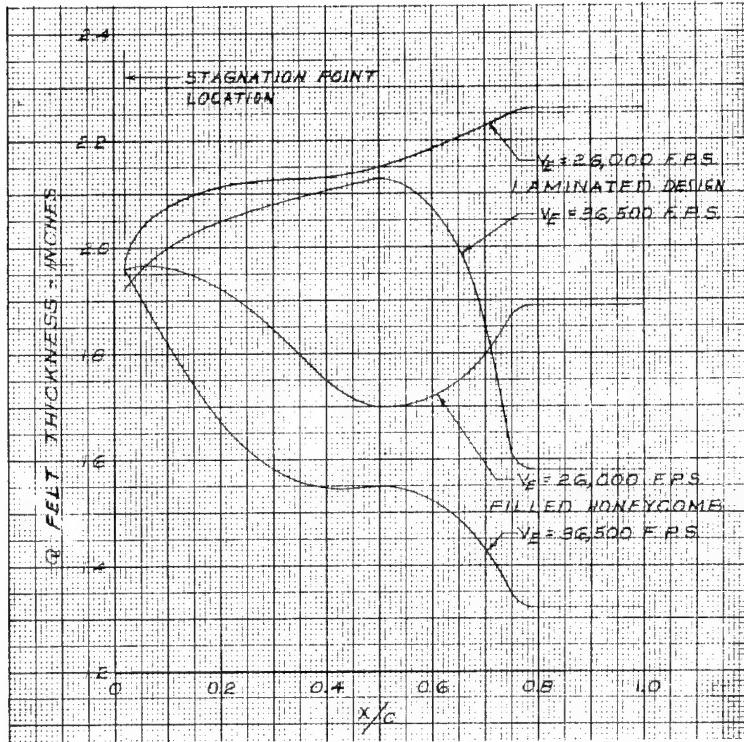
Figure 32 Q-FELT INSULATION THICKNESS, WINDWARD SIDE, DOUBLE WALL
CONCEPTS, FIBERGLASS OUTER SHELL
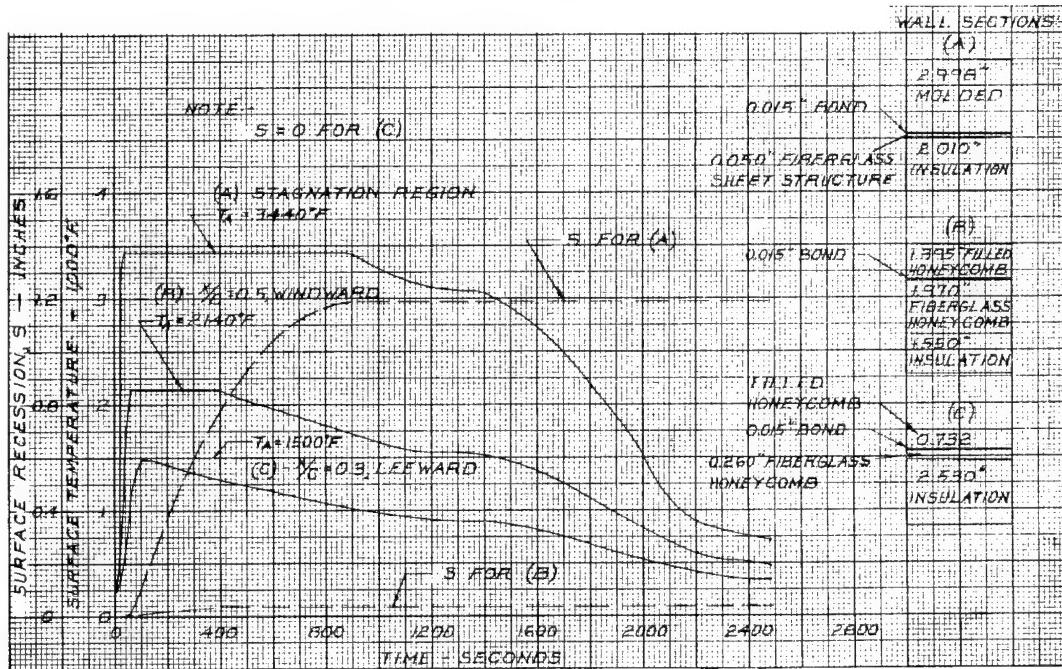
Figure 33 ABLATION AND SURFACE TEMPERATURE HISTORIES, $(L/D)_{max}$, 36,500 FPS
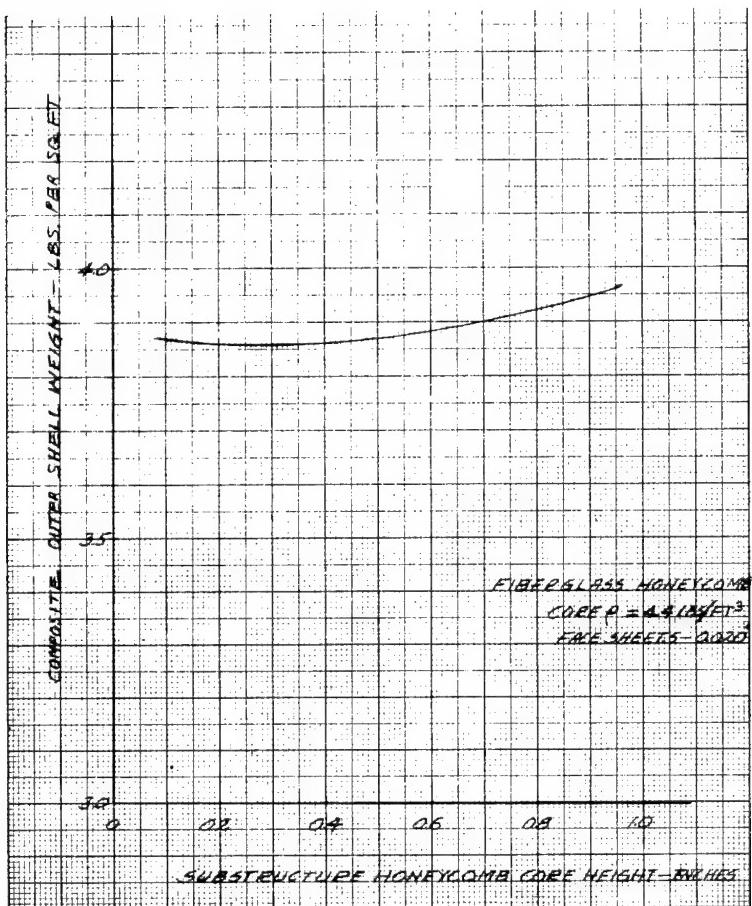
Figure 34 COMPOSITE OUTER SHELL UNIT WEIGHT VERSUS FIBERGLASS HONEYCOMB
CORE HEIGHT--LEEWARD SIDE
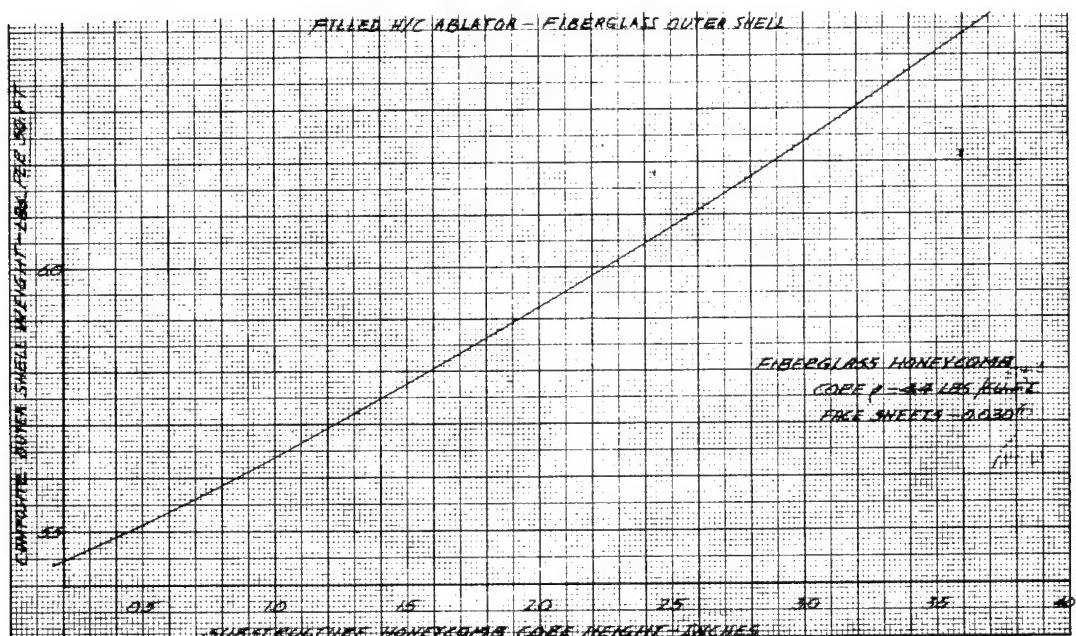
Figure 35 COMPOSITE OUTER SHELL UNIT WEIGHT VERSUS FIBERGLASS HONEYCOMB
CORE HEIGHT--WINDWARD SIDE
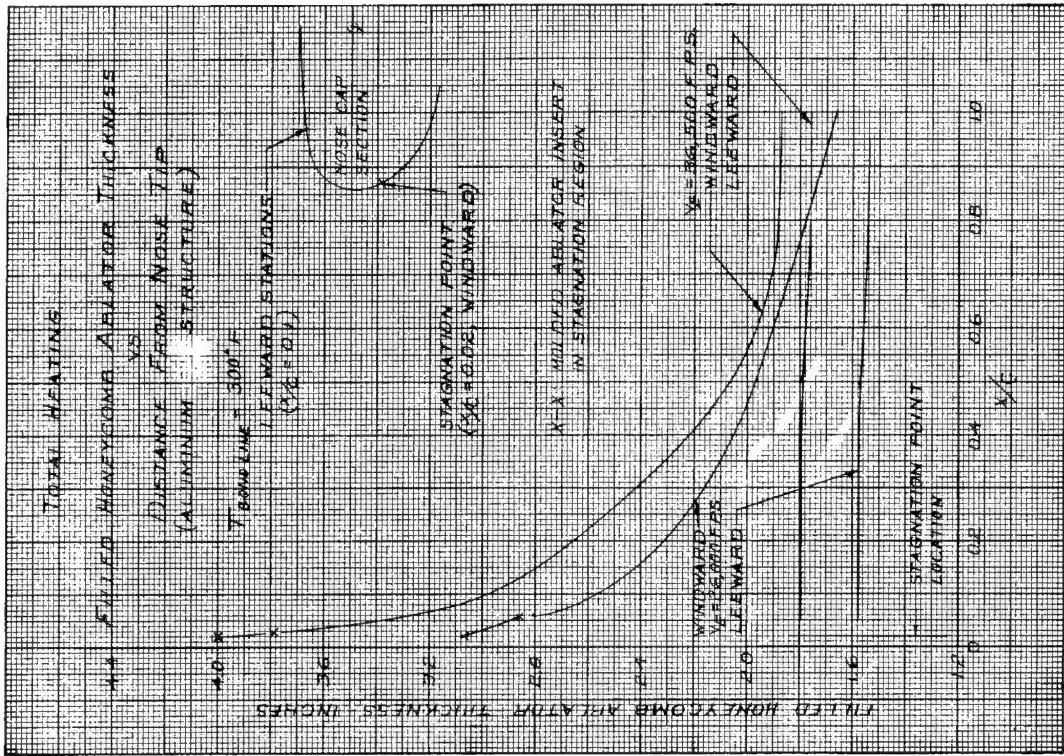
Figure 37 TOTAL FILLED H/C ABLATOR THICKNESSES VERSUS BODY LOCATION
(ALUMINUM STRUCTURE VEHICLE)
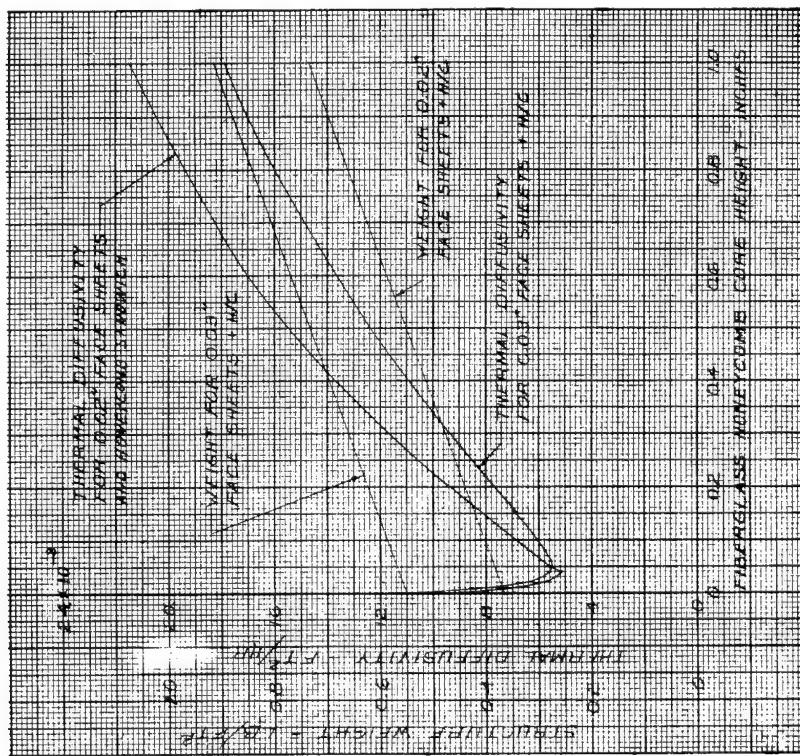
Figure 36 STRUCTURE WEIGHT AND THERMAL DIFFUSIVITY VERSUS FIBERGLASS
HONEYCOMB CORE HEIGHT
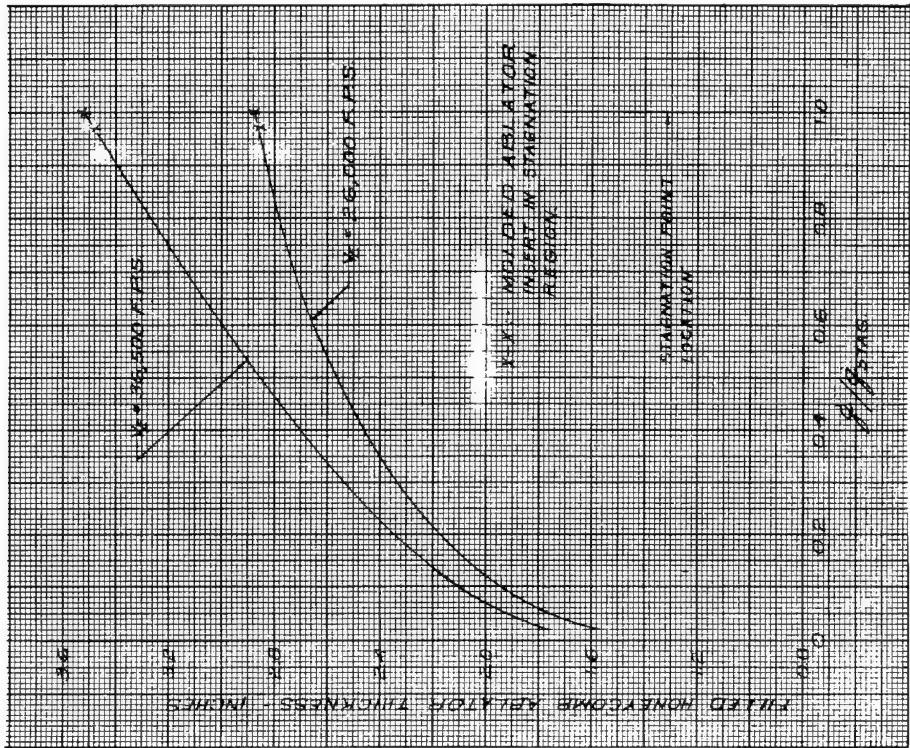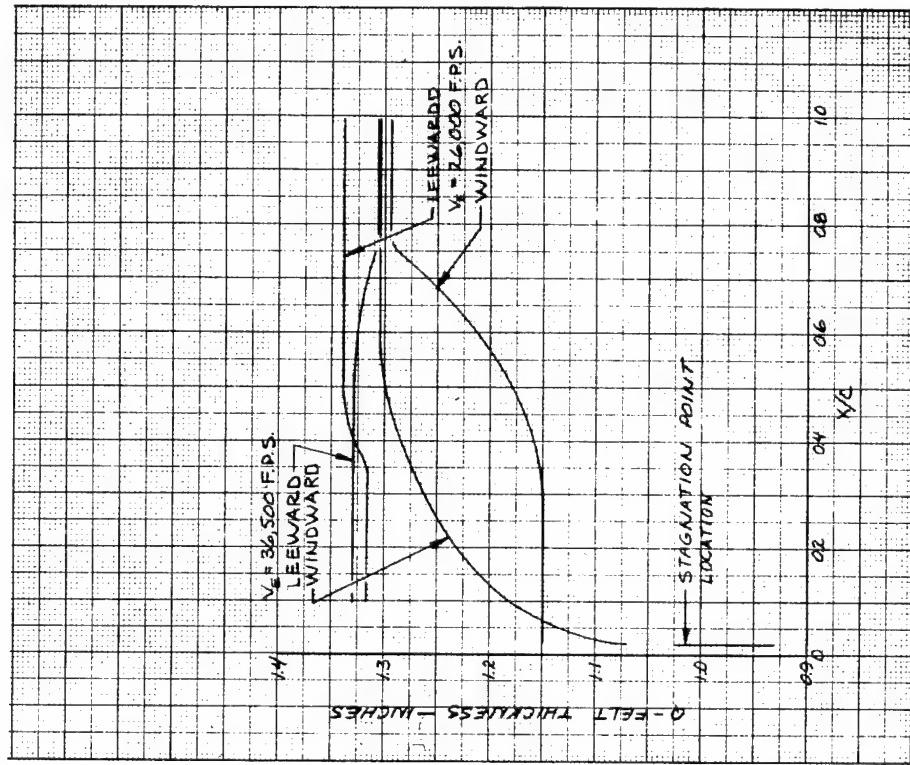
Figure 38 FILLED H/C ABLATOR THICKNESSES VERSUS LOCAL CONVECTIVE HEATING
(ALUMINUM STRUCTURE VEHICLE)

Figure 39 Q-FELT INSULATION THICKNESS VERSUS BODY LOCATION, ALUMINUM
STRUCTURE VEHICLE

-52-

3.5 Structural Analysis

This section of the report contains the results of the structural analyses which were performed for both the double and single wall concepts described in section 3.1. The criteria which governed these analyses are presented in section 3.5.1, and the loading conditions resulting therefrom are presented in section 3.5.2.

Details of the analyses of the two integrated designs are presented in section 3.5.3. This portion of the report includes design support studies, structural sizing of the integrated fiberglass shells, sizing of the inner aluminum pressure shell, and presentation of cold soak stresses, reentry stresses and space flight thermal deflections.

The analyses for the nonintegrated double and single wall concept designs begin in section 3.5.4.1, which treats two fiberglass outer shell designs, one for each ablator. Structural analysis of two steel shells is presented in section 3.5.4.2 and the analyses of the aluminum single shells for each ablator follow in section 3.5.5 and 3.5.6.

The final section 3.5.7 presents the structural weight summary for each design.

3.5.1 Structural Design Criteria

3.5.1.1 Substructure capabilities

The substructure of each design concept was required to survive reentry at both 26,000 fps and 36,500 fps. The inner aluminum pressure shell of the double wall concepts and also the single aluminum shell vehicle were designed to withstand 7 psi (limit) internal pressure. These structures were also required to survive a mission in which they were vented, with a venting lag of one psi differential between the outer and inner pressure.

3.5.1.2 Factors of safety

Limit loads as defined herein are the maximum applied loads that the structure would be expected to encounter during its mission. Ultimate loads were obtained by multiplying limit loads by a factor of safety. No structure was designed to fail at less than ultimate load.

Failure of the load-carrying structural composite was assumed to occur when the structure became unstable (buckled) or when the ultimate stress of a fiberglass, steel, or aluminum load-carrying

member was exceeded. Furthermore, local strain exceeding the ultimate strain allowable was the criterion for cracking of the ablator. For the purposes of this report, cracking of the ablator before or during reentry heating was not allowed, even when such an occurrence did not fail the fiberglass substructure.

The factors of safety used in the analyses were as follows:

a) For unpressurized structures, the factor of safety on limit applied loads was 1.5. No factor was used on thermal stresses or strains.

b) For internally pressurized structures, a factor of 1.33 was used on internal pressure in the presence of limit external loads for yield. The maximum distortion energy criterion was used for yielding of aluminum or steel. The ultimate conditions were a factor of 2.0 on internal pressure in the presence of limit applied loads, and a factor of 1.5 on applied loads in the presence of limit or zero internal pressure.

3.5.1.3 Ablator strength at elevated temperatures

The structural strength of any ablator above 600°F was ignored in the analyses of ablator-substructure composites.

3.5.2 Vehicle Loads

3.5.2.1 Weight distribution

The total weight of a lifting entry vehicle (assumed herein to be an HL-10) was taken to be 10,800 pounds with a distribution as shown in figure 40 and a c.g. location at $X/C = 0.53$. Any ascent cargo in addition to the amount included in the overall weight was assumed to be carried in the adapter section.

3.5.2.2 Ascent and abort loads

The ascent loading conditions considered in the analyses were those which would be imposed by a Saturn C-1 booster vehicle. Initially, launch temperatures ranging from 30 to 125°F were considered. The upper limit of 125°F was used in the structural design, since at lower temperatures the ablator strength increases.

For abort analyses, it was assumed that, rather than having an abort tower, the vehicle would be mounted on a propulsion module by means of a structural fairing which ties into the vehicle at station $X/C = 0.75$. A propulsion module would be mounted on the

Saturn C-1 and would disengage when an abort is initiated. For this method of abort, the following conditions and loads were assumed.

a) Pad abort = 10 g axial acceleration

b) Abort at maximum dynamic pressure (M = 1.5)

$\underline{1}$ Initiation of abort: 6 g axial acceleration and 750 lb/ft^2 dynamic pressure (stagnation pressure = 11.3 psi).

$\underline{2}$ Just before end of thrust: 2 g axial acceleration and 1000 lb/ft^2 dynamic pressure (stagnation pressure = 15.1 psi). An angle of attack variation of ± 15 degrees during an abort was also assumed.

The internal pressure inside of the outer shell of the entry vehicle would be determined by the local external pressure at the vent location on the upper surface of the vehicle and by the lag in venting. The local pressure there for a positive angle of attack would be very small, and hence a value of 0.4 psi was assumed for the internal pressure.

Figures 41 through 44 depict the axial loads, shears, and moments along the outer shell of the double wall vehicle concepts for the two max "q" abort conditions at $a = +15°$ and $-15°$. Because the longitudinal tie between the inner compartment and the outer shell was at X/C = 0.375, all axial inertia loads of the inner compartment would feed into the outer shell at that station.

For the aluminum single shell vehicle, axial internal inertia loads would be transferred to the shell all along the length rather than only at X/C = 0.375. Accordingly, the axial load distribution curves in figures 41 through 44 must be modified. Figure 45 presents the corrected axial load distributions for the aluminum single shell concept.

3.5.2.3 Space flight

The space flight environment would be characterized by zero applied loads and surface temperatures ranging from 250°F to -250°F, thereby producing thermal deflections that could cause interactions between the inner and outer shells of the double wall concepts.

The internal pressure in the pressure shell is taken as either 7 psi or, in the event of a malfunction or a leak, 0 psi. The 7 psi condition would cause inner-outer shell interactions in the double wall concepts.

-55-

3.5.2.4 Reentry

The trajectories considered for reentry are described in section
3.2. Initial temperatures range from 250°F to -250°F. For the
structural analyses, just the limits of ± 250°F were considered.
The 12 g undershoot trajectories cause larger pressures over the
vehicle than the overshoot trajectories. The severest reentry
pressures occur for the 12 g undershoot, L/D max, (a = 30°),
36,500 ft/sec trajectory, which has a maximum stagnation pres-
sure of 15.7 psi, compared to 6.1 psi for the C_L max (a = 60°)
undershoot trajectory. Pressure distributions corresponding to
a = 30° are shown in figures 7 and 8. Vehicle axial loads, shears,
and moments for the L/D max, undershoot trajectory are shown
in figure 46. Because the strengths of the ablators are tempera-
ture dependent, the strength of a composite would decrease with
time during reentry.

3.5.2.5 Approach to touchdown

This condition occurs after reentry when all the ablator has been
highly heated and can be considered structurally ineffective. From
the venting lag assumption there is a 1.0 psi differential between
ambient pressure and the internal pressure.

3.5.3 Double Wall Concepts - Integrated Designs

3.5.3.1 Design support studies

3.5.3.1.1 Inner and outer shell attachments

Any design attaching the inner pressure shell to the outer
shell must include adequate load paths between the two shells,
and must accommodate the thermal contraction and growth of
the outer shell at temperatures from -250°F to +700°F.
Furthermore, for minimum weight the design should allow
the stiffness of the inner shell to help support the outer shell
as much as possible when the latter is subjected to loads.

The thermal contraction of the outer shell from 70°F to -250°F
is approximately 0.32 inch per 100 inches of vehicle length,
while the expansion from 70 to 700°F is 0.25 inches for the
same interval of length. This expansion is less than the con-
traction because the coefficients of thermal expansion of the
materials are lower for higher temperatures than for cold
ones. High stresses ($\sim$ 25,000 psi on the aluminum shell)
would be induced if the shell were restricted against these
deflections in the axial direction. Accordingly, there should

be an axial load path connection between the inner and outer shells at only one station. This location was chosen at X/C = 0.375, which has the deepest cross section.

In the transverse plane, load paths must be provided for vertical and lateral load transfers between the two shells, and still be able to adequately accommodate the thermal deformations. The lateral load paths were selected at the top and bottom center lines at each frame location.

The placement of the vertical load paths was influenced by the results of analyses of outer shell frames at X/C = 0.375 and 0.75 subjected to the external pressure loads of reentry and approach to touchdown, and inner pressure shell frames subjected to internal pressure. Large deflections and stresses for inner and outer shell frames, especially at X/C = 0.75, indicated that either the frames must be very heavy in order to limit the deflections or that the inner and outer shell frames would make contact, and, accordingly, would rely on each other for support. For a minimum weight design, the latter was the obvious choice. In addition, at X/C = 0.75, an internally pressurized compartment conforming to the external shape would require either very heavy frame stiffening or, more likely, vertical posts between top and bottom surfaces to relieve the large circumferential bending moments. This is what has been assumed here. Figures 47 and 48 depict the vertical load path locations selected for frames at X/C = 0.75 and 0.375. Thermal stresses due to the expansion or contraction of the outer shell were found to be well within tolerable limits.

Three vertical paths were chosen along the bottom surface of each frame, because the largest external pressure loads occur there during reentry. These pressure loads are balanced mainly by inertia loads in the inner compartment. Providing several paths for these reactions lessens the bending in both the inner and outer shells, and thus permits a lighter design.

3.5.3.1.2 Frame spacing studies

Frames are used for attachment of the inner shell to the outer shell. Furthermore, they provide support for the shell when it is subjected to pressure loadings, especially in the flat regions along the bottom surface of the vehicle. Weight trade-off studies were performed to determine the effects of frame spacing on weight of the bottom surface.

The laminated ablator was used for these analyses, which considered spacings of 24, 30, and 36 inches at two locations on the vehicle, namely $X/C = 0.75$ and 0.375. The procedure was to idealize a longitudinal strip of the bottom surface as a beam of length "L" (L = frame spacing) clamped at each end, and subjected to external pressure. The design condition for the laminated ablator design was bending under the approach to touchdown pressure. The required honeycomb core depth for the fiberglass substructure was then found, and substructure weights per square foot computed for each frame spacing.

Next, frame stiffness requirements for circumferential bending were determined and then a frame cross section was selected such that, when combined with a honeycomb sandwich and ablator of width "L" it would be adequate for the maximum "q" reentry pressure loading, which was the design condition for the frame analyses. The particular fiberglass frame for $X/C = 0.75$, L = 24 inches, used in the analyses was an "I" section, 3 inches deep, 2 inches wide, and 0.10-inch thick. The frame selected for $X/C = 0.375$, L = 24 inches was another "I" section 2 inches deep, 2 inches wide, and 0.08-inch thick. The average weight per square foot of the frame and 24-inch width of shell was computed, and the radius of gyration (I/C_o) of the frame-shell composite calculated. It should be noted that the larger the I/C_o ratio, the greater is the moment the section can carry.

Next the 30- and 36-inch frame spacing cases were considered. Frames thicknesses for each were determined such that the total average weight per square foot of frame plus shell was the same as the 24-inch spacing case. Then the I/C_o's of those frame-shell composites were calculated.

At $X/C = 0.75$, the results of the calculations were as follows:

    <u>1</u>   L = 24 inches, $I/C_o = 0.044$

    <u>2</u>   L = 30 inches, $I/C_o = 0.037$

    <u>3</u>   L = 36 inches, $I/C_o = 0.026$

At $X/C = 0.375$, the results were $I/C_o = 0.035$ for L = 24 inches, and $I/C_o = 0.028$ for L = 30 inches.

Thus, at both locations, for a given average weight of frame and shell, the 24-inch frame spacings allowed greater moment carrying ability than the 30 and 36-inch spacing. This

meant that a 24-inch spacing design could be made lighter than the other two, hence it was selected as the design frame spacing aft of X/C = 0.375.

Forward of X/L = 0.375, where the bottom flat portion narrows down, frame bending becomes less severe, and consequently frames were placed at convenient locations with 35-inch and 36-inch spacings.

3.5.3.1.3 Frame design: derivation of frame design loads

The inner and outer shell frames of the double wall concepts are attached together at certain points at each frame location, which, at X/C = 0.75 and 0.375, are shown in figures 47 and 48. Since each attachment would be capable of transferring vertical loads between the shells, interactions occur that would affect the loads in the frames. The inner frames would help support the outer frames and vice versa. For the analyses an effective shell width of 24" was assumed with each frame.

Inner and outer shell frames at stations X/C = 0.375 and 0.75 were analyzed for the effects of both internal pressure in the inner shell and for a 12 g reentry. The latter condition would cause external pressure on the outer shell, inertia loads of the internal cargo and outer shell masses, and a required balancing shear flow in the outer shell. These loads were taken over a 24-inch width of shell. The internal mass distribution assumed for the analyses is that shown in figure 40. Figure 49 presents the particular locations of the inertial reactions and the values of the applied reentry loads for frames at X/C = 0.375 and 0.75.

Consistent with the design criteria, the ultimate loading conditions considered in the analyses were the following:

1   14 psi internal pressure, zero external loads

2   14 psi internal pressure, limit reentry loads

3   zero internal pressure, ultimate reentry loads

4   7 psi internal pressure, ultimate reentry loads

The interaction analyses were performed by making use of influence coefficients and requiring that inner and outer frame displacements be compatible at the attachment locations. Maximum loads in the frames were determined as a

function of the ratio of the inner frame composite stiffness (EI) to that of the outer frame composite. After some iterations it was found that at each X/C location inner and outer frame design bending moments and hoop forces for all of the double wall concepts were nearly the same because their cross-sectional stiffnesses were not significantly different. These loads were not sensitive to small changes in the outer shell thickness. This was significant because it meant that the same internal pressure shell design could be used for all the double wall concepts and that corresponding frames of all the outer shell designs would have the same design loads. The results of the interaction analyses for the X/C locations at 0.375 and 0.75 are presented in figures 50 and 51, in which bending moments in the inner and outer frame composites are plotted for various loading conditions. As can be seen from these figures, the maximum bending moments in the upper and lower halves of the frames X/C = 0.75 would be nearly the same, so that the frames could be designed with uniform cross sections. However, at X/C = 0.375, the bending moments over the upper halves of the inner and outer frames would be many times smaller than those over the lower halves. Thus, for a realistic design these frames should not have uniform cross sections. The upper and lower halves of each frame should be designed for the maximum upper and lower moments, respectively, in order to obtain a lighter design. Table IX summarizes the ultimate design loads for the inner and outer frame composites at X/C = 0.75 and at X/C = 0.375 (top and bottom).

Analyses were also performed to estimate the design loads for inner and outer frames at X/C = 0.164 based upon those for X/C = 0.375, without actually going through the interaction analyses. Loads were found to be proportional to frame spacing (35 instead of 24 inches at X/C = 0.164), pressures, and appropriate dimension squared. These results are included in table IX.

3.5.3.1.4 Stiffener requirements

For each ablator design, the flat portions of the vehicle at various locations were analyzed to determine the need for stiffeners. The pertinent loading conditions for this area of the vehicle were:

   1   buckling under in-plane loads of ascent,

   2   bending under max "q" reentry pressures for + 250° F, 12 g undershoot reentry, and

TABLE IX

FRAME DESIGN LOADS, DOUBLE WALL CONCEPTS

Location		Double Wall Concepts Ultimate Frame Design Loads				Design Condition	
		Inner		Outer			
		Moment in. -lb.	Force lb.	Moment in. -lb.	Force lb.	Inner	Outer
X/C = 0.164	(upper)	-21735	18165	6680	-5100	2	3
	(lower)	-99400	12425	-26600	-2230	2	4
X/C = 0.375	(upper)	-46600	14300	14300	-4030	2	3
	(lower)	-213000	9780	-44000	-1760	2	4
X/C = 0.750		96500	9225	-25000	-1310	1	3

Positive Moment ~ Tension inner fibers

Legend: Design Condition

1. Ultimate internal pressure, zero external loads.

2. Ultimate internal pressure, limit reentry loads.

3. Ultimate reentry loads, zero internal pressure.

4. Ultimate reentry loads, limit internal pressure.

<u>3</u>   bending under approach to touchdown pressures.

For the bending analyses three analogies were considered, namely:

   <u>a</u>   For no stiffener, an isolated strip of composite, 24. 0 inches long and 1. 0 inch wide, clamped at both ends.

   <u>b</u>   For the 8-inch stiffener spacing, an 8-inch span of composite plus stiffener, clamped on both ends.

   <u>c</u>   For the 16-inch stiffener spacing, a 16-inch span of composite, plus stiffener, clamped at both ends.

   Based on the established design condition for each concept, weight minimization studies were conducted involving honeycomb core depth, stiffener spacing and frame weights.

<u>1</u>   <u>Laminated ablator</u>

For the laminated ablator design, the flat portions of the vehicle at X/C = 0. 375, 0. 75 were analyzed. Analyses indicated that approach to touchdown was the design condition for the substructure at all three locations, occurring when the substructure has reached 700° F and the remaining ablator is structurally ineffective. At station X/C = 0. 75 the required honeycomb core depth was 0. 33 inches. Figure 52 shows that the moment-carrying ability of the laminated ablator design for the + 250° F reentries is considerably greater than what is actually required for those conditions.

Figure 53 shows the effect of the honeycomb core depth on the moment-carrying capability of the composite for no stiffener and for 8- and 16-inch spacing of the stiffener. Note that, for the design moment of 83 in-lbs/in. , the 8-inch stringer spacing is considerably overdesigned for minimum gauge core depth.

Figure 54 shows the weight of fiberglass versus bending moment for the no stiffener and 8- and 16-inch spacing cases. It is apparent that, for the design moment of 83 in-lbs/in. at X/C = 0. 75 and 88. 6 in-lbs/in. at X/C = 0. 375, the section with no stringer is lighter. Therefore,

there is no reason to use stiffeners for the substructure
of the laminated ablator along the bottom surface.

2   Filled H/C ablator

For the filled H/C ablator design, the flat portion of the
vehicle at $X/C = 0.75$ was investigated. Analyses indi-
cate that the $+ 250°F$ reentry condition would dictate the
design at $X/C = 0.75$ requiring a honeycomb core depth
of 1.35 inch. Figure 55 shows the effect of the honeycomb
core depth on the moment-carrying ability per unit width
of the composite for no stiffener, and for the 8- and 16-
inch spacings of the stiffener shown in the figure. Note
that, for the design moment of $260 \frac{\text{in. -lbs.}}{\text{in.}}$ (ult.), the
8-inch stiffener spacing indicates the smallest honeycomb
core depth. Figure 56 shows the weight of fiberglass
(stiffener and substructure only) versus bending moment
for the no stiffener and 8- and 16-inch spacing cases.
Here, the 8-inch spacing case appears to be the minimum
weight design. However, the fiberglass weights which ap-
pear in figure 56 do not include the weights of the circum-
ferential frames. Frame design calculations, which in-
cluded 24-inch effective width of the shell acting with the
frame, indicated an increased frame weight for the 8-inch
stiffener spacing case, due to the reduced honeycomb core
depth over that required for the no-stiffener case. Total
combined structural weights for the no-stiffener and 8-inch
stiffener spacing cases were found to be equal, thereby
cancelling the need for longitudinal stiffeners for the sub-
structure of the filled H/C ablator.

3.5.3.2 Structural sizing of outer shell

Various representative locations and sections of the outer shell of
the vehicle were idealized as simple geometrical shapes and
analyzed as composites to determine substructure requirements
enabling each integrated design to survive the imposed loading
conditions. A fiberglass honeycomb substructure was designed
for both the filled H/C and laminated ablators for reentry velocities
of 26,000 and 36,500 feet per second.

Analyses of a composite shell differ from those of a homogeneous

one in that the integrals $\int EdZ$, the extensional stiffness (B), and

$$\int \frac{E}{1-\nu^2} Z^2 dZ,$$ the bending rigidity (D), where the neutral axis

location is defined by $\int E Z dZ = 0,$ must be used instead of their

homogeneous shell counterparts of Et and $\dfrac{Et^3}{12(1-\nu)^2}$, respectively.

Formulae for homogeneous shell deflections, cross sectional loads, and buckling pressures or loads can be rederived in terms of B and D, and then used for composite shell calculations. Then, given a cross sectional force per inch of width, N, and a moment, M, in lbs/in., the resulting stress in any particular layer of the composite section may be obtained by solution of the following equation:

$$\sigma_i = E_i \left[\frac{N}{B} + \frac{MC_i}{\overline{EI}} \right],$$

where,

$$\overline{EI} \equiv \int E Z^2 dZ$$

The structural analyses of the various representative body sections chosen for investigation are presented below. A summary of the required fiberglass substructure thicknesses and the particular design conditions which governed these thicknesses for each location is presented in table X. In each analysis, the substructure was idealized as either a sphere, cone, cylinder or flat plate, as the case may apply, for each major portion of the vehicle such as the nose cap, main body, elevons and fins. Various geometries and dimensions used in the structural analyses are shown in figures 57 through 59.

3.5.3.2.1 Nose cap

The nose cap of the vehicle extends from $X/C = 0.06$, a distance of 20 inches. It consists of a spherical shell, of radius 15.75 inches, that fairs into a short cone, the dimensions of which are given in figure 57. Because of the difficulty of forming honeycomb to shapes of high curvature, fiberglass sheet construction and molded ablator were selected for this area of the vehicle.

-64-

TABLE X

DOUBLE WALL--INTEGRATED FIBERGLASS SHELL, STRUCTURAL SIZES AND WEIGHTS

Body Location	Ablator	Structure h_c (in.)	$t_{F.S.}$ (in.)	Weight	Design Condition
Nose Cap	Lam., F.H.C.	t = 0.05 in.		0.458 lb/ft^2	4(a)
Nose Cone	Lam., F.H.C.	t = 0.083		0.761	4(a)
1st cone (upper)	Lam., F.H.C.	0.100	0.02	0.603	4(a)
2nd cone (upper)	Lam., F.H.C.	0.154	0.02	0.623	4(a)
3rd cone (upper)	Lam., F.H.C.	0.215	0.02	0.646	4(a)
X/C = 0.375 (lower)	Lam.	0.240	0.02	0.654	4(b)
	F.H.C.	1.520	0.03	1.308	3(b)
X/C = 0.500 (upper)	Lam.	0.320	0.02	0.684	4(a)
	F.H.C.	0.430	0.02	0.725	3(a)
X/C = 0.500 (lower)	Lam.	0.33	0.02	0.688	4(b)
	F.H.C.	1.900	0.03	1.448	3(b)
X/C = 0.750 (upper)	Lam.	0.740	0.02	0.839	1
	F.H.C.	0.920	0.02	0.905	1
X/C = 0.750 (lower)	Lam.	0.310	0.02	0.680	4(b)
	F.H.C.	1.320	0.03	1.235	3(b)
Lower Sides	Lam., F.H.C.	0.100	0.02	0.603	4(a)
Elevons	Lam.	0.262	0.02	0.663	4(b)
	F.H.C.	2.080	0.02	1.330	3(b)
		Height (in.)	Area (in.)		
FRAMES X/C = 0.164 (upper)	Lam.	1.250"	0.251	0.066	3(c)
	F.H.C.	1.250	0.287	0.075	3(c)
X/C = 0.164 (lower)	Lam.	1.250	0.158	0.041	3(c)
	F.H.C.	2.500	0.647	0.169	3(b)
X/C = 0.375 (upper)	Lam.	2.000	0.420	0.160	3(c)
	F.H.C.	2.000	0.434	0.166	3(c)
X/C = 0.375 (lower)	Lam.	2.500	0.930	0.355	3(c)
	F.H.C.	3.500	1.802	0.688	3(b)
X/C = 0.750	Lam.	2.250	0.565	0.216	3(c)
	F.H.C.	2.750	0.906	0.346	3(b)

Legend: Design Condition

1. Buckling at Ascent
2. Space Flight
   a. Buckling due to shell interactions
   b. Bending, cracking of the ablator
   c. Bending, substructure failure
3. Reentry
   a. Buckling
   b. Bending, cracking of the ablator
   c. Bending, failure of the substructure
4. Approach to Touchdown
   a. Buckling
   b. Bending

The design criterion for the spherical shell portion of the nose cap was buckling under net external pressure. The maximum environmental pressures (external minus internal) experienced during a mission would be 14.7 psi for max "q" abort; 15.7 psi at maximum dynamic pressure for a 12 g undershoot reentry; and 1.66 psi at approach to touchdown, which represents 0.66 psi dynamic pressure plus a 1.0 psi lag in venting. In computing cross sectional bending rigidities and extentional stiffnesses, any ablator above 600° F was considered structurally ineffective.

Approach to touchdown when no ablator would be effective proved to be the structural design condition for both the molded ablator and the laminated ablator designs, requiring a fiberglass thickness of 0.05 inch. For ascent and reentry the effective ablator thicknesses strengthened the cross section more than enough to withstand the higher pressures. For instance, based upon ablator thicknesses for a 26,000 fps reentry, the margin of safety in buckling for the molded ablator design was 6.8 for ascent.

The cone section of the nose cap would be subjected to pressures of 6.9 psi for max "q" abort, 13.3 psi at max "q" reentry, and 1.56 psi at approach to touchdown. The structural design condition for both ablator designs again proved to be approach to touchdown, and required a fiberglass thickness of 0.083 inch.

3.5.3.2.2 Cone Sections, Upper Surface, X/C = 0.06 to 0.375

That portion of the upper surface of the vehicle from station X/C = 0.06 to 0.375 was idealized as three separate cone configurations. In each instance, the approach to touchdown once again was the design condition for both ablator designs, because the presence of the ablators during ascent and reentry provided enough stiffness for the shell to enable it to withstand the higher pressures.

<u>1 First Cone, Upper Surface, X/C = 0.06 to 0.164</u>

The first cone idealized the upper surface of the vehicle just aft of the nose cap (see figure 57). Its design criterion was buckling under external pressure. For a -15 degree angle of attack abort at max "q", the limit lateral pressure would be 2.2 psi. The maximum pressure expected during a 12 g reentry would be 2.35 psi at the side tangent, and at approach to touchdown it would be 1.1 psi. On the leeward side, with the ablator thickness for a 26,000 fps reentry, the reentry margin of safety

for the filled H/C ablator design was 1.0 and for the laminated ablator design was 2.90. Structural sizes are presented in table X.

2 Second Cone, Upper Surface, X/C = 0.164 to 0.268

The second cone represents an approximation of the upper surface of the vehicle just aft of the first cone and extends from X/C = 0.164 to 0.268 (see figure 57). Just as for the first cone, its design criterion was buckling under external pressure. For a -15 degree angle of attack abort at max "q", the limit lateral pressure would be 1.12 psi with an axial load of 8500 pounds. At max "q" reentry, the pressure would be 2.35 psi, and the axial force, 11,400 pounds. For the approach to touchdown condition, the pressure would be 1.1 psi.

3 Third Cone, Upper Surface, X/C = 0.268 to 0.375

The third cone represents an approximation of the upper surface of the vehicle between the second cone and the manufacturing break at X/C = 0.375 (see figure 57). It would be subjected to lateral pressures of 1.05 psi at max "q" abort, 2.35 psi at max "q" reentry, and 1.1 psi at approach to touchdown. The required fiberglass honeycomb thicknesses are included in table X.

3.5.3.2.3 Cylinder, Upper Surface, X/C = 0.5

The upper surface of the vehicle at X/C = 0.5 was idealized as a portion of a cylindrical shell, of radius 80 inches and length 24 inches. The severest ascent condition would be the initiation of a +15 degree angle of attack abort, which would produce an axial compressive load of 360 lbs/in. with essentially zero net lateral pressure. During max "q" reentry, the top portion of the cylinder would be subjected to an axial compressive load of 213 lbs/in. and a lateral pressure of 1.0 psi, while the side of the cylinder would have zero axial load and a pressure of 2.35 psi. The touchdown condition would produce a bukling pressure of 1.1 psi.

Based upon a +250° F, 26,000 fps reentry, the reentry condition of buckling under a 213 lbs/in. axial load and 1.0 psi lateral pressure designed the structure for the filled H/C ablator. The margin of safety for the ascent condition was 0.87, and for the touchdown condition was 1.25.

The critical condition for the laminated ablator design, how-
ever, was buckling under the approach to touchdown pressure.
For this design the higher strength of the laminated ablator
enabled the touchdown-designed structure to withstand the
reentry condition with a margin of safety of 0. 66, whereas
the weaker filled honeycomb ablator required more structure
to survive the same condition.   Table X lists the structural
thicknesses required for the two designs.

3. 5. 3. 2. 4   Flat Plate, Upper Surface, $X/C = 0.75$

The relatively flat top surface of the vehicle at $X/C = 0.75$,
just in front of the assumed ascent fairing tie-in to the
vehicle and on either side of the central hump, was idealized
as a flat plate 24 inches long and 60 inches wide (see figure
59 and figure 86 in section 4.2).

For a +15° angle of attack max "q" abort, the overall vehicle
axial load and bending moment (see figure 43) would produce
a limit compressive load of 560 lbs/in. in the plate accom-
panied by negligible net lateral pressure.   The max "q"
reentry line loads and pressures on the plate would be quite
small, and the approach to touchdown condition would impose
a lateral pressure of 1. 04 psi on the plate.

The design criteria for the plate are buckling under the
ascent in-plane compressive loads and bending under the
touchdown pressure.   For the ascent condition, the plate
was analyzed as simply supported on all four sides, and the
corresponding buckling formula[14] used was $N_{CR} = \frac{1.35 \, \pi^2 D}{L^2}$
For the case of bending under the touchdown pressure, the
plate was assumed to be clamped on the two ends at the
frame locations to simulate bending over the frames.

Ascent buckling proved to be the critical design condition
for both concepts, and the required substructure, reported
in table X provided margins of safety for the touchdown con-
dition of 3. 7 and 2. 8 for the filled H/ C and the laminated
ablator designs, respectively.

3. 5. 3. 2. 5   Flat Plate, Lower Surface, $X/C = 0.75$

This location on the flat bottom surface of the vehicle is
just in front of where the ascent fairing is assumed to tie in
to the vehicle and on either side of the center closure strip.
Its behavior is characterized by that of a flat plate between

frames, 24 inches long and 60 inches wide (see figure 59 and figure 86 in section 4.2).

For an initiation of a -15° angle of attack abort, the overall vehicle axial load and bending moment would produce a limit compressive load of 407 lbs/in. in the plate accompanied by negligible net lateral pressure. At max "q" reentry, the plate would be subjected to a tensile load of 86.4 lbs/in., a lateral external pressure of 3.57 psi, as well as thermal stresses (especially for a -250° F reentry), all of which tend to put the ablator in tension at the frame locations. At approach to touchdown, the plate would be subjected to a pressure of 1.15 psi.

The design criteria for the plate are buckling under the ascent in-plane compressive loads; bending under the reentry pressure, superimposed on an axial load and thermal stresses; and bending under the touchdown pressure. For the bending conditions, it was assumed to be clamped on the two ends at the frame locations to simulate bending over the frames. The plate was actually wide enough so as to analyze it as a longitudinal strip clamped on each end.

The performance of the two designs differed considerably at this location due to the large differences in strength and brittleness of two ablators. The critical condition for the laminated ablator design was the touchdown condition of bending under external pressure when the structure was hot (700° F) and no ablator was effective. The presence of the ablator on the structure during ascent provided enough stiffness to enable the plate to withstand buckling with a safety margin of 2.07. The performance of the laminated ablator design during reentry is shown in figure 52. This ablator's high stiffness and good ultimate strain capability ($\epsilon_{ult} = 1.2$ percent) would enable it to survive reentry with the large margin of safety evident in that figure. At maximum dynamic pressure for a +250° F initial reentry condition, which would occur 51 seconds after the start of entry, the thermal stresses throughout most of the composite would be small and would have little effect on the moment carrying capability of the composite. For a -250° F initial reentry condition, however, the thermal stresses would be more significant, as can be seen in figure 60. At this temperature the modulus of elasticity of the laminated ablator would be double its value at +250° F, and the additional stiffness this would give to the cross section would more than offset the detrimental effect of the thermal stresses in the moment carrying ability of the section, as evidenced in figure 52.

Unlike the laminated ablator's substructure, that for the
filled H/C ablator was designed by the reentry condition.
This ablator's structural performance in the bending environ-
ment of this condition would be considerably less than that of
the laminated ablator because of its lower stiffness and much
lower ultimate strain (0.4 percent versus 1.2 percent) as is
evident from figure 52. Cracking of the ablator was the design
criterion rather than failure of the substructure. The per-
tinent formular used in the analyses is the following:

$$\epsilon_{ULT} = 0.004 = \epsilon_{Thermal\ Stress} + 1.5\ \frac{N}{B} + 1.5\ \frac{MC_A}{D}$$

where

$$B = \int EdZ$$

$$D = \int \frac{E}{1-\nu^2}\ Z^2\ dZ$$

and where N = axial load/inch, M = cross sectional moment/
inch, and $\epsilon_{thermal\ stress}$ is the strain at a point in the
ablator due to the thermal stresses.

Typical thermal strains at max "q" reentry for a +250° F
and a -250° F initial temperature are plotted in figures 61
and 62. As can be seen, the +250° F thermal strains are
quite small. Although thermal stresses would be significant
in a -250° F reentry, the ablator at this temperature would
be stiff enough ($E = 0.25 \times 10^6$) so that the effect of the
thermal stresses would be more than offset by the additional
stiffness of the ablator relative to the +250° F condition. For
a +250° F reentry, the stiffness of the ablator would be low
enough ($E = 0.02 \times 10^6$) so that despite the absence of a
thermal stress problem the +250° F reentry would be the
critical design condition. This is evident in figure 52.

The substructure required to prevent cracking of the filled
H/C ablator for the +250° F, 36,500 fps initial reentry con-
dition consisted of 0.030 inch face sheets and a honeycomb
core height of 1.32 inch, which was only 0.02 inch more
than what was needed for the ablator thickness of a 26,000
fps reentry. These dimensions differ significantly from those
for the laminated ablator which requires 0.020 inch face sheets
and 0.31 inch core height.

3.5.3.2.6 Flat Plate, Lower Surface, X/C = 0.5

This flat plate, 24 inches long and 44 inches wide, represents
an approximation of the bottom surface of the vehicle at
X/C = 0.5 on either side of the center closure strip (see
figure 57). For a -15 degree angle of attack initiation of
abort, the overall vehicle axial load and bending moment
would produce a limit compressive load of 262 lbs/in. in
the plate. At max "q" reentry, the plate would be subjected
to a tensile load of 171 lbs/in., a lateral external pressure
of 4.75 psi, and thermal stresses, all tending to put the
ablator in tension. At approach to touchdown, the plate
would be subjected to a pressure of 1.20 psi.

The design criteria for the plate are buckling under the
ascent loads, and bending under the reentry and touchdown
pressures. For the buckling analyses, the plate was assumed
simply supported on all four sides, and for the bending
analyses, it was treated as a longitudinal strip 24 inches long
clamped at each end.

As in the case of the plate at X/C = 0.75, the laminated
ablator's substructure was designed by the approach to
touchdown bending condition. The ablator's stiffness was
sufficient to enable the composite to survive the ascent and
reentry environment with margins of safety of 8.0 and 1.4,
respectively.

The +250°F initial reentry condition again designed the sub-
structure for the filled H/C ablator because the low stiff-
ness and ultimate allowable strain of the ablator required a
stiff substructure to prevent cracking of the ablator. Despite
the presence of thermal stresses in a -250°F initial reentry
condition (see figure 62) the increased stiffness of the
ablator would enable the design to survive that condition
with a margin of safety of 0.72.

The design substructure for the filled H/C ablator consisted
of 0.030 inch face sheets and 1.90 inch core height, while
0.020 inch face sheets and 0.31 inch core height was sufficient
for the laminated ablator design.

3.5.3.2.7 Flat Plate, Lower Surface, X/C = 0.375

This flat plate, 36 inches long and 17 inches wide, idealized
the bottom surface of the vehicle bounded between the center
closure strip on one side, the axial load transfer longeron on
the other side, and the frames at X/C = 0.268 and 0.375 at
each end (see figure 57).

-71-

During ascent this plate would be only lightly loaded with a compressive load of 89 lbs/in. for a -15° angle of attack abort or a lateral pressure of 0.96 psi for a +15° angle of attack abort. Max "q" reentry would impose a tensile load of 127 lbs/in. and a lateral pressure of 5.44 psi, and the approach to touchdown pressure would be 1.23 psi. For the bending conditions, this plate was assumed to be simply supported along the two sides with the ends clamped at the frame locations.

The touchdown condition when all of the ablator would be ineffective designed the structure of the laminated ablator. As for the plates at $X/C = 0.5$ and 0.75, the high stiffness and allowable strain of the laminated ablator strengthened the cross section enough to enable it to survive the higher loads of reentry with a margin of safety of 2.3.

Reentry at +250° F again proved to be the critical design condition for the filled H/C ablator substructure. The structure was designed to be stiff enough to prevent the ablator from cracking, which was a more severe criterion than failure of the substructure itself. The margin of this composite for a -250° F initial reentry would be 1.12. Structural sizes are included in table X.

3.5.3.2.8 Lower Cylindrical Sides

The lower sides of the vehicle between the side and bottom tangent lines (see figure 57) are approximated by 90° cylindrical panels of radius 15.8 inches extending between the frames. The design criteria for these were buckling under the external pressures of ascent, reentry, and approach to touchdown, which for the lower cylindrical side in the first cone area would be 5.7 psi, 12.5 psi, and 1.53 psi, respectively.

The critical condition for both designs was the approach to touchdown which, because of the small radius of the cylinder, required a honeycomb core height of only 0.1 inch. The presence of the ablator during reentry stiffened the shell enough to give it a margin of safety of 6.3 with the filled H/C ablator.

In an actual design, the core height in the lower side area would be determined by fairing between the values required for the bottom and top surfaces of the vehicle, and the value

of 0. 1 inch would only represent a minimum allowable
height rather than the actual design height.

3. 5. 3. 2. 9 Elevons

The two full depth elevons would be deflected downwards 20°
for an L/D max reentry. At max "q", the pressure on the
bottom surface would be 7. 5 psi and on the upper surface
would be about 1. 0 psi. At approach to touchdown, assuming
there is a 1. 0 psi lag in venting, the lower surface net pressure
would be 1. 31 psi, which includes 0. 31 psi dynamic pressure.

The design criteria for the elevons were bending under the
reentry and touchdown pressures. For the structural
analyses, two ribs were assumed as shown in figure 58. The
upper and lower surfaces were analyzed by isolating a lateral
strip and treating it as a beam on four equidistant supports
subjected to uniform pressure.

The critical condition for the upper and lower surfaces in
the laminated ablator design was the approach to touchdown.
The ablator would provide enough stiffness to the cross sec-
tion to enable it to survive the larger reentry pressures
with a margin of safety of 3. 4.

The critical design condition for the upper surface of the
filled H/C ablator's substructure was the approach to touch-
down condition because of the small loads at other times,
but the +250°F max "q" reentry was the critical condition
for the lower surface. Just as in the case of the flat plate
locations on the bottom surface of the vehicle, the low stiff-
ness and ultimate allowable strain of the ablator would create
a need for a stiff substructure to prevent ablator cracking.
Based upon 0. 020 inch face sheets, a core height of 2. 08
inch would be required as contrasted to a core height of 0. 26
inch for the laminated ablator design.

3. 5. 3. 2. 10 Fins

The two tail fins would be subjected to external pressures
of 2. 35 psi at max "q" reentry and 1. 1 psi at approach to
touchdown, assuming the one psi lag in venting occurs in the
fin. Figure 58 depicts the structural arrangement in the fin.
A flat panel 43 inches by 26 inches, simply supported at the
top, bottom and on one side, and clamped on the fourth side,
was selected to represent the structure.

Bending under the approach to touchdown pressure was the
design condition for the laminated ablator's substructure.
Again, the presence of the ablator during max "q" reentry
stiffened the plate enough for it to withstand that condition
with a margin of safety of 3. 3.

The bending environment of a +250° F reentry proved to be
the critical condition for the filled H/C ablator design. A
stiff substructure would be required to prevent cracking of the
ablator because of its low ultimate strain to failure. Based
upon 0. 020 inch face sheets, the required honeycomb core
depth would be 1. 58 inch as contrasted to a core height of
0. 49 inch needed in the laminated ablator design.

3. 5. 3. 2. 11 Outer Shell Frame Designs

Based upon the design moments and hoop forces shown in
table IX, outer shell frames were designed at $X/C = 0. 75$,
0. 375, and 0. 164. In each case the loads were imposed on
a composite cross section of a frame and an effective width
of shell of 24 inches at $X/C = 0. 75$ and 0. 375, and 35 inches
at $X/C = 0. 164$.

1 Frame, $X/C = 0. 75$

The condition of max "q" reentry and zero internal
pressure in the inner shell would cause the severest
loads at this location. For both ablator designs reentry
at +250° F proved to be more critical than at -250° F

-74-

despite the presence of thermal stresses, because of
the increased stiffness of the ablators and fiberglass at
that temperature.

For the laminated ablator design buckling of the inner
flange of the frame was the failure criterion. Its margin
of safety for a -250°F reentry was 0.58. The frame for
the filled H/C ablator's substructure was designed to be
stiff enough to prevent ablator cracking, which proved
to be the design criterion rather than buckling of the
frame because of the ablator's low ultimate strain to
failure. Its margin of safety for a -250°F reentry was
0.86. The required frame sizes are listed in table X.

2 Frame, $X/C = 0.375$

The critical condition for the bottom half of the frame
at $X/C = 0.375$ was max "q" reentry with 7 psi in the
inner pressure shell. Again, the +250°F reentry was
more critical than the -250°F for both designs, the
margins of safety being 0.58 and 1.4 for the laminated
and filled H/C ablator composites, respectively. From
table X it can be seen that the frame required to pre-
vent cracking of the filled H/C ablator was considerably
heavier than the one required for the laminated ablator.

The critical condition for the top half of the frames at
$X/C = 0.375$ was max "q" reentry with zero internal
pressure in the inner shell. This condition would load
the ablator in compression so that tensile cracking
would not occur. Rupture of the frame inner flange
would be the failure criterion for both designs.

3 Frame, $X/C = 0.164$

The design loads for the upper and lower outer frame
halves at $X/C = 0.164$ occurred for the same conditions
as those for $X/C = 0.375$, and the failure criteria were
correspondingly the same as discussed in the section
for frames at that location. Frame weights are pre-
sented in table X.

3.5.3.3 Inner Pressure Vessel Design

An aluminum pressure vessel of honeycomb construction was designed for the double wall concepts to contain 7 psi internal pressure and to encompass as much usable internal volume as possible. Structural areas, frame locations, and inner-outer shell attachment points were the same as those previously selected for the outer shell design. Structural design criteria governing the analyses are listed in section 3.5.1.

3.5.3.3.1 Load Environment

During normal flight conditions the pressure vessel was assumed to contain a limit pressure of 7 psi. However, to account for possible leakage or a malfunction it was also required to survive a one psi net external pressure venting lag. In addition, the pressure vessel was maintained at a constant 70°F temperature throughout the entire mission.

Other loading conditions imposed on the pressure vessel would be those caused by the inertia of the internal masses during ascent and reentry, and by interactions between the inner and outer shells. These interaction loads would occur when the outer shell as a whole bends under imposed loads or temperatures when one side of the vehicle is hot (+250°F) and the other side is cold (-250°F). These space flight conditions caused the severest thermal bending of the outer shell and thus the worst inner-outer shell interactions.

A brief discussion is presented here to describe how the inner-outer shell interaction loads were derived. As is mentioned in the section on space flight deflections of the outer shells, 3.5.3.4.3, there is no relative motion permitted between the inner and outer shells at X/C = 0.375. To determine interaction loads the inner and outer shells were considered as two beams, one inside the other, constrained to permit only relative motion in the longitudinal direction, imposing zero slope change and deflection conditions at X/C = 0.375. Loading conditions were taken from the space flight deflection analyses for the laminated ablator design, which produced the larger thermal deflections for the conditions of bottom hot-top cold and top hot-bottom cold. From these relationships for the outer shell, inner shell reaction moments were computed by considering the relative stiffnesses of the two shells and are shown in figure 63. Axial tensile and compressive loads for

both the upper and lower surfaces of the inner shell for these
reaction moments were then evaluated.

3.5.3.3.2 Structural Design

A summary of structural sizes, unit weights, and critical
design conditions appears in table XI.

1   Frames

Inner shell frames were designed at vehicle X/C loca-
tions of 0.164, 0.375, and 0.75. The analyses were com-
plicated by the fact that because of the attachment points
between the inner and outer shells, frame designs for
either shell were dependent upon the other (see section
3.5.3.1). A summary of frame design loads and geo-
metries is presented in tables IX and XI, respectively.

At X/C = 0.75 a frame of uniform cross-section was
found to be sufficient to satisfy the design condition of
14 psi ultimate internal pressure. At stations X/C = 0.164
and 0.375 separate designs for the locations were found to
be inefficient because of the large difference between design
loads at the upper and lower attachment points. The con-
dition of limit max "q" reentry and 14 psi ultimate internal
pressure produced the design frame loads at X/C = 0.375
and 0.164.

2   Nose Cap

The nose cap consists of a spherical shell of radius 13.3
inches fairing into a cone of height 8.6 inches and 15
inches base radius. The design condition for both was
buckling under the lag in venting condition.

3   First Cone

The first cone section, corresponding to the first cone of
the outer shell (see figure 57) was idealized as an equiva-
lent cylinder of radius 20.8 inches. The design condition
was buckling under a maximum compressive line load of
744 lbs/in. (ult) caused by space flight interactions while
the pressure shell was vented.

4   Second Cone

The second cone (see figure 57) was idealized as an
equivalent cylinder of radius 31.3 inches and length 36.4

-77-

TABLE XI

INNER ALUMINUM PRESSURE VESSEL
Structural Sizes and Weights

Body Location	Structure		Weight (lb/ft^2)	Design Condition
Nose Cap	t = 0.014 in.		0.204	4(a)
Nose Cone	t = 0.022		0.320	4(a)
	h_c	$t_{F.S.}$		
1st cone (upper)	.110	0.010 in.	0.429	2(a)
2nd cone (upper)	.132	0.010	0.436	2(a)
3rd cone (upper)	0.180	0.010	0.459	2(c)
X/C = 0.375 (lower)	0.867	0.015	0.861	2(a)
X/C = 0.500 (lower)	1.081	0.015	0.941	2(a)
X/C = 0.500 (upper)	.27	0.010	0.492	2(a)
X/C = 0.750 (lower)	1.020	0.015	0.919	2(c)
X/C = 0.750 (upper)	0.970	0.015	0.900	2(c)
	Height (in.)	Area (in^2)		
FRAMES X/C = 0.164 (lower)	2.25	0.970	0.403	3(c)
X/C = 0.164 (upper)	1.50	0.354	0.147	3(c)
X/C = 0.375 (upper)	2.75	0.445	0.270	3(c)
HC = 0.375 (lower)	4.00	1.465	0.888	3(c)
X/C = 0.750	3.50	0.839	0.317	2(c)

Legend: Design Condition

1. Buckling at Ascent
2. Space Flight
   a. Buckling due to shell interactions
   b. Bending; cracking of the ablator
   c. Bending; substructure failure
3. Reentry
   a. Buckling
   b. Bending; cracking of the ablator
   c. Bending; failure of the substructure
4. Approach to Touchdown
   a. Buckling
   b. Bending

inches. Its design condition, the same as for the first cone, was buckling under an ultimate load of 720 lbs/in.

5   Third Cone--Upper Surface

Buckling under space flight interaction loads (718 lbs/in) for a vented condition designed the third cone upper surface, idealized as an equivalent cylinder having a radius of 41.87 inches and a length equal to 37.45 inches.

6   Third Cone--Lower Surface (X/C = 0.375

Axial load transfer longerons along the lower surface at this location (see figure 57) resulted in the structure being idealized as a flat plate, clamped on all four sides, having a length and width of 36 inches and 22 inches, respectively. The combined effects of a compressive space flight interaction load and the internal pressure loading produced a bi-axial stress condition in the plate at the longeron location, and yielding of the inner face sheet at the center of the longeron was the design criterion.

7   X/C = 0.50--Upper Surface

Space Flight interaction loads when the shell was vented proved to be the design condition at this location. The upper surface structure at X/C = 0.50 was considered to be an equivalent cylinder having a radius equal to 77.50 inches, and a length of 24.0 inches. A uniform, ultimate compressive line load of 432 pounds per inch was the design buckling load.

8   X/C = 0.75--Upper Surface and Lower Surface

For the upper surface at X/C = 0.75 and lower surface at X/C = 0.75 and 0.50, a unit width strip 24.0 inches long, clamped on both ends, was considered under the combined loadings of bending over the frame and axial tension due to the ultimate internal pressure of 14.0 psi, and the axial tensile forces due to the appropriate space flight interaction. The resulting designs for the three areas are included in table XI.

9   Aft Bulkhead

The aft portion of the pressure vessel was considered to be closed off by a flat bulkhead at X/C = 0.85 and a

semicylindrical tube inside the rear hump, extending
back between the elevons to the end of the vehicle (see
figure 86 in section 4.2). The portion of the bulkhead
on either side of the tube was analyzed as a flat plate of
honeycomb construction, 29.5 inches high, 56.7 inches
long, simply supported on all four sides, and loaded by
lateral pressure. The cylindrical tube was designed for
buckling under the one psi lag in venting condition.

3.5.3.4 Thermal Stresses and Deflections

3.5.3.4.1 Cold Soak (-250°F)

When fabricating either the filled H/C or laminated ablator
vehicles the material would be bonded to the fiberglass struc-
ture and then cured at a temperature of 200°F. This then
would become the zero stress level temperature for the cross-
section of the composite. When the temperature of the com-
posite is changed, the different thermal strains of both the
ablator and fiberglass substructure would induce thermal
stresses. If it is assumed that plane sections of the com-
posite remain plane and there is no net force over the cross
section and changes in curvature are suppressed, then the
thermal stresses can be calculated by using the following
formula:

$$\sigma = \frac{E}{1-\nu}\, \epsilon, \text{ where: } \epsilon = \left\{ \frac{\displaystyle\int \frac{E\,\alpha\Delta T}{1-\nu}\, dz}{\displaystyle\int \frac{E}{1-\nu}\, dz} - \alpha\,\Delta T \right\},$$

ΔT is measured from 200°F and the integrals are through
the thickness.

When the temperature is lowered to -250°F, $\Delta T = -450°$, the
resulting thermal interaction stresses and strains could be
significant. In figures 64 and 65, ablator strains and fiber-
glass stresses, based upon the material properties given in
table II, are plotted as a function of the ablator/fiberglass
thickness ratio. Notice that the larger the ratio, the smaller
are the ablator strains but the larger are the fiberglass
stresses. The laminated ablator causes higher fiberglass
stresses than the filled H/C ablator because of its greater
stiffness and thermal strain, but the margin of safety of the
laminated ablator in a composite would be considerably higher

than that of the filled H/C ablator because of the latter's much lower ultimate strain to failure (0.4 versus 1.2 percent).

Figures 66 and 67 present the effect of varying the soak temperature on the ablator strains and fiberglass stresses for two different values of the ablator/fiberglass thickness ratio in ablator-fiberglass composites. The closer the soak temperature is to the zero stress temperature of 200°F, the smaller are the induced thermal stresses and strains.

3.5.3.4.2 Thermal Stresses during Reentry

During reentry, time dependent thermal stresses would be induced within any ablator-fiberglass cross section because of the varying temperatures and temperature-dependent material properties through the thickness. These stresses, computed by the same formula presented in the previous paragraph, would have to be superimposed on stresses due to any applied loads in order to obtain total stresses in the ablator and fiberglass.

Figures 68 through 81 present typical ablator strain-time and fiberglass stress-time histories for the L/D max, 36,500 fps, overshoot trajectory at a point on the lower and upper surface of the vehicle for both ablator designs and for reentries starting at initial temperatures of +250°F and at -250°F. Ablator strain-time histories are more meaningful than stress-time histories because the ultimate strain to failure of both ablators is nearly constant over a wide range of temperatures, but the ultimate allowable stress is strongly temperature-dependent, so that it would not be immediately apparent from a stress-time history how near the ablator is to failure unless the temperature-dependent ultimate stresses are plotted on the same graph.

A comparison of figure 68 to figure 70 and of figure 76 to figure 78 indicates that the greatest tensile and compressive strains in both ablator designs would occur for a -250°F rather than a +250°F reentry. Moreover, the large tensile strains in a -250°F reentry would occur in cold layers of the ablator when they would still have considerable strength, but in a +250°F reentry the tensile strains would become large in an ablator layer only when the temperature is high and the ablator is structurally ineffective. Furthermore, the stresses in the fiberglass substructure would be more severe for the -250°F initial reentry condition (see figures 69, 71, 77, and 79). Thus, reentry at -250°F produces a more severe thermal

loading environment than reentry at +250°F. However, it must be pointed out that in computing margins of safety for a design, the stresses and strains due to external loading must be superimposed on the thermal ones to give the total state of stress or strain in the materials. Since at -250°F the moduli of elasticity of the ablators and fiberglass are greater than at +250°F, the section is stiffer and was shown in paragraph 3.5.3.2.5 to be capable of carrying more load than at +250°F, despite the larger thermal stresses.

At the start of a -250°F reentry, the composite would be in a state of cold soak thermal stress. Figures 70 and 78 show that the thermal strain at a point in the ablator increases over its cold soak value unitl the temperature pulse reaches the point, whereupon the strain starts to diminish. The greatest ablator tensile strain would occur at the backface of the ablator and could be considerably higher than the cold soak value.

The severest reentry pressures and decelerations would occur at max "g" for an L/D max, 12 g undershoot trajectory, 51 seconds after the start of reentry. Figures 60 through 62 are plots of thermal strains through the thickness of the filled H/C and laminated ablator designs at $X/C = 0.5$ on the bottom side of the vehicle for that time. Ablator strains due to the external loading would have to be superimposed on those strains to find the true state of strain in the ablator. Note that the strains due to a +250°F reentry (figure 61) are negligible compared to those for a -250°F reentry (figure 62).

3.5.3.4.3 Space Flight Deflections

Space flight deflections of the outer shell were computed for both the filled H/C and laminated ablator designs. Environmental conditions of bottom hot (+250°F)--top cold (-250°F) and of top hot-bottom cold were investigated. The temperature distributions used in the analyses are shown in figure 82. Results of the deflection analyses are presented in table XII and longitudinal ablator strains around the circumference at a typical station are plotted in figures 83 and 84.

1   Temperature Distribution

For the computation of temperature distributions, steady state space flight conditions were assumed in which the vehicle did not change its orientation with respect to the sun, the primary external energy source. Based upon

-82-

TABLE XII

STRUCTURAL SHELL--SPACEFLIGHT DEFLECTIONS*
(36,500 fps ablator thicknesses)

	Vehicle Nose		Vehicle Tail	
	Vertical (positive up) (inches)	Axial elongation (inches)	Vertical (positive up) (inches)	Axial elongation (inches)
Filled H/C Ablator design--top hot, bottom cold	-0.44	-0.32	-1.78	-0.63
Filled H/C Ablator design--top cold, bottom hot	0.35	-0.32	1.54	-0.56
Laminated Ablator design--top hot, bottom cold	-0.65	-0.35	-2.34	-0.78
Laminated Ablator design--top cold, bottom hot	0.52	-0.38	2.16	-0.70

*Zero deflection and rotation at $X/C = 0.375$.

the assumption of negligible heat flow through the thickness and around the circumference, the temperature at any location on the side of vehicle facing the sun was computed using the following formula for radiation equilibrium temperature:

$$K_s\, a \cos \theta = \sigma \epsilon\, (T_{wall})^4$$

where K_s is the solar flux constant of 442 Btu/hr-ft^2, θ is the incidence angle, T_{wall} is the wall temperature in degrees Rankine, a and ϵ are the ablator's absorptivity and emissivity, respectively, and σ is the Stefan-Boltzman constant. For absorptivity equal to emissivity, the maximum wall temperature at zero incidence angle was +250°F.

At all points on the shadow side of the vehicle, where there would be no incoming solar radiation, a minimum temperature of -250°F was used. It was found that the heat conduction through the wall thickness necessary to keep the surface temperature from falling below -250°F would produce a temperature rise of only a few degrees through the thickness, so that the use of uniform temperatures through the thickness for the structural analyses was justified.

At the sun-shadow (90°) interface, a fairing process was used to insure a continuous solution.

As a check on the validity of neglecting circumferential heat flow, an analytical method by Charnes and Raynor,[15] which yields temperature distributions while considering circumferential heat transfer, was applied. It was found that the change in distribution caused by circumferential heat flow was negligible due to the large size of the vehicle and the small conductivity of the ablator.

2   Deflection Analyses

For analytical purposes, the entire outer shell was considered as a free beam composed of five segments representative of sections at X/C = 0. 125, 0. 300, 0. 500, 0. 750, and 0. 950. Conditions of zero slope and deflection were imposed at X/C = 0. 375, because this was the vehicle location at which there is no relative motion between the inner and outer shells.

Thermal moments and axial forces were computed for each average cross section mentioned above, and were then applied at the ends of each respective beamlike segment. Resulting deflections, listed in table XII, represent the gross deformation of the outer shell relative to $X/C = 0.375$. Figures 83 and 84 represent longitudinal ablator strains around the circumference of the vehicle at $X/C = 0.75$.

3.5.4 Double Wall Concept: Nonintegrated Designs

3.5.4.1 Fiberglass Outer Shell

In addition to the integrated fiberglass outer shells previously considered, nonintegrated shells of similar construction were analyzed for each of the two ablators considered. In this instance the load-carrying ability of the ablators was ignored, which meant that each fiberglass substructure was required to take all the loads by itself as if the ablator were not present. In addition, the requirement was made that the ablator should not crack, which meant that the composite section had to be stiff enough to prevent this from occurring.

The areas of the vehicle analyzed and the applied loads were the same as those discussed in section 3.5.3.2 for the integrated designs. Results of the analyses are presented in table XIII along with the critical design conditions for each area.

The entire top surface of the vehicle's outer shell, including the spherical and conical regions of the nose, the cylinder at $X/C = 0.5$, and the palte at $X/C = 0.75$, were designed by buckling criteria. Because the presence of the ablator was ignored, the honeycomb core heights of the structure had to be increased over those required for the integrated designs in order to provide the necessary stiffness to the substructure. However, the in-plane loads were low enough so that no increase in face sheet thickness was required.

For the laminated ablator's substructure, the areas of the vehicle shell designed by bending under reentry loads (i.e., the flat bottom locations, elevons, and fins) required some increase in core heights over its integrated counterpart to enable the fiberglass structure alone to take the loads, but no increase in face sheet thicknesses was necessary. Because of the strain capabilities of the laminated ablator, cracking of the ablator was not a design problem.

TABLE XIII

DOUBLE WALL-FIBERGLASS SHELL
STRUCTURAL SIZES AND WEIGHTS

Body Location	Ablator	Structure		Weight	Design Condition
Nose Cap	Lam., F.H.C.	$t = 0.11$ in.		1.008 lb/ft^2	3(a)
Nose Cone	Lam., F.H.C.	$t = 0.17$		1.558	3(a)
		h_c (in)	$t_{F.S.}$ (in)		
1st cone (upper)	Lam., F.H.C.	0.145	0.02	0.620	3(a)
2nd cone (upper)	Lam., F.H.C.	0.220	0.02	0.647	3(a)
3rd cone (upper)	Lam., F.H.C.	0.300	0.02	0.677	3(a)
X/C = 0.375 (lower)	Lam.	0.417	0.02	0.720	3(c)
	F.H.C.	1.530	0.03	1.308	3(b)
X/C = 0.500 (upper)	Lam., F.H.C.	0.480	0.02	0.743	1, 3(a)
X/C = 0.500 (lower)	Lam.	0.628	0.02	0.797	1
	F.H.C.	1.900	0.03	1.447	3(b)
X/C = 0.750 (upper)	Lam., F.H.C.	1.040	0.020	0.948	1
X/C = 0.750 (lower)	Lam.	0.715	0.020	0.829	1
	F.H.C.	1.320	0.030	1.234	3(b)
Lower Sides	Lam., F.H.C.	0.300	0.020	0.677	3(a)
Elevons	Lam.	0.594	0.020	0.785	3(c)
	F.H.C.	2.080	0.020	1.230	3(b)
Fins	Lam.	0.492	0.020	0.747	4(b)
	F.H.C.	1.580	0.020	1.147	3(b)
		Height (in)	Area (in^2)		
FRAMES X/C = 0.164 (upper)	Lam.	1.250	0.287	0.075	3(c)
	F.H.C.	1.250	0.287	0.075	3(c)
X/C = 0.164 (lower)	Lam.	2.500	0.726	0.190	3(c)
	F.H.C.	2.500	0.648	0.169	3(b)
X/C = 0.375 (upper)	Lam.	2.000	0.434	0.166	3(c)
	F.H.C.	2.000	0.434	0.166	3(c)
X/C = 0.375 (lower)	Lam.	2.750	1.189	0.454	3(c)
	F.H.C.	3.500	1.802	0.688	3(b)
X/C = 0.750	Lam.	2.500	0.642	0.245	3(c)
	F.H.C.	2.750	0.906	0.346	3(b)

Legend: Design Condition

1. Buckling at Ascent
2. Space Flight
   a. Buckling due to shell interactions
   b. Bending, cracking of the ablator
   c. Bending, Substructure failure
3. Reentry
   a. Buckling
   b. Bending, cracking of the ablator
   c. Bending, failure of the substructure
4. Approach to Touchdown
   a. Buckling
   b. Bending

Structural sizes in the areas designed by bending for the filled H/C ablator's substructure, however, remained the same as for its integrated counterpart because of the requirement that the ablator should not crack. A substructure stiff enough to prevent albator cracking was more than strong enough to take the loads by itself, as can be readily seen from table XIII by comparing the bottom surface nonintegrated laminated ablator's structure to that of the filled H/C ablator's structure.

The frames with their effective widths of shell would be subjected to the same loads and conditions as those discussed in section 3.5.3.2 for the integrated designs. Without the presence of the ablator on the effective width of shell, the laminated ablator substructure frames had to be increased in size in order to take the loads. However, for the filled H/C ablator substructure, those frames that had been sized to prevent ablator cracking in the integrated design were more than strong enough to take the loads by themselves, so that they were sufficient for the nonintegrated design, too. The difference between requiring the frames to take loads by themselves and requiring, in addition, that they be stiff enough to prevent the filled H/C ablator from cracking can be readily seen from table XIII by comparing the laminated to the filled H/C frame designs.

3.5.4.2 Steel Outer Shell

In order to compare the fiberglass double wall designs to an existing metallic double wall concept, stainless steel honeycomb outer shell for each of the two ablators was analyzed, based upon the same maximum bond line temperature of 700°F. The shell would enclose the same inner aluminum pressure vessel as would the fiberglass designs. This concept of a steel honeycomb outer shell and an aluminum honeycomb inner shell is typical of the Apollo space craft, which is presently being built. In this design, the load-carrying ability of the ablator was ignored in the analyses, and the substructure was again required to be stiff enough to prevent cracking of the ablator.

Design details of the steel outer shells, such as frame spacings, inner-outer shell attachment locations, and locations of manufacturing breaks, were taken as the same as those for the fiberglass outer shells. The particular type of stainless steel assumed for the analyses was PH 15-7 Mo TH 1050. For minimum gauge face sheets of 0.008 inch thickness, which were found to be sufficient at all vehicle locations where honeycomb was used, the honeycomb core density was 5.6 lbs/ft^3, based on 1/8 inch cell size.

TABLE XIV

DOUBLE WALL -- STEEL SHELL STRUCTURAL SIZES AND WEIGHTS

Body Location	Ablator	Structure		Weight	Design Condition
Nose Cap	Lam., F.H.C.	t = 0.042 in.		1.675 lb/ft^2	3(a)
Nose Cone	Lam., F.H.C.	t = 0.068		2.712	3(a)
		h_c	$t_{F.S.}$		
1st cone (upper)	Lam., F.H.C.	0.100 in.	0.008 in.	0.883	3(a)
2nd cone (upper)	Lam., F.H.C.	0.100	0.008	0.883	3(a)
3rd cone (upper)	Lam., F.H.C.	0.124	0.008	0.894	3(a)
X/C = 0.375 (lower)	Lam.	0.213	0.008	0.935	3(c)
	F.H.C.	0.912	0.008	1.268	3(b)
X/C = 0.500 (upper)	Lam., F.H.C.	0.246	0.008	0.951	1
X/C = 0.500 (lower)	Lam.	0.322	0.008	0.989	1
	F.H.C.	1.042	0.008	1.323	3(b)
X/C = 0.750 (upper)	Lam., F.H.C.	0.530	0.008	1.086	1
X/C = 0.750 (lower)	Lam.	0.452	0.008	1.047	1
	F.H.C.	0.802	0.008	1.211	3(b)
Lower Sides	Lam., F.H.C.	0.132	0.008	0.900	3(a)
Elevons	Lam.	0.103	0.008	0.836	3(c)
	F.H.C.	0.742	0.008	1.185	3(b)
Fins	Lam.	0.100	0.008	0.885	4(b)
	F.H.C.	0.562	0.008	1.101	3(b)
		Height	Area		
X/C = 0.164 (upper)	Lam	1.000 in	0.081 in^2	0.092 lb/ft^2	3(c)
	F.H.C.	1.000	0.081	0.092	3(c)
X/C = 0.164 (lower)	Lam.	1.500	0.211	0.240	3(c)
	F.H.C.	1.500	0.233	0.266	3(b)
X/C = 0.375 (upper)	Lam.	1.250	0.143	0.238	3(c)
	F.H.C.	1.250	0.143	0.238	3(c)
X/C = 0.375 (lower)	Lam.	2.000	0.293	0.489	3(c)
	F.H.C.	2.500	0.338	0.562	3(b)
X/C = 0.750	Lam.	1.600	0.165	0.274	3(c)
	F.H.C.	1.800	0.185	0.307	3(b)

(The last group of rows is labeled "Frames")

Legend: Design Condition

1. Buckling at Ascent
2. Space Flight
    a. Buckling due to shell interactions
    b. Bending, cracking of the ablator
    c. Bending, substructure failure
3. Reentry
    a. Buckling
    b. Bending; cracking of the ablator
    c. Bending; failure of the substructure
4. Approach to Touchdown
    a. Buckling
    b. Bending

The areas of the vehicle analyzed and the applied loads and temperature environments were the same as those discussed in section 3.5.3.2 for the double wall fiberglass designs. The two requirements of having the structure able to withstand the applied loads without the aid of the ablator and not allowing the ablator to crack, produced the design conditions and failure criteria of the various vehicle areas for the two ablator designs to be exactly the same as their nonintegrated fiberglass outer shell counterparts, which were discussed in detail in section 3.5.4.1.

Structural sizes and critical design conditions for the representative areas on the steel honeycomb substructure for both the laminated and filled H/C ablator designs are listed in table XIV. Just as for the fiberglass structure the differences in structural design, considering both ablators, were due to the criterion of no ablator cracking, which required stiffer frames and substructure along the bottom surface of the vehicle for the filled H/C ablator than for the laminated ablator.

3.5.5 Single Wall Concept-Aluminum Shell (Filled H/C Ablator)

A single aluminum shell vehicle of honeycomb construction, covered with the filled H/C ablator, was designed to contain 7 psi internal pressure and perform the same missions as the double wall vehicles. The load-carrying ability of the ablator was not relied upon in the analyses, but, consistent with the previously described concepts, the ablator-structure composite was required to be stiff enough to prevent ablator cracking. The structural design criteria governing the analyses are in section 3.5.1, and a description of the loading environments is in section 3.5.2.

The following paragraphs summarize the structural design. A 2014-T6 aluminum alloy was used for the face sheets, and 7075-T6 for the frames. The honeycomb core density was 4.5 lbs/ft^3. A sketch of the vehicle, showing the selected frame locations, is in figure 85, and dimensions and unit weights of the structure at representative locations on the vehicle are presented in table XV.

3.5.5.1 Frame Spacing Trade-Offs

Weight trade-off studies were performed for Stations X/C = 0.375 and 0.75 along the bottom surface of the vehicle to determine optimum frame spacing for the single-wall concept, subjected to the space flight loading environment of internal pressure and no external loads.

TABLE XV

SINGLE WALL-ALUMINUM SHELL (FILLED H/C ABLATOR)
Structural Sizes and Weights

Body Location	Structure		Weight (lb/ft^2)	Design Condition
Nose Cap	0.065 in.		0.945	3(a)
Nose Cone	0.100		1.454	3(a)
	h_c	$t_{F.S.}$		
1st cone (upper)	0.100 in.	0.010 in.	0.429	3(a)
2nd cone (upper)	0.107	0.010	0.431	3(a)
3rd cone (upper)	0.148	0.010	0.446	3(a)
X/C = 0.375 (lower)	0.995	0.015	0.909	2(b)
X/C = 0.500 (upper)	0.315	0.010	0.509	3(a)
X/C = 0.750 (upper)	0.885	0.015	0.868	2(b)
X/C = 0.750 (lower)	0.945	0.015	0.891	2(b)
Elevons (upper)	0.100	0.010	0.428	4(b)
Elevons (lower)	1.140	0.020	1.109	3(b)
Fins	0.880	0.020	1.012	3(b)
Aft Bulkhead	1.16	0.020	1.115	2(c)
	Height	Area		
FRAMES — X/C = 0.208 (upper)	2.50 in.	0.610 in^2	0.444	3(b)
FRAMES — HC = 0.208 (lower)	4.00	1.720	1.251	3(b)
FRAMES — X/C = 0.375 (upper)	3.50	0.910	0.662	3(b)
FRAMES — X/C= 0.375 (lower)	5.00	4.552	3.310	3(b)
FRAMES — X/C = 0.750	4.00	1.924	1.399	2(b)

Legend: Design Condition

1. Buckling at Ascent
2. Space Flight
   a. Buckling due to shell interactions
   b. Bending, cracking of the ablator
   c. Bending, substructure failure
3. Reentry
   a. Buckling
   b. Bending, cracking of the ablator
   c. Bending, failure of the substructure
4. Approach to Touchdown
   a. Buckling
   b. Bending

The first part of the analyses involved determining the required honeycomb core depths and face sheet combinations for frame spacing of 20, 24, 30, and 36 inches. The analytical model consisted of a unit width strip of honeycomb construction running longitudinally between frames, and clamped at both ends at the frame locations. The applied loads consisted of lateral pressure and axial tension due to the internal pressure.

Results indicated that face sheet thicknesses of 0.015 inch provided a lighter design for the strip than 0.010 or 0.012 inch for frame spacings of 24 to 36 inches, and was only 1-1/2 percent heavier than the 0.012 inch face sheet design for the 20 inch frame spacing. Accordingly, face sheet thicknesses of 0.015 inch were selected.

The frame analyses consisted of treating a composite frame section composed of an "I" section frame with an effective width of shell equal to the frame spacings of 20, 24, 30, and 36 inches. The face sheet thicknesses of the shell were 0.015 inch; the minimum core heights for each frame spacing case were the ones obtained in the strip analyses.

The composite frame section for each frame spacing was subjected to the moments and hoop forces produced by the internal pressure, and frames were designed to enable the composite section to resist the loads. Combined wieghts of frame and shell were than computed for each frame spacing.

Results indicated that the 20 inch spacing provided lighter designs at both $X/C = 0.375$ and 0.75 than did the other spacings. For instance, at $X/C = 0.375$, spacings of 24 and 30 inches provided designs that were 12 and 37 percent heavier than the 20 inch spacings, and at $X/C = 0.75$, the corresponding weight increases over the 20 inch spacing design were 6 and 22 percent respectively. Since spacings of much less than 20 inches would not be practical in an actual design, smaller spacings were not considered, and 20 inch spacing was selected for the vehicles.

3.5.5.2 Structural Design

a) Nose Cap

The nose cap, consisting of a spherical shell that fairs into a short cone, has the same dimensions as the one for the double wall concepts shown in figure 57. Buckling under max "q" reentry pressure with the vehicle vented was the design criterion for both the spherical shell and the cone.

-91-

b)   Cone sections, upper surface, A/C = 0.06 to 0.386

The upper surface of the vehicle from X/C = 0.06 to 0.386
was idealized as separate cone configurations extending between
frame locations.   Three cones were analyzed: between X/C =
0.06 to 0.133, from X/C = 0.208 to 0.267, and from X/C =
0.327 to 0.386.   The design condition for all three was buckling
under the pressures of max "q" reentry when the vehicle was
vented.

c)   X/C = 0.50--Upper Surface

The upper surface of the vehicle at X/C = 0.500 was idealized
as a portion of a cylinder of 80.0 inches radius, with a length
of 20.0 inches.   Buckling due to the max "q" reentry loads
designed the structure, considered to be at a temperature of
+250°F.

d)   X/C = 0.75--Upper Surface

The structure at this location was idealized as a unit width
strip between frames spaced at 20.0 inches, clamped at both
ends.   The design condition, to prevent cracking of the filled
honeycomb ablator, was a combination of bending and axial
tension due to ultimate internal pressure.

e)   Lower Surface, X/C = 0.375 and 0.75

Locations along the flat lower surface of the vehicle were
idealized as unit width strips, clamped at each end at the
frame locations, subjected to lateral pressure and axial
force caused by the internal pressure in the vehicle in space
flight which was a more severe condition than max "q" reentry.
The criterion of design was to prevent the filled H/C ablator
from cracking.

f)   Elevons

A honeycomb structure with two supporting ribs was the result-
ant design for the elevons (see figure 58).   The criterion of
preventing the filled honeycomb ablator from cracking pro-
duced designs for the lower surface of the elevons under
influence of max "q" reentry pressures, while the approach
to touchdown designed in the upper surface.

g) Fins

Each fin was structurally idealized as a 26.0 inch by 43.0 inch
plate, clamped on one edge and simply supported along the
remaining three sides (see figure 58). Cracking of the filled
honeycomb ablator under the bending loads of max "q" reentry
pressure was the design criterion.

h) Aft Pressure Bulkhead

The pressurized portion of the aluminum shell was considered
to be closed off by a flat bulkhead at $X/C = 0.85$ and a semi-
cylindrical tube forming the rear hump, extending back between
the elevons to the end of the vehicle (see figure 85). The
bulkhead, completely enclosed within the outer shell, would
have a layer of insulation but no ablator protecting it. The
portion of the bulkhead on either side of the tube was analyzed
as a flat plate of honeycomb construction, 33 inches high,
56.7 inches long, simply supported on all four sides, and
loaded by lateral pressure. The cylindrical tube was designed
for buckling under the one psi lag in venting condition.

i) Frames

For the single wall concept, frames were designed at body
locations of $X/C = 0.208$, 0.375, and 0.75. In arriving at the
design loads for the frames, internal inertia load locations
were chosen in the same locations as for the double wall con-
cepts, and the same vertical posts were used for the frame
at $X/C = 0.75$ (see figure 47 and 49). An effective width of
shell of 20 inches was taken to act with the frame cross sections
in resisting the applied loads. The condition of ultimate
internal pressure and limit reentry produced ultimate design
loads for frames at $X/C = 0.208$, and 0.375, while those for
the frame at $X/C = 0.750$ resulted from a condition of ultimate
internal pressure only (space flight). At both X/C locations of
0.208 and 0.375 there were different frame designs for the
upper and lower portions of the frames, due to the large
differences in magnitude of the design loads at these respec-
tive positions, while at $X/C = 0.750$, this difference was
small enough to permit a frame design of uniform cross
section.

At $X/C = 0.208$ the upper and lower portions of the frame
composites were subjected to bending moments of 16180 in. -
lbs. and 69540 in. -lbs., (ablator in tension) and tensile loads
of 8980 lbs. and 6550 lbs., respectively. At $X/C = 0.375$,

the design loads for the upper and lower areas of the vehicle were bending moments of 37200 in. -lbs. and 204,000 in. -lbs. (ablator in tension) and tensile loads of 9750 lbs. and 7130 lbs., respectively.

The frame composite at X/C = 0.75 was designed for an ultimate moment of 89460 in. -lbs. and a tensile load of 6420 lbs.

Cracking of the ablator proved to be the critical design condition for all the frames. The resulting frame dimensions and weights appear in table XV.

3.5.6 Single Wall Concept-Aluminum Shell (Laminated Ablator)

In addition to the structural sizing of an aluminum shell for use with the filled H/C ablator, one was also sized for the laminated ablator. The only difference in the two sets of analyses was that cracking of the laminated ablator was not a critical condition at any location because of its increased strain capability whereas cracking of the filled H/C ablator was the design condition at many locations. The structure for the laminated ablator only had to be stiff enough to take the applied loads by itself; it was not required to be stiffer.

The results of the analyses are presented in table XVI. Note that the frame weights, especially at X/C = 0.375, are considerably lighter than the corresponding ones in table XV for the filled H/C ablator design.

3.5.7 Total Structure Weights

Total structure weights were computed for the integrated and non-integrated fiberglass shells, the steel shells, and the single aluminum shells, for both the filled honeycomb and laminated ablators. A structure weight was also calculated for the inner aluminum pressure shell. Table XVII summarizes the results of these calculations. In all cases the structures required to support the filled honeycomb ablator were heavier than those required for the laminated ablator. However, it should be noted that when the combined weights of ablator (see table XVIII) and structure were considered, the filled honeycomb ablator provided the more efficient design.

For each total weight calculation, the individual design face sheet, bond, core and frame weights were calculated in pounds per square foot, then integrated along the vehicle length to obtain the total desired structure weight. For each double shell concept, an additional weight of 50 pounds was added to account for the inner-outer shell attachment fittings, and 71 pounds added to account for edge closure members along the top and bottom closure strips of the outer shell.

TABLE XVI

SINGLE WALL - ALUMINUM SHELL (LAMINATED ABLATOR)
STRUCTURAL SIZES AND WEIGHTS

Body Location	Structure		Weight	Design Condition
Nose Cap	0.065 in.		0.945 lb/ft^2	3 (a)
Nose Cone	0.100		1.454	3 (a)
	h_c (in.)	$t_{F.S.}$(in.)		
1st cone (upper)	0.100	0.010	0.429	3 (a)
2nd cone (upper)	0.107	0.010	0.431	3 (a)
3rd cone (upper)	0.148	0.010	0.446	3 (a)
X/C = 0.375 (lower)	0.617	0.015	0.767	2 (c)
X/C = 0.500 (upper)	0.315	0.010	0.509	3 (a)
X/C = 0.500 (lower)	0.633	0.015	0.773	3 (c)
X/C = 0.750 (upper)	0.619	0.015	0.768	2 (c)
X/C = 0.750 (lower)	0.640	0.015	0.776	2 (c)
Elevons (upper)	0.100	0.010	0.428	4 (b)
Elevons (lower)	0.316	0.020	0.800	3 (c)
Fins	0.211	0.020	0.761	3 (c)
Aft Bulkhead	1.16	0.020	1.115	2 (c)
	Height(in)	Area (in^2)		
FRAMES X/C = 0.208 (upper)	1.500	0.277	0.201	3 (c)
X/C = 0.208 (lower)	2.250	0.775	0.563	3 (c)
X/C = 0.375 (upper)	2.750	0.393	0.286	3 (c)
X/C = 0.375 (lower)	4.000	1.615	1.174	3 (c)
X/C = 0.750	3.500	0.759	0.552	2 (c)

Legend: Design Condition

1. Buckling at Ascent
2. Space Flight
   a. Buckling due to shell interactions
   b. Bending, cracking of the ablator
   c. Bending, substructure failure

3. Reentry
   a. Buckling
   b. Bending, cracking of the ablator
   c. Bending, failure of the sub-structure
4. Approach to Touchdown
   a. Buckling
   b. Bending

TABLE XVII

TOTAL STRUCTURE WEIGHTS
(Pounds)

Structure	Nose Area	Elevon.	Fin	Shell	Frame	Total
Integrated Fiber-glass (outer shell)						
a. Laminated	8	120	72	618	129	947
b. Filled H/C	8	242	111	782	218	1361
Nonintegrated Fiber-glass (outer shell)						
a. Laminated	17	143	72	675	156	1063
b. Filled H/C	17	242	111	797	218	1385
Nonintegrated Steel (outer shell)						
a. Laminated	36	161	86	800	181	1264
b. Filled H/C	36	216	107	859	200	1418
Aluminum Pressure Vessel (Inner Shell)	4	---	---	413	242	659
Aluminum Single Shell						
a. Laminated	16	95	60	503	380	1054
b. Filled H/C	16	96	98	635	953	1798
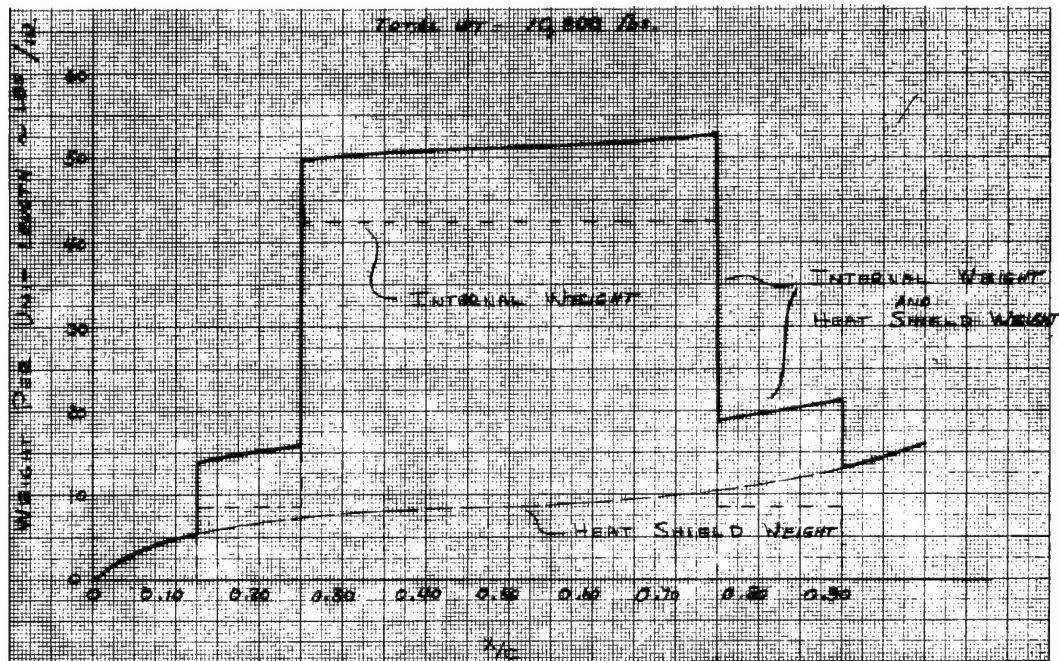
Figure 40 VEHICLE WEIGHT DISTRIBUTION
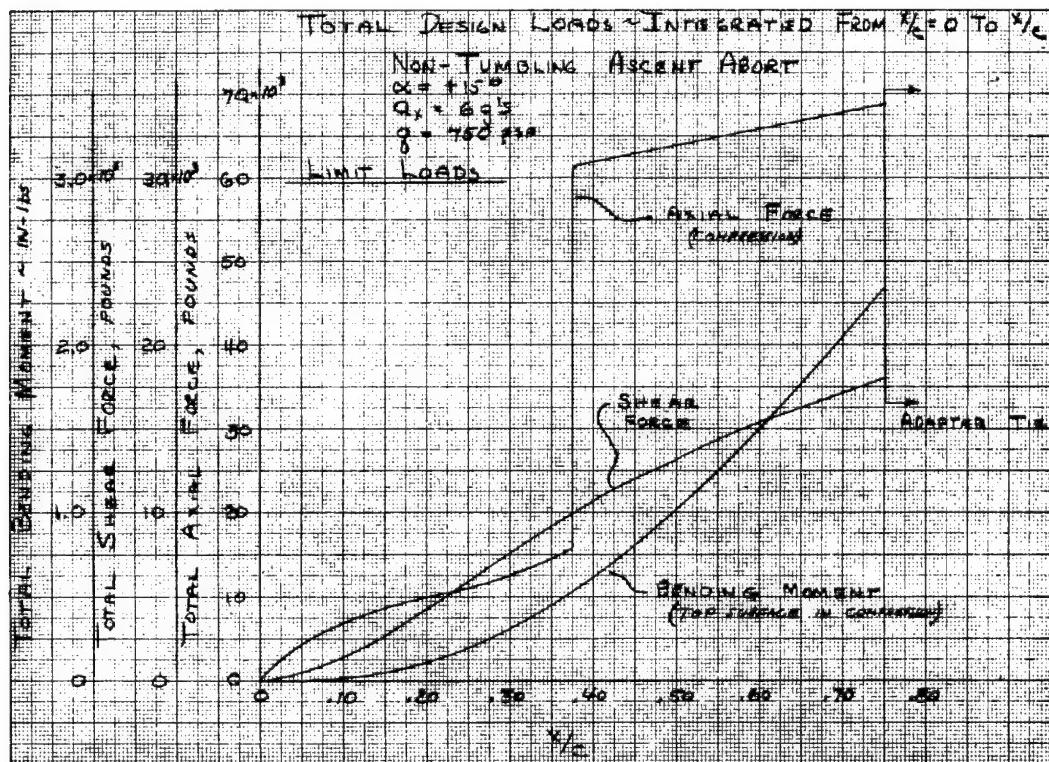
Figure 41 VEHICLE CROSS SECTIONAL LOADS, START OF max "q" ABORT, $\alpha = +15°$
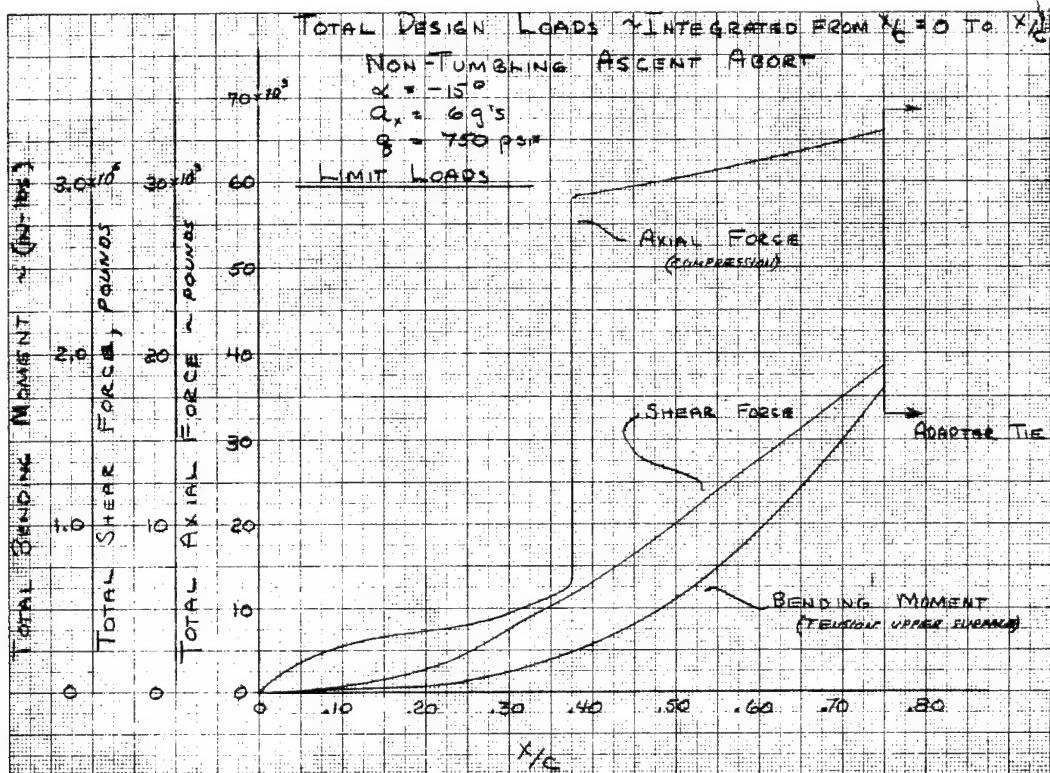
Figure 42 VEHICLE CROSS SECTIONAL LOADS, START OF max "q" ABORT, a = -15°
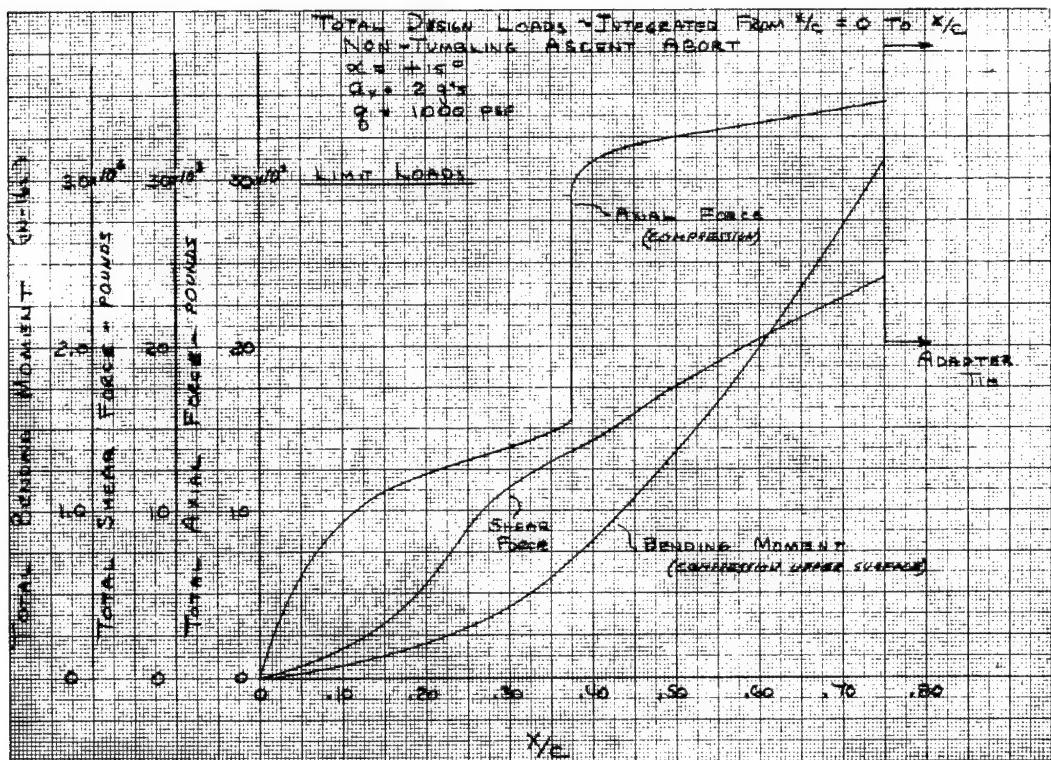
Figure 43 VEHICLE CROSS SECTIONAL LOADS, END OF max "q" ABORT, a = +15°
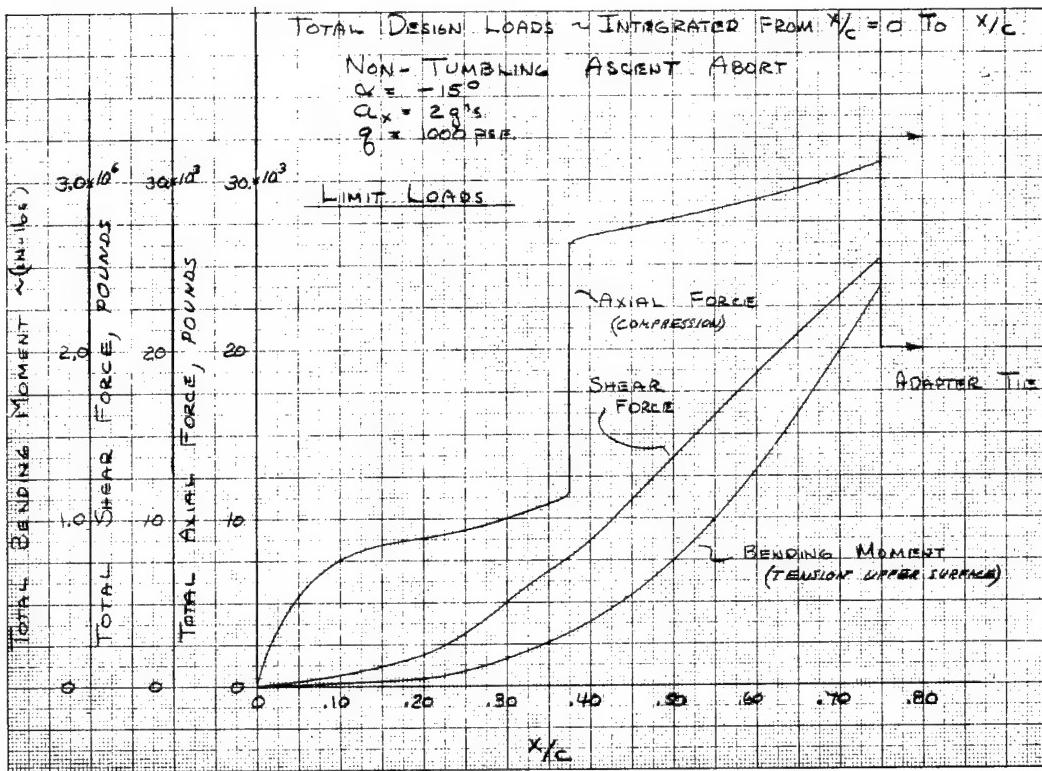
Figure 44 VEHICLE CROSS SECTIONAL LOADS, END OF max "q" ABORT, a =-15°
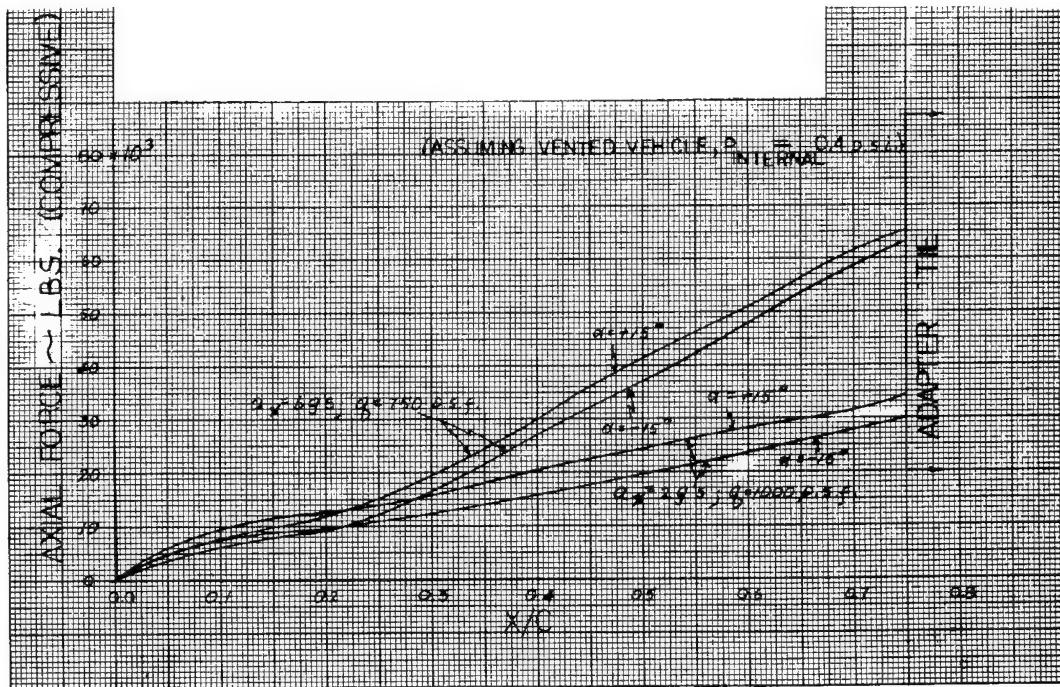
Figure 45 CROSS SECTIONAL AXIAL FORCES, ASCENT ABORT, ALUMINUM SINGLE
SHELL CONCEPT
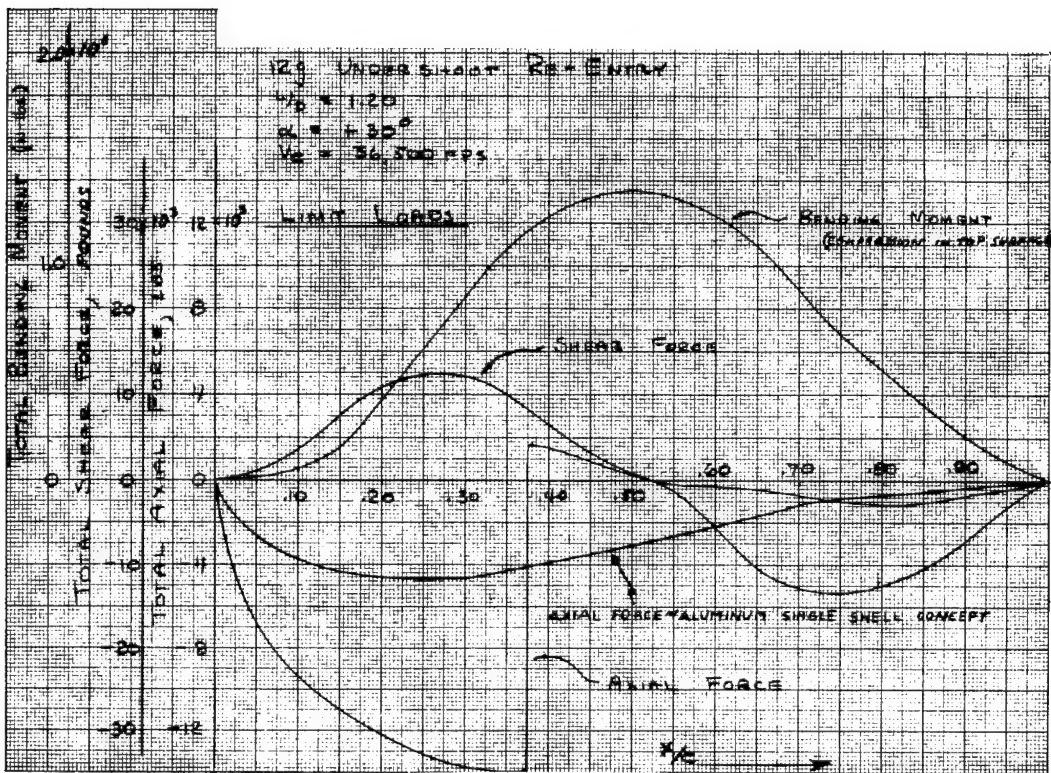
Figure 46 VEHICLE CROSS SECTIONAL LOADS, max "q" 12 g UNDERSHOOT REENTRY
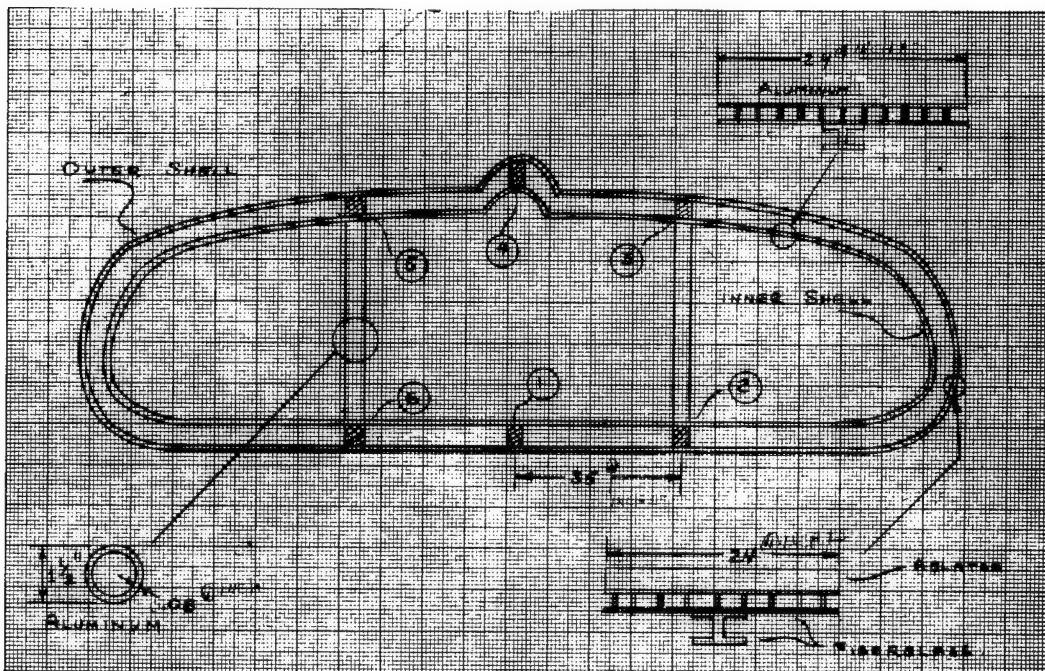
Figure 47 FRAME ATTACHMENT LOCATIONS AT X/C = 0.75
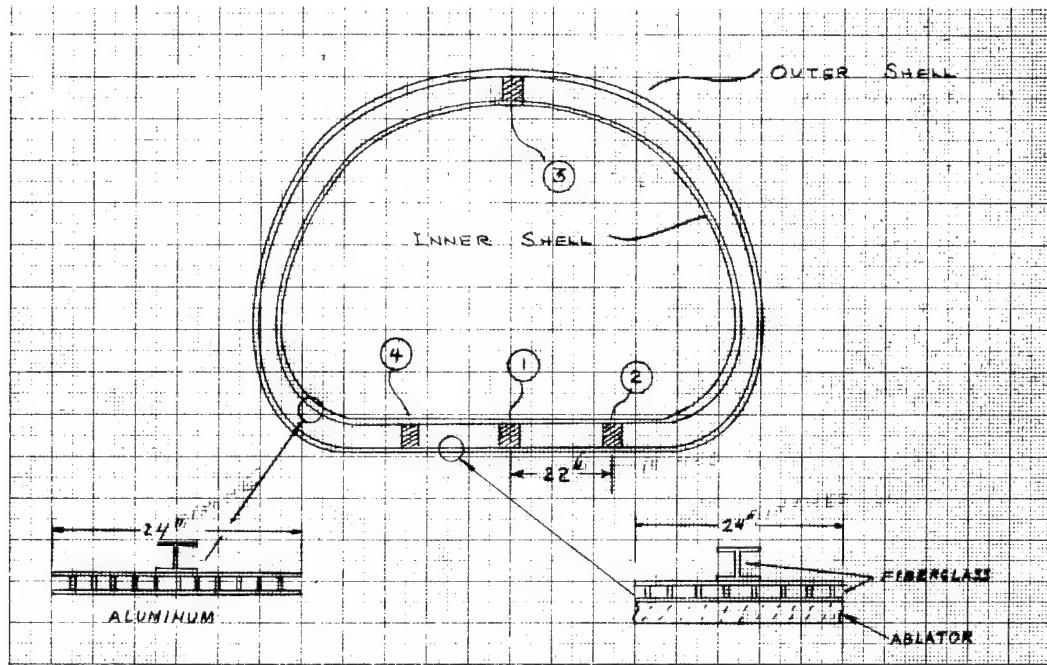
Figure 48 FRAME ATTACHMENT LOCATIONS AT X/C = 0.375
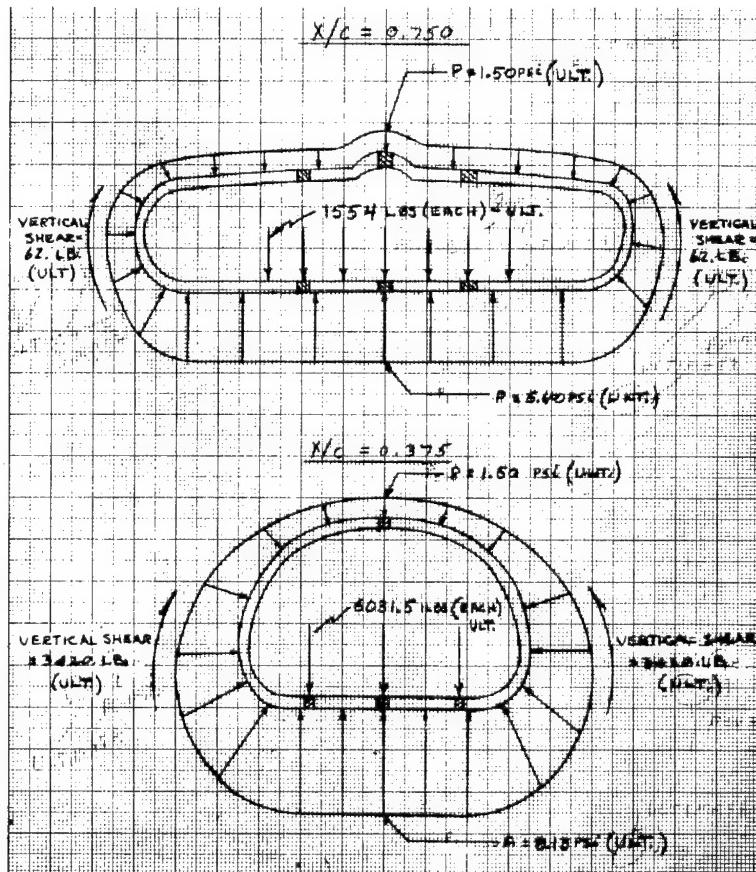
Figure 49 FRAME LOADING FOR A max "q" 12 g UNDERSHOOT REENTRY

-101-
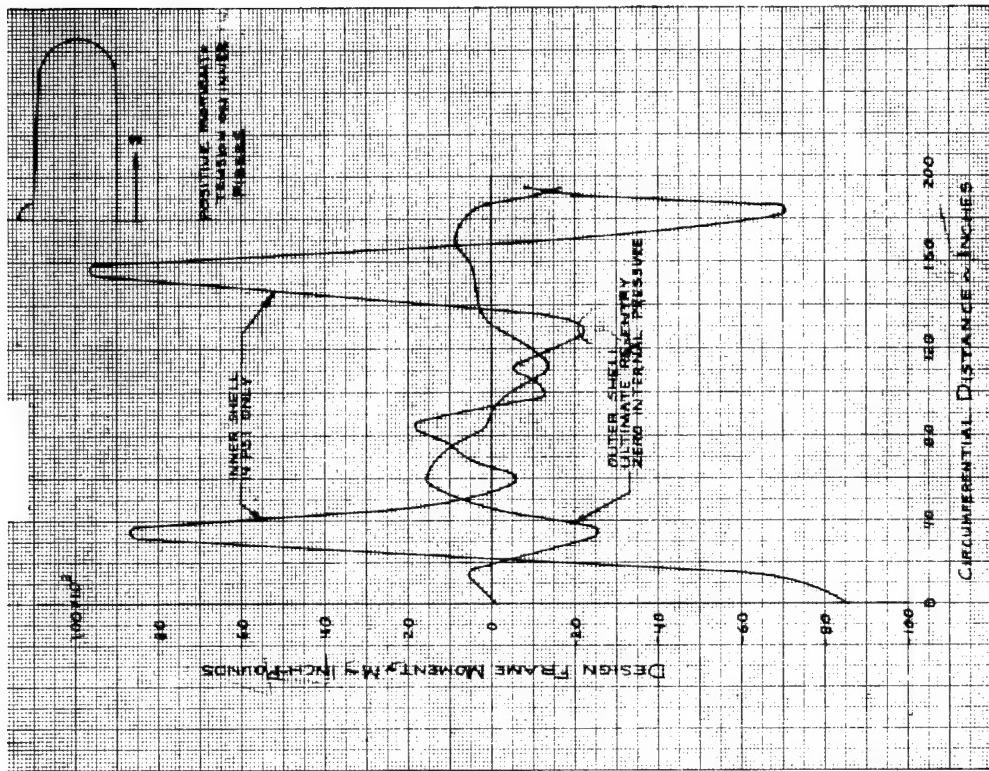
Figure 51   DESIGN FRAME MOMENTS VERSUS CIRCUMFERENTIAL DISTANCE
AT X/C = 0.750
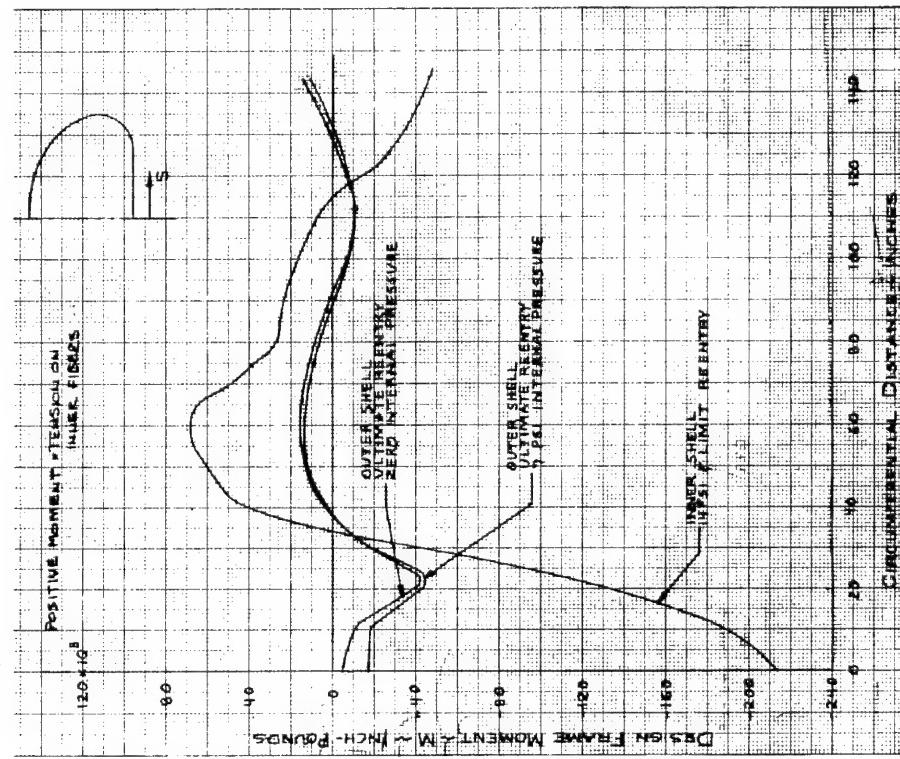
Figure 50   DESIGN FRAME MOMENTS VERSUS CIRCUMFERENTIAL DISTANCE
AT X/C = 0.375

-102-

Figure 53 ALLOWABLE ULTIMATE BENDING MOMENT VERSUS FIBERGLASS HONEYCOMB CORE DEPTH FOR THE TOUCHDOWN CONDITION (+700°F)

Figure 52 ULTIMATE BENDING MOMENT VERSUS HONEYCOMB CORE DEPTH AT X/C = 0.75 FOR A max "q" 12 g REENTRY

-103-

Figure 55 ALLOWABLE ULTIMATE BENDING MOMENT VERSUS HONEYCOMB CORE DEPTH FOR THE FILLED H/C ABLATOR AT max "q" +250°F REENTRY
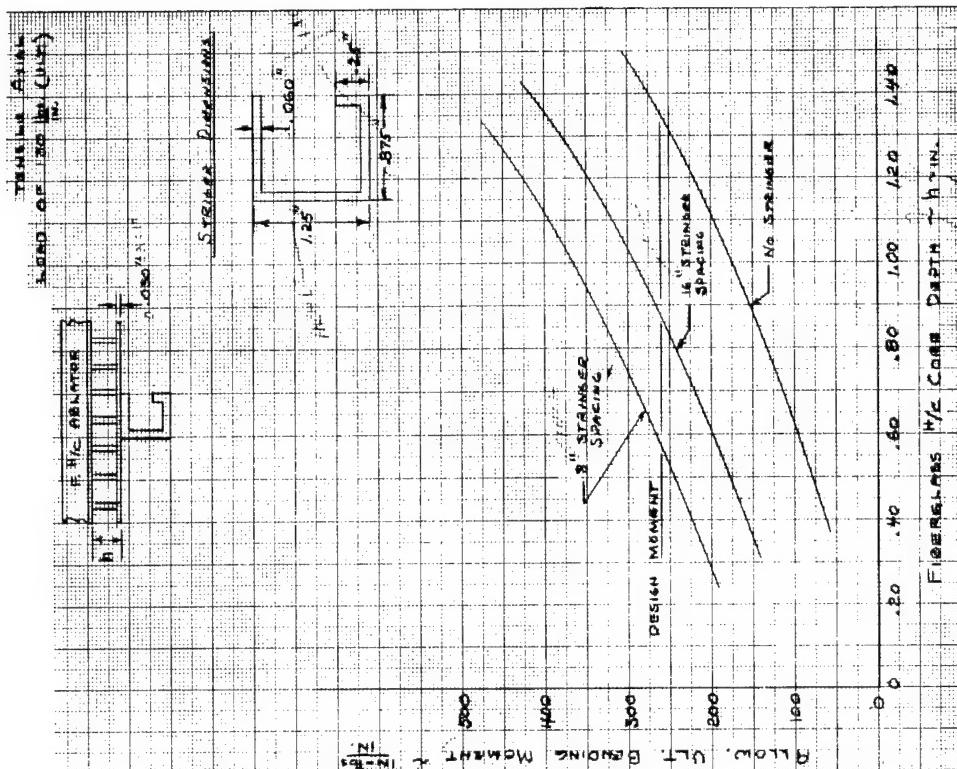
Figure 54 ALLOWABLE ULTIMATE BENDING MOMENT VERSUS FIBERGLASS WEIGHT PER SQUARE FOOT FOR THE TOUCHDOWN CONDITION (+700°F)
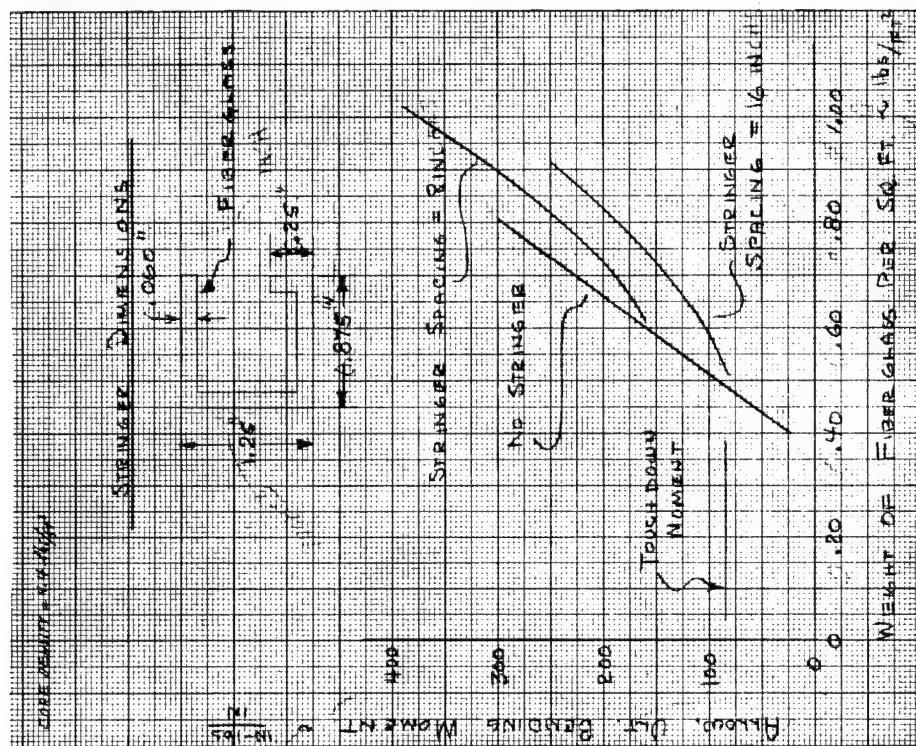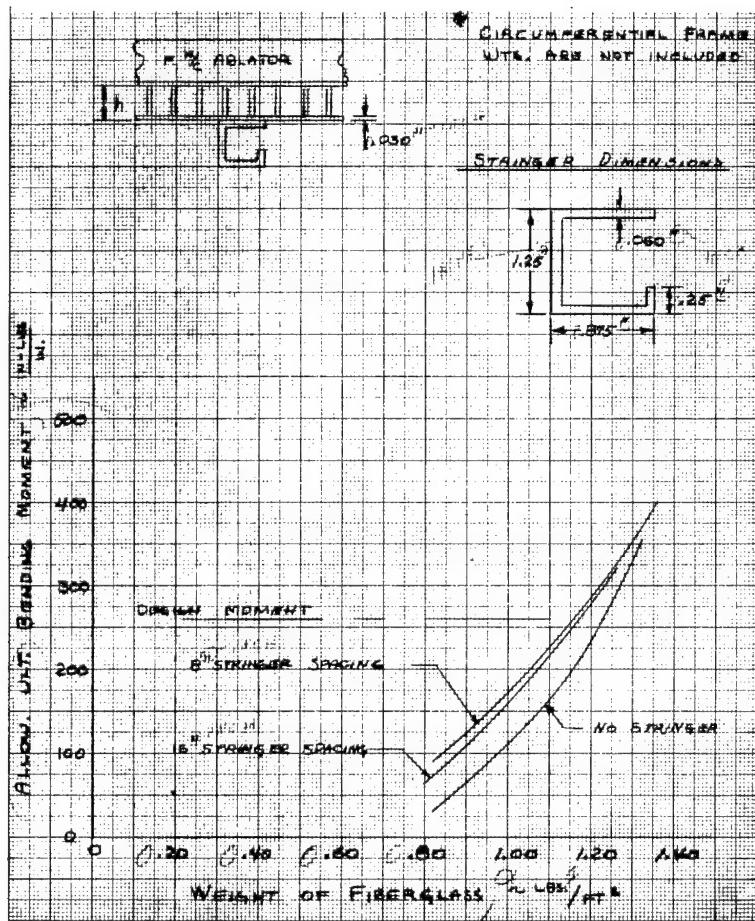
Figure 56 ALLOWABLE ULTIMATE BENDING MOMENT VERSUS FIBERGLASS WEIGHT
FOR THE FILLED H/C ABLATOR AT max "q" +250°F REENTRY
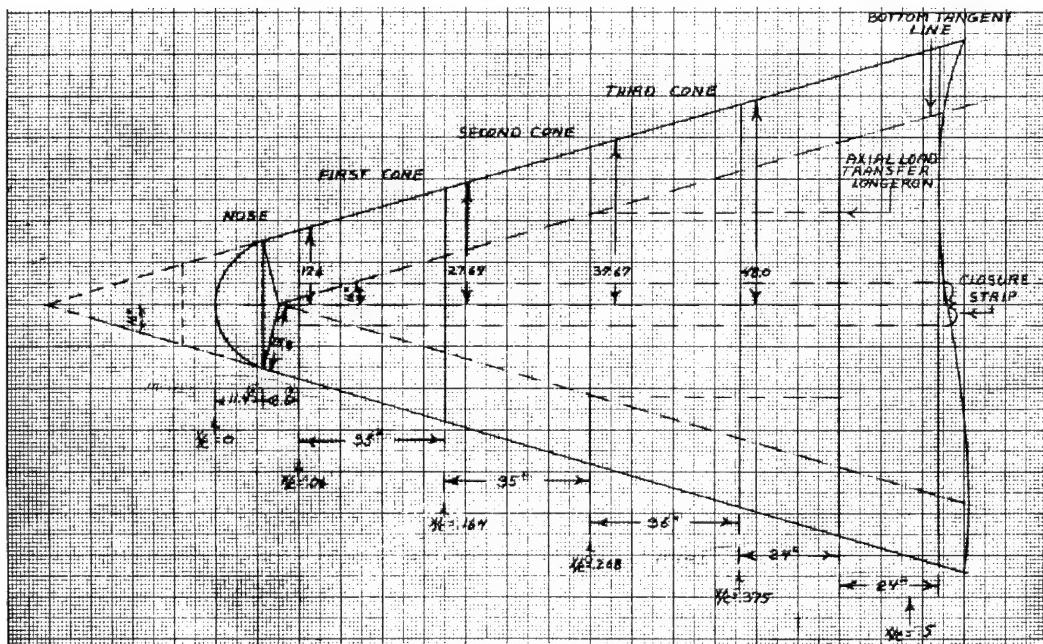
Figure 57 GEOMETRIES FOR STRUCTURAL ANALYSES
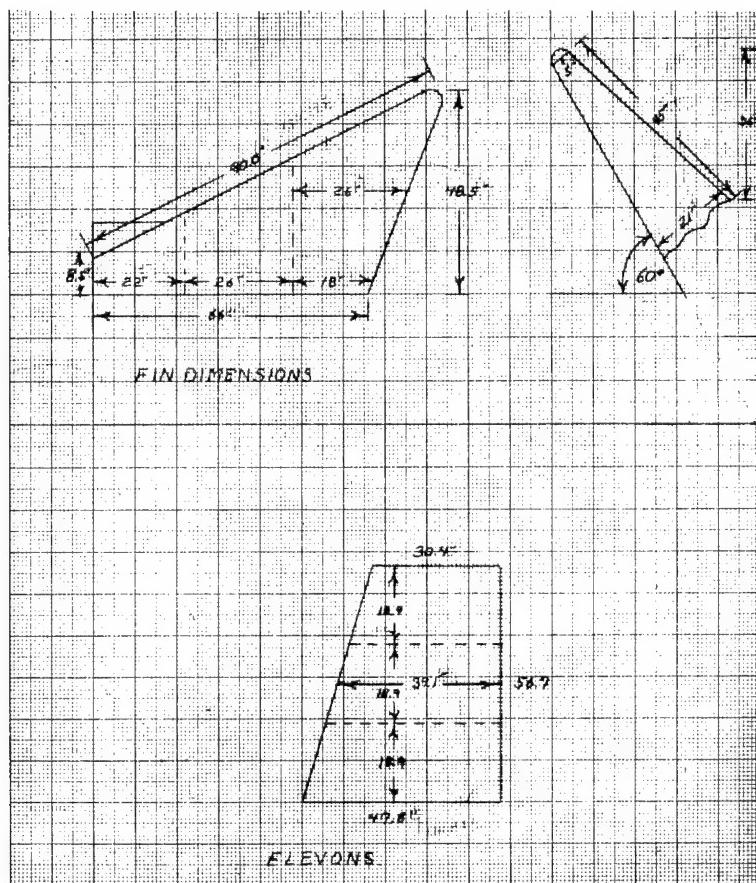
Figure 58 GEOMETRIES FOR FINS AND ELEVONS
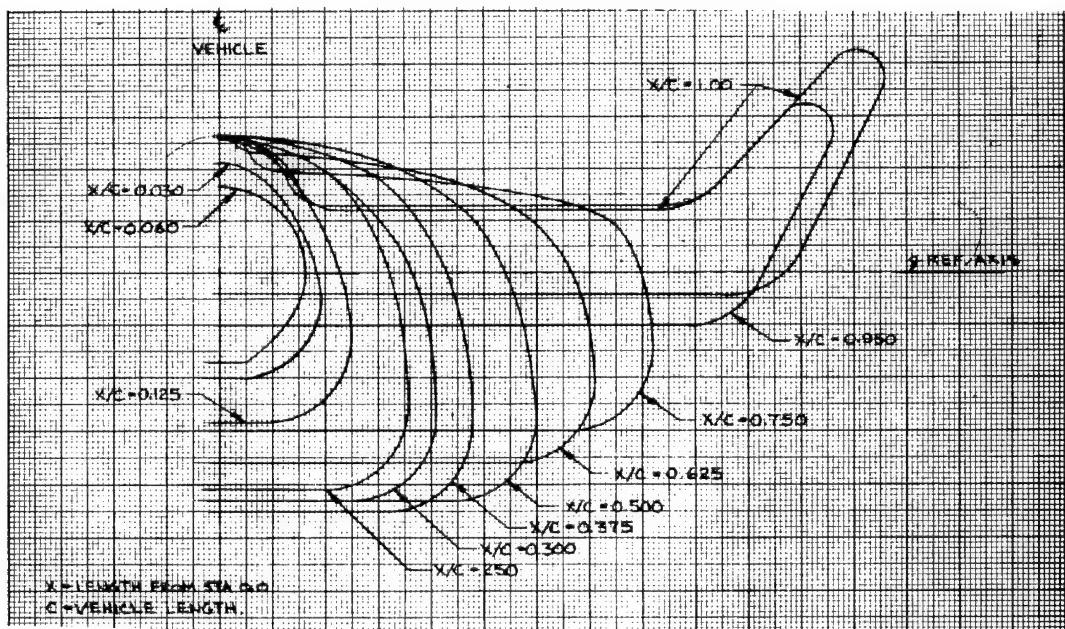
Figure 59 VEHICLE CROSS SECTIONS
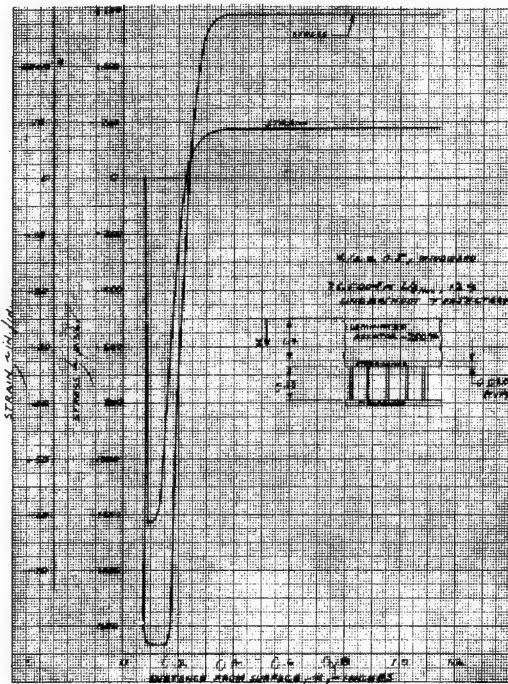
Figure 60 LAMINATED ABLATOR THERMAL STRESS AND STRAIN THROUGH THICKNESS,
t = 51 SECS., 36,500 FPS, (L/D)$_{max}$, 12 g UNDERSHOOT, -250°F
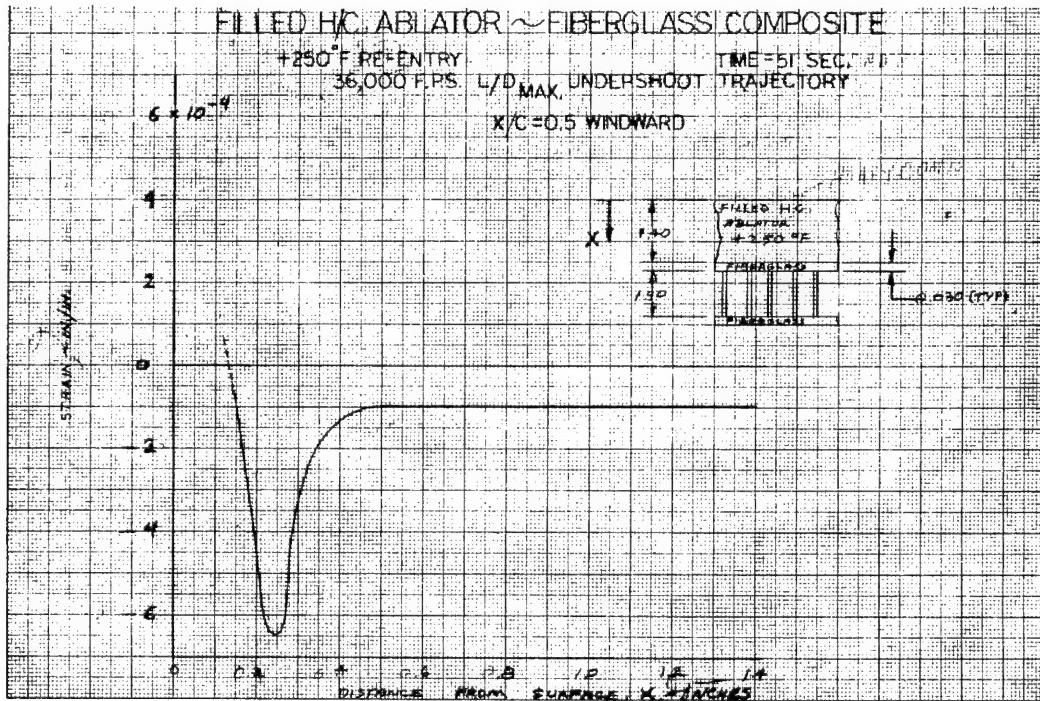

Figure 61 FILLED H/C ABLATOR THERMAL STRAIN THROUGH THICKNESS, t = 51 SECS.,
36,500 FPS., (L/D)$_{max}$, 12 g UNDERSHOOT, +250°F
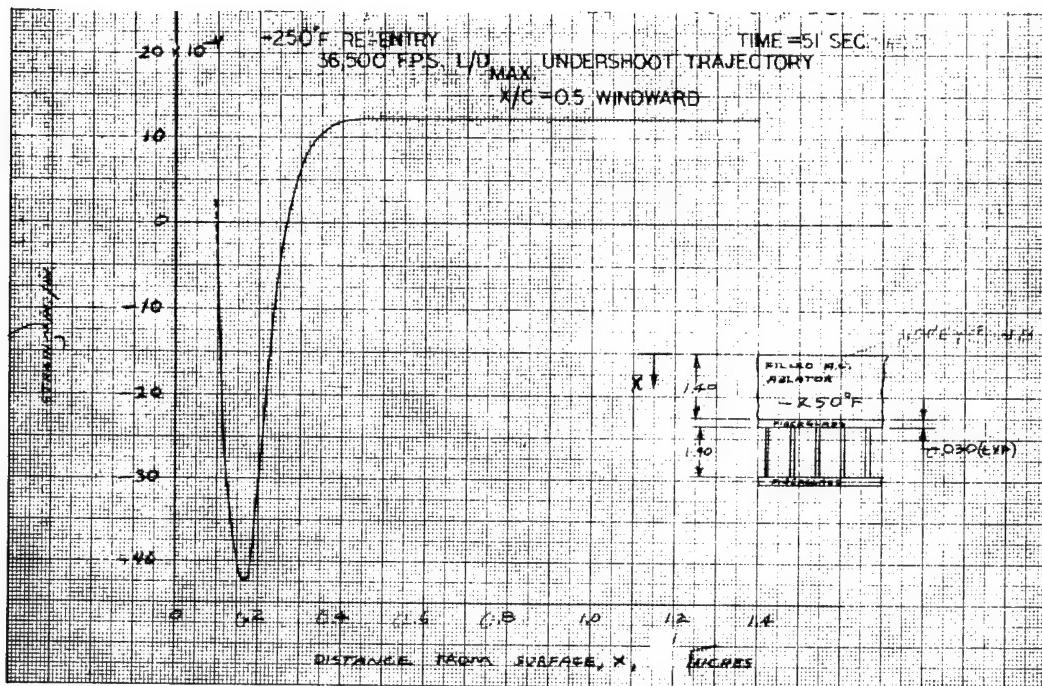
Figure 62 FILLED H/C ABLATOR THERMAL STRAIN THROUGH THICKNESS, t = 51 SECS.,
36,500 FPS., $(L/D)_{max}$, 12 g UNDERSHOOT, -250°F
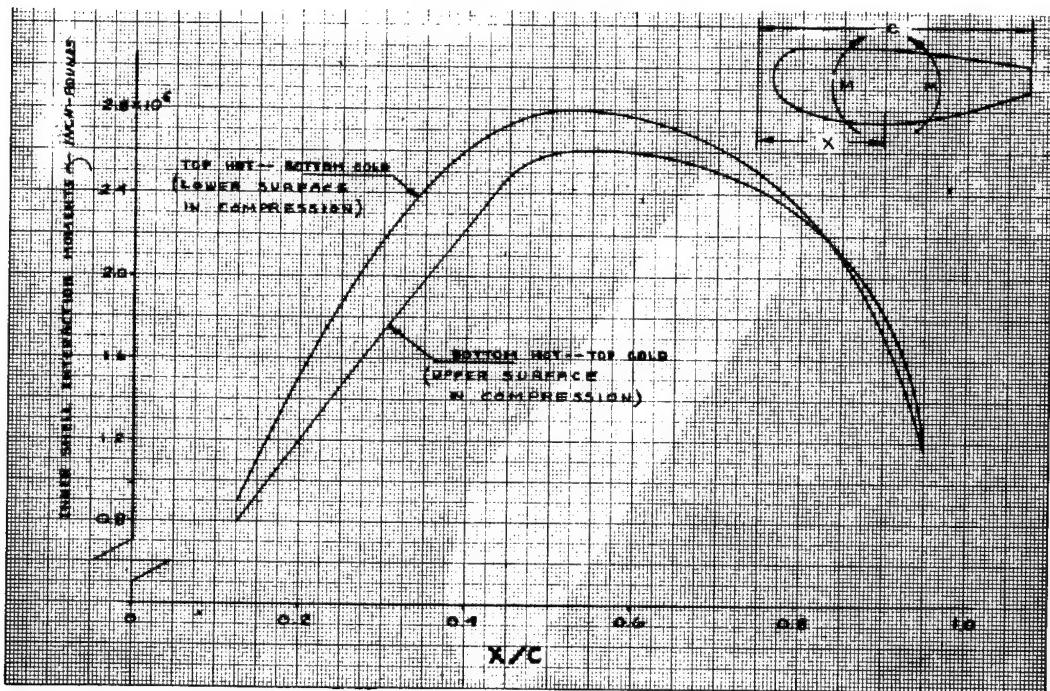
Figure 63 SPACE FLIGHT INTERACTION MOMENTS FOR THE INNER PRESSURE SHELL,
DOUBLE WALL CONCEPT
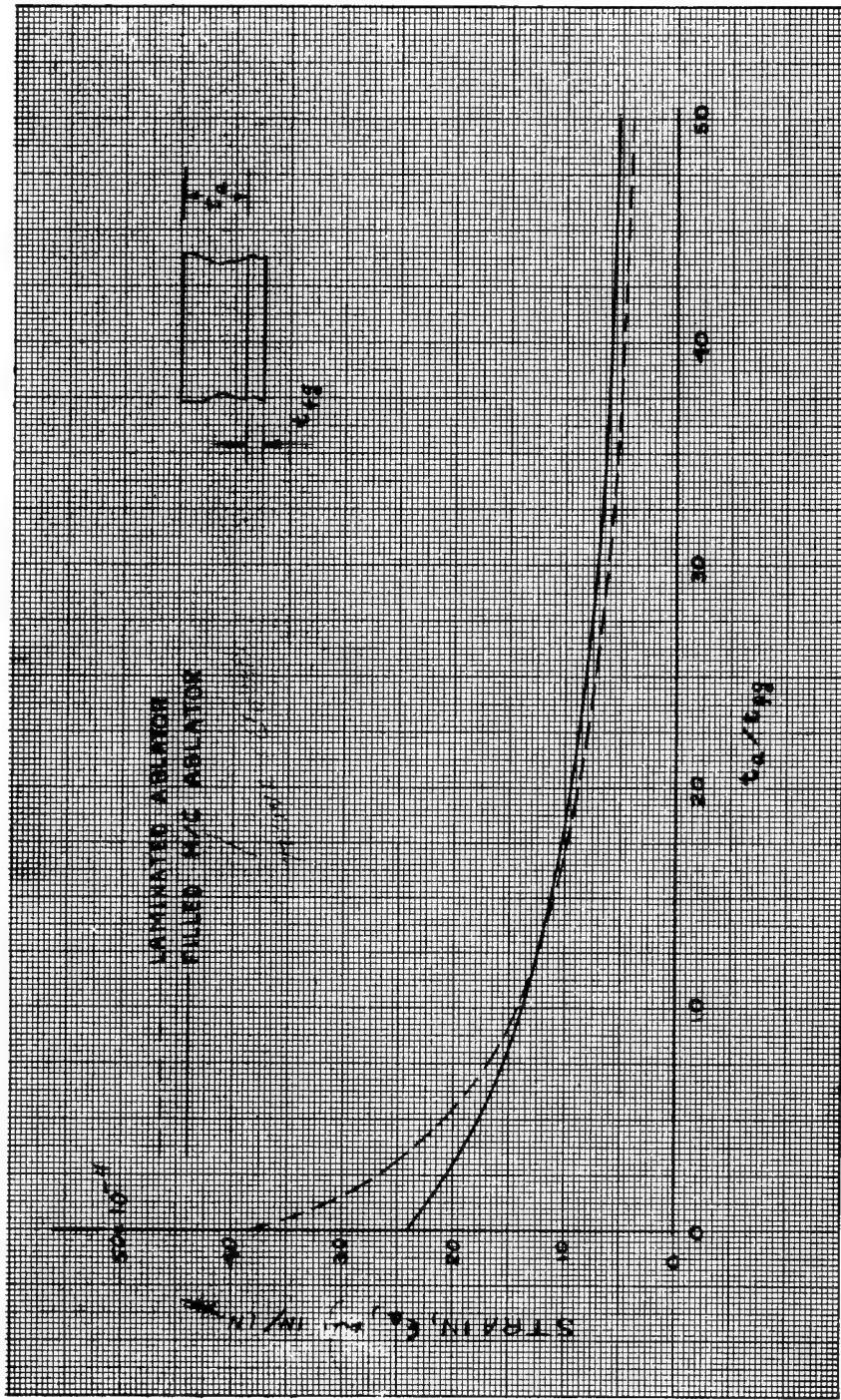
Figure 64 ABLATOR THERMAL STRAIN VERSUS ABLATOR TO FIBERGLASS THICKNESS
RATIO, -250°F, COLD SOAK
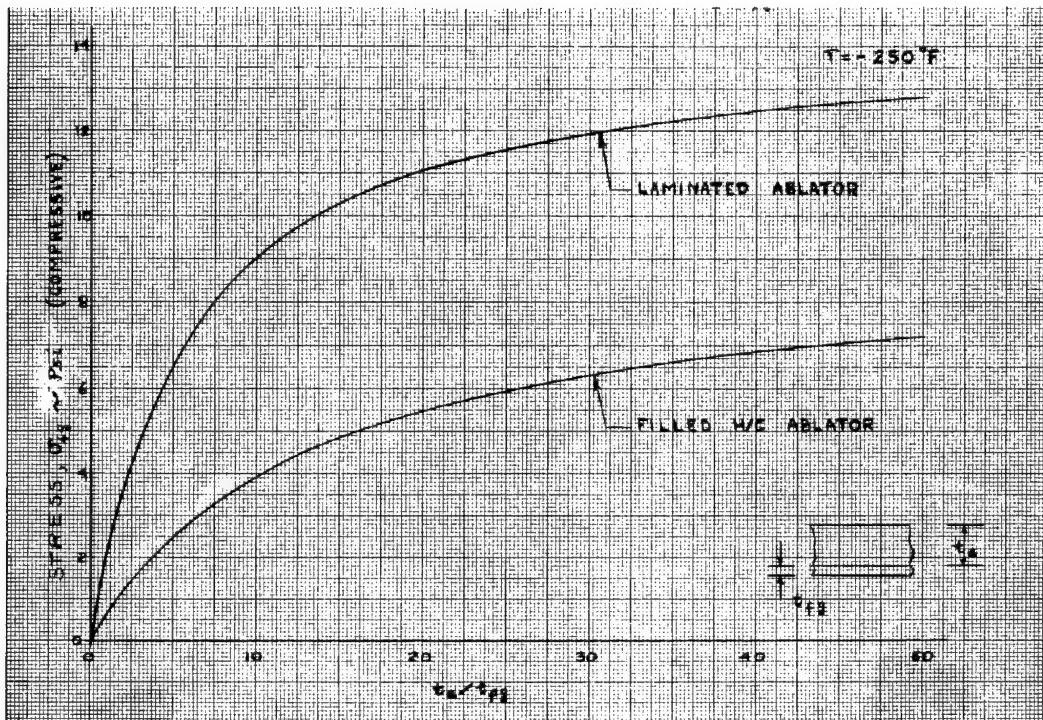
Figure 65 FIBERGLASS THERMAL STRESS VERSUS ABLATOR TO FIBERGLASS
THICKNESS RATIO, -250°F, COLD SOAK
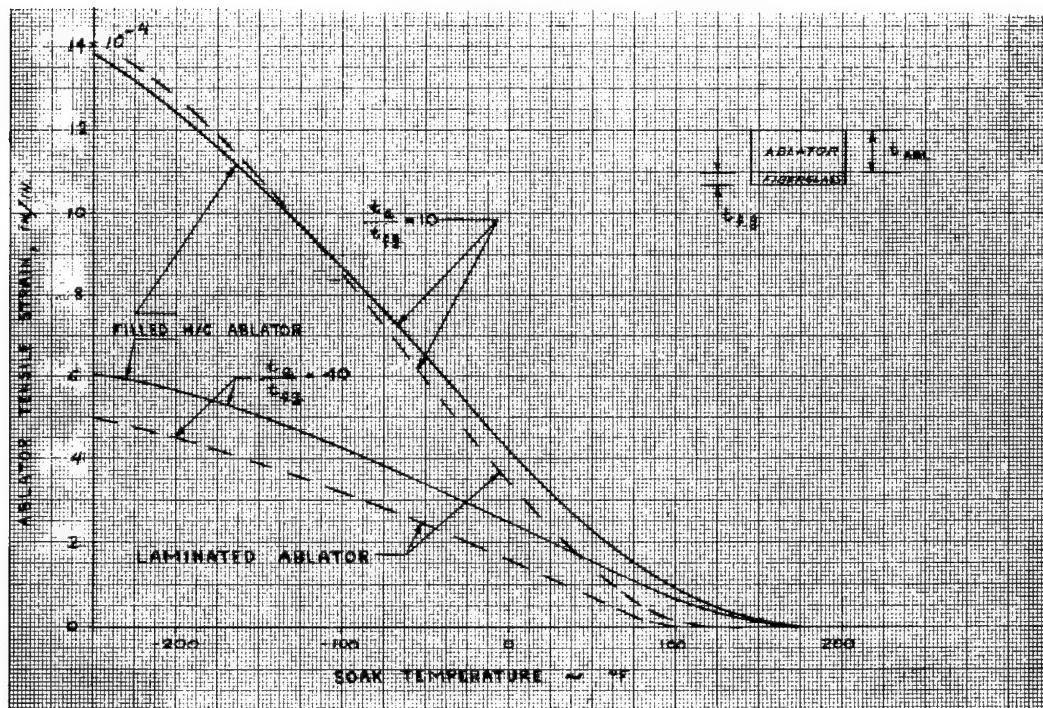
Figure 66 ABLATOR THERMAL STRAIN VERSUS SOAK TEMPERATURE, FOR BOTH
ABLATORS, WITH TWO ABLATOR TO FIBERGLASS THICKNESS RATIOS

-110-
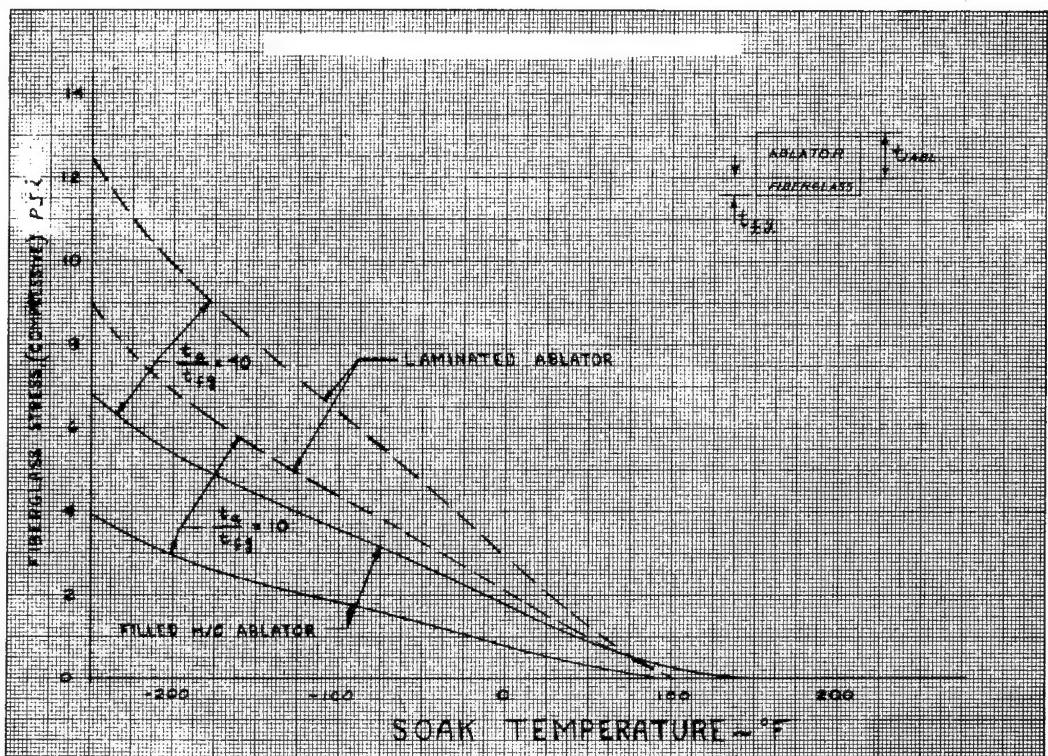
Figure 67 FIBERGLASS THERMAL STRESS VERSUS SOAK TEMPERATURE, FOR
BOTH ABLATORS, WITH TWO ABLATOR TO FIBERGLASS THICKNESS RATIOS

Figure 69 THERMAL STRESS VERSUS TIME, FIBERGLASS FACE SHEETS, X/C = 0.5 WINDWARD, +250°F REENTRY, V_E = 36,500 FPS, OVERSHOOT, $(L/D)_{max}$

Figure 68 THERMAL STRAIN VERSUS TIME, FILLED HONEYCOMB ABLATOR, X/C = 0.5 WINDWARD, +250°F REENTRY, V_E = 36,500 FPS, OVERSHOOT, $(L/D)_{max}$
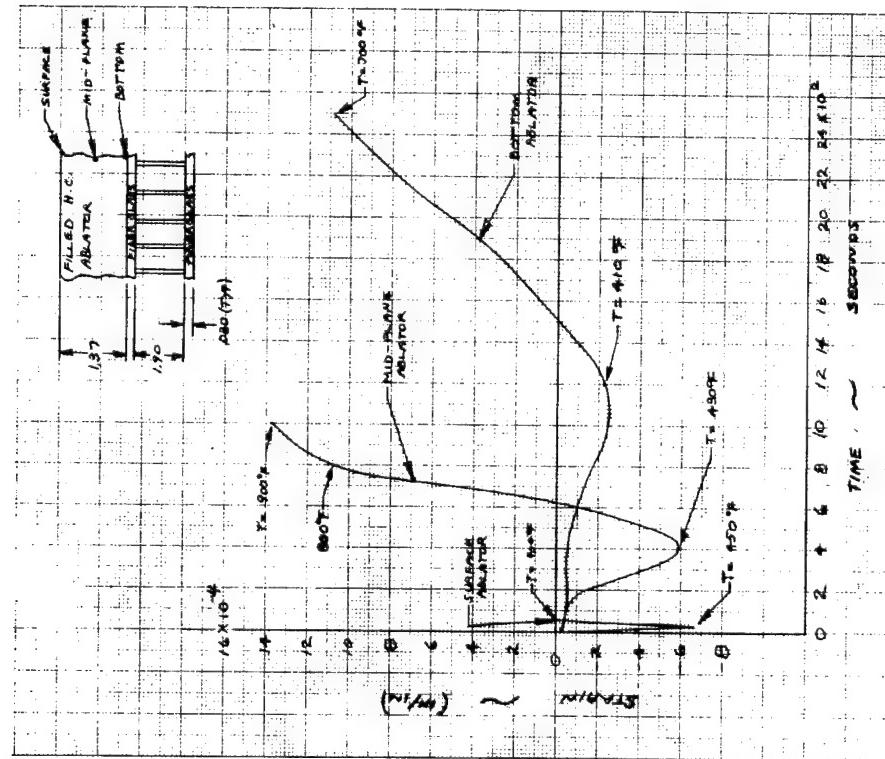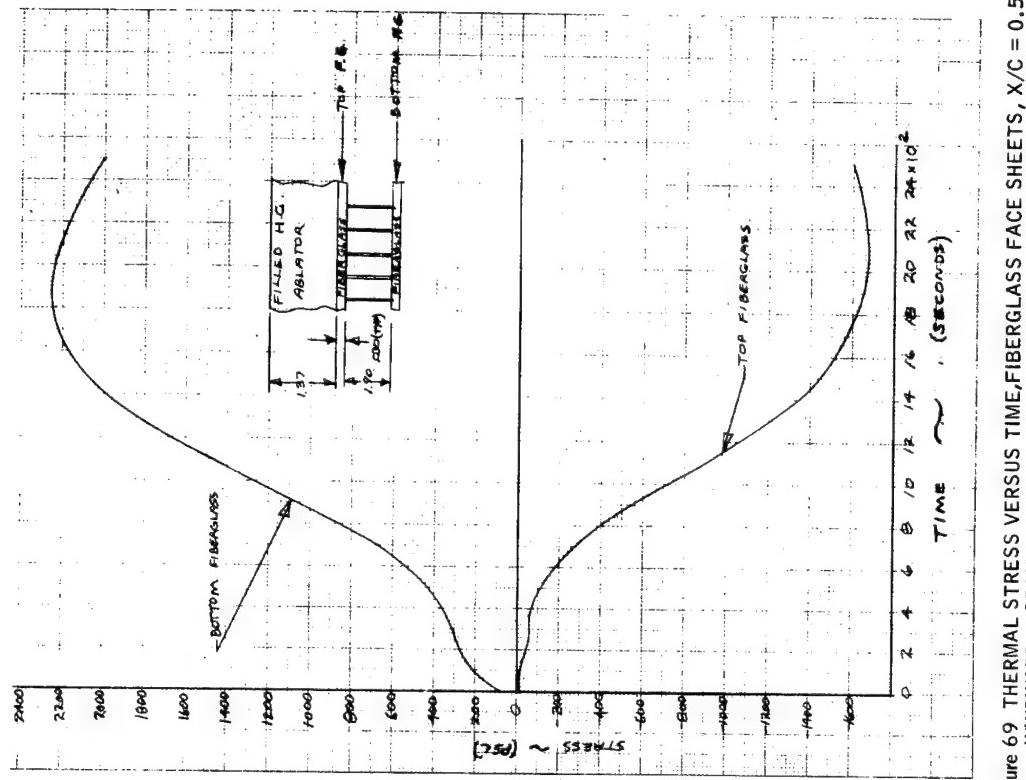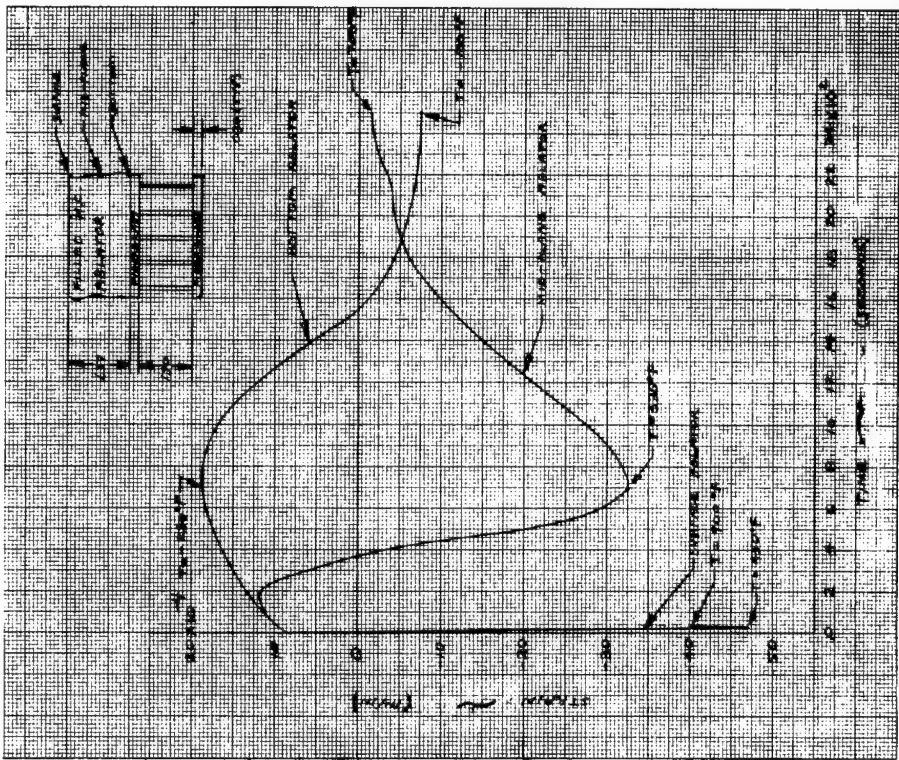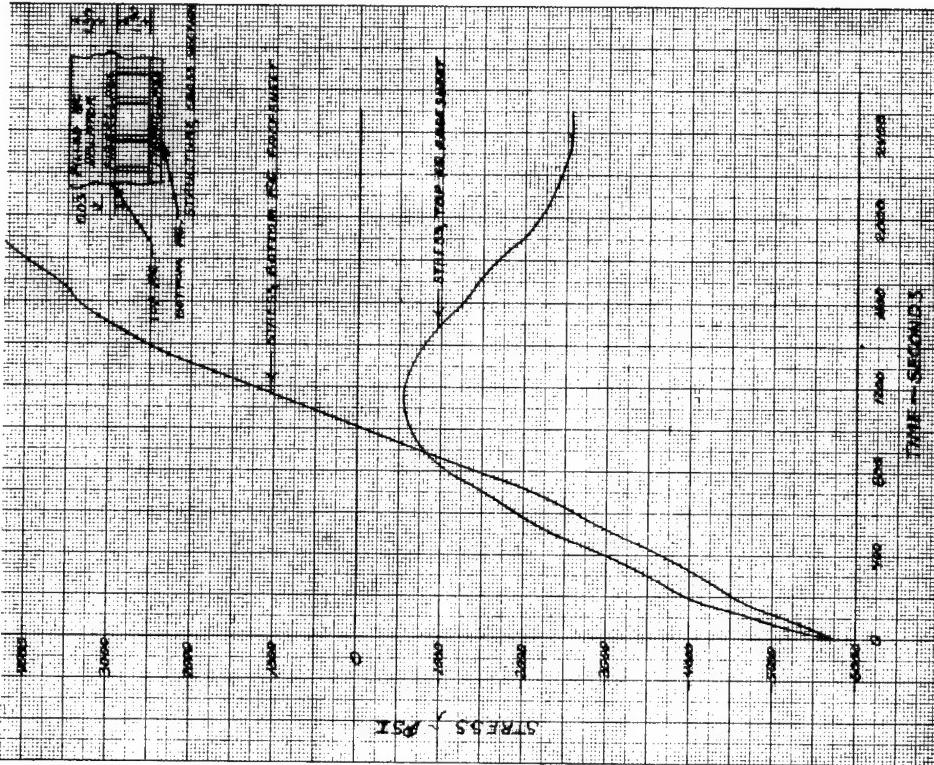
Figure 70 THERMAL STRAIN VERSUS TIME, FILLED HONEYCOMB ABLATOR, X/C = 0.5 Figure 71 THERMAL STRESS VERSUS TIME, FIBERGLASS FACE SHEETS, X/C = 0.5
WINDWARD, -250°F REENTRY, V_E = 36,500 FPS, OVERSHOOT, (L/D)$_{max}$ WINDWARD, -250°F REENTRY, V_E = 36,500 FPS, OVERSHOOT, (L/D)$_{max}$
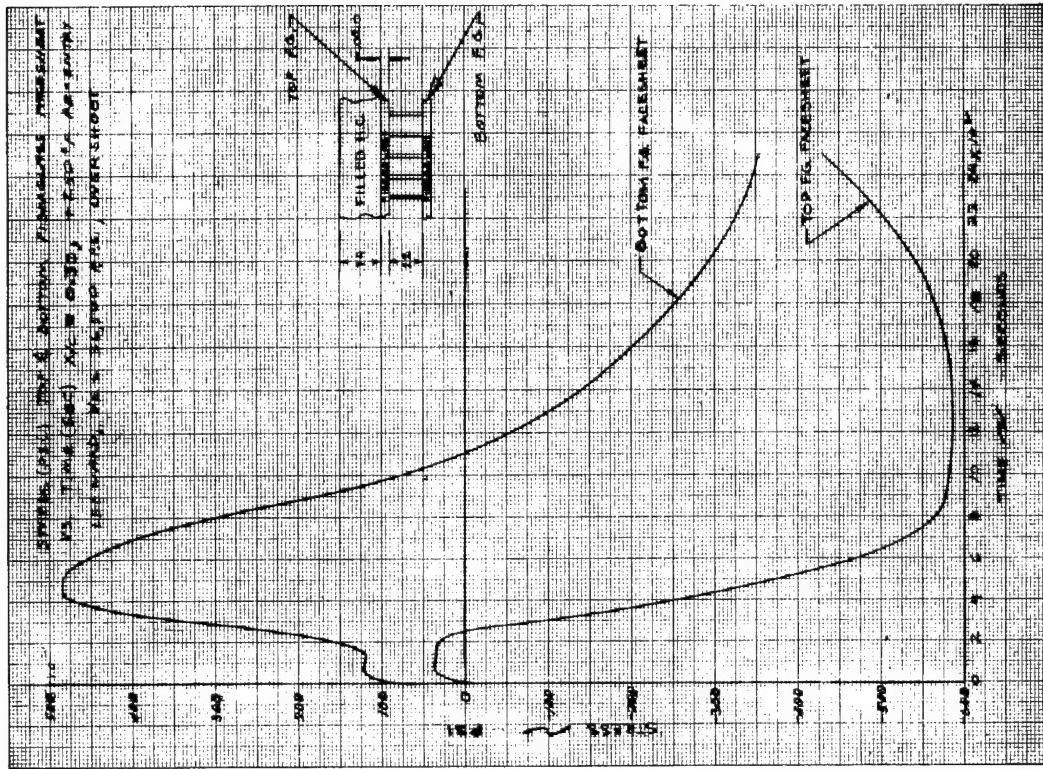
Figure 73 THERMAL STRESS VERSUS TIME, FIBERGLASS FACE SHEETS, X/C = 0.30
LEEWARD, +250°F REENTRY, V_E = 36,500 FPS, OVERSHOOT, $(L/D)_{max}$
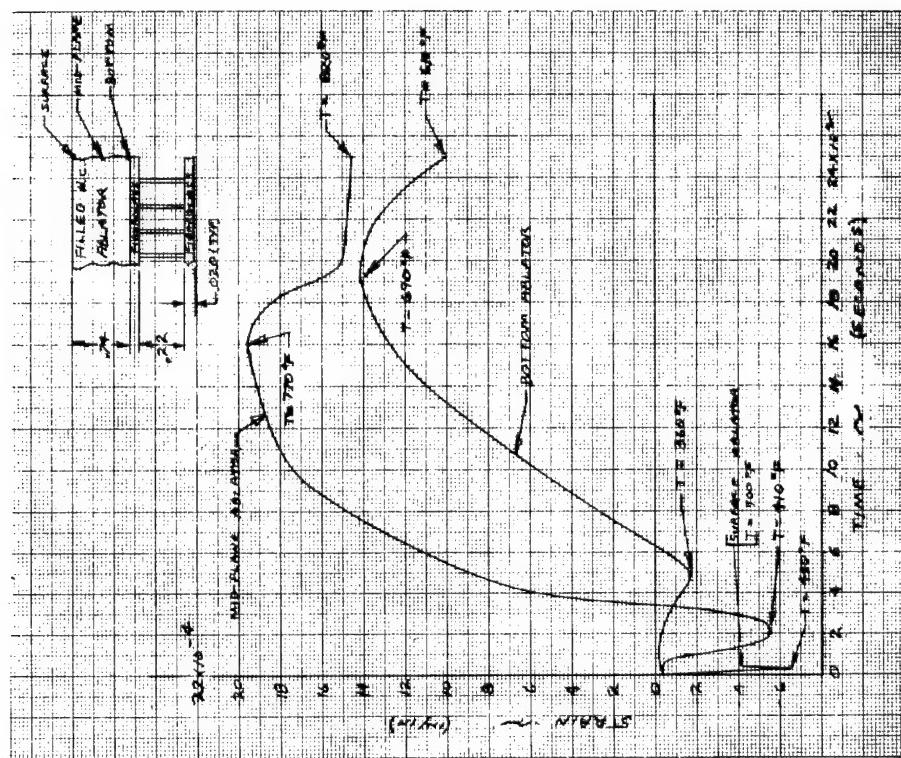
Figure 72 THERMAL STRAIN VERSUS TIME, FILLED HONEYCOMB, ABLATOR, X/C = 0.30
LEEWARD, +250°F REENTRY, V_E = 36,500 FPS, OVERSHOOT, $(L/D)_{max}$

Figure 75 THERMAL STRESS VERSUS TIME, FIBERGLASS FACE SHEETS, X/C = 0.3 LEEWARD, -250°F REENTRY, V_F = 36,500, OVERSHOOT, $(L/D)_{max}$

Figure 74 THERMAL STRAIN VERSUS TIME, FILLED HONEYCOMB ABLATOR, X/C = 0.3 LEEWARD, -250°F REENTRY, V_E = 36,500 FPS OVERSHOOT, $(L/D)_{max}$

Figure 77 THERMAL STRESS VERSUS TIME, FIBERGLASS FACE SHEET, X/C = 0.5 WINDWARD, +250°F REENTRY, V_E = 36,500 FPS, OVERSHOOT, (L/D)$_{max}$
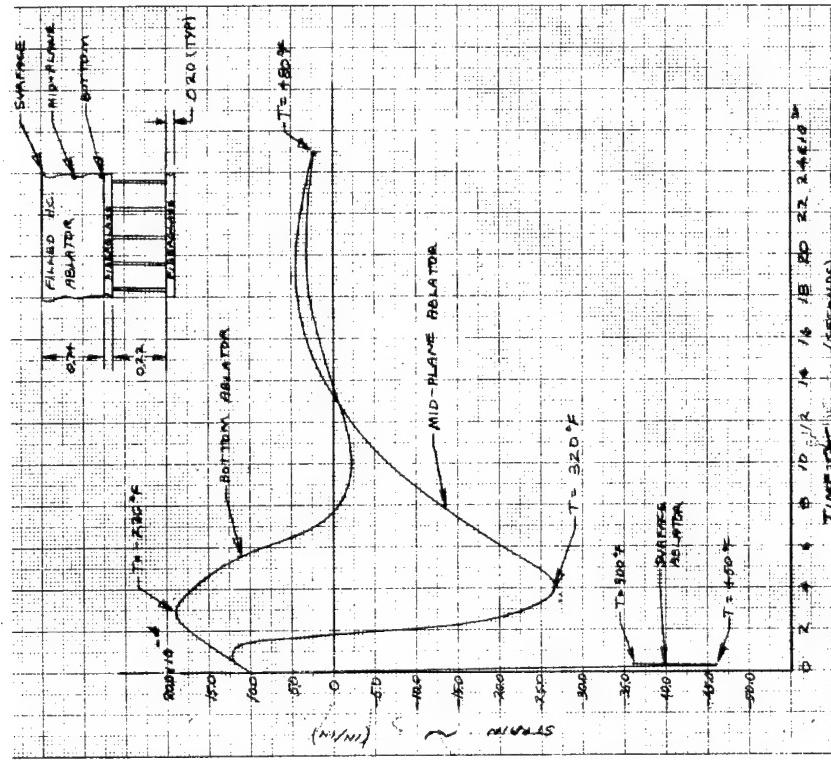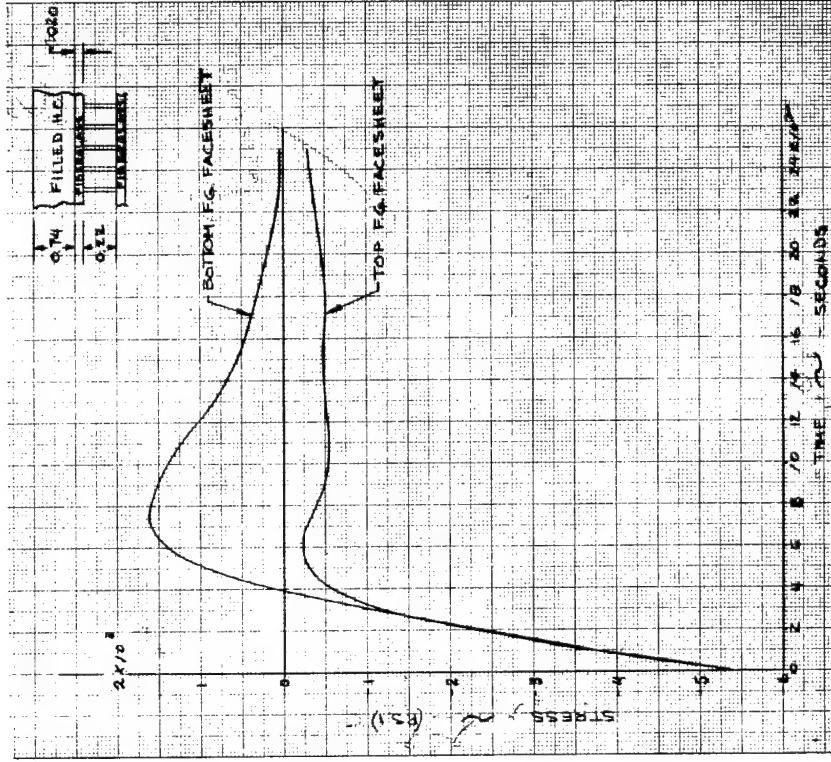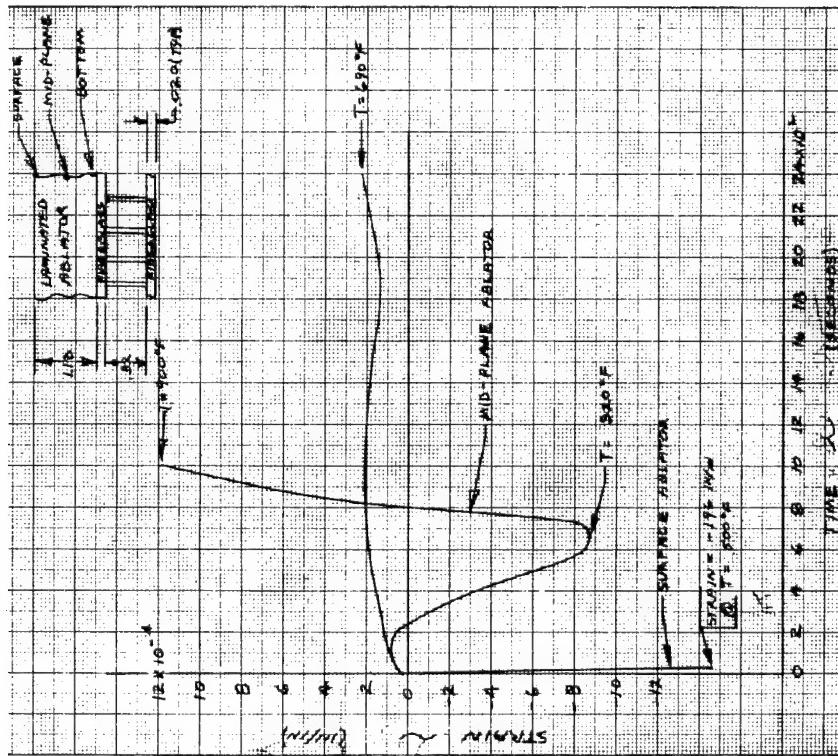
Figure 76 THERMAL STRAIN VERSUS TIME, LAMINATED ABLATOR, X/C = 0.5 WINDWARD, +250°F REENTRY, V_E = 36,500 FPS, OVERSHOOT, (L/D)$_{max}$
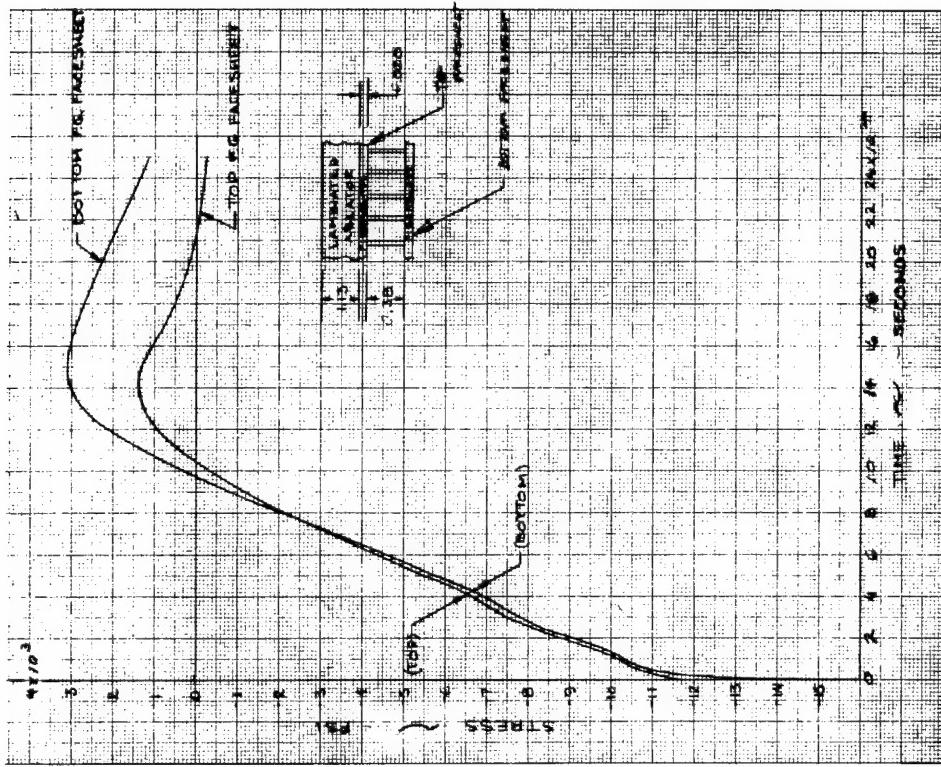
Figure 79 THERMAL STRESS VERSUS TIME, FIBERGLASS FACE SHEET, X/C = 0.5, WINDWARD, -250°F REENTRY, V_E = 36,500 FPS, OVERSHOOT, $(L/D)_{max}$
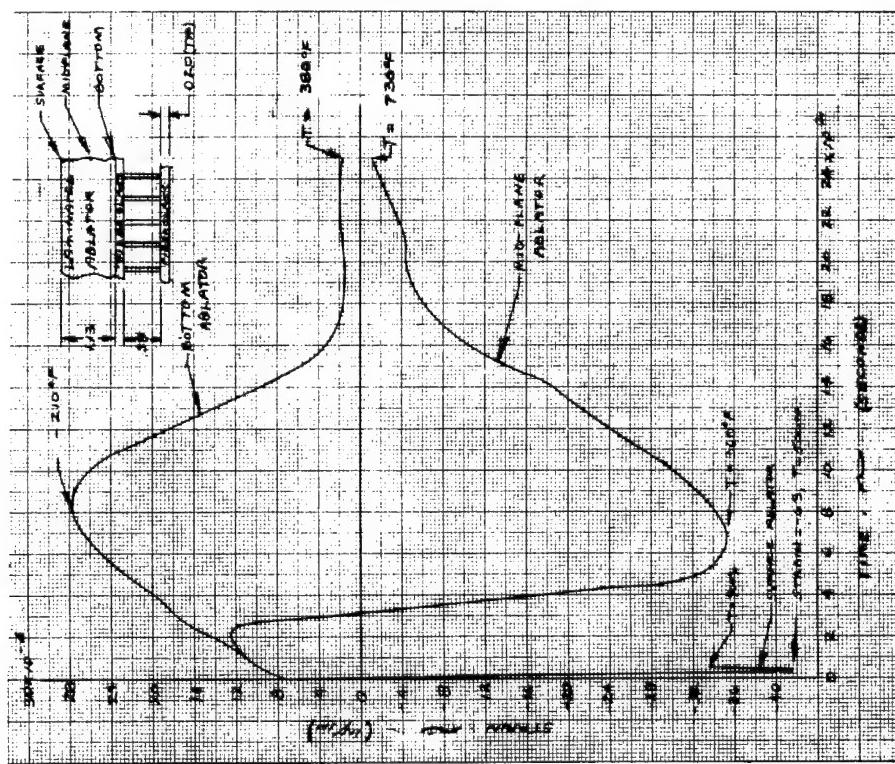
Figure 78 THERMAL STRAIN VERSUS TIME, LAMINATED ABLATOR, X/C = 0.5, WINDWARD, -250°F REENTRY, V_E = 36,500 FPS, OVERSHOOT, $(L/D)_{max}$

-117-

Figure 81 THERMAL STRESS VERSUS TIME, FIBERGLASS FACE SHEET, X/C = 0.3
LEEWARD, -250°F REENTRY, V_E = 36,500 FPS, OVERSHOOT, $(L/D)_{max}$

Figure 80 THERMAL STRAIN VERSUS TIME, LAMINATED ABLATOR, X/C = 0.3
LEEWARD, -250°F REENTRY, V_E = 36,500 FPS, OVERSHOOT, $(L/D)_{max}$
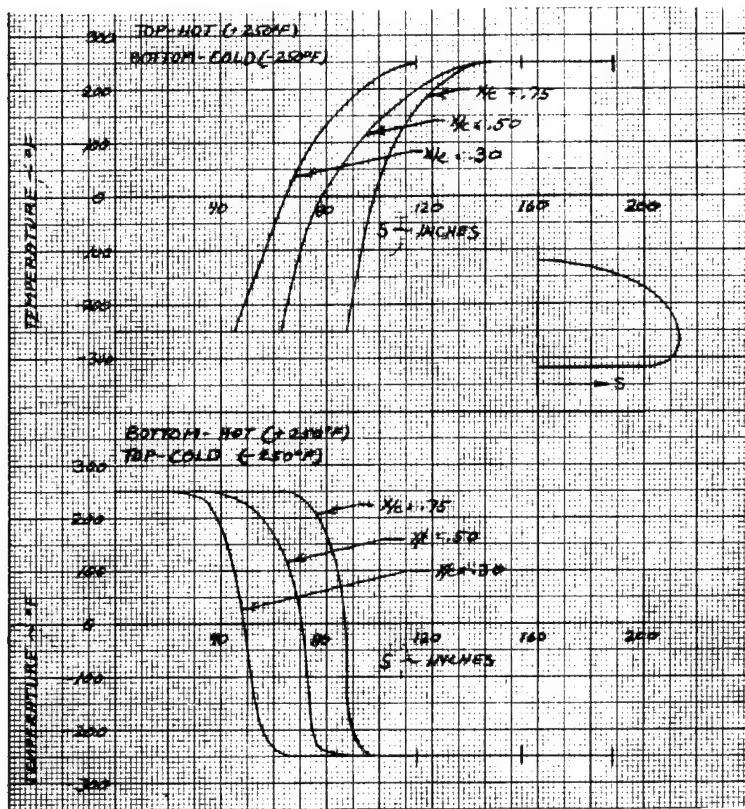
Figure 82 SPACE FLIGHT TEMPERATURES VERSUS CIRCUMFERENTIAL DISTANCE
FROM THE WINDWARD MERIDIAN, FOR VARIOUS BODY LOCATIONS
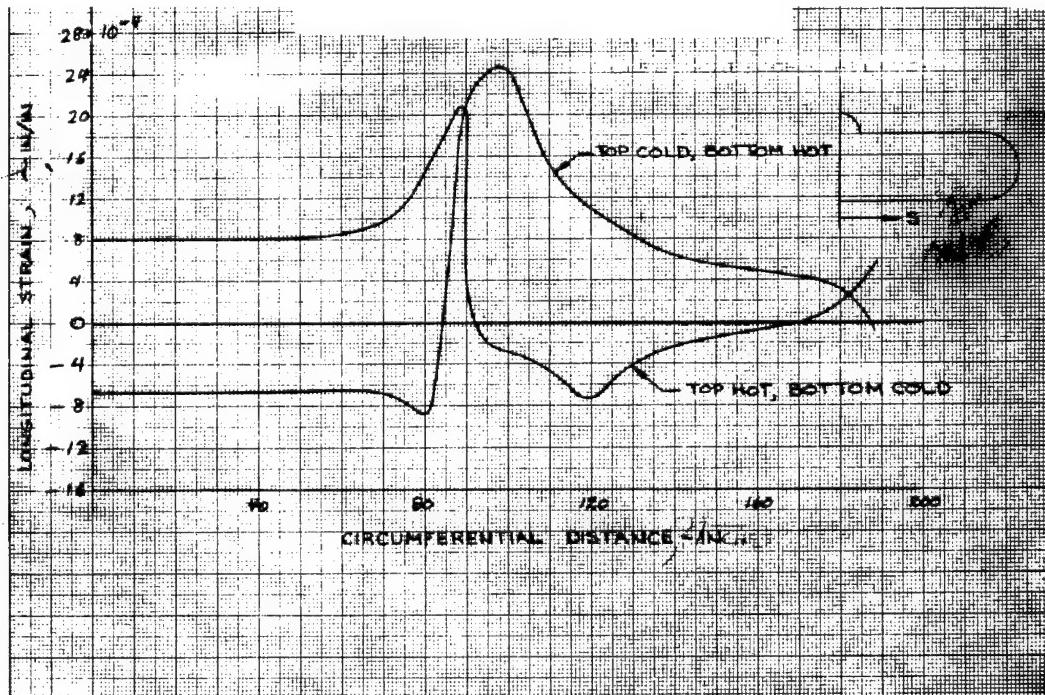
Figure 83 SPACE FLIGHT LONGITUDINAL STRAIN VERSUS CIRCUMFERENTIAL
DISTANCE AT X/C = 0.75, FOR THE FILLED H/C ABLATOR
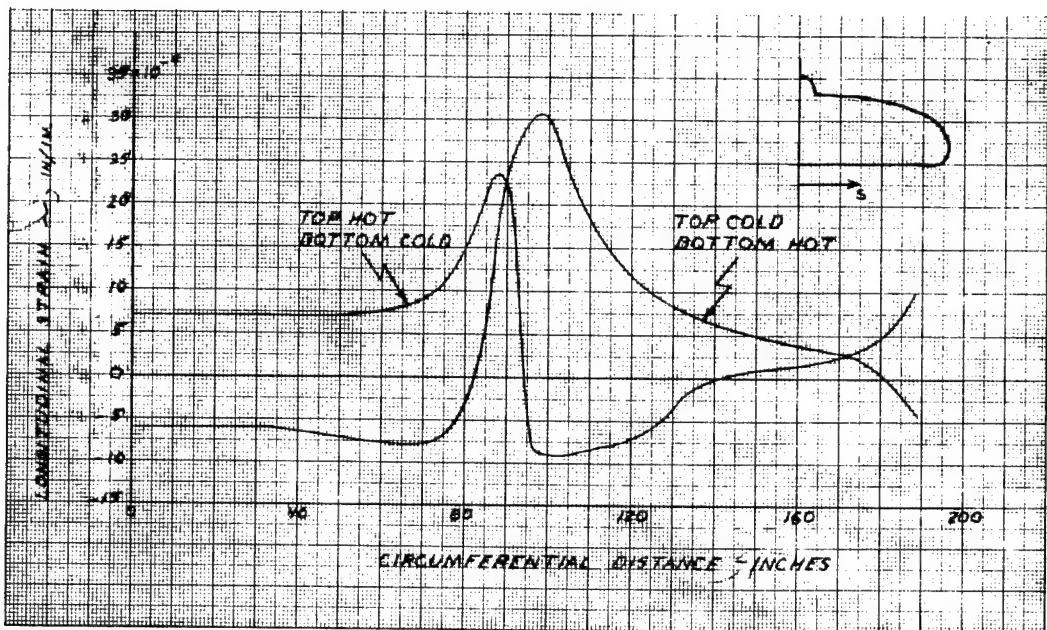
Figure 84 SPACE FLIGHT LONGITUDINAL STRAIN VERSUS CIRCUMFERENTIAL
DISTANCE AT X/C = 0.75, FOR THE LAMINATED ABLATOR
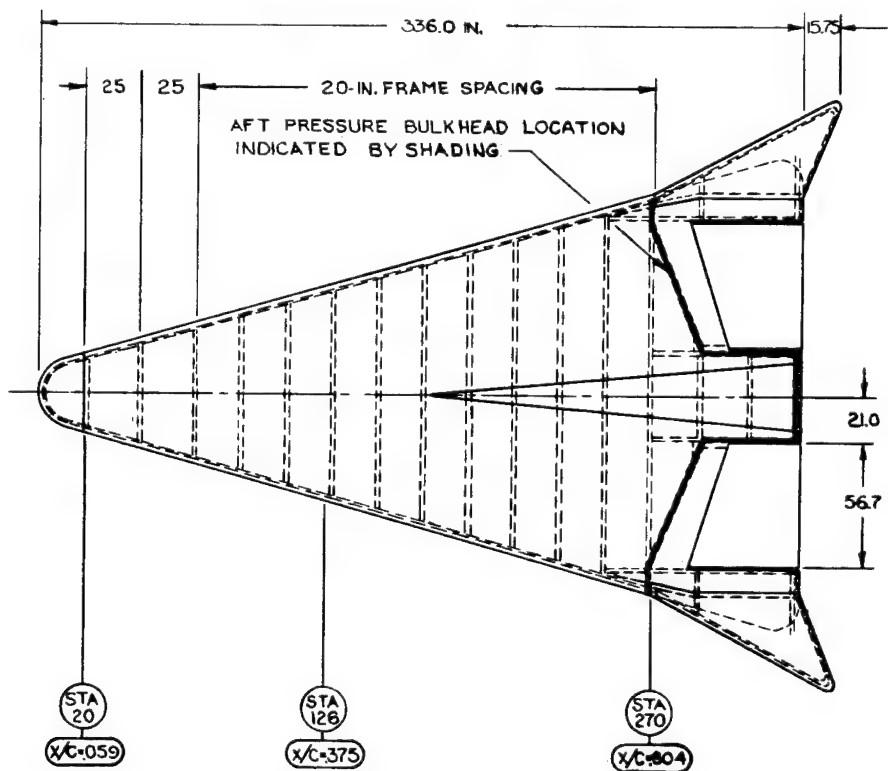
Figure 85 ALUMINUM SINGLE SHELL STRUCTURE

3.6 Weight Comparisons for Vehicle Design Concepts

The various combinations of ablator and substructure considered for both the single and double wall type of construction analyzed in this study are listed below.

1.   Fiberglass shell-filled H/C ablator (integrated)

2.   Fiberglass shell-laminated ablator (integrated)

3.   Fiberglass shell-filled H/C ablator

4.   Fiberglass shell-laminated ablator

5.   Steel shell-filled H/C ablator

6.   Steel shell-laminated ablator

7.   Aluminum shell-filled H/C ablator

8.   Aluminum shell-laminated ablator (structure only)

In the case of each honeycomb outer shell of the double wall construction, items (1) through (6), the bond line temperature between the ablator and substructure was not allowed to exceed 700°F. The inner shell consisted of an aluminum honeycomb pressure vessel. For the single pressurized shell construction the bond line was not allowed to exceed 300°F.

Table XVIII summarizes the individual ablator, insulation, structures and total weights of the vehicle configurations listed above. Table XIX presents outer shell weights per unit area at certain locations for the two integrated designs.

3.6.1 Total Weight Comparisons

The total weight calculations indicate small differences between the filled H/C and laminated ablators for the integrated designs, the filled H/C ablator design being the lighter of the two by 0.5 to 2.3 percent. In addition, both integrated designs are somewhat lighter than the steel shell designs but here again the differences are only slight and thus, no significant weight advantage can be seen. However, all the double wall concepts are significantly lighter than the single aluminum shell concept by about 27 percent.

TABLE XVIII

VEHICLE WEIGHT BREAKDOWNS

Concept	Outer Shell wt. (lbs.)	Inner Shell wt. (lbs.)	Total Structure wt. (lbs.)	26000 fps Reentry			36500 fps Reentry		
				Ablator & Bond wt. (lbs.)	Insulation wt. (lbs)	Total wt. (lbs.)	Ablator & Bond wt. (lbs)	Insulation wt. (lbs.)	Total wt. (lbs.)
Fiberglass Shell -Filled H/C Ablator (Integrated)	1361	659	2020	2338	482	4840	2850	459	5329
Fiberglass Shell- Laminated Ablator (Integrated)	947	659	1606	2741	519	4866	3346	504	5456
Fiberglass Shell -Filled H/C Ablator	1385	659	2044	2338	482	4864	2850	459	5353
Fiberglass Shell -Laminated Ablator	1063	659	1722	2741	519	4982	3346	504	5572
Steel Shell- Filled H/C Ablator	1418	659	2077	2338	538	4953	2850	529	5456
Steel Shell- Laminated Ablator	1264	659	1923	2741	542	5206	3346	526	5795
Aluminum Shell -Filled H/C Ablator	1798	---	1798	4085	295	6188	4629	299	6726
Aluminum Shell -Laminated Ablator (Structure Only)	1054	---	1054	----	---	---	----	---	---

TABLE XIX

OUTER SHELL UNIT WEIGHTS-DOUBLE-WALL CONCEPTS(LBS/FT^2)

26,000 F.P.S.

Body Location		Filled H/C Ablator	Insulation	Integrated Fiberglass Substructure	Total	Laminated Ablator	Insulation	Integrated Fiberglass Substructure	Total
X/C = .375	(upper)	1.31	1.25	0.83	3.39	1.59	1.24	0.80	3.63
	(lower)	3.47	0.89	1.98	6.34	4.16	1.07	1.01	6.24
X/C = .750	(upper)	1.28	1.11	1.24	3.63	1.63	1.12	1.04	3.79
	(lower)	2.34	0.93	1.58	4.85	2.88	1.12	0.90	4.90

36,500 F.P.S.

Body Location		Filled H/C Ablator	Insulation	Integrated Fiberglass Substructure	Total	Laminated Ablator	Insulation	Integrated Fiberglass Substructure	Total
X/C = .375	(upper)	1.90	1.26	0.83	3.99	2.35	1.24	0.80	4.39
	(lower)	4.13	0.78	1.98	6.89	4.92	1.05	1.01	6.98
X/C = .750	(upper)	1.87	1.15	1.24	4.26	2.31	1.18	1.04	4.53
	(lower)	3.21	0.67	1.58	5.46	4.16	0.81	0.90	5.87

3.6.2 Ablator Weight Comparison

A comparison of ablator weights in table XVIII indicates that the filled H/C ablator would be 17 percent lighter than the laminated ablator, due primarily to its considerably lower density (30.8 lbs/ft^3 versus 45.4 lbs/ft^3). No measurable difference in ablator weight was found between using a fiberglass or a steel substructure. The strong influence of the maximum allowable ablator-structure bond line temperature is evident by comparing the ablator weight for the vehicle using the single aluminum shell concept, based on a bond line temperature of 300°F, to those for the double wall concepts, which were derived for a 700°F maximum bond line temperature. The temperature of 300°F was chosen for the aluminum shell because its strength properties above this temperature start to decrease fairly rapidly. The difference between a 300°F and 700°F bond line temperature causes a weight differential of about 1800 pounds and is the primary cause for the large total weight of the single aluminum shell vehicle.

3.6.3 Insulation Weight Comparisons

A comparison of the required Q-Felt insulation weights indicates relatively small differences among those for the double wall concepts, which average about 200 pounds heavier than for the single aluminum shell. This occurs because of the lower allowable structural temperature of the latter concept.

3.6.4 Structural Weight Comparisons

Several interesting conclusions may be drawn from the structural weights in table XVIII. Looking at the two integrated shells, the one for the laminated ablator is 414 pounds lighter than that for the filled H/C ablator. This difference is due to the small strength and ultimate allowable tensile strain (0.4 percent versus 1.2 percent) of the filled H/C ablator than that of the laminated design. In order for a filled H/C ablator-substructure composite shell to have the same load-carrying ability as one with a laminated ablator, the substructure for the filled H/C ablator must be stiffer than that for the laminated ablator. This is especially the case when the composite is subjected to bending loads. The filled H/C composite must not only be capable of carrying the loads, but must also be stiff enough to prevent the ablator from cracking because of its low allowable strain capability.

The weight advantage obtained by the laminated ablator substructure nearly offsets the weight penalty for the ablator itself relative to the

filled H/C concept, especially over the bottom surface of the vehicle, as can be seen from table XIX.

Table XVIII indicates that the fiberglass outer shells are lighter than the steel outer shells. This is due to the fact that only minimum gauge thicknesses were required in many areas of the vehicle. If the structural loads had been greater, a steel design would probably have been lighter than a fiberglass one, due to its greater strength efficiency.

Finally, the structures for the single aluminum shells are lighter than their double shell counterparts. In the case of the laminated ablator designs this weight difference is approximately equal to the weight of the inner pressure shell of the double wall concept. For the filled H/C ablator designs, however, the weight difference is only 252 pounds. This is caused by the larger weight penalty incurred by the pressurized aluminum single shell over the unpressurized fiberglass outer shell due to the criterion that the ablator shall not crack.

3.6.5 Weight Savings of Integrated Wall Construction

The weight savings that can be realized from structural integration may be found in table XVIII by comparing the substructure weights for the integrated and nonintegrated fiberglass designs, the difference being that, in one case, the load-carrying ability of the ablator is relied upon in the structural analyses and in the other case it is not. The weight savings are small because structure is needed for the touchdown condition when no ablator is effective, due to the high temperatures, and because the lightest design utilizes the low strength filled H/C ablator.

Weight savings due to integrated construction with a strong ablator would be more significant if the structural loads on ascent or early reentry were larger relative to the loads of touchdown than the ones considered in this study. For instance, the use of the laminated ablator in an integrated design of a large pressurized single shell vehicle would very likely result in appreciable weight savings.

3.6.6 Effect of Low Ultimate Strain of Ablator

Another result that can be inferred from table XVIII is the structural weight that can be saved in a nonintegrated design by improving the ultimate strain to failure capability of the thermally efficient filled H/C ablator. The only difference in the structural weight between the various combinations of ablators and substructure was caused by the requirement of no ablator cracking, which was the critical design

criterion for much of the substructure for the filled H/C ablator but
not the laminated ablator's substructure. This caused differences
between the filled H/C and laminated ablator substructures of 322
pounds in the fiberglass outer shell, 154 pounds in the steel outer shell,
and 738 pounds in the single aluminum shell. Becuase the single
aluminum shell is internally pressurized, it is more highly loaded
than an outer shell of a double wall concept, and the resulting weight
penalty for the required stiffness is significantly larger.

4.0 MANUFACTURING TECHNIQUES

The manufacturing techniques involved in fabricating, assembling, and refurbishing the various conceptual vehicles are discussed in this section.

The fabrication of the ablators and the structural shells is presented in section 4.1. The assembly of an outer shell around the inner pressure shell, along with a feasible scheme for inner-outer shell attachments, is presented in section 4.2. Finally, in section 4.3, the process involved in refurbishing a used outer shell with new ablator is discussed.

4.1 Fabrication

In this section, the manufacturing processes required to fabricate the fiberglass, steel, and aluminum honeycomb shell structures, the two ablators, and the insulation are described.

4.1.1 Fiberglass Outer Shell

The outer shell would be made of fiberglass honeycomb sandwich construction bonded to structural frames for support. The proposed fabrication method would consist of a wet layup of the inner and outer face sheets followed by a bonding together of the cured face sheets and honeycomb filler to make a panel which would be, in turn, bonded to other panels and structural members to make a complete assembly. An alternate successfully used method would be to employ a dry layup method in which face sheets are purchased as "prepregs" and a dry adhesive is required to bond them to the honeycomb core in an autoclave to form panels.

The structural members such as the ring frames, channel at the nose, and splice members would all be made up of wet layups requiring a large number of molds. The procedure would be to layup fiberglass in a mold, saturate with resin, vacuum bag, paddle out excess resin and air, and cure under vacuum. The panel closeouts would also be made of a wet layup.

The panel fabrication would consist of the wet layup of the first face sheet in a mold that would give the proper contour to the sheet. The sheet would be laid up and cured, and then the second face sheet would be laid up and cured.

Fiberglass honeycomb core would be spliced to the proper thickness and, if curvature were severe, would be hot formed to the approximate required shape. The sandwich would then be assembled with a tape adhesive between core and face sheets, vacuum bagged, and cured

-127-

under proper conditions. The fiberglass honeycomb matrix for the honeycomb filled ablator would be bonded to the outer face sheet by the same procedure.

The edge members may be bonded at the same time as the sandwich with proper fixturing. The resulting panels may be as large as 10 feet x 6 feet just forward of the fins, to 16 inches x 36 inches just aft of the nose cone. Smaller panels may be required around the rear control surfaces. The panels would be assembled to the structural members in a supporting fixture to assure alignment.

4.1.2 Stainless Steel Outer Shell

The steel outer shell would be made of 15-7 Mo age-hardened stainless steel honeycomb sandwich construction bonded to structural frames for support. The structural members would all be stretch formed, trimmed, and machined to configuration. The honeycomb panels fabricated to the desired contours would be purchased from an outside vendor since much specialized equipment, tooling, and know-how are required to form them. After inspection, these panels would be assembled by welding on the appropriate fixture and welding facility. The structural members would also be attached by welding. The whole assembly would have to be rigidly fixtured to assure conformance to the mold line of the master facility tooling.

4.1.3 Aluminum Shells

Both the inner aluminum pressure shell of the double shell concepts and the single shell concept vehicle would be made of honeycomb sandwich construction and supporting frames. The materials required for the shells would consist of commercial aluminum sheet, standard aluminum honeycomb, and a tape adhesive. The fabrication of the inner pressure shell would require the building up of an aluminum honeycomb sandwich panel and welding the panels together and to the supporting structural members, which would be stretch formed from commercially extruded stock.

The incoming aluminum sheet would be selectively etched to form the proper thickness face sheets with thicker edges for welding of closeouts and joining panels together. The first shell would be laid on the mold, tape adhesive applied, the honeycomb centered on the sheet, and the second face sheet with adhesive tape next to the honeycomb fitted in place. When possible, closeout members may be bonded in place at this time. The whole assembly would be bagged and autoclaved to form the aluminum honeycomb panel which could range in size from 1 by 2 feet to 4 by 8 feet. These panels would be welded together and to supporting structural members in suitable fixtures to assure alignment.

4.1.4 Ablator Fabrication

   a. Filled H/C Ablator

A typical epoxy ablator would consist of a resin system heavily
filled with silica and glass fibers for char reinforcement and with
phenolic microballoons for reduction of density and thermal con-
ductivity. This mix would be loaded into the cells of fiberglass
honeycomb that have been bonded to the outer shell structure.
Following completion of the filling of the honeycomb with ablator,
the assembly would be bagged for a vacuum cure and final dimen-
sional stabilizing. It may then be machined to any desired surface
finish or dimensional tolerance.

The molded charring ablator, used for high curvature areas,
would consist of the same basic mixture as the filled honeycomb
ablator described above. To mold the material, a metal matched
mold of the desired shape may be used or it may be vacuum bag
molded over one forming surface in an autoclave. To bond molded
parts to the substructure, several acceptable adhesive systems
have been developed, and the choice would depend on the stress
analysis of the particular system and environment.

   b. Laminated Ablator

The laminated felt ablator would have a somewhat different com-
position than the filled honeycomb ablator in order to make it
amenable to fabrication by layup techniques. Organic fibers
would be added (Vinyon and Orlon) to a sufficient extent to make
possible the forming of the fibrous portion into a continuous web
or felt. The phenolic microballoons would be added during the
felting operation and would be distributed uniformly in the finished
felt. This felt would then be laid up on the desired surface and
the liquid resin system brushed or poured on to the felt to impreg-
nate it thoroughly. Ablator thickness may be modified as desired
by the addition of layers during the layup process. For the proposed
system, a reinforcement of the felt would be obtained by alternating
layers of felt with thin sheets of fiberglass scrim cloth, a screen-
like material with an open weave, which should reinforce the felt
composition without materially affecting the ablator's thermal
properties. After layup, the assembly would be vacuum bagged
for cure and post cure.

4.1.5 Insulation

For all concepts considered in the study, the inside of the vehicle would
be insulated by a layer of Q-Felt, varying from about 1-1/2 to 2-1/2

inches thick, mounted on the inside surface of the outer shell. This is a silica felt which could be attached to the structure using an adhesive that is tacky at application and is room temperature cured.

4.2 Assembly of Double Wall Vehicle

This section outlines a proposed breakdown of the vehicle into major structural subassemblies. A method for joining these subassemblies is described along with a feasible method for attachment that permits thermal expansion of the external shell relative to the inner pod(s). A frame arrangement providing for an efficient strength/weight ratio is presented.

a. Manufacturing Breaks and Joining Methods

The outer shell would be manufactured in several sections. The configuration of each of these sections is dictated by one or more of the following factors: production limitations imposed by shapes and sizes, joining methods, structural and thermal integrity, and physical acceptance of the inner pod by the outer shell. The proposed breakdown consists of: a nose cap, right and lefthand body shells, an upper longitudinal closure strip, a lower longitudinal closure strip, right and lefthand elevons, and right and lefthand tip fins (figure 86).

An alternate breakdown would be the same as above except for a semi-cylindrical shell between station 20.0 (nose cap interface station) and station 126.0 (maximum vehicle depth station at $X/C = 0.35$). This scheme may be required if aerothermal analyses or testing show that it is inadvisable to have longitudinal seams in the vicinity of the nose cap and its attendant high heating. This breakdown is not considered in the subsequent discussion.

The nose cap will be fabricated of molded or laminated ablator and fiberglass structure and will be spliced to the remainder of the vehicle at station 20.0 (figure 87, section A-A). This station was selected to insure that the stagnation point and its attendant area of high pressures and heating will occur forward of the splice.

The left and right body shells extend from station 20.0 to the trailing edge of the vehicle. The shells are mirror images that splice at Butt Line zero at the upper and lower surfaces. The fiberglass structure and ablator ends some distance from either side of BL 0.0, approximately 5 inches, to provide access for joining the two halves to each other and installation of fittings for attachment of the inner pod to the external shell (figure 87, section B-B). The ends of the ring frames will be joined in this access area by means of splice members applied to the ring frames. The splice members will extend beyond the limits of the open access area in order to pick up the bending loads from the
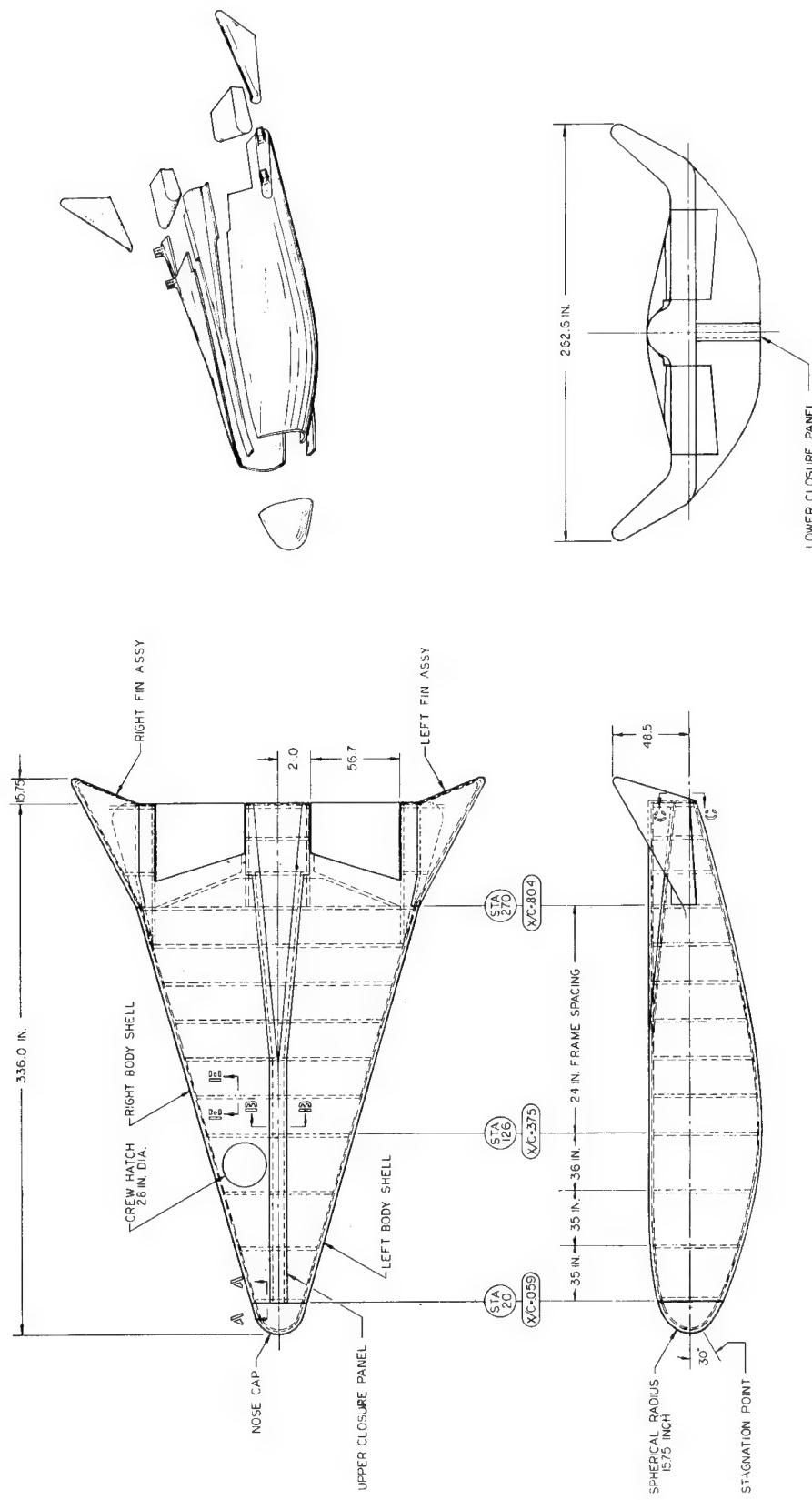
Figure 86 STRUCTURES ARRANGEMENT, DOUBLE WALL CONCEPT, FIBERGLASS SHELL
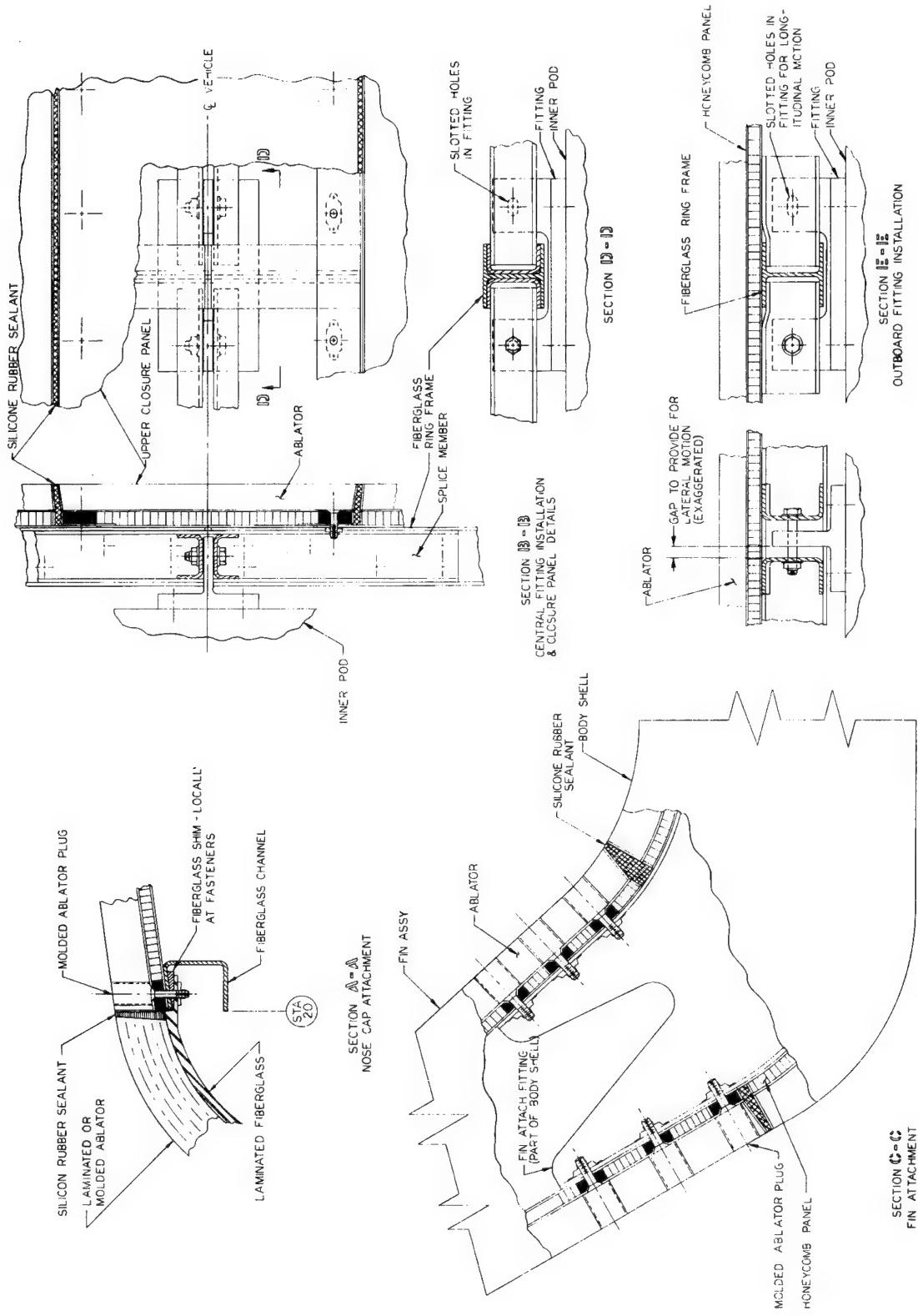
Figure 87 ASSEMBLY DETAILS, DOUBLE WALL CONCEPT, FIBERGLASS SHELL

-132-

fiberglass sandwich panel and transmit them across the access area
(figure 87, section B-B). These splice members may be fiberglass
sheets or shapes, such as channels, which may be nested in the ring
frames and attached by mechanical fasteners.

After the left and right shell halves have been joined and the nose cap
is in place, the upper and lower longitudinal closure strips may be
bolted in place over the access openings.

Each tip fin will be constructed so that it may be slipped over two or
more attachment fittings which extend from each of the shell halves
(figure 87, section C-C). These fittings will be an integral part of
the shell structure unless otherwise dictated by manufacturing re-
quirements. The fins will be physically attached by means of
a series of bolts installed from the exterior of the vehicle.

At the interface area of each of these exterior shell structure portions,
there will be a gap of approximately 0.2 - 0.3 inch between the fiber-
glass panels in order to accomodate a silicone rubber filler required to
seal the joint. The edge of the ablator will be inclined at some small
draft angle to the normal. The edge of the ablator which acts as the
closure member (such as the nose cap or the longitudinal closure
strips) will have a corresponding angle but will be greater by approxi-
mately 3 degrees so that the gap at the exterior surface of the ablator
will be smaller than the gap at the bond line between the ablator and
the fiberglass sandwich panel. The rubber gasket may be cast in place
by the following procedure: first, the interface surface of the closure
member is coated with a release agent. The closure panel is then
mounted in place but shimmed an amount to provide desired gasket
compression at final assembly.

The silicone rubber is then injected into the gap or cavity, which ex-
tends for the full length of the closure member. It is allowed to cure,
after which time the panel and shims are removed and the panel is
ready for final assembly. This procedure will result in a sealing
member which conforms to the shape of the joint and exerts a con-
tinuous pressure or sealing action against mating parts at all times
when they are in final installed positions.

A 28-inch diameter personnel hatch is provided in the forward right
hand shell at station 108.0. It is assumed that in docking operations
personnel transfer between vehicles would be required and that
the access would logically be through the central fairing in the aft
end of this vehicle. Due to the requirements of minimum permissable
access holes and the necessary structure in this area, the fairing radius
would have to be enlarged to permit use of this area for personnel access.

In order to fasten the sections together, it will be necessary to counter-bore through the ablator material to provide for the installation of bolts, screws, etc. These counterbored holes may be tapped and then filled with threaded plugs fabricated from molded ablator material. After installation these plugs may be machined down to match the external contour of the ablator.

b. Frame Spacing

The principal crew or crew and cargo compartment area is expected to be within limits of $X/C = 0.059$ (station 20.0) and $X/C = 0.804$ (station 270.0). Between station 20.0 and station 126.0 the ring frames are spaced at approximately 35 inches and between station 126.0 and station 270.0 they are spaced at approximately 24 inches (figure 86).

In the vicinity of station 126.0 ($X/C = 0.375$) rigid or nonthermally compensating fittings between the outer shell and the inner pod will be employed. These fittings will be mounted on the vehicle centerline and will be required to transmit the longitudinal launch loads between the outer shell and the inner pod. The ring frames at the vehicle center line are not tied to the honeycomb sandwich panel and are relatively weak in resisting these longitudinal loads. Therefore, diagonal inter-costals will be attached to the ring frames in the area of the fittings on one end and the other end will be attached to the adjacent ring frame where it is bonded to the fiberglass honeycomb sandwich panel. At the outboard fitting locations longerons running between the two frames on either side of station 126.0 will be required to shear the fitting loads out into the shell.

Aft of station 270.0 ($X/C = 0.804$) frame locations along with longerons and intercostals will be located and oriented as dictated by a combination of structural and internal mechanical requirements.

c. Attachments between Inner Pod and Outer Shell

In the previous section it was stated that a fitting providing a rigid connection between the inner pod and outer shell would be located at BL 0.0 and station 126.0 upper and lower surfaces. Other fittings will be required at frame stations along the vehicle center line (BL 0.0) top and bottom surfaces. These fittings will permit longitudinal translation between the inner pod and the outer shell to compensate for the difference between their respective rates of thermal expansion and temperature environments. These fittings restrain lateral and vertical translation (figure 87, section D-D).

Additionally, other fittings will be installed at approximately midsemi-span at frame stations. These fittings are designed to permit both longitudinal and lateral translation while restraining vertical (Z axis) translation (figure 87, section E-E).

The attachment between these fittings and the inner pod will be accomplished when the inner pod is mated to the left and right shell halves and they, in turn, are mated to each other. The nose cap, upper and lower closure strips and tip fins may be attached at any time subsequent to this operation.

For this study, the inner pod has been assumed to be a pressurized unit conforming to the shape of the exterior shell and extending from the nose rearward to approximately station 270.0 (X/C = 0.8). The remainder of the interior of the vehicle is assumed to be taken up with control surfaces, actuators and other miscellaneous equipment.

It is realized, also, that the inner pod could be made up of one or more pressurized units for crew and personnel requirements and one or more randomly sized and oriented, pressurized or unpressurized cargo and equipment cells. These random cells could either be attached to primary structure or serve as structural units.

4.3 Refurbishing

A study was made of the feasibility of reusing the outer structural shell by refurbishing the ablator. The two ablators under consideration must be considered separately since the different types of heat shield material will require different considerations in respect to the reapplication of a new ablator. The temperature of a reusable fiberglass outer shell structure would have to be limited to 500°F because of the degradation in properties of fiberglass even at short periods above this temperature. Where reuse of the shell is not considered, a short time temperature as high as 700°F could be considered. In the case of aluminum honeycomb single shell construction, the temperature would have to be limited to about 300°F for a reusable structure. When a 15-7 Mo outer shell structure is used, temperatures as high as 1050°F could be tolerated by the material. The exact limiting temperature would be dependent on the heat transfer to the inner pressure shell.

Assuming that the thermal design limits the temperature of the shell structure to that compatible with the material used, there will probably be 1/4 to 1/2 inch of uncharred ablator remaining on the vehicle (at least in the case of fiberglass and aluminum). A part or all of this would have to be removed, depending on the type of ablator used.

4.3.1 Filled H/C Ablator

In the case of the honeycomb filled ablator, there can be no assurance that a new fiberglass honeycomb could be satisfactorily bonded to a portion of the former heat shield which might still be in good condition on the vehicle. Therefore, all of the original heat shield would have to be removed at least down to the surface of the tape adhesive.

The process by which this would be removed would be by rough machining, finish machining, and hand finishing to the surface of the tape. The tape adhesive bond usually has a distinctly different color and hardness than the ablator material and is sufficiently thick to act as an indicator for machining operations, especially of the hand finishing type.

The proposed method would involve the following procedures:

1) Disassemble the vehicle into components.

2) Install outer shell with charred ablator in fixture, utilizing original inspection logs to locate and orient the structure.

3) Rough machine to 1/4 inch nominal from the outer face sheet of the shell structure.

4) Drill gage holes through the ablator to the surface of adhesive utilizing flat end release clutch drills.

5) Inspect and plot OML of outer shell structure based on gaging from 4 above. Rerun new numerical tape of machining facility.

6) Finish machine ablator to as close to the adhesive tape as possible.

7) Hand sand, scrap, power sand to below tape surface to give a smooth finish.

8) Inspect and rework face sheet and shell structure where required.

9) Replot new OML of shell structure.

There would be no difference in the ablator removal process from one type of outer shell structure to another, except for possible minor differences in the repair of damage to the face sheet and structural members.

4.3.2 Laminated Ablator

In considering the feasibility of refurbishing the laminated ablator, the fact that this is applied as a wet layup makes it appear possible that the original ablator need only be removed until a fairly uniform thickness of uncharred ablator remains. With this original ablator as a base, the new ablator could be layed up to the desired thickness. The integrity of the bond joint between the old and the new ablator would have to be evaluated but there is good reason to assume that with this type of ablator no problem would exist.

Inspection of the shell structure and gaging of the thickness of the old and new heat shield would constitute a major but not insurmountable problem. Since all of the ablator would not be removed, actual inspection of the outer face sheet could not be made. However, by close comparison of original records of the inner surface and existing inner surface at time of refurbishing coupled with a complete nondestructive inspection of the shell, an accurate evaluation of the shell condition could be made. The means of gaging the thickness of both the old and the new ablator is a problem since the drilling of gage holes is very difficult as no tape adhesive is present to afford protection to the outer shell structure. There is a good possibility that advanced techniques in nondestructive testing can afford a solution to this inspection problem.

The procedure to be used in preparing the old felt ablator for refurbishing is as follows:

1) Disassemble the vehicle into components.

2) Install outer shell with charred ablator on fixture, utilizing the original inspection logs to locate and orient structure.

3) Rough machine to 1/4 inch nominal from the outer face sheet of the shell structure.

4) Drill gage holes through the ablator to the surface of the shell structure.

5) Inspect and plot OML of outer shell structure.

6) Rework face sheet and structure where required.

7) Clean and prepare surface for application of new ablator.

The procedure for removal of the old ablator would be the same regardless of the type of shell structure used.

5.0 VEHICLE FABRICATION COST ANALYSIS

An integral part of the feasibility study was an analysis of the costs which would be incurred in fabricating the main ablator and primary structure of a vehicle such as the one considered herein for the various concepts considered. The analysis consisted of estimating the cost per vehicle based on the individual costs for materials, labor, tooling and special facility equipment. It should be noted that the cost figures presented do not take into account any detail design aspects of the vehicle such as doors, windows or other discontinuities, since no definition of such was specified in the statement of work. The addition of these items will increase the overall cost considerably, depending on the number and complexity of the openings, which are primarily a function of the mission requirements. For comparison purposes, cost estimates were determined for three structural designs and two prime ablators. The prime heat shields considered were the filled honeycomb and laminated ablators. The double wall structural designs were the fiberglass and 15-7 Mo steel honeycomb outer shells with ablator (both to be assembled around an inner aluminum honeycomb pressure shell), while the single wall design was an aluminum honeycomb shell with ablator.

In addition, the costs involved in refurbishing the ablators so that the outer shell structure could be reused were also considered. Analyses were performed to indicate the economics involved for multimission reusability and its effect on the turnaround time of the vehicle.

The cost figures were made on a square footage rather than a weight basis whenever applicable. The areas used for the cost analyses were as follows: ablator-900 ft^2; outer shell structure-950 ft^2; inner pressure shell -607 ft^2, and for the Q-Felt insulation, 640 ft^2. A summary of the cost analysis, based on an estimated labor cost of \$10.00 per man-hour is presented in the paragraphs below.

It should be noted that the cost estimates as outlined herein represent only a portion of the total cost that would be incurred in an operational vehicle such as the one analyzed in this study. Other considerations must be taken into account, such as costs per launch, the number of launches required to perform the mission and the subsequent cost per pound of payload in orbit. These costs will be considerably greater than those for fabrication of the heat shield and structure of the vehicle. For a given launch weight, the heavier the basic entry vehicle, the less becomes the useful payload the vehicle can carry; subsequently, the launch cost per pound of payload will be greater. If one considers the Saturn C-1 B as the launch booster, cost for the booster and operational support is estimated to be in the order of \$45,000,000 per flight. These launch costs, therefore, will put a great emphasis on vehicle weight in the overall mission economics.

5.1 Ablator and Structure Costs

The cost estimates presented herein for the fabrication of the various ablator and structural materials considered during this study are composed of both labor and material costs, which are based on the processes described in section 4.1. The labor costs include such items as inspection, cleaning, bonding, curing, machining, repair and overall quality control of the hardware. Estimates for fabricating the heat shield can be quoted with a fair degree of confidence since each item considered is based on actual cost figures. A summary for each design, less tooling and special facility equipment requirements, is presented in table XX. It will be noted that the laminated ablator is cheaper to fabricate than the filled honeycomb ablator by about 13 percent.

In considering the use of 15-7 Mo age-hardened stainless steel honeycomb for the outer shell structure it was assumed that the panels would be a vendor purchased item since much specialized equipment and tooling are required. In arriving at a cost figure for the two main structures, a figure of $550 per square foot was used as the weighting factor.

The fabrication costs per square foot for an aluminum honeycomb structure will be the same whether it is the inner pressure vessel or the aluminum single shell vehicle, based on the preliminary data available. In estimating these figures, it was assumed that the aluminum honeycomb sandwich will be made in house with the components purchased as commercial materials.

A comparison of the total vehicle costs in table XX indicates that the steel outer shell-aluminum pressure shell vehicle would be 53 percent more expensive to fabricate than the one with the fiberglass outer shell because of the much higher cost of the steel outer shell. The aluminum single shell vehicle, because it has only one structural shell instead of two, would be 22 percent cheaper.

5.2 Special Facility Equipment

In fabricating a vehicle such as the one considered herein, a number of special facilities are required. These facilities include such items as curing ovens, vacuum and refrigeration equipment, a specialized machining facility, a large welding facility, forming and autoclaving equipment, cleaning equipment, and inspection equipment. Total cost of these facilities is estimated to be $1,631,000 for fabrication of an entire vehicle using the filled H/C ablator and $1,642,000 for a vehicle

TABLE XX

FABRICATION COSTS
(In Dollars)

Vehicle	Cost Item	Ablator		Structure		Insulation Q-Felt	Complete Vehicle with Ablator	
		Filled H/C	Laminated	Outer	Inner		Filled H/C	Laminated
Fiberglass Shell, Aluminum Inner Shell	Materials	44,000	40,000	40,000	23,000	4,000		
	Labor	331,000	286,000	241,000	193,000	16,000		
	Total	375,000	326,000	281,000	216,000	20,000	892,000	843,000
Stainless Steel Shell, Aluminum Inner Shell	Materials	44,000	40,000	531,000	23,000	4,000		
	Labor	331,000	286,000	225,000	193,000	16,000		
	Total	375,000	326,000	756,000	216,000	20,000	1,367,000	1,318,000
Aluminum Single Shell	Materials	44,000	40,000	34,000		4,000		
	Labor	331,000	286,000	265,000		16,000		
	Total	375,000	326,000	299,000		20,000	694,000	645,000

with the laminated ablator. These costs are independent of the design concept considered. It should be noted that these cost figures do not take into account any facility equipment which may currently exist to do the work but are rather an estimate of what would be required if none were available.

5.3 Tooling

The tooling items required for the fabrication of the vehicle are quite extensive. These include the master facility tools and splashes from molds for edge members, honeycomb panels, and structural members; machining tools and templates, handling fixtures, special assembly fixtures, vacuum bags, panel closeout molds, inspection fixtures, and final assembly fixtures. The cost of special tooling including tool engineering, tool proofing, and Quality Control is $2,102,000 for a fiberglass honeycomb outer shell, $339,000 for a 15-7 Mo stainless steel honeycomb outer shell, $1,665,000 for an aluminum honeycomb single shell, and $637,000 for the ablator. The total tooling costs for a complete vehicle with the filled H/C ablator would be $3,123,000 for the fiberglass outer shell vehicle, $2,396,000 for the steel outer shell vehicle, and $2,624,000 for the single aluminum shell vehicle.

In the above figures, it was assumed that the stainless steel honeycomb panels would be vendor-purchased items since much specialized equipment and tooling are required. Therefore, the cost of tooling for the steel construction as presented herein reflects only that tooling which would be required for assembly.

5.4 Refurbishing

The costs of refurbishing a used outer shell with a new coating of ablator are presented below. These costs were based on the refurbishing operations outlined in section 4.3.

5.4.1 Filled H/C Ablator

The cost of a fully refurbished filled H/C ablation shield is the removal cost of $163,000 plus the ablator fabrication cost of $375,000 from table XX. This gives a total cost for the refurbished heat shield of $538,000. A comparison of the savings of a refurbished heat shield over the fabrication of a new outer shell plus ablator is given below for the various concepts:

Refurbished Ablator	Fiberglass H/C Shell + Ablator	Steel H/C Shell + Ablator	Aluminum H/C Shell + Ablator
$538,000	$656,000	$1,131,000	$674,000

5.4.2. Laminated Ablator

The total cost of removing the laminated type ablator is $100,000.
In order to arrive at a cost figure for a refurbished felt heat shield,
the cost of removal, $100,000, must be added to the cost for install-
ing a new laminated heat shield--$326,000-- as given in table XX.
This amounts to a total of $426,000. A comparison of the savings
of a refurbished felt heat shield over the fabrication of a new outer
shell plus felt ablator is given below:

Refurbished Ablator	Fiberglass H/C Shell + Ablator	Steel H/C Shell + Ablator	Aluminum H/C Shell + Ablator
$426,000	$607,000	$1,082,000	$625,000

5.4.3 Feasibility of Reusability

Based on the estimated refurbishing costs of the vehicle, trade-offs
between refurbishing or discarding a used fiberglass outer shell of
a double wall concept were made as well as comparisons between
the reusability aspects of single and double wall concepts. These
cost figures favor refurbishment of the outer shell, especially
when many missions are involved. The difference in cost between
a refurbished fiberglass outer shell and a new one is about $118,000
for the filled H/C ablator and $181,000 for the laminated ablator.
As an illustrative example of the significance of these figures,
suppose that a vehicle is to be used to resupply a space station over
a period of time involving 24 flights and that the time between flights
is short enough to require four complete vehicles to be built,
assuming the inner shells are reusable. Then, the difference be-
tween building 20 additional outer shells and refurbishing the
original four, each five times, is $2,360,000 for the filled H/C
ablator and $3,620,000 for the laminated ablator.

Based on the above figures, it appears that further study into the feasibility of refurbishing heat shields on recoverable space vehicles considering cost alone, is warranted. The economics, however, have to be adjusted to include the weight penalties of a thicker heat shield, due to the lower allowable maximum temperature for a fiberglass structure that is to be reused, and the changes in the shell structural properties caused by reentry heating.

It is also possible to make a qualitative comparison between reusability of a double wall vehicle versus that of a single shell vehicle, even though the basic costs of refurbishing are the same. Reusability of a double shell vehicle would consist of reusing the inner pressure vessel and either replacing or refurbishing the used outer shell. Short turnaround times are possible with double wall construction because the outer shell is removable. After a mission, the outer shell would be disassembled and replaced by a new unit, fabricated beforehand. The vehicle could then be readied for another flight. In the meantime, refurbishing of the used outer shell could be initiated to make it ready for a future mission if so desired. Thus, the time involved in refurbishing would not affect the turnaround time of the vehicle.

On the other hand, refurbishing a single shell vehicle would require a lengthy turnaround time, which must include the time required to remove the used ablator and fabricate a new one. Furthermore, the relatively high curing temperature of the ablator bond ($\sim 300\,°F$) might require that electronic and other sensitive equipment be removed from the vehicle during that process, further adding to the basic refurbishing cost and turnaround time. Accordingly, if several flights are required with relatively short turnaround times, more single shell than double shell vehicles would have to be built to perform those missions, and the resulting fabrication costs based upon the single shell concept would be higher, despite its lower initial cost relative to a double shell vehicle.

As was mentioned previously, the launch cost to put a pound of useful payload in orbit is dependent on vehicle weight, which thus becomes an important factor in the economics of reusability and/or refurbishability and the type of vehicle construction used. For example, in table XVIII, the single wall design was shown to be more than 1300 pounds heavier than the double wall construction. Should an increase in vehicle heat shield and structure weight of this magnitude reduce the useful payload capability of the vehicle enough to require an additional flight to accomplish the objectives of the mission, then the additional cost of launching such a vehicle would overshadow the savings obtained in the initial fabrication.

6.0 PARAMETRIC STUDIES

Parametric studies were performed in an attempt to determine the effects on the performance and weight of the thermo-structural composite (ablator plus substructure) due to variations in the thermal and mechanical properties of the ablator material.

6.1 Thermal Properties and Ablation Characteristics of the Filled Honeycomb Ablator

The intent of this portion of the study was to determine the relationship between required filled-honeycomb ablator weight and variations in each thermal property of the material. These relationships were established by determining the ablator weight required to limit bondline temperature to 700°F assuming a uniform initial temperature of 250°F. This was done for discrete changes in a particular thermal property -- all other properties being held at their nominal values for the specific body station being investigated.

The trajectory selected for the parametric studies was the L/D max, 36, 500 fps overshoot, which proved to be the design trajectory for most of the heat shield on the double wall vehicles.

Three typical body locations were investigated and are described below:

  a. Stagnation Region

The stagnation region represents the region of most severe thermal environment. The location selected for this study was a point 20 inches aft of the stagnation point.

  b. Windward Side, X/C = 0.5

Weight variations at the X/C = 0.5 station on the windward element of the vehicle constitute the best index of heat shield weight variation for the whole vehicle. The reference slab, or vehicle wall section, or thermal properties is shown below:

-144-
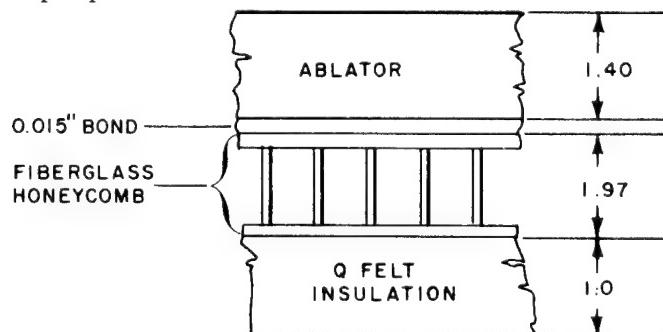
c. Leeward Side

A typical station in the separated flow region of the vehicle was included in this study. Weight variations predicted at this station are common to about one quarter of the total vehicle surface, because the air flow will be separated over the major portion of the leeward side of the vehicle during reentry.

Results of this study are presented graphically in figures 88 through 93. Each of these graphs contains predicted results for only those vehicle stations at which the particular subject thermal property has been demonstrated to have at least appreciable, if not predominant, influence on ablator weight. For example, each thermal property most directly related to the ablation process will certainly be of primary importance in regions subjected to the highest heating rates, and will have little or no effect at vehicle stations experiencing low heating rates.

The following paragraphs discuss each of the thermal properties that were varied independently over a predetermined range of deviations from their nominal values. It must be noted that the range of values selected (and covered in figures 88 through 93) do not necessarily represent physically realizable thermal properties of the filled honeycomb ablator material or any derivative thereof.

a. Thermal Conducitivty

Because the thermal conductivity of a material is basic to all heat transfer processes occuring within that material, the effects of variations in thermal conductivity were investigated at each of the three references stations. In the analyses, the effects of proportional reductions in thermal conductivity at all temperature levels were considered. These proportional changes were achieved by applying constant multipliers of 0.7, 0.85, and the nominal multiplier of 1.0 to the temperature-dependent thermal conductivity (see figure 20 for nominal thermal conductivity-temperature relationship). The results of the thermal conductivity variation analyses are presented in figure 88, and indicate a potential weight saving of fifteen to twenty per cent, the largest percentage savings to be realized, as expected, at the leeward location.

b. Density

Figure 89 indicates that a decrease in density of 25 percent from the nominal value of 30.8 lb/ft^3 would result in potential weight savings of 12.0 to 17.0 percent at high to low heating regions; again, the leeward side showing the highest potential for percentage weight savings. These percentages are based on a nominal thermal conductivity at all density levels. In actuality, a decrease in density would usually cause a decrease in conductivity, so that weight reductions due to both effects would be realized, although they would not necessarily be directly additive.

-145-

c. Specific Heat

The specific heat of the present family of ablation materials is almost entirely insensitive to variations in material density and the associated compounding changes required to produce the several densities. Thus, a significant change in specific heat would necessarily imply a most basic alteration in the ablator composition, and, therefore, in all other material properties. Accordingly, changes in specific heat alone were not investigated.

d. Ablation Temperature

The filled honeycomb ablator material exhibits large variations in ablation temperature with heating rate. The desirability of a high or low ablation temperature level can be determined only by a complete analysis of the interactions of all thermal properties considered as a whole. It was found that the aggregate effect of all thermal properties considered as a whole. It was found that the aggregate effect of all other thermal properties of the filled honeycomb ablator material was, as expected, to render the ablator weight requirement relatively insensitive to ablation temperature level for vehicle regions exposed to low or moderate heating. The effect of varied ablation temperature at the stagnation region is more pronounced as can be seen from figure 90.

e. Heat of Vaporization and Laminar Transpiration Factor

Although these two properties were analyzed separately, it is convenient to discuss them together. The "heat of vaporization" and "laminar transpiration factor" are defined, respectively, by the terms H_v and η_L in the expression:

$$F = H_v + \eta_L (H_s - H_w)$$

The results of varying the heat of vaporization from a value of -1439.0 BTU/Lb to $+ 4000$ BTU/lb are shown in figure 91. Weight variations for increases in the laminar transpiration factor up to 2.0 are given in figure 92.

f. Emissivity

The influence of ablator emissivity on ablator weight is indicated in figure 93 which shows only minor weight savings by an increase in emissivity from 0.75 to 0.80.

It should be noted here that the small effects of ablation characteristics were anticipated as relatively low temperatures prevail over most of the vehicle surface through most of the reentry period. This is also true with respect to the surface (temperature and emissivity) characteristic.

Conclusions

a. Promising Areas of Weight Reductions

The most promising areas of ablator improvement with regard to potential weight reduction are the thermal conductivity and density of the material. A reduction of 30 percent in thermal conductivity has been shown to afford a potential weight saving of 16 to 21 percent. A 25 percent density reduction is predicted to lower ablator requirements by 12 to 17 percent. Furthermore, when a density reduction is accompanied by a conductivity reduction, as is often the case, a total weight savings representing a combination (but not necessarily directly additive) of the two effects will be realized.

b. Marginal Weight Reduction Areas

Extreme improvements in the heat of vaporization and laminar transpiration factor have been shown to yield possible ablator weight reductions of 7 and 13 percent respectively, in the stagnation region. These particular thermal properties, however, have far greater significance in the stagnation region than elsewhere. Therefore, potential weight reduction of the total ablator is much less than the percentages quoted. Also, although the heat of vaporization may be amenable to favorable modification with reasonable effort, improvement in the laminar transpiration factor would almost certainly require a long-term, full-scale development program not justified in the case of the mission analyzed.

Overall heat shield weight has been shown to be relatively insensitive to variation in ablation temperature -- even in the stagnation region, where it is influence would be most pronounced. Specifically, an increase of 500°F in ablation temperature is indicated to allow a reduction of 17 percent of the stagnation region ablator weight -- a small gain on an overall ablator weight basis.

Only a modest ablator weight reduction of 2 to 3 percent could be realized by increasing the ablator surface emissivity from its present nominal value to 0.75 to 0.8.

6.2 Structural Characteristics

In the following sections, structural parametrics relating to thermal stresses, axial and bending load carrying abilities of composite cross sections, and stiffnesses for buckling loads are presented.

6.2.1 Cold Soak Thermal Strain

In section 3.5.3.4, the cold soak thermal strain performances of the filled H/C and laminated ablator designs were presented. Corresponding

thermal strains for any ablator substructure composite are shown in figures 94 and 95, in which ablator strains and substructure stresses are plotted as a function of the modulus (E) times thickness ratio of the ablator to that of the substructure ($E_A t_A$ / $E_{FG} t_{FG}$) for various values of the differences in the coefficients of thermal expansion of the two materials. These curves are based on the assumptions of plane sections remaining plane, zero net force over the cross section, and no changes in curvature. The curves show that the smaller the differences between the coefficient of thermal expansion, the smaller will be the induced stresses and strains. Also, increasing the ablators E or thickness will decrease the ablator strains.

Figures 96 and 97 depict the effects on ablator strain of changing the difference between the zero stress temperature and the soak temperature for two different values of the Et ratio and for four values of the differences in coefficients of thermal expansion. Clearly, the nearer the two temperatures are to each other, the smaller will be the induced strains.

6.2.2 Reentry Thermal Strains

As discussed in section 3.4.3.4, reentry from a -250°F soak produced higher tensile and compressive ablator strains than a +250°F reentry, and accordingly the following studies emphasized the -250°F conditions more than the +250°F one.

The effects of changing the zero stress temperature from +200°F to 70°F on ablator strains during a typical +250°F and -250°F reentry are shown in figures 98 and 99. The reference case was the filled H/C ablator design at X/C = 0.5 on the bottom surface, subjected to the 36,500 fps L/D max overshoot trajectories. For the -250°F reentry, lowering the zero stress temperature would relieve the tensile ablator strains.

The effect of increasing the coefficient of thermal expansion of the filled H/C ablator by a factor of 1.5 on the thermal strains of a -250°F reentry is shown in figure 100. This increase makes the difference between the ablator and fiberglass a's larger, which results in larger thermal strains.

The effects of changing the ablator modulus of elasticity on ablator strains for a -250°F reentry are presented in figure 101, which also depicts just how the modulus was changed: The value of 0.25×10^6 psi at -250°F remained unaltered but decreased with temperature to a value of 0.06×10^6, three times the reference value. This would bring the E variation with temperature a little closer to that of the laminated abaltor whose E decreases from 0.56×10^6 to 0.21×10^6 psi.

6.2.3 Tensile Load

When an ablator-fiberglass cross section is subjected to a tensile load, the presence of the ablator can add to or impair the load carrying ability of the fiberglass, depending on its properties, provided no ablator cracking is allowed. Figure 102 depicts parametrically the load a cross section can carry as a function of the E times thickness ratio of the ablator to the substructure for several values of ultimate strain to failure of the ablator. The intercept of the ϵ = 1.2 percent curve with the vertical axis represents the load carrying ability of the fiberglass alone. If the ablator E and ϵ_{ULT} are too low, the full load carrying capability of the substructure is not utilized.

6.2.4 Bending Load

In the performance analysis for the filled H/C ablator designs, cracking of the ablator was the design criterion for the bottom surface of the vehicle and the frames rather than failure of the substructure. The worst loading condition was the +250°F reentry during which the modulus of the ablator was low as well as its ultimate allowable strain. Figures 103 through 105 point out the significance of a low E and ϵ_{ULT} of the ablator. For three different ablator thicknesses and various values of E, honeycomb core heights required to prevent ablator cracking in a composite section loaded by a typical bending moment were plotted as a function of ultimate ablator strain. Referring to figure 104, the reference point for the filled H/C ablator is labelled on the plot. A factor of two increase in the strain would decrease the core height considerably, and somewhat more than a factor of two increase in E. The core height required by the substructure to take the loads without the presence of the ablator can be found by extraplating the E = 0 curve out to ϵ_{ULT} = 6.6 percent. The required core height is much less. Thus, the full load carrying ability of the substructure is not utilized in a filled H/C ablator-fiberglass composite. For the laminated ablator design, however, with an ablator E of 0.21 x 10^6 and ϵ_{ULT} of 1.2 percent the strength of the composite is considerably greater than that of the fiberglass alone.

From figures 103 through 105, it is clear that the performance of the filled H/C ablator design can best be improved by increasing the ultimate strain of the material.

The effects of applying the same bending moment as in the previous cases on an ablator-fiberglass honeycomb cross section in the presence of -250°F cold soak thermal stress are shown in figures 106 through 108. The thermal stresses, which are proportional to to the differences in the coefficients of thermal expansion of the materials, impair the performance of the composite, which would require a greater core height to carry the same moment.

-149-

6.2.5 Buckling Load

The compressive buckling load of a flat plate or a very short cylinder is directly proportioned to D, the bending stiffness of the cross section. The effects of the ablator modulus of elasticity and of the substructure core height on D for three different ablator thicknesses are shown in figures 109 through 111. The E = 0 curves would represent the D of the substructure alone. Note that even for a small ablator E of 0.02×10^6 (filled H/C ablator) the core height for a required value of D is considerably reduced.

The buckling load for a cone or cylinder under external pressure is directly proportional to the quantity $D(B/D)^{1/4}$, where B is the extentional rigidity of the wall cross section. The effects of ablator E and of the substructure core height on this quantity are shown in figures 112 through 114. Just as for D alone, the presence of the ablator in a cross section significantly increases the buckling load.

Figure 89 ABLATOR WEIGHT VERSUS DENSITY
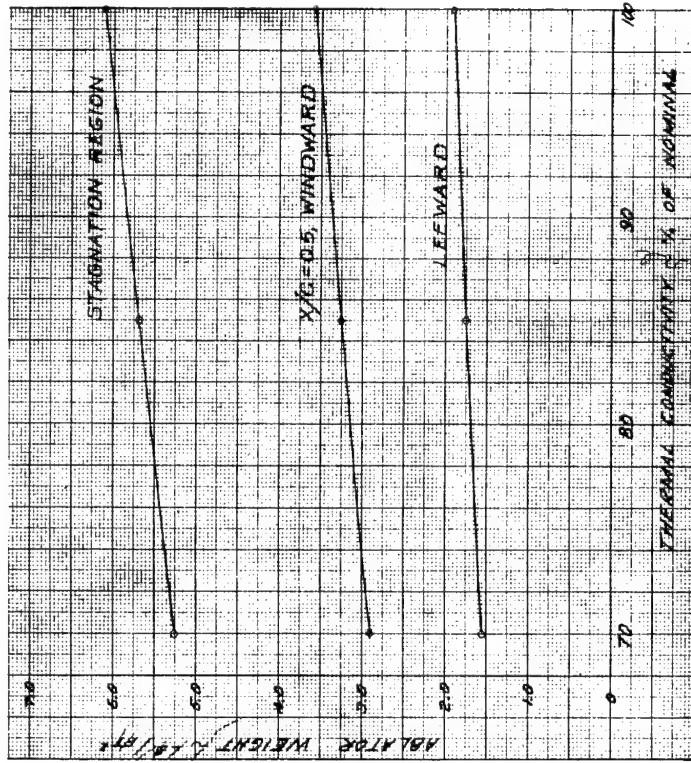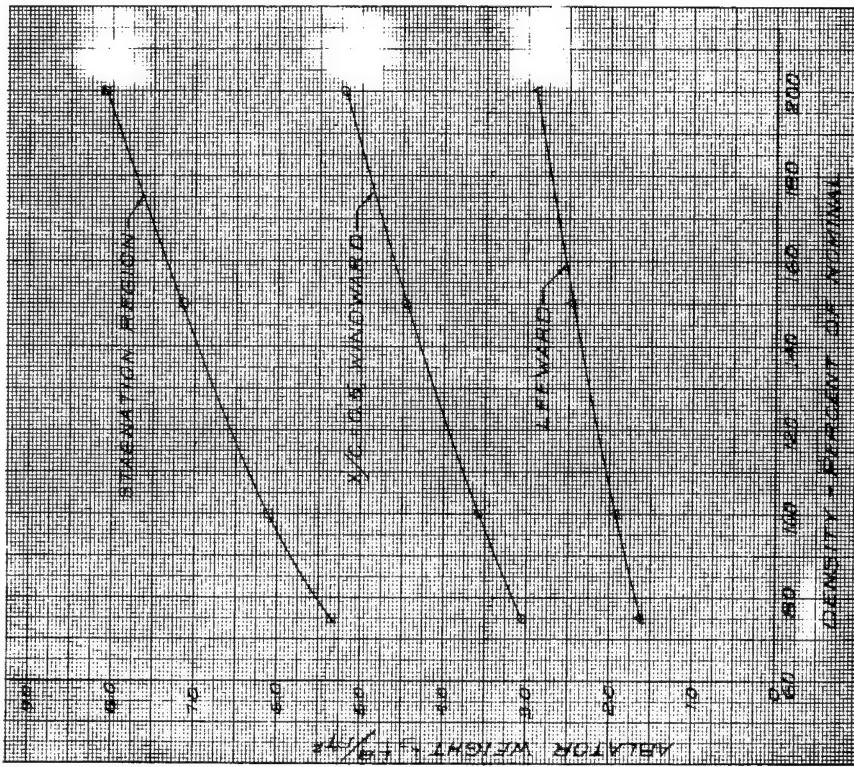
Figure 88 ABLATOR WEIGHT VERSUS THERMAL CONDUCTIVITY
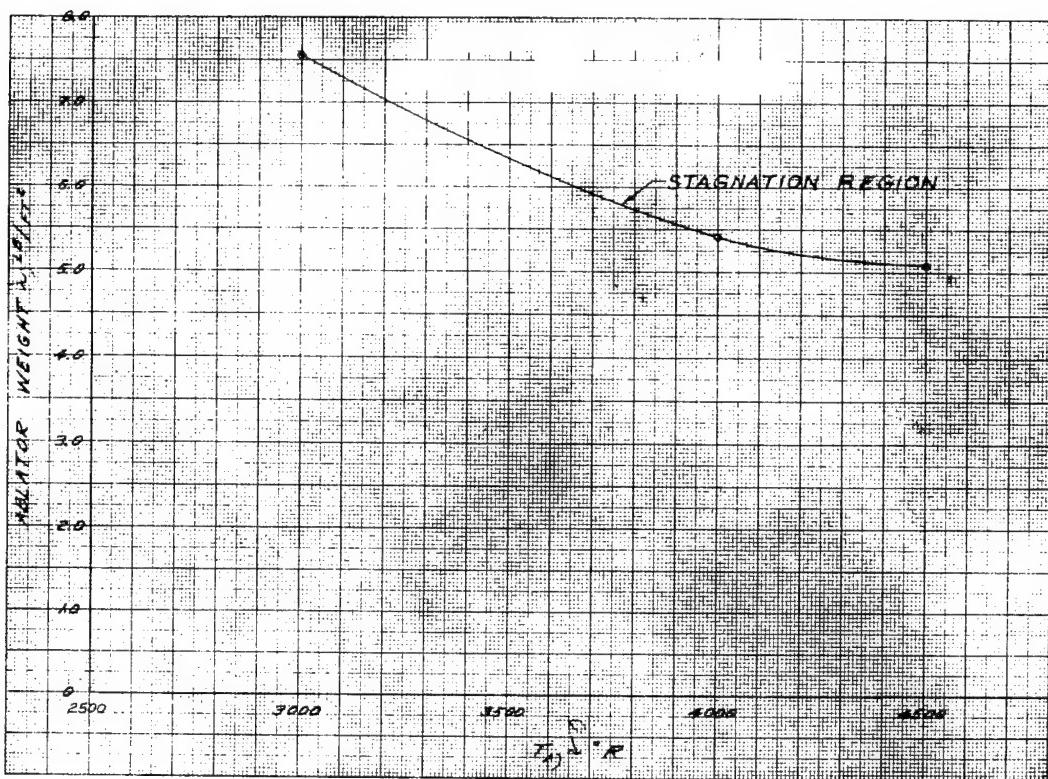
Figure 90 ABLATOR WEIGHT VERSUS ABLATION TEMPERATURE
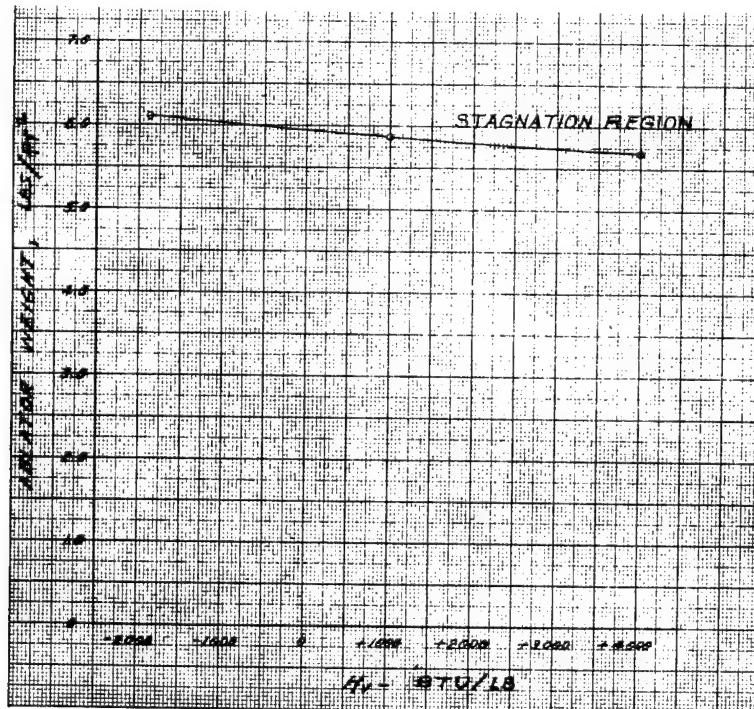
Figure 91 ABLATOR WEIGHT VERSUS HEAT OF VAPORIZATION

-152-
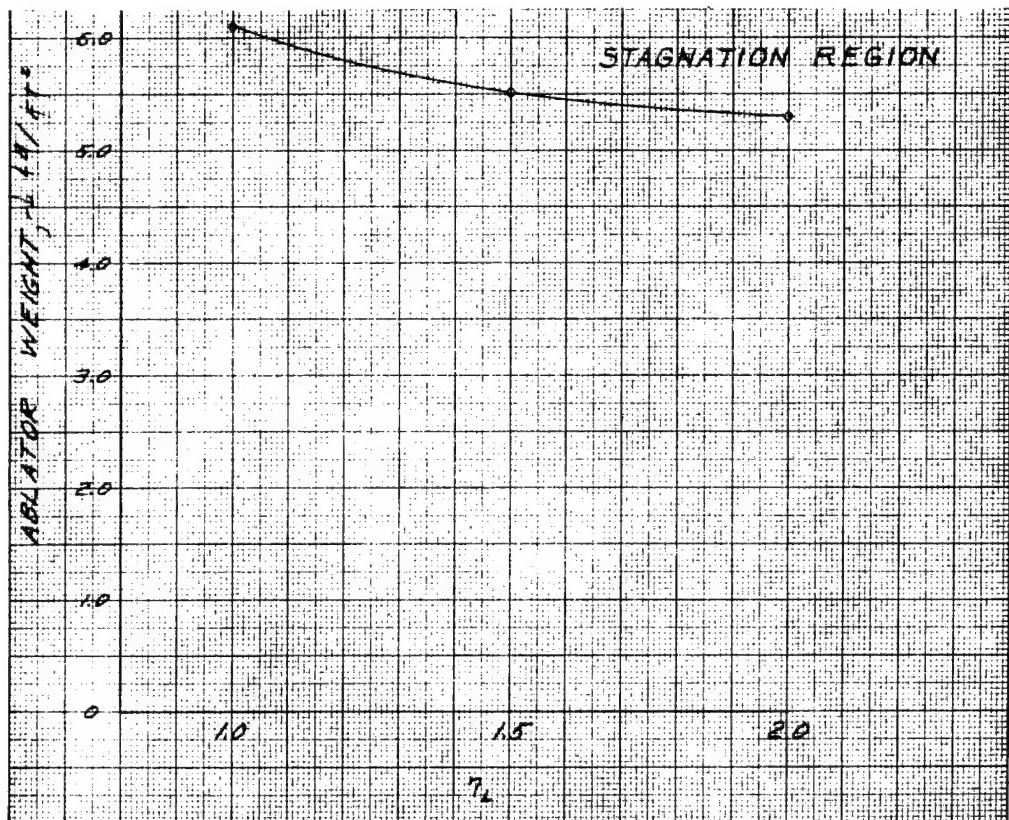
Figure 92 ABLATOR WEIGHT VERSUS LAMINAR TRANSPIRATION FACTOR
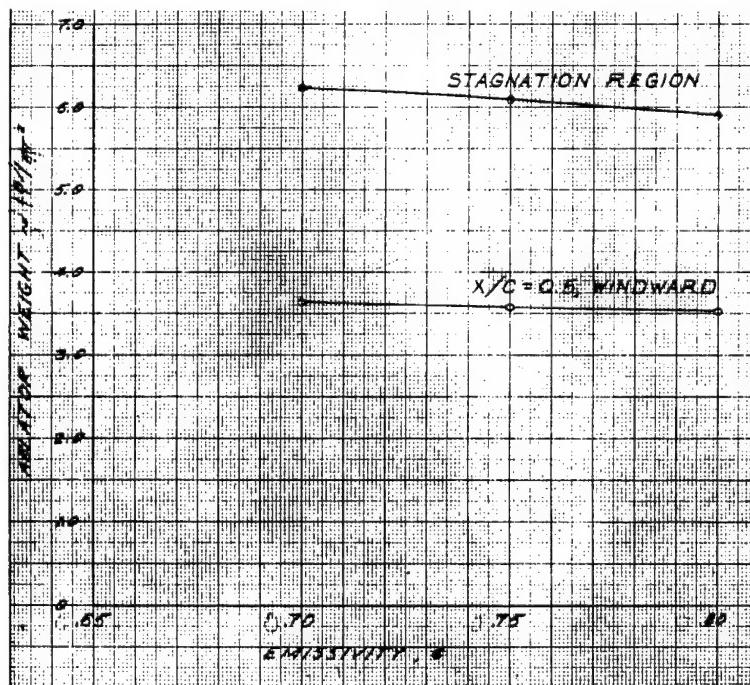
Figure 93 ABLATOR WEIGHT VERSUS EMISSIVITY

-153-
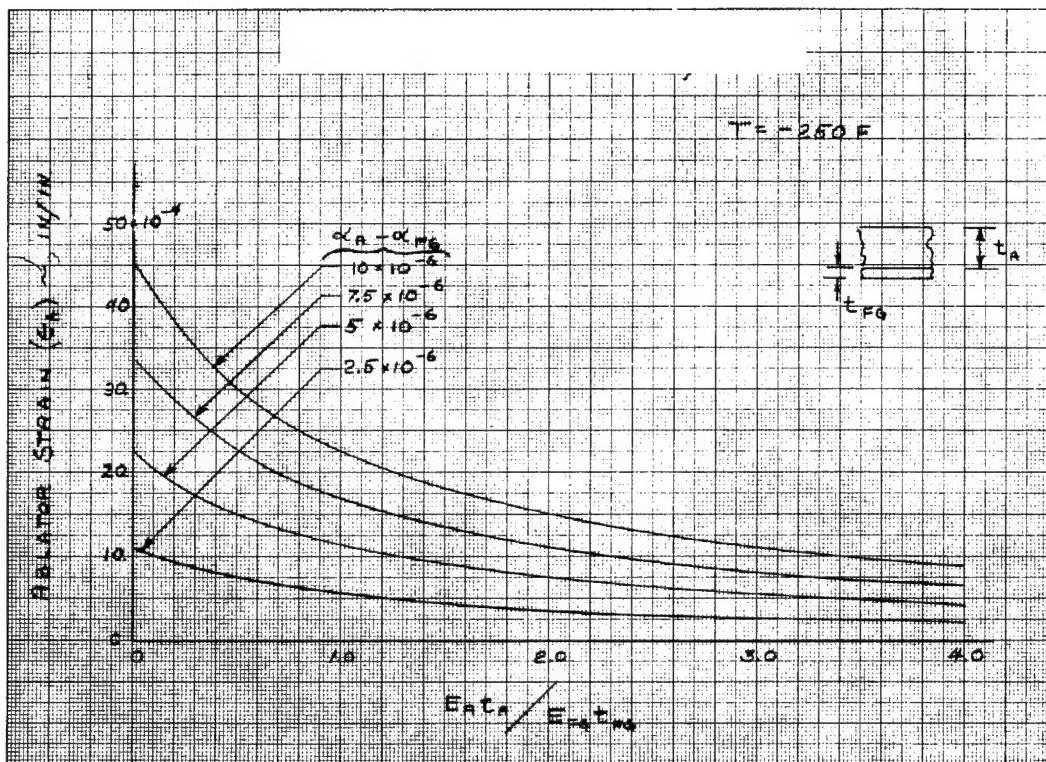
Figure 94 ABLATOR THERMAL STRAIN VERSUS EXTENSIONAL STIFFNESS
RATIO, T = −250°F, COLD SOAK
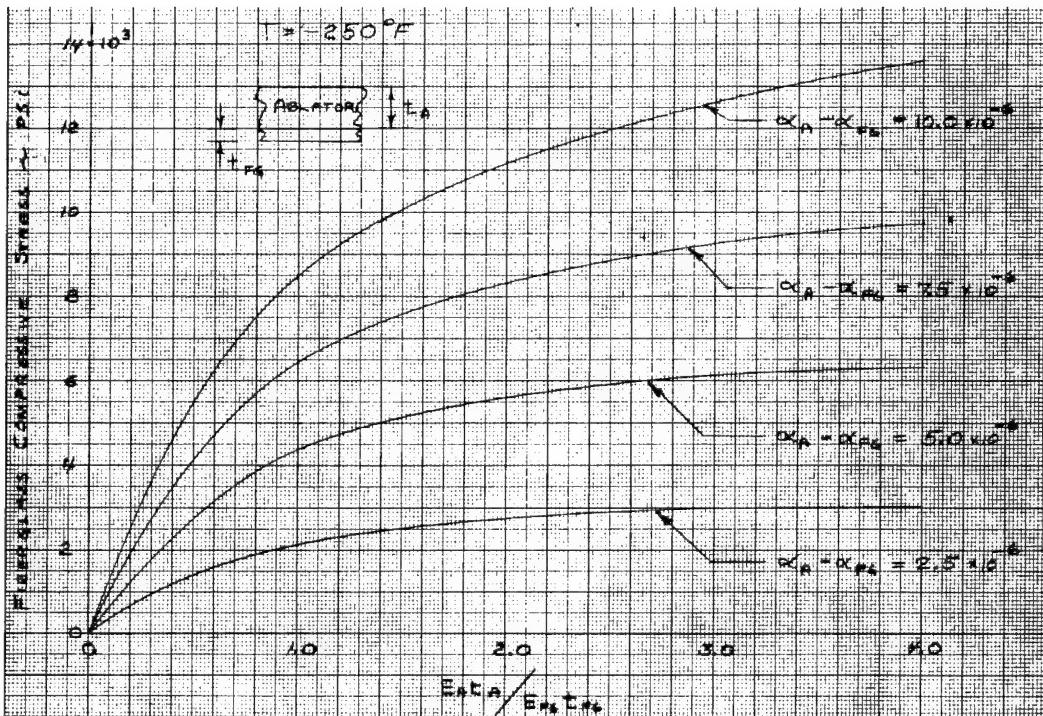
Figure 95 FIBERGLASS THERMAL COMPRESSIVE STRESS VERSUS EXTENSIONAL
STIFFNESS RATIO T = -250°F, COLD SOAK
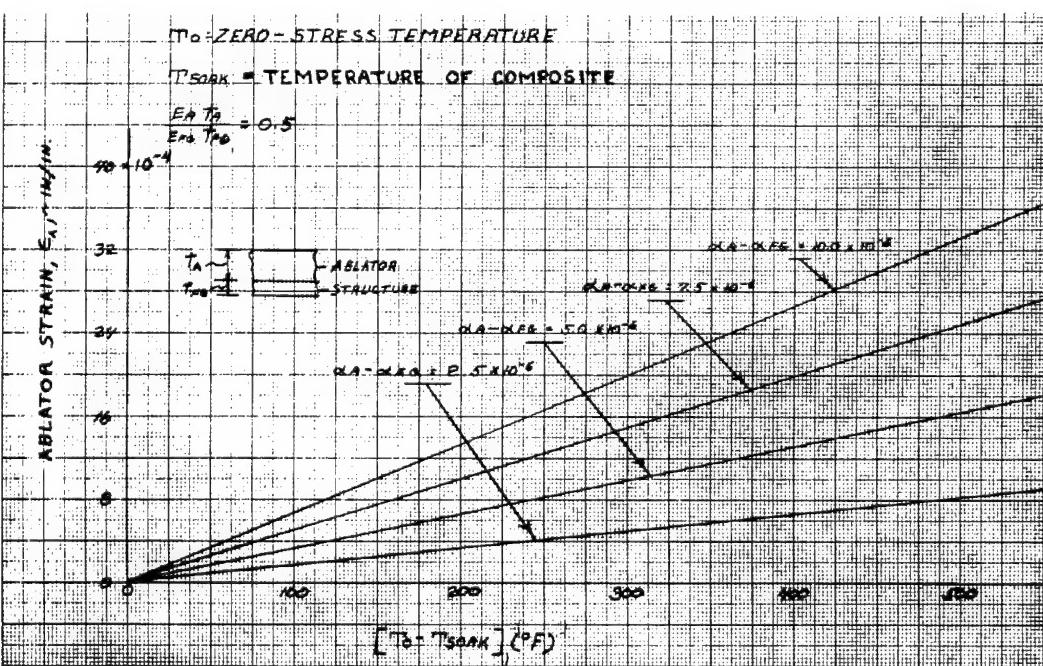
Figure 96 ABLATOR THERMAL STRAIN VERSUS SOAK TEMPERATURE FOR ABLATOR
TO FIBERGLASS STIFFNESS RATIO = .50
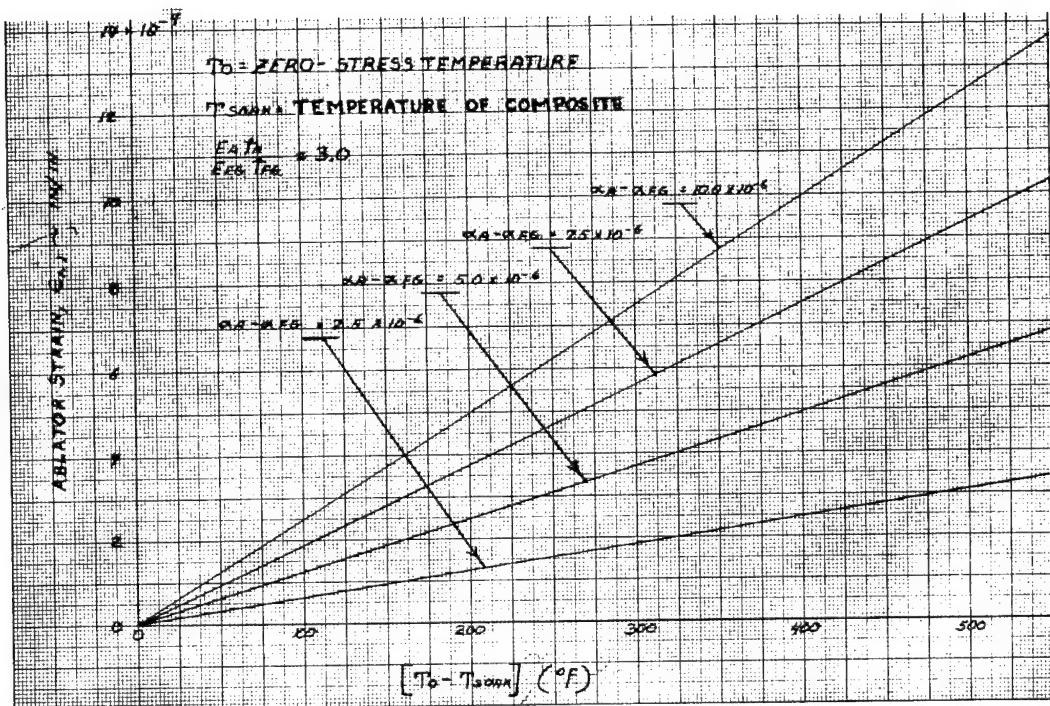
Figure 97 ABLATOR THERMAL STRAIN VERSUS SOAK TEMPERATURE FOR ABLATOR
TO FIBERGLASS STIFFNESS RATIO = 3.0
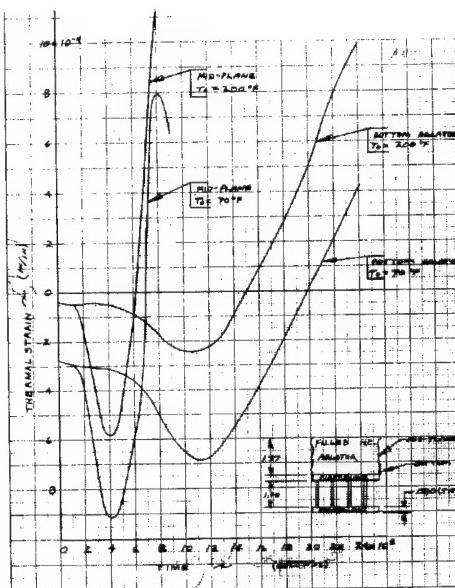
Figure 98 COMPARISON OF STRAIN VERSUS TIME FOR ZERO STRESS TEMPERATURE
EQUAL TO 70°F AND 200°F. FILLED HONEYCOMB ABLATOR, X/C = 0.5
WINDWARD, +250°F REENTRY, V_E = 36,500 FPS, OVERSHOOT
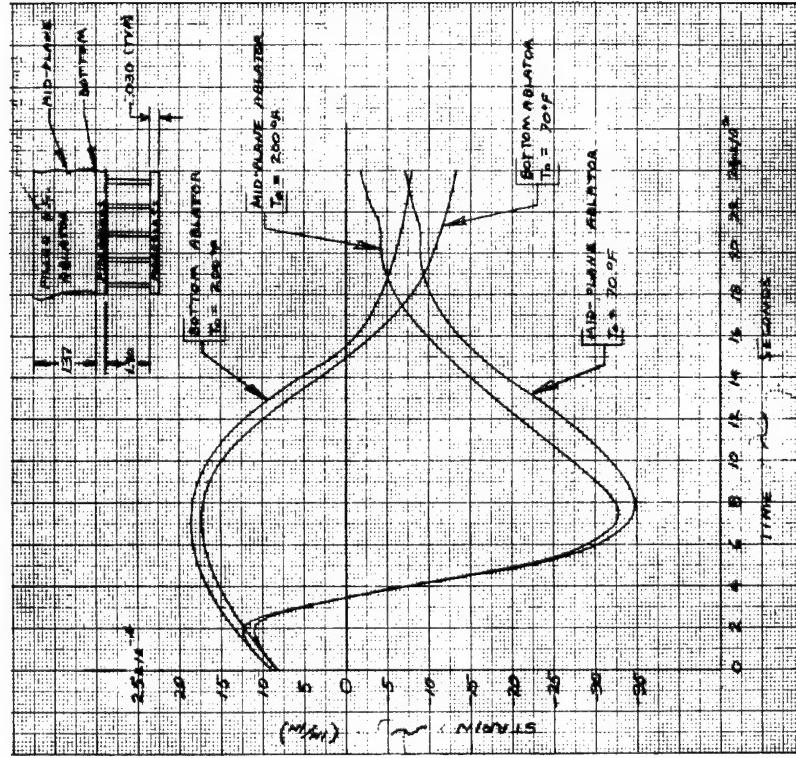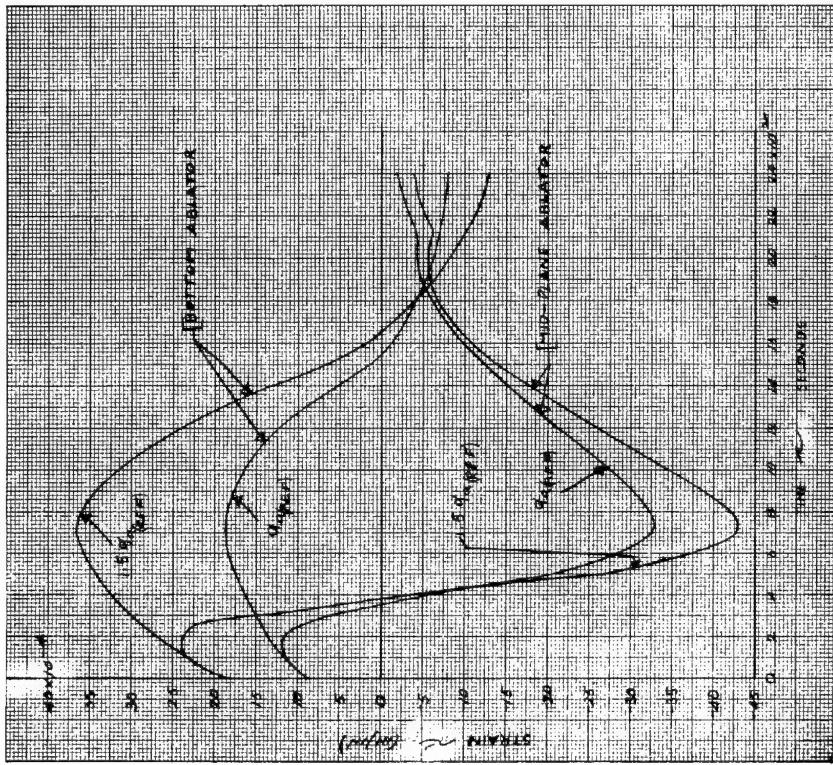
Figure 99   COMPARISON OF STRAIN VERSUS TIME FOR ZERO STRESS TEMPERATURES EQUAL TO 70°F AND 200°F. FILLED HONEYCOMB ABLATOR, X/C = 0.5 WINDWARD,-250°F REENTRY, V_E = 36,500FPS, OVERSHOOT

Figure 100   COMPARISON OF STRAIN VERSUS TIME WITH A CHANGE IN THE COEFFICIENT OF THERMAL EXPANSION OF ABLATOR,X/C = 0.5 WINDWARD,-250°F REENTRY, V_E = 36,500 FPS, OVERSHOOT

-157-
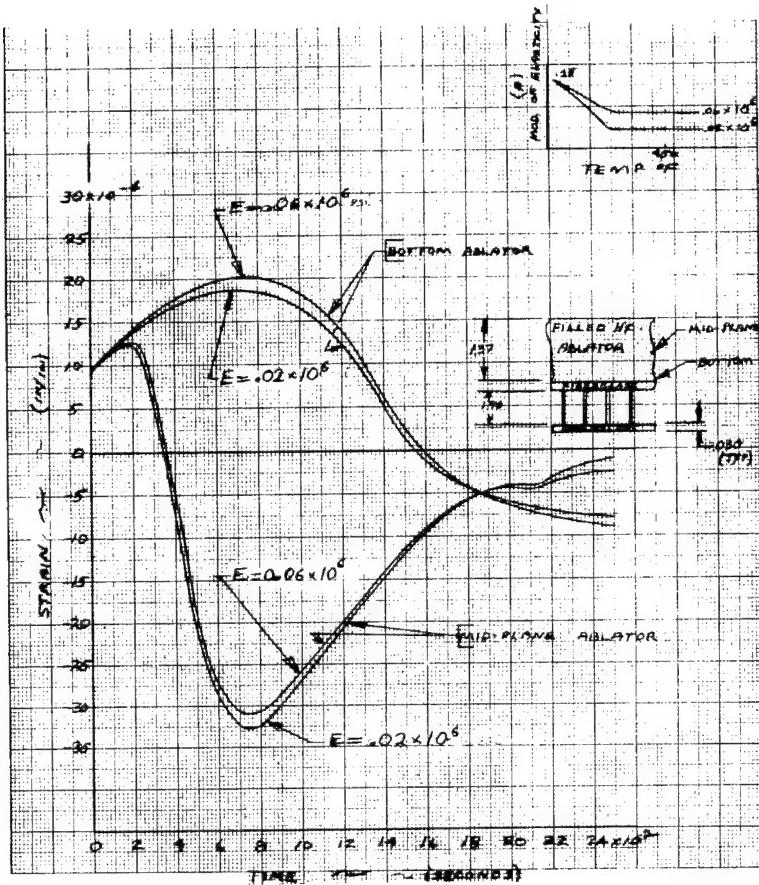
Figure 101 COMPARISON OF STRAIN VERSUS TIME FOR A CHANGE IN MODULUS
OF ELASTICITY OF FILLED HONEYCOMB ABLATOR, X/C = 0.5
WINDWARD, -250°F REENTRY, V_E = 36,500 FPS, OVERSHOOT
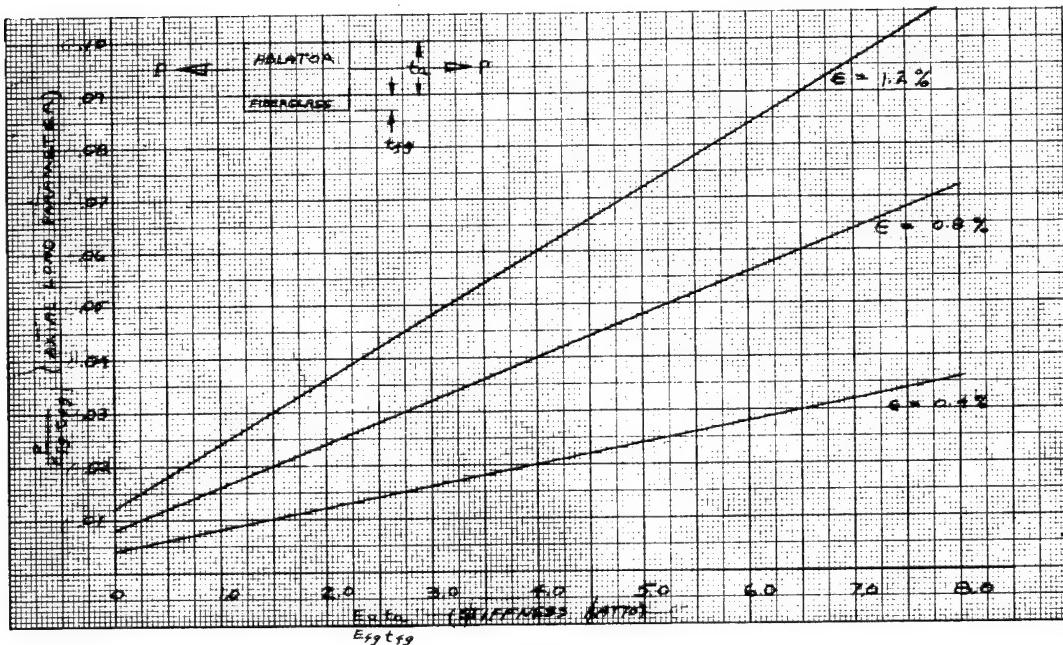
Figure 102 AXIAL LOAD PARAMETER VERSUS ABLATOR TO FIBERGLASS
STIFFNESS RATIO

-158-
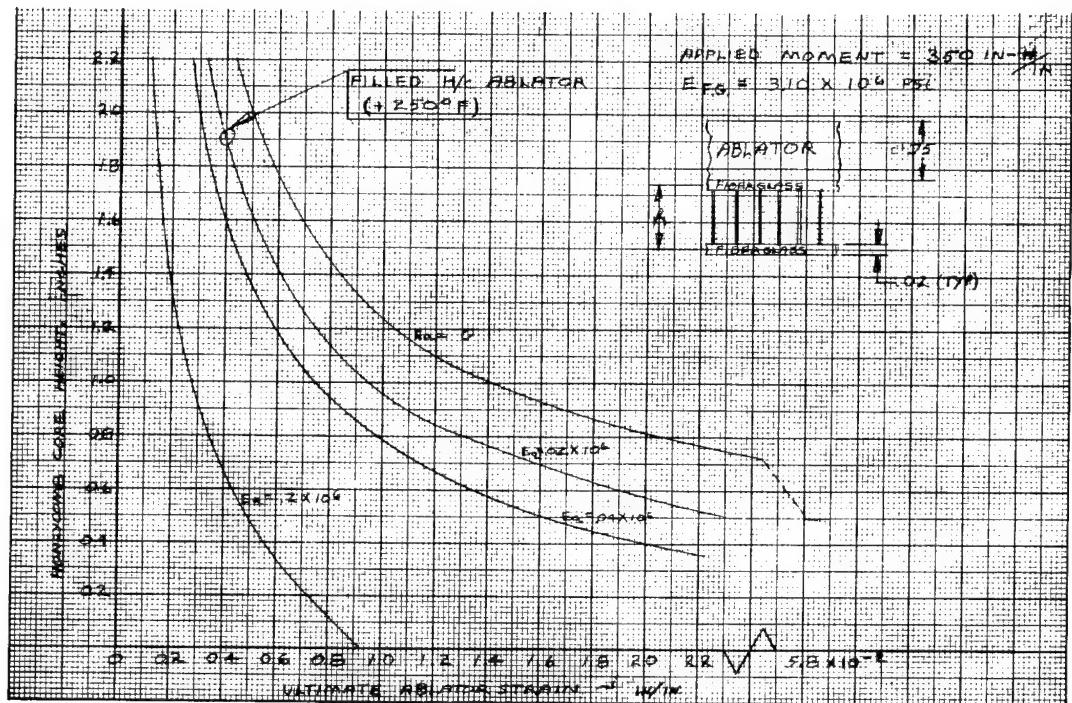
Figure 103 REQUIRED HONEYCOMB CORE HEIGHT VERSUS ULTIMATE ABLATOR
STRAIN FOR A GIVEN MOMENT OVER CROSS SECTION, ABLATOR
THICKNESS = .75
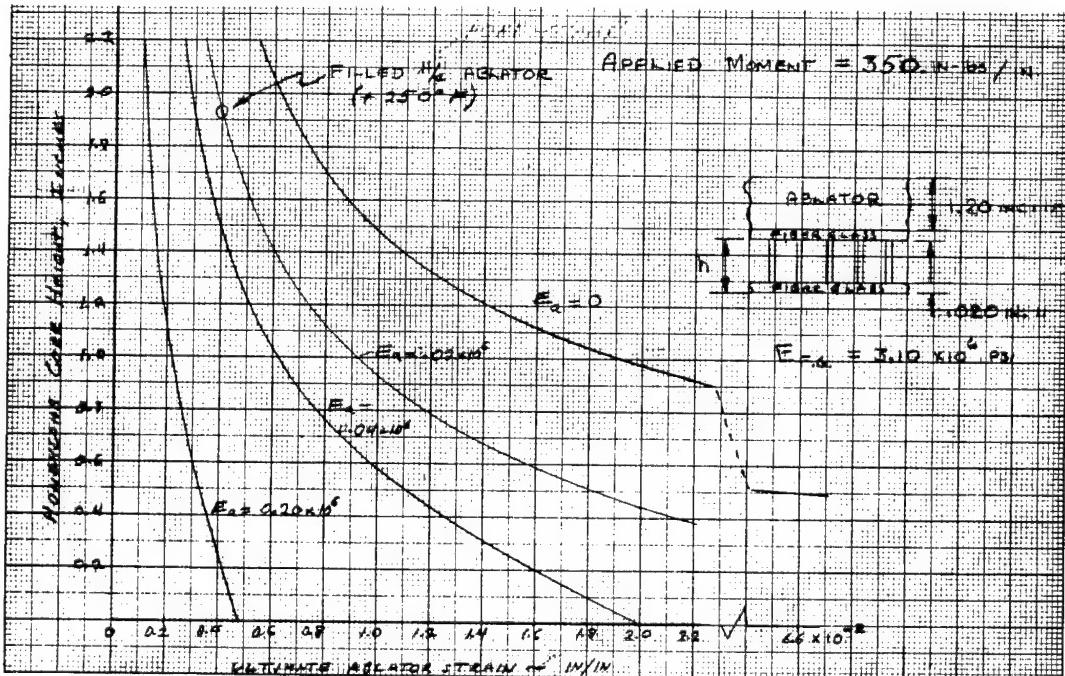
Figure 104 REQUIRED HONEYCOMB CORE HEIGHT VERSUS ULTIMATE ABLATOR
STRAIN FOR A GIVEN MOMENT OVER CROSS SECTION, ABLATOR
THICKNESS = 1.2

-159-
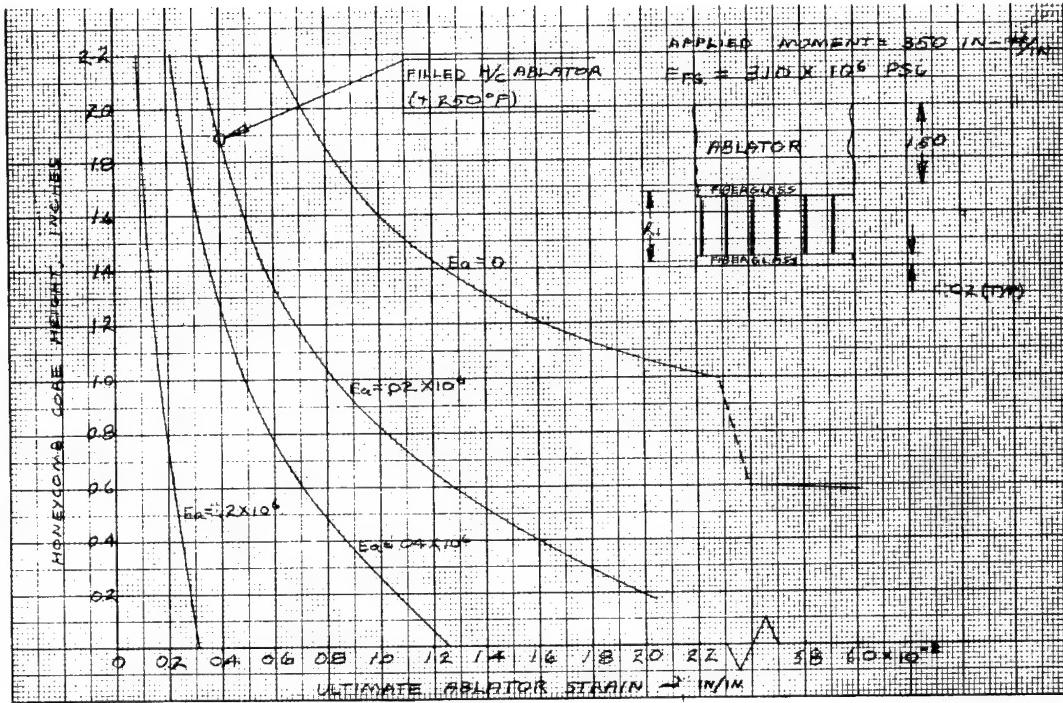
Figure 105 REQUIRED HONEYCOMB CORE HEIGHT VERSUS ULTIMATE ABLATOR
STRAIN FOR A GIVEN MOMENT OVER CROSS SECTION, ABLATOR
THICKNESS = 1.5
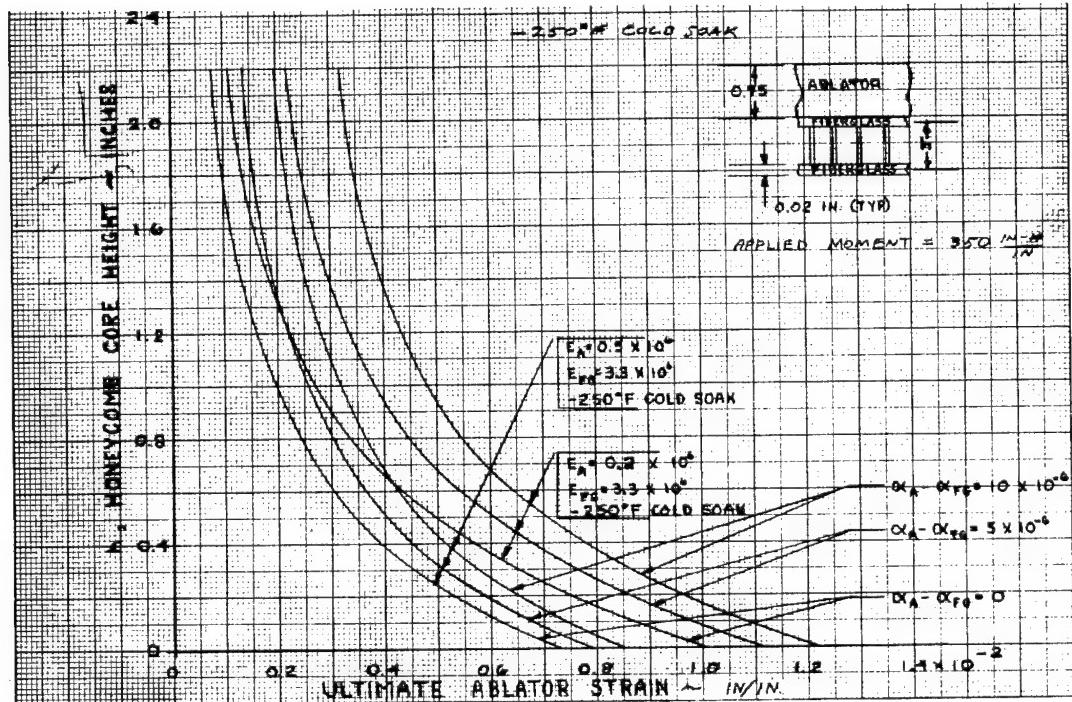
Figure 106 REQUIRED HONEYCOMB CORE HEIGHT VERSUS ULTIMATE ABLATOR
STRAIN FOR A GIVEN MOMENT OVER CROSS SECTION, -250°F
COLD SOAK, ABLATOR THICKNESS = 0.75
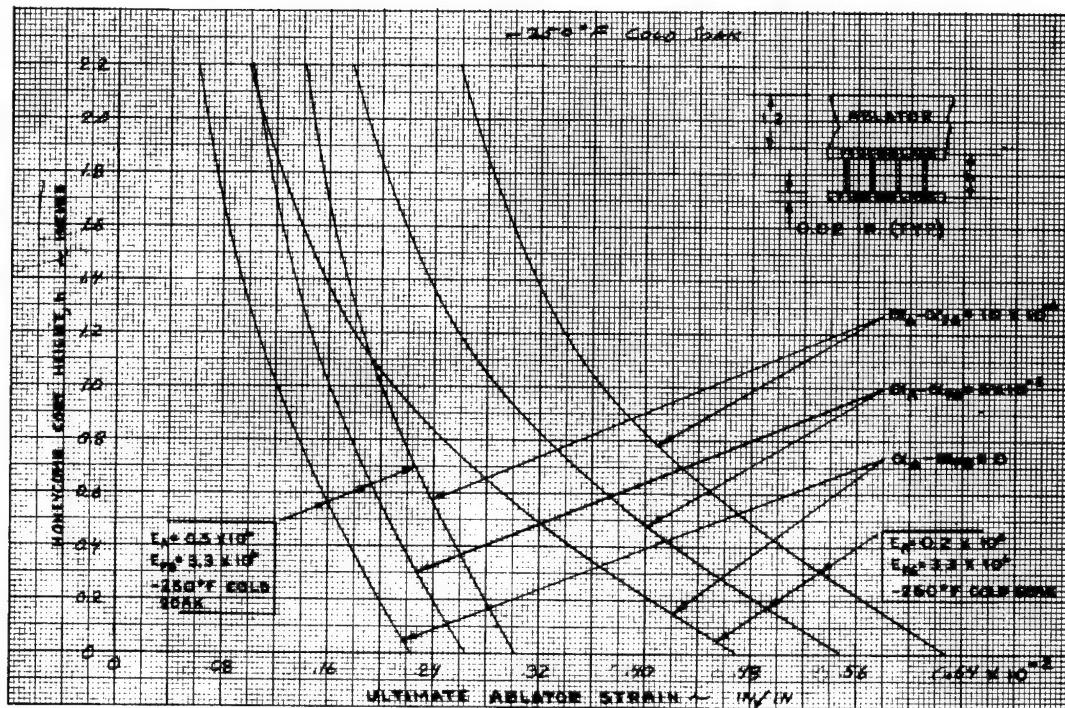
Figure 107 REQUIRED HONEYCOMB CORE HEIGHT VERSUS ULTIMATE ABLATOR
STRAIN FOR A GIVEN MOMENT OVER CROSS SECTION, -250,F
COLD SOAK, ABLATOR THICKNESS = 1.2
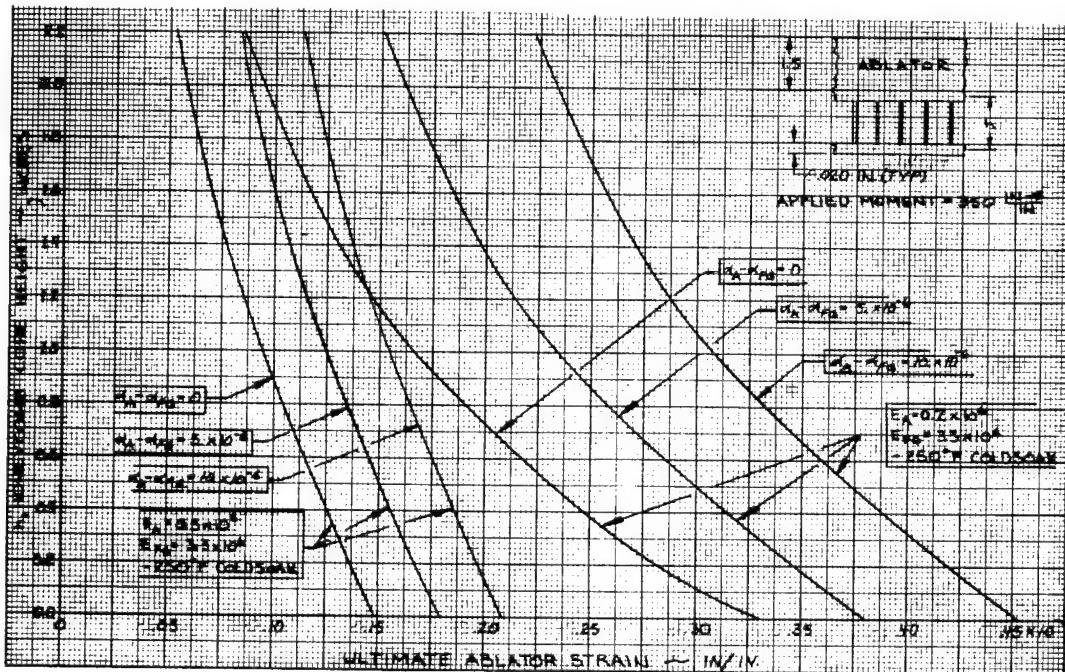
Figure 108 REQUIRED HONEYCOMB CORE HEIGHT VERSUS ULTIMATE ABLATOR
STRAIN FOR A GIVEN MOMENT OVER CROSS SECTION, -250°F
COLD SOAK, ABLATOR THICKNESS = 1.5

Figure 110 EFFECT OF ABLATOR MODULUS AND CORE HEIGHT ON BENDING
RIGIDITY, ABLATOR THICKNESS = 1.2
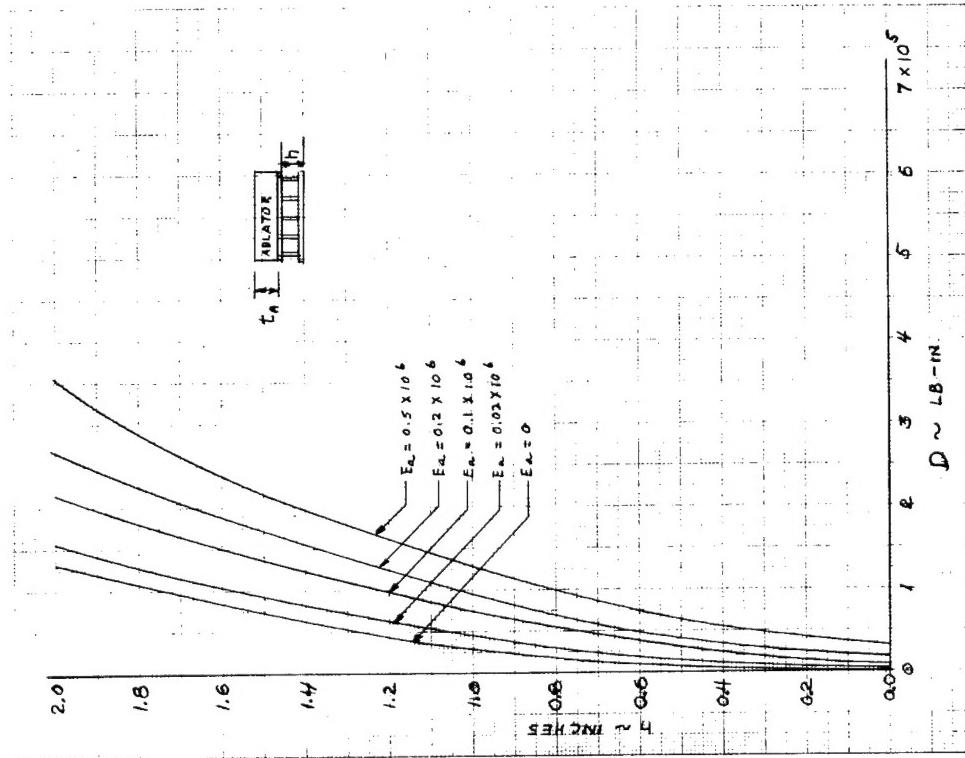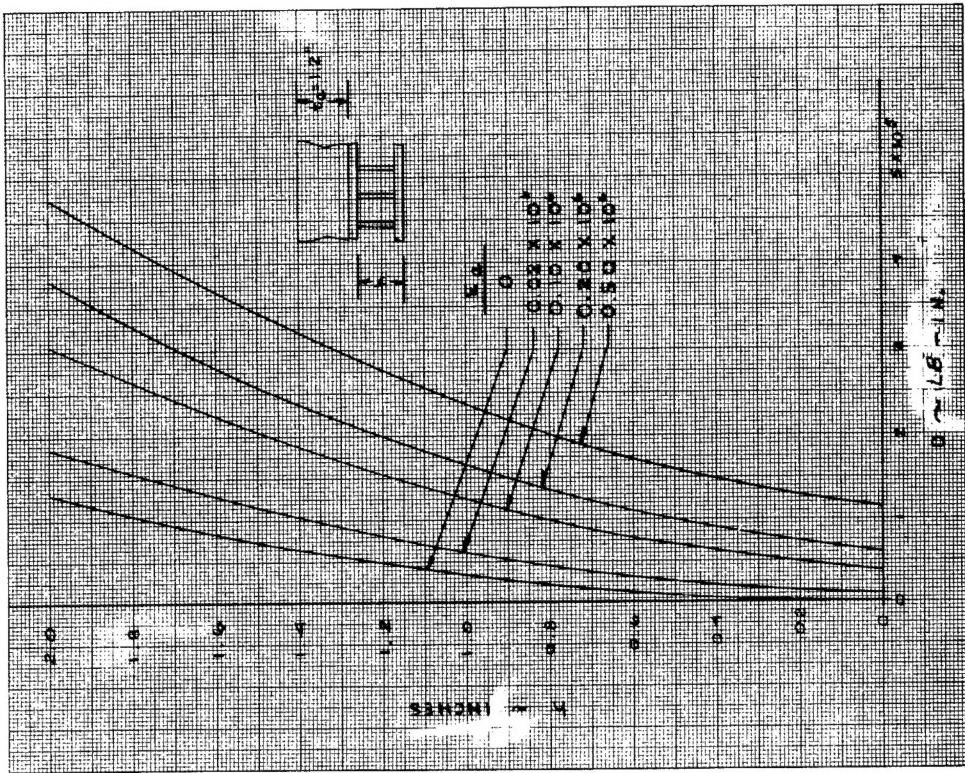
Figure 109 EFFECT OF ABLATOR MODULUS AND CORE HEIGHT ON BENDING
RIGIDITY, ABLATOR THICKNESS = 0.75
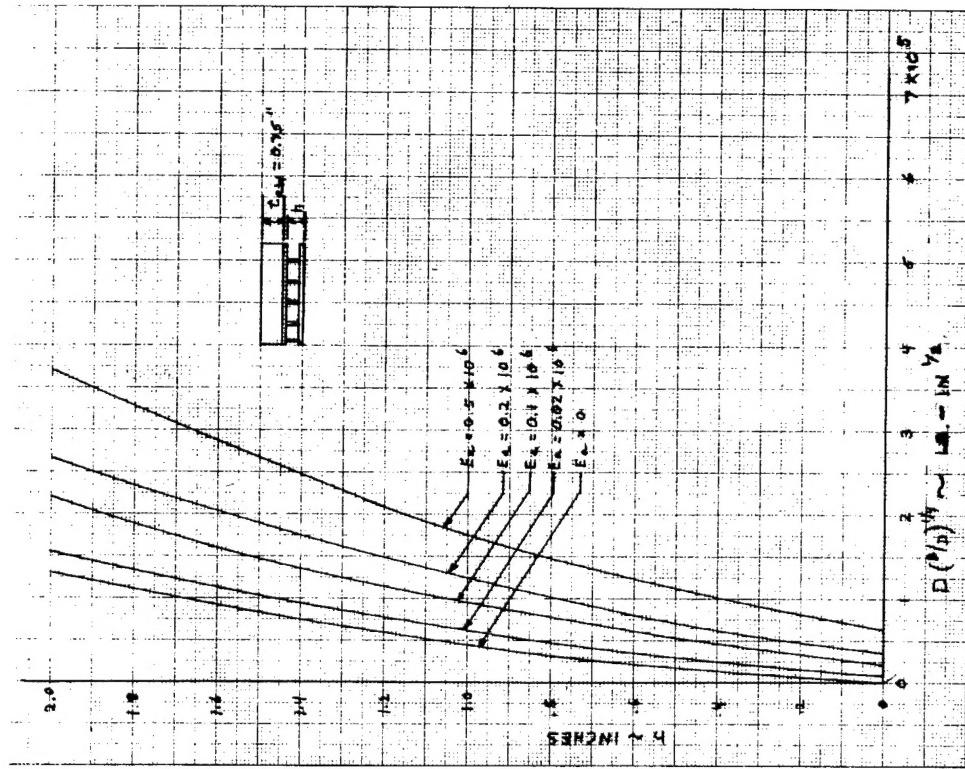
Figure 112 EFFECT OF ABLATOR MODULUS AND HONEYCOMB CORE HEIGHT ON CONE BUCKLING PARAMETER, ABLATOR THICKNESS = 0.75
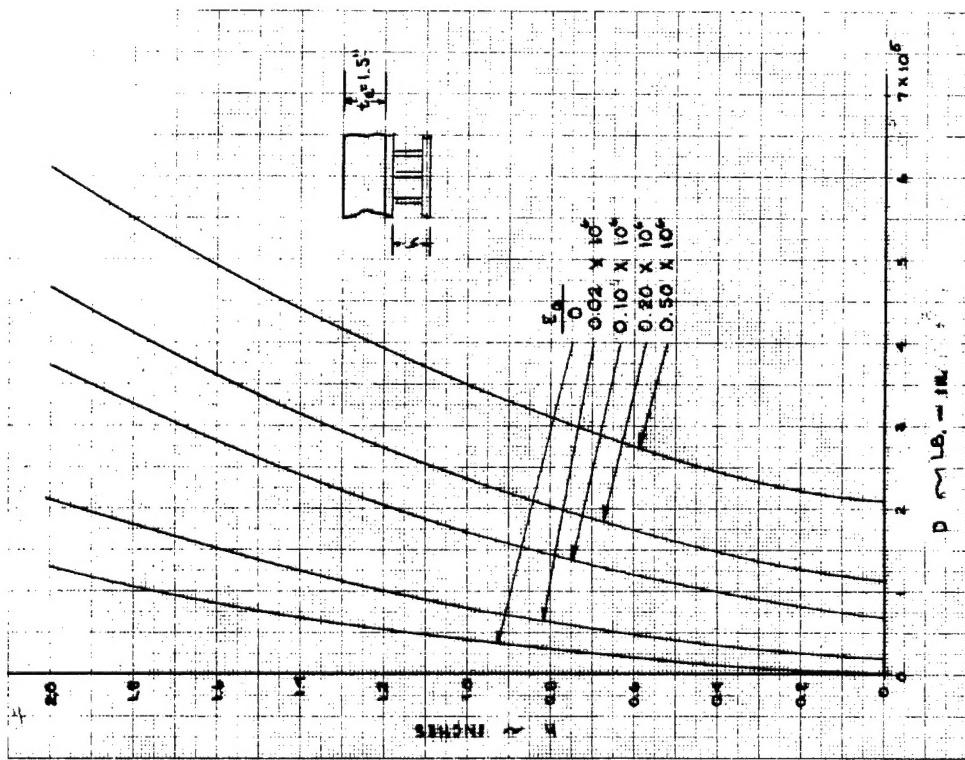
Figure 111 EFFECT OF ABLATOR MODULUS AND CORE HEIGHT ON BENDING RIGIDITY, ABLATOR THICKNESS = 1.5

Figure 114 EFFECT OF ABLATOR MODULUS AND HONEYCOMB CORE HEIGHT ON CONE BUCKLING PARAMETER, ABLATOR THICKNESS = 1.5
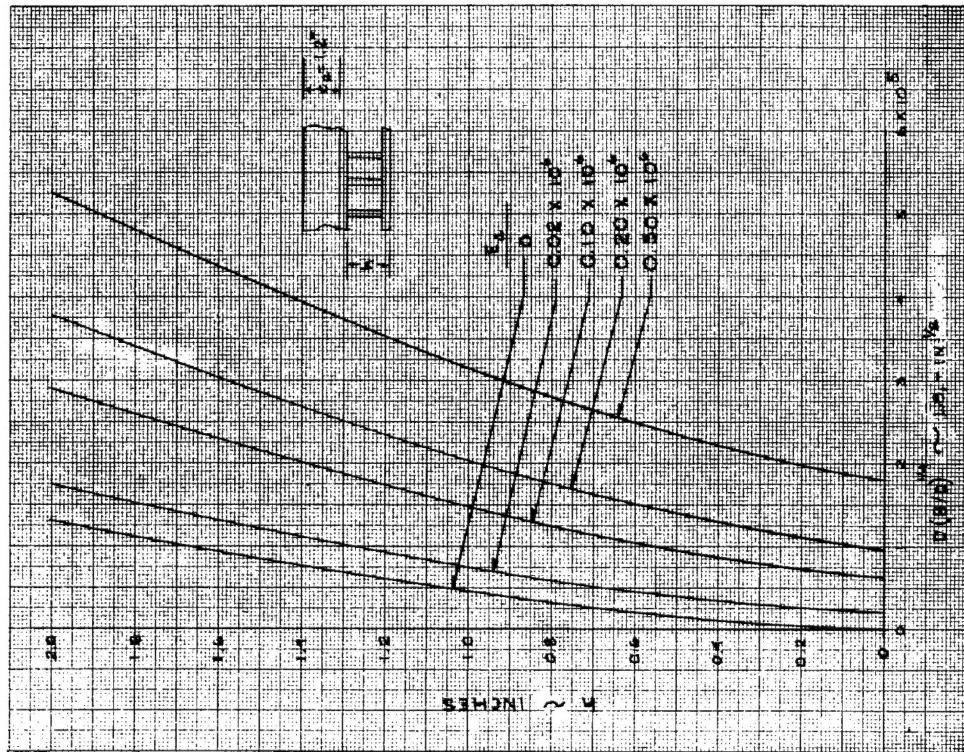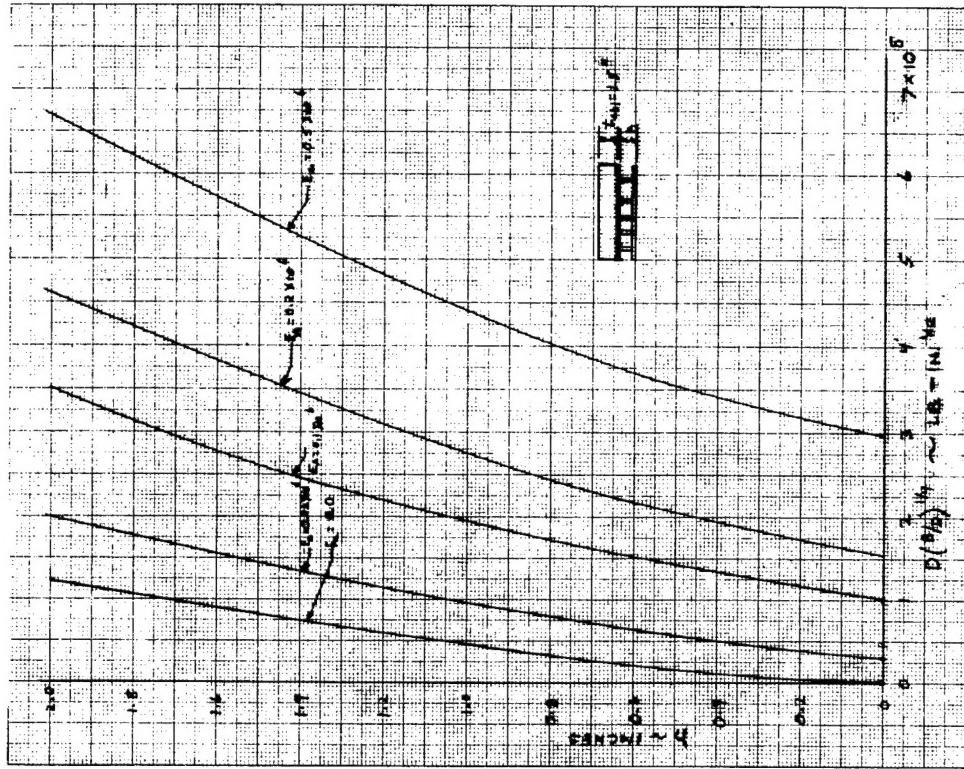
Figure 113 EFFECT OF ABLATOR MODULUS AND HONEYCOMB CORE HEIGHT ON CONE BUCKLING PARAMETER, ABLATOR THICKNESS = 1.2

REFERENCES

1. Preliminary Concept Report, Contract NAS 1-3531, Avco RAD-SR-64-24, (29 January 1964).

2. MIL-HDBK-5, Metallic Materials and Elements for Flight Vehicle Structures.

3. Cherni, G.G., Introduction to Hypersonic Flow, Academic Press, New York, (1961).

4. Miller, D.S., R. Hijman, M.E. Childs, Mach 8 to 22 Studies of Flow Separations due to Deflected Control Surface, AIAA Journal, (February 1964).

5. Van Tassell, W., A. Pallone, Similar Solutions of the Compressible Laminar Boundary-Layer Equations for Air in Equilibrium Dissociation and Ionization with and without Air Injection in the Stagnation Region, Avco RAD-TM-61-22 (28 June 1961).

6. Hoshizaki, H., The Effect of shock-generated Vorticity Surface Slip, and Temperature Jump on Stagnation Point Heat Transfer Rates, J. Aero Science (February 1960).

7. Waldman, G., N. Thyson, Three-Dimensional Stagnation Point Heating, Avco RAD-TM-62-92 (November 1962).

8. NASA-Langley Research Center letter to J.M. Newell from F.L. Thompson (8 November 1963).

9. Kivel, B., K. Bailey, Tables of Radiation from High Temperature Air, Avco-Everett Research Report 21 (December 1957).

10. Allen, R.A., A. Textoris, New Measurements and a New Interpretation for High Temperature Air Radiation, AIAA Preprint 64-72 (January 1964).

11. Allen, R.A., P.H. Rose, J.C. Camm, Non-Equilibrium and Equilibrium Radiation at Super-Satellite Reentry Velocities, Avco-Everett Research Report 156 (September 1962).

12. Mascola, N.E., and J.D. Brown, Digital Program 1327, Avco RAD Internal Memorandum S230-REM/JB-472 (29 March 1963).

13. Brown, J.D., Extension of Program 1327, Avco RAD Internal Memorandum S230-JB-686 (12 August 1963).

14. Timoshenko, S., and Woinowsky-Krieger, S., Theory of Plates and Shells, McGraw-Hill (1959).

15. Charnes and Raynor, Solar Heating of a Rotating Cylindrical Space Vehicle, ARS Journal (May 1960).